

AD-774 264

ROLLING ELEMENT BEARING RETAINER  
ANALYSIS

Joseph A. Mauriello, et al

Avco Lycoming Division

Prepared for:

Army Air Mobility Research and Development  
Laboratory

November 1973

DISTRIBUTED BY:



National Technical Information Service  
U. S. DEPARTMENT OF COMMERCE  
5285 Port Royal Road, Springfield Va. 22151

ACCESSION BY	WHITE Section <input checked="" type="checkbox"/>
STC	BUU Section <input type="checkbox"/>
BCC	<input type="checkbox"/>
REASON FOR USE	
Justification	
BY DISTRIBUTION/AVAILABILITY CODES	
SIM	AVAIL REG OR SPECIAL
OA	

#### DISCLAIMERS

The findings in this report are not to be construed as an official Department of the Army position unless so designated by other authorized documents.

When Government drawings, specifications, or other data are used for any purpose other than in connection with a definitely related Government procurement operation, the United States Government thereby incurs no responsibility nor any obligation whatsoever; and the fact that the Government may have formulated, furnished, or in any way supplied the said drawings, specifications, or other data is not to be regarded by implication or otherwise as in any manner licensing the holder or any other person or corporation, or conveying any rights or permission, to manufacture, use, or sell any patented invention that may in any way be related thereto.

Trade names cited in this report do not constitute an official endorsement or approval of the use of such commercial hardware or software.

#### DISPOSITION INSTRUCTIONS

Destroy this report when no longer needed. Do not return it to the originator.

10

Unclassified  
Security Classification

AD-774264

DOCUMENT CONTROL DATA - R & D		
(Security classification of title, body of abstract and indexing annotation must be entered when the overall report is classified)		
1. ORIGINATING ACTIVITY (Corporate author) <b>Avco Lycoming Division 550 S. Main Street Stratford, Connecticut 06497</b>		2a. REPORT SECURITY CLASSIFICATION <b>Unclassified</b>
		2b. GROUP
3. REPORT TITLE <b>ROLLING ELEMENT BEARING RETAINER ANALYSIS</b>		
4. DESCRIPTIVE NOTES (Type of report and inclusive dates) <b>Final Report</b>		
5. AUTHOR(S) (First name, middle initial, last name) <b>Joseph A. Mauriello      A. B. Jones Normand Lagasse      William Murray</b>		
6. REPORT DATE <b>November 1973</b>	7a. TOTAL NO. OF PAGES <b>273 267</b>	7b. NO. OF REPS <b>11</b>
8a. CONTRACT OR GRANT NO. <b>Contract DAAJ02-67-C-0080</b>	8a. ORIGINATOR'S REPORT NUMBER(s)	
8b. PROJECT NO. <b>Task LG:62203D14414</b>	8b. SPONSORING MILITARY ACTIVITY <b>USAAMRDL Technical Report 72-45</b>	
8c.	8d. OTHER REPORT NO(S) (Any other numbers that may be assigned this report) <b>Lycoming Report No. 105.7.10</b>	
10. DISTRIBUTION STATEMENT <b>Approved for public release; distribution unlimited.</b>		
11. SUPPLEMENTARY NOTES	12. SPONSORING MILITARY ACTIVITY <b>Eustis Directorate U.S. Army Air Mobility R&amp;D Laboratory Fort Eustis, Virginia</b>	
13. ABSTRACT <p>An integrated analytical and experimental program was conducted to analyze the operation of rolling element bearing retainers and attendant lubrication effects. Analytical models to represent ball and roller bearing operation were derived with regard to the elastic deflections at the rolling element/race contacts, tractive forces generated at the bearing component interaction surfaces, and viscous drag effects.</p> <p>Program objectives were conducted in two phases. The first phase was to analyze the forces and the lubrication conditions that exist between the rolling element and retainer pockets when the bearing is operating at high-load and high-speed conditions. Once completed, the derived analysis was incorporated into an iterative computer program to produce bearing solutions for arbitrary load and speed conditions.</p> <p>The second phase of the program was to conduct an experimental test program to validate the computer analysis. Bearing performance was investigated over a wide range of loads, speeds, and lubrication conditions. Also, data were acquired on ball bearings subjected to retainer skid at high-speed, low-load operating conditions. To accomplish the test program, it was necessary to modify an existing test rig and to design special instrumentation for acquisition of the desired operating data.</p>		

DD FORM 1 NOV 1973 OBSOLETE FOR NAVY USE.

Unclassified

Reproduced by  
**NATIONAL TECHNICAL  
INFORMATION SERVICE**  
U.S. Department of Commerce  
Springfield, VA 22151

Unclassified  
Security Classification

14 KEY WORDS	LINK A		LINK B		LINK C	
	ROLE	WT	ROLE	WT	ROLE	WT
Bearing Retainer Lubrication of Bearings Rolling Element Bearing Retainer						

Unclassified  
Security Classification

1a)

12036-73



DEPARTMENT OF THE ARMY  
U. S. ARMY AIR MOBILITY RESEARCH & DEVELOPMENT LABORATORY  
EUSTIS DIRECTORATE  
FORT EUSTIS, VIRGINIA 23604

The research described herein was conducted by AVCO Lycoming Division under the terms of Contract DAAJ02-69-C-0080. The work was performed under the technical management of Mr. E. R. Givens, Propulsion Division, Eustis Directorate, U.S. Army Air Mobility Research and Development Laboratory.

The objectives of the program were to analyze the forces exerted on the retainer pockets of rolling element bearings during high-load, high-speed operating conditions that exist within the rolling-contact areas of the bearing.

Appropriate technical personnel of this Directorate have reviewed this report and concur with the conclusions contained herein.

ic)

Task 1G162203D14414  
Contract DAAJ02-69-C-0080  
USAAMRDL Technical Report 72-45  
November 1973

ROLLING ELEMENT BEARING RETAINER ANALYSIS

Final Report

Avco Lycoming Report No. 105.7.10

By

Joseph A. Mauriello  
Normand Lagasse  
A. B. Jones  
William Murray

Prepared by

Avco Lycoming Division  
Stratford, Connecticut

for

EUSTIS DIRECTORATE  
U.S. ARMY AIR MOBILITY  
RESEARCH AND DEVELOPMENT LABORATORY  
FORT EUSTIS, VIRGINIA

Approved for public release; distribution unlimited.

## SUMMARY

An integrated analytical and experimental program was conducted to analyze the operation of rolling element bearing retainers and attendant lubrication effects. Analytical models to represent ball and roller bearing operation were derived with regard to the elastic deflections at the rolling element/race contacts, tractive forces generated at the bearing component interaction surfaces, and viscous drag effects.

Program objectives were conducted in two phases. The first phase was to analyze the forces and the lubrication conditions that exist between the rolling element and retainer pockets when the bearing is operating at high-load and high-speed conditions. Once completed, the derived analysis was incorporated into an iterative computer program to produce bearing solutions for arbitrary load and speed conditions.

The second phase of the program was to conduct an experimental test program to validate the computer analysis. Bearing performance was investigated over a wide range of loads, speeds, and lubrication conditions. Also, data were acquired on ball bearings subjected to retainer skid at high-speed, low-load operating conditions. To accomplish the test program, it was necessary to modify an existing test rig and to design special instrumentation for acquisition of the desired operating data.

## FOREWORD

This final report describes a program conducted by Avco Lycoming Division for the U. S. Army Air Mobility Research and Development Laboratory under Contract DAAJ02-69-C-0080, Task 1G162203D14414.

U. S. Army technical direction was provided by Mr. R. Givens.

We wish to acknowledge Mr. R. Chasman of the Air Force Aero Propulsion Laboratory for his support of the program, and Drs. J. Walowit and A. L. Gu of Mechanical Technology, Inc., for their contributions to the elastohydrodynamic traction computer subroutines and to the equations of shear forces on the high-speed bearing retainers.

## TABLE OF CONTENTS

	<u>Page</u>
SUMMARY . . . . .	iii
FOREWORD . . . . .	v
LIST OF ILLUSTRATIONS . . . . .	ix
LIST OF TABLES. . . . .	xiv
LIST OF SYMBOLS . . . . .	xv
INTRODUCTION . . . . .	1
MATHEMATICAL ANALYSIS . . . . .	5
Ball Bearing Mathematical Model. . . . .	5
Roller Bearing Mathematical Model . . . . .	21
Elastohydrodynamic Film Thickness Calculation. . . . .	41
Elastohydrodynamic Traction Coefficients . . . . .	46
Analysis of Shear Forces on a Lubricated, High-Speed Bearing Retainer. . . . .	62
VERIFICATION TEST PROGRAM. . . . .	83
Test Rig Description and Operation . . . . .	83
Test Bearing Description . . . . .	93
Instrumentation. . . . .	121
Data Acquisition . . . . .	129
Test Procedure. . . . .	134
Test Results. . . . .	140
COMPUTER PROGRAM RESULTS . . . . .	176
Ball Bearing Computer Deck . . . . .	176
Roller Bearing Computer Deck . . . . .	184
CONCLUSIONS . . . . .	188
RECOMMENDATIONS . . . . .	189
LITERATURE CITED . . . . .	190

**APPENDIXES**

	<u>Page</u>
I. Ball Bearing Computer Program FORTRAN Source Deck . . . . .	191
II. Format for Ball Bearing Computer Input Information .	222
III. Typical Ball Bearing Problem for Computer Program	224
IV. Roller Bearing Computer Program FORTRAN Source Deck . . . . .	227
V. Format for Roller Bearing Computer Program Input Information . . . . .	244
VI. Typical Roller Bearing Problem from Computer Program. . . . .	246
VII. MIL-L-23699-Type Oil Properties Available for Use in Program Inputs . . . . .	248
VIII. Solution for Roller Bearing Case Operating at 20,000 RPM and Radial Load of 200 Pounds . . . . .	249
DISTRIBUTION . . . . .	251

## LIST OF ILLUSTRATIONS

<u>Figure</u>		<u>Page</u>
1	Race Control Concept . . . . .	2
2	Ball Referred to XYZ Coordinate System . . . . .	7
3	Initial and Final Positions of Inner and Outer Race Curvature Centers . . . . .	11
4	Bearing Referred to XYZ Coordinate System . . . . .	15
5	Forces and Moments Acting on Outer-Piloted Cage .	18
6	Forces and Moments Acting on Inner-Piloted Cage .	19
7	Bearing Details . . . . .	22
8	Roller Contact Forces and Roller Orientation Schematic . . . . .	25
9	Roller Pocket Forces and Cage Whirl Forces . . . . .	33
10	Ball Motion Occurring in High-Speed Angular-Contact Ball Bearing; General Case . . . . .	43
11	Contact Areas on Race and Ball . . . . .	44
12	Coefficient of Friction Versus Shear Rate Parameter for Heating Parameter = $10^{-6}$ . . . . .	48
13	Coefficient of Friction Versus Shear Rate Parameter for Heating Parameter = $5 \times 10^{-4}$ . . . . .	49
14	Velocity Components Active in Contact Areas . . . . .	51
15	Tractive Force Versus Slip Velocity . . . . .	55
16	Race Contact, Velocity Distribution, and Tractive Force Distribution in a Ball-Race Contact . . . . .	56

<u>Figure</u>		<u>Page</u>
17	Sliding Velocity and Tractive Force Distribution in a Ball-Race Contact .....	57
18	Analysis of Retainer-Ball Traction; Schematic . . .	63
19	Dimensionless Pressure Profile for Ball-Retainer Contact ( $\eta = 0$ ). . . . .	67
20	Dimensionless Load per Unit Length . . . . .	71
21	Film Thickness and Maximum Pressure for Retainer-Ball Contact . . . . .	73
22	Traction Versus Load for Ball and Roller Contacts	76
23	Film Thickness and Maximum Pressure for Retainer-Roller Contact, . . . . .	77
24	Geometry Used in Calculating Retainer-Race Traction; Schematic . . . . .	79
25	Section Used in Calculating Drag on Ball; Schematic	82
26	Bearing Test Rig; Cross-Sectional View . . . . .	85
27	Bearing Test Facility . . . . .	86
28	Bearing Test Rig; Right Front View . . . . .	87
29	Bearing Test Rig; Front View . . . . .	88
30	Air Pressure Differential Versus Bearing Thrust Load . . . . .	89
31	Test Rig Facilities; Schematic Diagram . . . . .	91
32	Typical Data Sheets . . . . .	92
33	Ball Bearing PSK 18123 . . . . .	95

<u>Figure</u>		<u>Page</u>
34	Ball Retainer Rework PSK 17438 . . . . .	97
35	Ball Bearing S/N 003 Inner Race Roundness and Concentricity . . . . .	100
36	Ball Bearing S/N 003 Outer Race Roundness and Concentricity . . . . .	101
37	Ball Bearing S/N 006 Inner Race Roundness and Concentricity . . . . .	102
38	Ball Bearing S/N 006 Outer Race Roundness and Concentricity . . . . .	103
39	Ball Bearing S/N 003 Outer Race Surface Texture and Groove Radius . . . . .	105
40	Ball Bearing S/N 003 Thrust Inner Race Surface Texture and Groove Radius . . . . .	107
41	Ball Bearing S/N 006 Outer Race Surface Texture and Groove Radius . . . . .	109
42	Ball Bearing S/N 006 Thrust Inner Race Surface Texture and Groove Radius . . . . .	111
43	Roller Retainer Rework PSK 17478 . . . . .	115
44	Roller Bearing Outer Ring Roundness and Concentricity . . . . .	117
45	Roller Bearing Inner Ring Roundness and Concentricity . . . . .	118
46	Roller Bearing Outer Race Surface Finish . . . . .	119
47	Roller Bearing Inner Race Surface Finish . . . . .	120
48	Instrumentation Location . . . . .	122

<u>Figure</u>		<u>Page</u>
49	Ball Bearing Retainer Strain-Gage Location and Rework . . . . .	124
50	Hall Generators Installed in Ball Bearing Retainer Pockets . . . . .	127
51	Ball Bearing Magnetic Field Mapping . . . . .	128
52	Slip Ring and Driving Plate . . . . .	130
53	Typical Multiplexer Outputs . . . . .	132
54	Build No. 1 Bearing Failure; Shaft Unbalance . . .	133
55	Build No. 2 Bearing Failure; Insufficient Pocket Clearance . . . . .	135
56	Improved and Original Retainer to Driving Ring Strain-Gage Lead Paths . . . . .	136
57-64	Retainer Web Force and Retainer Speed Versus Time, Showing Nature of Impact Loads . . . . .	142-149
65-72	Retainer Web Force Expanded With Computed Web Force Superimposed . . . . .	150-157
73-74	Harmonic Analysis of Experimentally Determined Retainer Web Force (Average of 16 Spectra) for Ball Bearing Smooth Race . . . . .	159-160
75	Harmonic Analysis of Computed Retainer Web Force for Ball Bearing Smooth Race . . . . .	161
76-79	Retainer Web Filtered and Unfiltered Retainer Force Wave Form With Computed Forces Superimposed . . . . .	162-165
80	Retainer Speed Ratio Versus Axial Thrust Load .	167

<u>Figure</u>		<u>Page</u>
31-82	Expanded Trace of Rough-Race Bearing Retainer Web Forces . . . . .	169-170
83-86	Bearing Retainer Web Force and Speed Versus Time . . . . .	172-175
87	Pocket Loading Versus Radial Load (Axial Load = 1000 Pounds) . . . . .	178
88	Pocket Film Thickness Versus Pocket Load (Axial Load = 1000 Pounds, Radial Load = 500 Pounds) . . . . .	179
89	Retainer Speed Versus Axial Load. . . . .	181
90	Roller Bearing Program Data; Residual Cage Torque Versus Cage Slip (Inner Race Speed = 20,000 RPM) . . . . .	186
91	Roller Bearing Program Data; Cage Slip Versus Radial Load (Inner Race Speed = 20,000 RPM) . . . . .	187

## LIST OF TABLES

<u>Table</u>		<u>Page</u>
I	Stability Map - FRCTN Subroutine. . . . .	60
II	Stability Map - Analytical Function From FRCTN Subroutine. . . . .	60
III	Stability Map - $f = C_1 G_1^{1/4}$ . . . . .	61
IV	Stability Map - $f = C_1 G_1^{1/2}$ . . . . .	61
V	Physical Properties of MIL-L-23699 Oil, Code 0-64-2 . . . . .	90
VI	Test Ball Bearing Inspection Data, Detail Internal Geometry . . . . .	99
VII	Roller Bearing Engineering Data . . . . .	113
VIII	Ball Bearing Test Conditions . . . . .	137
IX	Roller Bearing Test Conditions. . . . .	138
X	Summary of Test Results, Build No. 2 . . . . .	141
XI	Inner and Outer Race Temperatures, Build No. 3 .	168
XII	Inner and Outer Race Temperatures, Build No. 4 .	171
XIII	Bearing Problem Parameters. . . . .	177
XIV	Ball Kinematics; Inner Ring Speed = 20,000 RPM, Radial Load = 0 . . . . .	183
XV	Roller Bearing Problem Parameters . . . . .	185

### LIST OF SYMBOLS

A	area of cage guiding surface, in. <sup>2</sup>
A <sub>1</sub>	axial distance between inner and outer race curvature centers, in.
A <sub>2</sub>	radial distance between inner and outer race curvature centers, in.
A <sub>3</sub>	drag area on rolling elements, in. <sup>2</sup>
A <sub>i</sub>	drag area on races, in. <sup>2</sup>
A <sub>Y, Z</sub>	pilot surface load parameters for Y and Z directions, lb
a <sub>i</sub>	semimajor axis of contact ellipse, in.
b	semiwidth of roller contact, in.
b <sub>i</sub>	semiminor axis of pressure ellipse, in.
C	radial clearance of rolling element in retainer pocket, in.
C <sub>D</sub>	drag coefficient
C <sub>f</sub>	friction factor for flow between race and retainer
C <sub>i</sub>	C <sub>1</sub> = 1.0, C <sub>2</sub> = -1.0
D <sub>1</sub>	outside diameter of retainer or pilot surface, in.
D <sub>2</sub>	inside diameter of retainer or pilot surface, in.
D'	retainer pilot diameter, in.
D <sub>C<sub>1</sub></sub>	outside diameter of cage, in.
D <sub>C<sub>2</sub></sub>	inside diameter of cage, in.
d	rolling element diameter, in.

E	pitch diameter, in.
$E(\epsilon_i)$	complete elliptical integral of the second kind
$E_R, E$	Young's modulus for bearing rings (R) and rolling elements (E), lb/in. <sup>2</sup>
$E'$	instantaneous pitch diameter of ball, in.
$E''$	materials parameter in Dowson and Higginson equation, lb/in. <sup>2</sup>
F	reaction of bearing, in.
$\bar{F}$	external radial load, lb
$F_1, F_2$	hydrodynamic forces in retainer pocket, lb
$F_C$	rolling element centrifugal force, lb
$\bar{F}_C$	centrifugal force on cage, lb
$F_D$	viscous drag force on rolling element, lb
$F_F$	retainer pilot surface Coulomb drag force, lb
$F_P$	normal force in roller/pocket contact, lb
$F_{Pi}$	total load of roller against retainer pocket, lb
$F_{Px}$	friction force generated at retainer contact in pocket in X direction, lb
$F_{Pz}$	friction force generated at ball retainer contact in ball pocket in Z direction, lb
$F_R$	net viscous drag force on retainer, lb
$F_T$	tractive force in roller/race contact, lb
$F_V$	tangential force in roller/pocket contact, lb
$F_X$	bearing reaction force in X direction, lb

$F_{X_i}$	friction force directed along major axis (X) of pressure ellipse, lb
$F_Y$	bearing reaction force in Y direction, lb
$F_{Y_i}$	friction force directed along minor axis (Y) of pressure ellipse, lb
$F_Z$	bearing reaction force in Z direction, lb
$F'_{P_x}$	load per unit length of roller against retainer pocket, lb/in.
$F'Z$	total tractive force between roller and retainer pocket, lb
$F'_{Z_y}$	tractive force per unit length between roller and retainer pocket, lb/in.
$\bar{F}_V$	roller bearing externally applied radial load in the Z direction, lb
$\tilde{F}_i$	dimensionless tractive forces
$f$	friction factor/coefficient - rolling element to race contacts
$f_i$	race curvature - groove radius divided by ball diameter
$f_r$	coefficient of sliding friction for pilot surface
$G_1$	shear rate parameter
$G_2$	thermal heating parameter
$G_3$	pressure-viscosity parameter
$H$	horizontal component of pilot surface load ( $P_c$ ), lb
$H_j$	spacing between retainer and race, in.
$h$	elastohydrodynamic film thickness, in.
$h_o$	minimum elastohydrodynamic film thickness, in.

$h_p$	film thickness of midpoint of roller to cage contact, in.
$h_{p_x}$	film thickness at any point X along roller to cage contact, in.
$\tilde{h}$	dimensionless film thickness
I	mass moment of inertia of rolling element, in.-sec <sup>2</sup> -lb
i	i = 1 for outer race contact; i = 2 for inner race contact
K	coefficient of friction for retainer-rolling element contacts
$K(\epsilon_1)$	complete elliptical integral of the first kind
$K_c$	Coulomb friction coefficient for roller-retainer contact
$K_f$	thermal conductivity of the lubricant, Btu/ <sup>o</sup> F-hr-ft
$K'_1$	constant = 0.5482
$K'_w$	constant = 2.447
$l_F$	flat length of roller, in.
$l_T$	total length of roller less two corner radii, in.
$l'$	distance from roller dim point to contact pattern end, in.
$M_c$	total torque on retainer, lb-in.
m	mass of rolling element, lb-sec <sup>2</sup> /in.
$m_c$	mass of cage, lb-sec <sup>2</sup> /in.
$m_R, E$	Poisson's ratio for bearing rings (R) and rolling element (E)
$M_V$	viscous drag between rings and retainer, lb-in.
$M_Y$	inertial moment of ball about Y axis, lb-in.
$M_Z$	inertial moment of ball about Z axis, lb-in.
$M'_Y$	bearing reactive moment about Y axis, lb

$n$	number of rolling elements
$P$	race contact force, lb
$P_c$	retainer pilot surface to guiding race land load, lb
$P_{c_r}$	normal pilot contact force if $\bar{F}_c$ is absent, lb
$F_D$	diametral clearance of bearing, in.
$P_{HZ}$	Hertz pressure, lb/in. <sup>2</sup>
$P_i$	race contact normal loads, lb
$F_{ix}$	load per unit length of contact at X along roller contact, lb/in.
$P_p$	normal contact load between ball and retainer in pocket, lb
$\tilde{P}$	dimensionless load per unit length
$p$	pressure, lb/in. <sup>2</sup>
$p_x$	roller loading, lb-in.
$\tilde{p}$	dimensionless pressure
$Q_p$	spin torque at ball to retainer pocket contact, lb-in.
$Q_{s_i}$	spin torque at race contact, lb-in.
$Q_v$	viscous drag torque on cage, lb-in.
$\bar{Q}$	torque unbalance on cage, lb-in.
$q$	roller azimuth index
$R$	equivalent radius of contact against a plane surface, in.
$R_c$	roller crown radius, in.

$R_E$	radius of rolling element, in.
$R_R$	radius of race surface, in. /sec
$\Re$	Reynolds number
$r$	corner radius of roller, in.
$r_r$	roller radius, in.
$S_m$	maximum Hertz stress, psi
$S_R, S_B$	RMS surface roughness parameters
$T_i$	inlet lubricant temperature, $^{\circ}$ F
$T_o$	temperature of lubricant, $^{\circ}$ F
$t_r$	thickness of retainer, in.
$U$	velocity term in Dowson and Higginson equation, in. /sec
$U_i$	sliding velocity of ring on cage, in. /sec
$U_R$	linear velocity of roller, in. /sec
$U_y$	linear velocity of race, in. /sec
$u_s$	sliding speed at rolling element to race contact, in. /sec
$u_x, u_y$	rolling element to retainer sliding velocities, in. /sec
$V$	vertical component of pilot surface load ( $P_c$ ), lb
$V_{Bi}$	linear velocity in the Y direction at a strip on a ball, in. /sec
$V_E$	surface velocity of roller, in. /sec
$V_o$	orbital velocity of rolling element, rad/sec
$V_{Ri}$	linear velocity in the Y direction at a strip on the race, in. /sec

$V_{XR_i}$	linear velocity on a strip on the race in the X direction, in./sec
$V_{yB_i}$	linear velocity of the ball in the Y direction at the center of the contact area, in./sec
$V_{XB_i}$	linear velocity on a strip on the ball in the X direction, in./sec
$V_{y_i}$	surface velocity of ring relative to retainer, in./sec
$V_{xB_i}$	linear velocity on a strip on the ball in the X direction, in./sec
$V_{yR_i}$	linear velocity of a raceway in the Y direction at the center of the contact area, in./sec
$W$	normal pocket load = $P_p$ , lb
$w$	load per unit width of contact, lb/in.
$\tilde{w}$	dimensionless load
$W_i$	total axial effective contact length between retainer and ring, in.
$X_1$	ball center (axial) coordinate relative to outer race center of curvature, in.
$X_2$	ball center (radial) coordinate relative to outer race center of curvature, in.
$y^*$	semistrip width, in.
$z$	radial clearances at cage outside and inside diameter
$\alpha_o$	pressure coefficient of viscosity, in. <sup>2</sup> /lb
$\beta_1^*$	temperature viscosity coefficient used by Crook, °F
$\beta_i$	race contact angle, deg
$\gamma_i$	geometric parameter = $d/\cos \beta_i/E'$
$\Delta$	total approach of inner and outer rings, in.

$\Delta_o$	total compression at roller to race contact, in.
$\Delta_i$	approach of ball to race at the $i^{\text{th}}$ contact, in.
$\Delta_{ix}$	approach of roller to race at X along roller contact, in.
$\delta$	total approach of inner to outer race, in.
$\Delta_q$	total compression of roller, in.
$\delta_o$	maximum compressive stress in contact area, Hertz stress
$\delta_x$	inner ring displacement in X direction, in.
$\delta_y$	inner ring displacement in Y direction, in.
$\delta_z$	inner ring displacement in Z direction, in.
$\epsilon_i$	modular angle of a pressure ellipse, rad
$\xi, \eta$	dimensionless coordinates
$\sigma$	angular position of pilot surface load line, rad
$\nu$	lubricant viscosity, lb-sec/in. <sup>2</sup>
$\mu_o$	lubricant viscosity in inlet region of elastohydrodynamic contacts, lb-sec/in. <sup>2</sup>
$\rho$	mass density of lubricant, lb-sec <sup>2</sup> /in. <sup>4</sup>
$\tau$	shear stress, lb/in. <sup>2</sup>
$\tilde{\tau}$	dimensionless shear stresses
$\tau_i$	Hertz auxiliary parameter
$\tau_y$	shear stress in lubricant film in Y direction, lb/in. <sup>2</sup>
$\omega$	rolling element azimuth angle measured clockwise, deg

$\omega_i$	angular velocity of the $i^{\text{th}}$ ring relative to the retainer, rad/sec
$\omega_{s_j}$	spin velocity component at race contact, rad/sec
$\omega_x$	rolling element angular velocity about X axis, rad/sec
$\omega_y$	rolling element angular velocity about Y axis, rad/sec
$\omega_z$	rolling element angular velocity about Z axis, rad/sec
$\dot{\omega}_x$	angular acceleration of rolling element about X axis, rad/sec <sup>2</sup>
$\Omega_1$	angular velocity of ball about X axis = $\omega_x$ rad/sec
$\Omega_2$	angular velocity of ball about Z axis = $\omega_z$ rad/sec
$\Omega_E$	retainer (cage) speed, rpm
$\Omega_i$	absolute angular velocity of the bearing rings, rad/sec
$c$	elastic constants, in. <sup>2</sup> /lb

## INTRODUCTION

The analysis of rolling element bearing systems, which had earlier been prohibitive for manual calculation, has been facilitated by the advent of digital computers. Bearing systems present highly redundant, nonlinear mathematical models for which closed-form solutions are not available. Solutions must be obtained by numerical iterative techniques.

During the past ten years, many computer programs for bearing analysis have been created to meet the varying needs of industry. The best known is a five-degree-of-freedom program derived and written by A. B. Jones.<sup>2</sup> This program forms the basis of most of the computer work accomplished in the bearing analysis field, and is extensively used throughout the aerospace industry for the design and analysis of high-speed rolling element bearings.

The program uses Newton-Raphson iterative techniques to solve for equilibrium of the individual bearings and the entire bearing system simultaneously under the action of applied external loads while considering high-speed effects. Solutions are arrived at by systematically varying the shaft deflections until the integrated reaction forces of the rolling elements against the races balance the applied forces.

This analysis for ball bearings, however, does not consider the forces acting among the retainer, the rolling elements, and the piloting surfaces of the bearings, nor does it account for the tractive forces generated at the race contact areas. Bearing kinematics are established by constraining the balls' angular velocity vector to lie in a radial plane, i.e., no ball rotation about the axis dictated by the ball gyroscopic moment. Also, the analysis is subject to the race control hypothesis, which dictates that the ball will roll without spin at the race contact (inner or outer) that offers the greatest resistance to spinning. High-speed bearings with relatively large centrifugal ball loads against the outer race would, therefore, be predominantly outer race controlled. The significance of outer and inner race control is shown geometrically in Figure 1.

A race control assumption was imposed in the previous analysis because a ball in angular contact cannot exhibit pure rolling at both inner and outer race contacts simultaneously. Therefore, the ball must have a

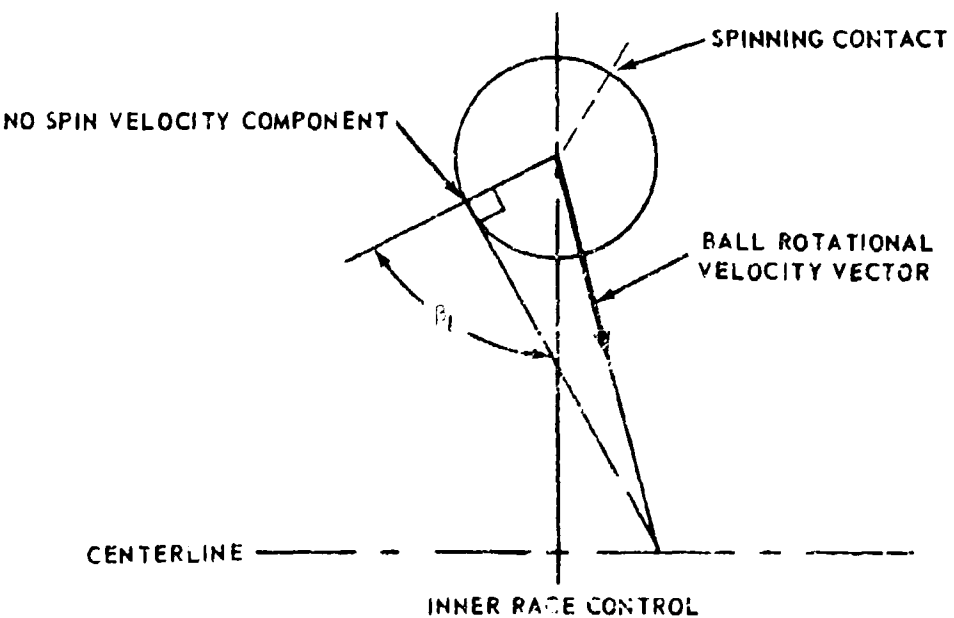
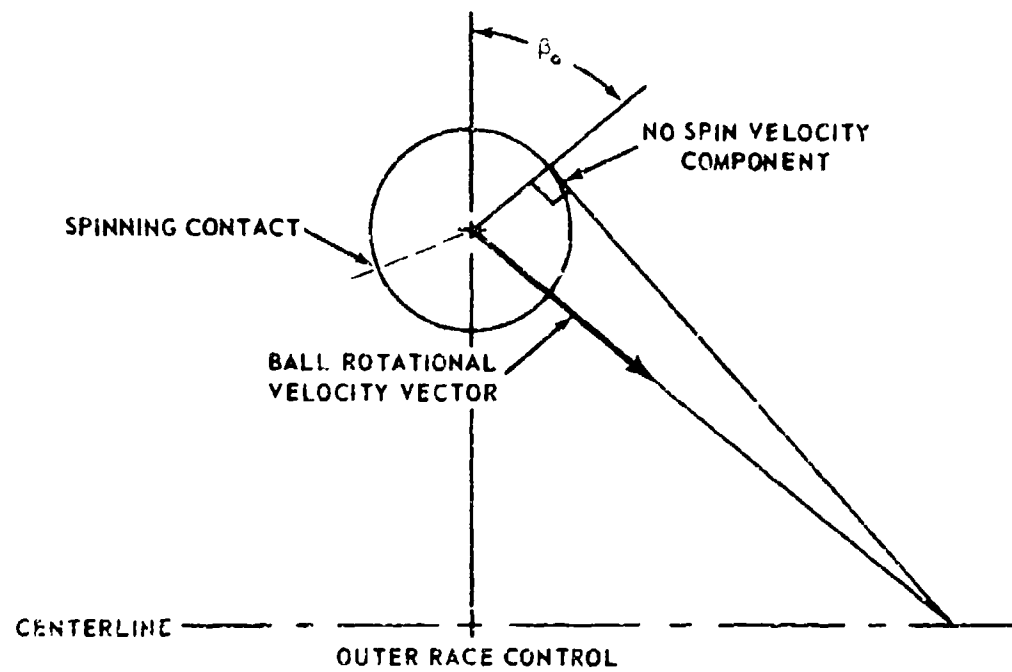


Figure 1. Race Control Concept.

spin velocity component at one or both race contacts which is equivalent to a twisting of the race body with respect to the ball about the normal to the center of the pressure area. Outer race control is considered to be advantageous for high-speed bearings because it results in minimum ball gyroscopic moments and maximum stability. It does have the disadvantage of placing the spin velocity component at the inner race with attendant heat generation, where oil cooling is most difficult.

Also implicit in the analysis is the concept that all friction resistance to the gyroscopic moment is generated at the controlling race and that tractive slip does not occur at any of the race contacts, which, of course, results in analytical solutions predicated upon zero retainer slip. The roller bearing analysis used is, in general, subject to the same limitations as those described for the ball bearing with the obvious exception of the race control and gyroscopic considerations, which are not applicable to rollers.

Recent work conducted by Harris,<sup>5</sup> Popiawski and Mauriello,<sup>9</sup> Boness,<sup>3</sup> and others has indicated that some of the assumptions discussed above and incorporated within the basic Jones analysis are only approximately valid. Specifically:

1. The ball angular velocity vector in an angular contact ball bearing does not lie exclusively in a radial plane. There is an angular velocity component in the circumferential direction.
2. The raceway control hypothesis is not applicable to all modes of bearing operation.
3. Tractive slip does occur at the rolling element-to-race contacts with attendant retainer slippage.
4. Resistance to the ball gyroscopic moment is not confined exclusively to the controlling race.

Some of these weaknesses have been resolved by various analysts in special computer models treating individual bearings. However, some fundamental problem areas have yet to be addressed, most notably the thermal effects due to contact area slip upon the tractions generated in an EHD (elastohydrodynamic) contact. This effect is of the utmost importance

in that the contact area traction is the key element in the establishment of the ball kinematics and thereby the entire solution.

The task undertaken as reported herein was to derive a new mathematical model for ball and roller bearings that is general and is not subject to the assumptions and restrictions described above. This undertaking required a reformulation of the existing Jones analytical model to include the following salient points:

1. EHD tractive forces and moments in the contact areas accounting for the thermal effects accompanying sliding
2. EHD film thickness accounting for spin as well as rolling velocities in the contact areas
3. Ball angular velocity in three degrees of freedom
4. Tensions and normal loads acting at the rolling element-to-retainer contacts
5. Viscous forces acting among the retainer inside diameter, outside diameter, and their respective bearing race surfaces
6. Rolling element viscous drag forces
7. Equilibrium of the retainer assembly to be established to predict retainer speed deviation from the theoretical epicyclic value.

Rig testing was conducted to verify and modify the theoretical analysis. The test program included the modification of a test rig and the design of special instrumentation to obtain the required verification data. Tests were run on a 100-millimeter ball bearing at speeds up to 20,000 rpm with axial and radial loads up to 1,000 pounds.

## MATHEMATICAL ANALYSIS

### BALL BEARING MATHEMATICAL MODEL

A complete presentation of the mathematical model developed for the ball bearing solution is presented in this section. The approach taken is an extension of the analysis related in Reference 2 to include retainer loads and lubrication considerations. The numerical procedure that has been employed is composed of essentially two major iterative loops, one within the other. Each loop has specific criteria which must be satisfied to obtain the desired solution. The innermost loop of the analysis deals with individual ball equilibrium which is achieved when Equations (26) through (30) are simultaneously satisfied. These equations represent force equilibrium in the X and Z directions, and moment equilibrium about the X, Y, and Z axes, respectively. The second loop of the analysis establishes equilibrium of the bearing rings with respect to externally applied loads. These criteria are achieved when Equations (34) through (37) are satisfied. These equations represent force equilibrium on the bearing races in the X, Y, and Z directions and moment equilibrium about the Y axis, respectively. A second function of this loop establishes retainer torque balance by iterating upon retainer speed accounting for ball-to-race tractive forces, ball-to-retainer loads, viscous drag between retainer and ring surfaces, and ball drag. In this manner, the retainer speed is established and its deviation from the theoretical epicyclic value can be determined. These considerations are expressed in Equations (46) through (49), which deal with force equilibrium in the X, Y, and Z directions and moment equilibrium about the X axis.

The balls in a high-speed ball bearing operating under other than a centric thrust load do not orbit at uniform speed if unrestrained by the cage. Consequently, they move fore and aft within the clearance of the pockets, and at times they may be in contact with the fore or aft wall of the retainer pocket.

When a ball is in contact with either the fore or aft wall of the pocket, its orbital speed is that of the cage and is generally different from its unconstrained orbital speed. Slippage between ball and race, always present to some degree, is greatly altered in form and intensity at this time. Also, frictional forces of the ball in the pocket are significantly increased.

At the instant a ball contacts a pocket wall, an impact force is produced. This force may be the maximum force exerted on the pocket when speeds are high and bearing loadings are light. As loading intensity is increased, the impact severity changes little, whereas the slippage-dependent forces increase greatly.

The mathematical model for this study neglects the impact forces and constrains the ball to orbit at the constant speed of the cage. Also, the fore and aft clearance in the pocket is zero to ensure the worst possible case of cage loading, neglecting impact forces; i.e., all balls are in contact with their pockets at all times. For purposes of assessing the properties of the film between ball and pocket, the true clearance is employed.

The ball referred to an XYZ coordinate system is shown in Figure 2. The X axis is parallel to the axis of the bearing and rotates about the latter with the angular cage (retainer) velocity  $\Omega_E$ .

In the following, the subscript 1 refers to the outer ring or outer-ring contact. The subscript 2 refers to the inner ring or inner-ring contact.

$$\left. \begin{array}{l} C_1 = 1 \\ C_2 = -1 \end{array} \right\} \quad (1)$$

$\omega_i$  is the angular velocity of the  $i^{\text{th}}$  ring relative to the cage and is related to the absolute angular velocity  $\Omega_i$  of the ring and the cage velocity  $\Omega_E$ .

$$\omega_i = \Omega_i - \Omega_E \quad (1)$$

$i = 1$  for outer ring

$i = 2$  for inner ring

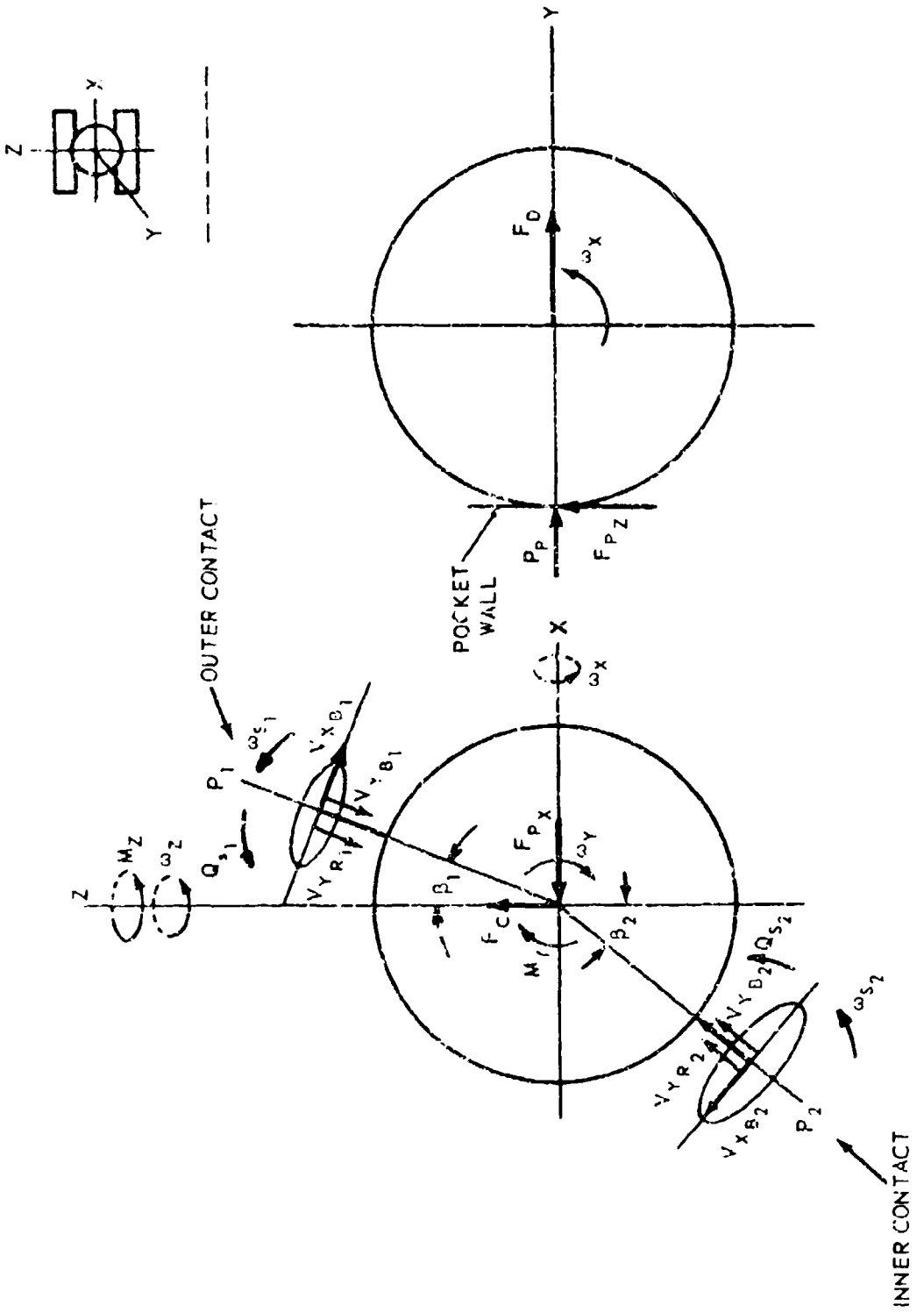


Figure 2. Ball Referred to  $XYZ$  Coordinate System.

$\omega_X$ ,  $\omega_Y$ , and  $\omega_Z$  are the angular velocities of the ball about X, Y, and Z.

$F_C$  is the centrifugal force, and  $M_Y$  and  $M_Z$  are the inertial moments about Y and Z.

$$M_Y = I \omega_Z \Omega_E \quad (3)$$

$$M_Z = -I \omega_Y \Omega_E \quad (4)$$

$$F_C = m \frac{E'}{2} \Omega_E^2 \quad (5)$$

I is the mass moment of inertia of the ball about its center, and m is the mass of the ball. E' is the instantaneous pitch diameter.

$P_i$  is the contact force, and  $a_i$  and  $b_i$  are the semimajor and semiminor axes of the pressure ellipse.

$V_{YR_i}$  is the linear velocity of a raceway in the Y direction at the center of a pressure area.

$$V_{YR_i} = \frac{(\Omega_i - \Omega_E) (E' + c_i d \cos \beta_i)}{2} \quad (6)$$

$V_{YB_i}$  is the linear velocity of the ball at the  $i^{th}$  contact in the Y direction.

$$V_{YB_i} = \frac{c_i d}{2} (\omega_X \cos \beta_i - \omega_Z \sin \beta_i) \quad (7)$$

$\beta_i$  is the operating contact angle at the  $i^{\text{th}}$  contact.

$V_{X_B_i}$  is the velocity of slip of race on ball in the X direction.

$$V_{X_B_i} = - \frac{d}{2} \omega_Y \quad (8)$$

$\omega_{S_i}$  is the angular velocity of spin of the  $i^{\text{th}}$  race with respect to the ball and is

$$\omega_{S_i} = C_i \left[ (\Omega_i - \Omega_E - \omega_X \sin \beta_i - \omega_Z \cos \beta_i) \right] \quad (9)$$

$F_{X_i}$  and  $F_{Y_i}$  are friction forces directed along the major and minor axes of the pressure ellipse.  $Q_{S_i}$  is a friction moment about the normal at the center of the ellipse. These items are the result of sliding between the race and ball, which are separated by an EHD film. Their values and the values of their derivatives are calculated in a subroutine, BALFTJ. \*

Input to subroutine BALFTJ<sup>11</sup> consists of:

- \*\*1. Pressure-viscosity coefficient of the lubricant - in.<sup>2</sup>/lb
- \*\*2. Temperature-viscosity coefficient of the lubricant - /°F
- 3. Viscosity of the lubricant at inlet temperature - lb-sec/in.<sup>2</sup>
- \*\*4. Thermal conductivity of the lubricant - Btu/°F-hr-ft
- 5. Inlet temperature - °F
- 6. Young's modulus for ball and for race - lb/in.<sup>2</sup>
- 7. Poisson's ratio for ball and race
- 8. Dimensions  $a_i$  and  $b_i$  of the pressure area - in.
- 9. Load on the contact  $P_i$  - lb
- 10. Linear velocity of the race  $V_{Y_R_i}$  - in./sec
- 11. Linear velocity of the ball  $V_{Y_B_i}$  - in./sec
- 12. Velocity of slip of race on ball in the direction of the major axes  
 $V_{X_B_i}$  - in./sec
- 13. Angular velocity of spin  $\omega_{S_i}$  - rad/sec

---

\* Discussed under "Elastohydrodynamic Traction Coefficients"

\*\*Values can be obtained from Appendix VII.

14. Ball diameter  $d$  - in.
15. Race groove radius  $f_i d$  - in.
16. Pitch diameter  $E^i$  - in.
17. Cosine of the contact angle  $\cos \beta_i$
18. Value of  $C_i$
19. Incrementing factor for  $V_{YBi}$
20. Incrementing factor for  $V_{XBi}$
21. Incrementing factor for  $\omega_{Si}$
22. Incrementing factor for  $P_i$

BALFTJ returns  $F_{X_i}$ ,  $F_{Y_i}$ , and  $Q_{Si}$  and their derivatives with respect to  $V_{X_i}$ 's,  $V_{Y_i}$ 's,  $\omega_{Si}$ 's, and  $P_i$ 's. It also returns minimum film thickness  $h_0$ .

$P_P$  is the normal force of retainer on ball.

$$P_P = F_{Y_1} + F_{Y_2} - F_D \quad (10)$$

$F_D$  is a viscous drag force.\*

$P_i$  is the contact force and is the result of the elastic approach  $\Delta_i$  of ball and race body.

Figure 3 shows the initial and final positions of the inner and outer race curvature centers.  $\beta$  is the initial contact angle and  $f_i$  the race curvature factor.

From Figure 3,

$$\Delta_1 = \left[ X_1^2 + X_2^2 \right]^{1/2} - (f_i - .5) d \quad (11)$$

$$\Delta_2 = \left[ (A_1 - X_1)^2 + (A_2 - X_2)^2 \right]^{1/2} - (f_2 - .5) d \quad (12)$$

$A_1$  and  $A_2$  are defined analytically in Equations (31) and (32).

---

\*Calculated as described under "Analysis of Shear Forces on a Lubricated, High-Speed Bearing Retainer."

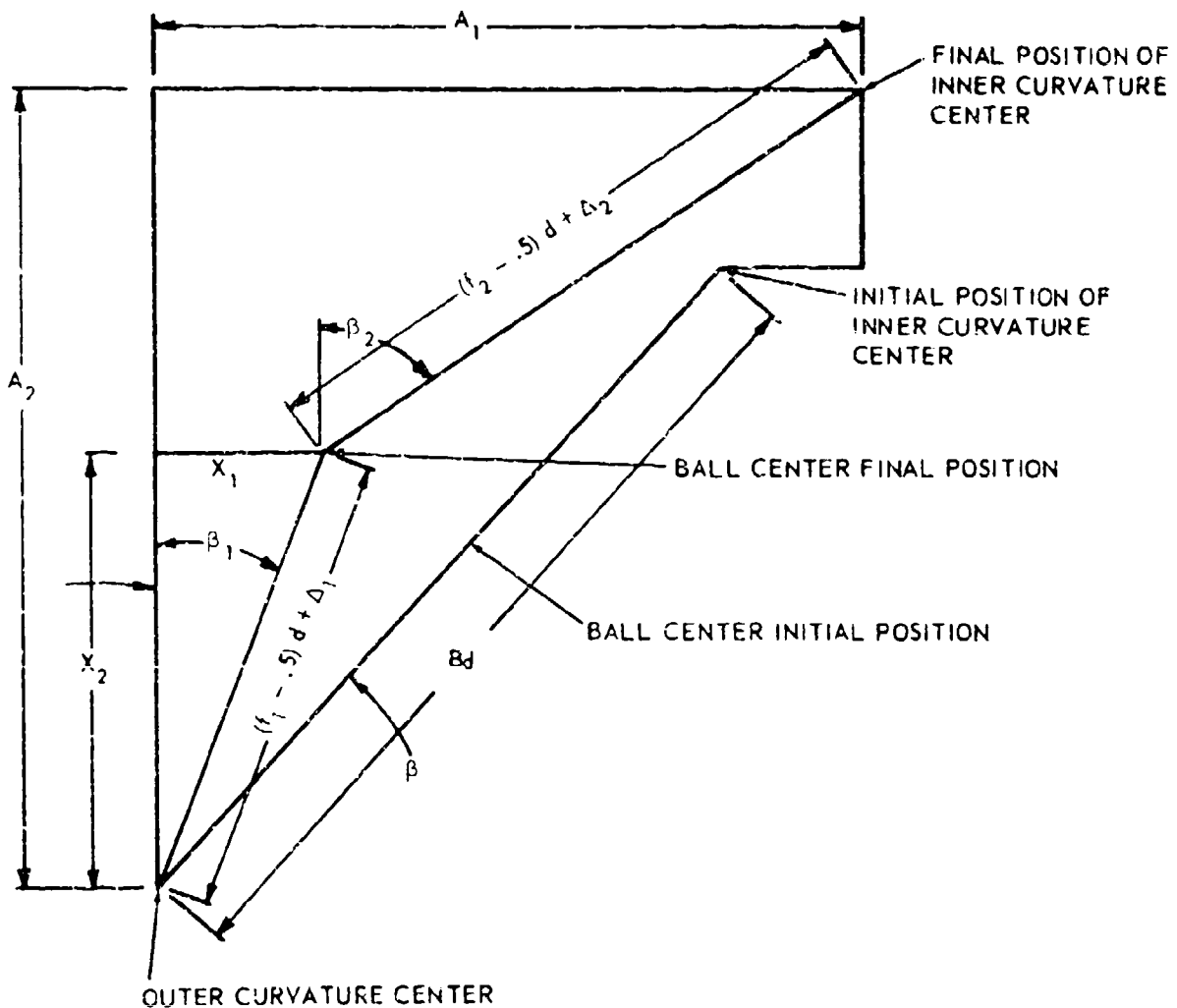


Figure 3. Initial and Final Positions of Inner and Outer Race Curvature Centers.

$$\tan \beta_1 = \frac{x_1}{x_2} \quad (13)$$

$$\tan \beta_2 = \frac{A_1 - x_1}{A_2 - x_2} \quad (14)$$

$$E' = E + 2 \left[ x_2 - (f_1 - .5) d \cos \beta \right] \quad (15)$$

The dimensions of the pressure area are found as follows:

$\epsilon_i$  is the modular angle of the ellipse.

$$\epsilon_i = \sin^{-1} \left[ 1 - \left( \frac{b_i}{a_i} \right)^2 \right]^{1/2} \quad (16)$$

It is related to the geometries of the bodies in the neighborhood of the contact by an auxiliary parameter  $\tau_i$ .

$$\cos \tau_i = \frac{\frac{1}{f_i} - \frac{2C_i y_i}{1 + C_i y_i}}{4 - \frac{1}{f_i} - \frac{2C_i y_i}{1 + C_i y_i}} \quad (17)$$

where

$$y_i = \frac{d \cos \beta_i}{E'} \quad (18)$$

$\epsilon_i$  and  $\tau_i$  are related by

$$\cot^2 \epsilon = \frac{(1 - \cos \tau_i) E(\epsilon_i)}{2[K(\epsilon_i) - E(\epsilon_i)]} \quad (19)$$

$K(\epsilon_i)$  and  $E(\epsilon_i)$  are the complete elliptic integrals of the first and second kind having the modular angle  $\epsilon_i$ .

The semiminor axis of the pressure area is

$$b_i = \left[ \frac{3(\vartheta_R + \vartheta_E) E(\epsilon_i) P_i d \cos \epsilon_i}{4\pi \left( 4 - \frac{1}{f_i} - \frac{2C_i \tau_i}{i + C_i \tau_i} \right)} \right]^{1/3} \quad (20)$$

and the semimajor axis is

$$a_i = \frac{b_i}{\cos \epsilon_i} \quad (21)$$

$\vartheta_R$  and  $\vartheta_E$  are elastic constants for race and ball, respectively.

$$\vartheta_R = \frac{4(1 - m_R^2)}{E_R} \quad (22)$$

$$\vartheta_E = \frac{4(1 - m_E^2)}{E_E} \quad (23)$$

The symbols  $m_R$  and  $m_E$  are Poisson's ratio for race and ball.  $E_R$  and  $E_E$  are Young's modulus for race and ball.

The relation between contact force and elastic deflection is nonlinear.

$$\Delta_i = \frac{3P_i(\vartheta_R + \vartheta_E) K(\epsilon_i)}{8\pi a_i} \quad (24)$$

The maximum normal pressure occurs at the center of the pressure area and is

$$\delta_{o_i} = \frac{3P_i}{2\pi a_i b_i} \quad (25)$$

The equilibrium of the ball requires that

$$-P_1 \sin \beta_1 + P_2 \sin \beta_2 + F_{X_1} \cos \beta_1 - F_{X_2} \cos \beta_2 - F_{p_X} = 0 \quad (26)$$

$$-P_1 \cos \beta_1 + P_2 \cos \beta_2 - F_{X_1} \sin \beta_1 + F_{X_2} \sin \beta_2 + F_C + F_{p_Z} = 0 \quad (27)$$

$$(F_{Y_1} \cos \beta_1 - F_{Y_2} \cos \beta_2 - F_{p_Z}) \frac{d}{2} + Q_{S_1} \sin \beta_1 - Q_{S_2} \sin \beta_2 = 0 \quad (28)$$

$$(F_{X_1} + F_{X_2}) \frac{d}{2} + M_Y - Q_P = 0 \quad (29)$$

$$(-F_{Y_1} \sin \beta_1 + F_{Y_2} \sin \beta_2 - F_{p_X}) \frac{d}{2} + Q_{S_1} \cos \beta_1 - Q_{S_2} \cos \beta_2 + M_Z = 0 \quad (30)$$

$F_{p_X}$  and  $F_{p_Z}$  are pocket frictional forces.\*

The variables in the above set of equations are  $X_1$  and  $X_2$ , and the angular velocities  $\omega_X$ ,  $\omega_Y$ , and  $\omega_Z$ . The equations are solved numerically.

Figure 4 shows the bearing referred to an XYZ coordinate system. The outer ring is fixed while the inner ring can move. The inner ring can have three linear displacements,  $\delta_X$ ,  $\delta_Y$ , and  $\delta_Z$ , relative to the outer ring and is constrained from rotations about Y and Z.

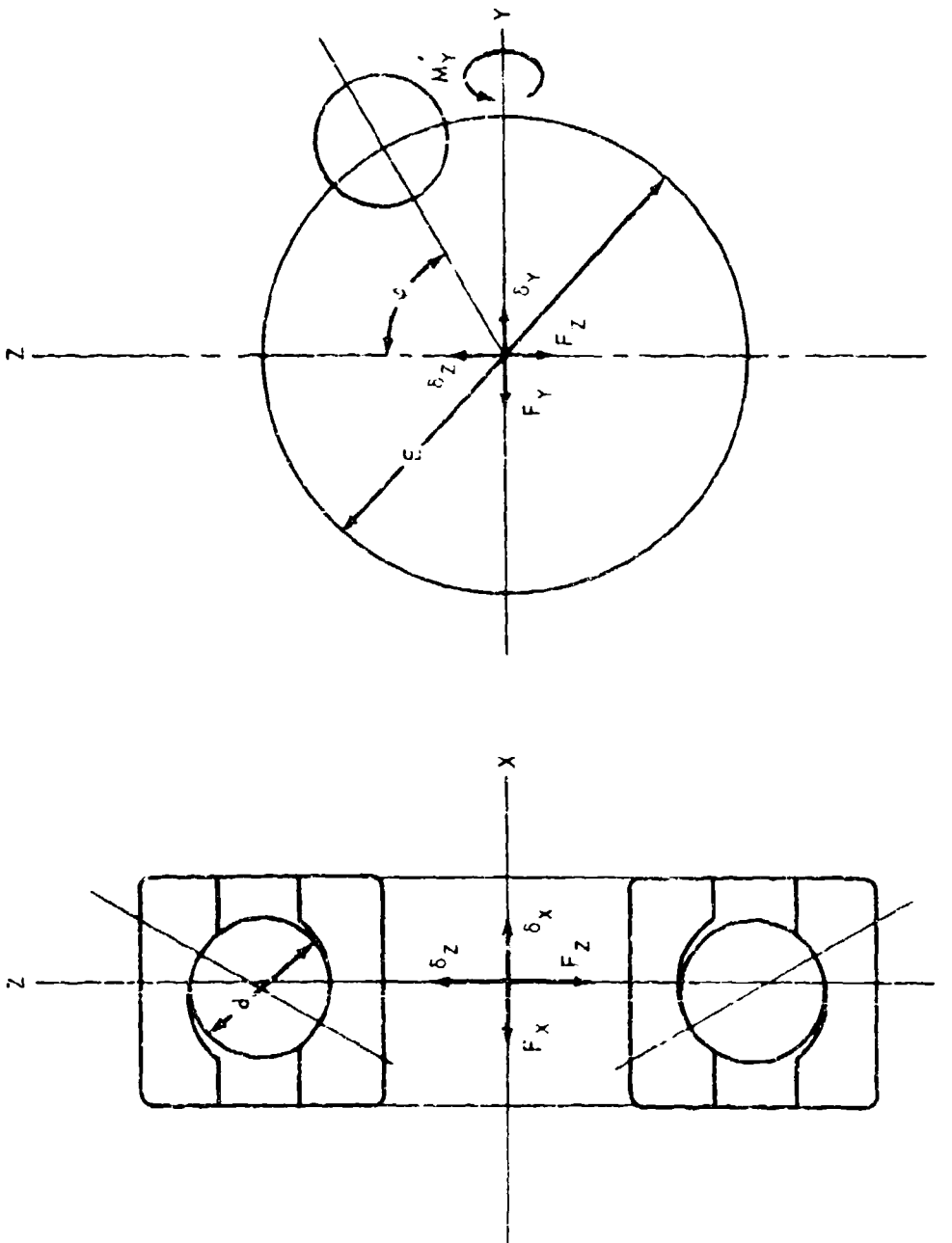
The YZ plane in Figure 4 contains the locus of the inner race curvature centers.

For arbitrary values of the three displacements, there will be the reactions  $F_X$ ,  $F_Z$ , and  $M_Y$ , which act in the directions shown in Figure 4.

---

\*Calculated as described under "Analysis of Shear Forces on a Lubricated, High-Speed Bearing Retainer."

Figure 4 . Yearing Referred to XYZ Coordinate System.



The values of  $A_1$  and  $A_2$  in Equation (14) depend on the displacements at the inner ring center.

$$A_1 = Bd \sin \beta + \delta_x \quad (31)$$

$$A_2 = Bd \cos \beta + \delta_Y \sin \varphi + \delta_Z \cos \varphi \quad (32)$$

$$B = f_1 + f_2 - 1 \quad (33)$$

$\varphi$  is the ball azimuth measured clockwise from the YZ plane as viewed from +X.

The bearing reactions are:

$$F_x = \sum_{j=1}^n \left[ P_{2j} \sin \beta_{2j} - F_{x_{2j}} \cos \beta_{2j} \right] \quad (34)$$

$$F_y = \sum_{j=1}^n \left[ \left( P_{2j} \cos \beta_{2j} + F_{x_{2j}} \sin \beta_{2j} \right) \sin \varphi_j - F_{y_{2j}} \cos \varphi_j \right] + A_y \quad (35)$$

$$F_z = \sum_{j=1}^n \left[ \left( P_{2j} \cos \beta_{2j} + F_{x_{2j}} \sin \beta_{2j} \right) \cos \varphi_j + F_{y_{2j}} \sin \varphi_j \right] + A_z \quad (36)$$

$$M_y = \sum_{j=1}^n \left\{ \left[ P_{2j} R \sin \beta_{2j} - F_{x_{2j}} (R \cos \beta_{2j} - f_{2j} d) \right] \cos \varphi_j + F_{y_{2j}} f_{2j} d \sin \beta_{2j} \sin \varphi_j \right\} \quad (37)$$

where n is the number of balls.

$A_y$  and  $A_z$  are zero for an outer-piloted cage and are nonzero for inner-piloted cage; they are calculated as follows:

$$R = \frac{E}{2} + (f_2 - .5)d \cos \beta \quad (38)$$

$M_Y$  does not enter into the calculations but is an item of interest.

Figure 5 shows the forces and moments acting on an outer-piloted cage.  $QV_1$  and  $QV_2$  are viscous shear moments.\*  $P_C$  is the reaction of the piloting ring against the cage.  $F_F$  is a Coulomb friction force between cage and guiding surface and acts at the angle  $\theta$ .

$$P_C = [H^2 + V^2]^{1/2} \quad (39)$$

$$H = \sum_{j=1}^n [-P_{P_j} \cos \varphi_j - F_{P_{Z_j}} \sin \varphi_j] \quad (40)$$

$$V = \sum_{j=1}^n [-P_{P_j} \sin \varphi_j - F_{P_{Z_j}} \cos \varphi_j] \quad (41)$$

$$F_F = \mu P_C \quad (42)$$

$$\tan \theta = \frac{H}{V} \quad (43)$$

Figure 6 similarly illustrates an inner-piloted cage. Equations (37) through (41) apply here also.

With an inner-piloted cage,  $P_C$  and  $F_F$  are reactive on the inner ring, and  $A_Y$  and  $A_Z$  for use with Equations (35) and (36) are

$$A_Y = -P_C (\sin \theta - \mu \cos \theta) \quad (44)$$

$$A_Z = -P_C (\cos \theta + \mu \sin \theta) \quad (45)$$

---

\* Calculated as described under "Analysis of Shear Forces on a Lubricated, High-Speed Bearing Retainer."

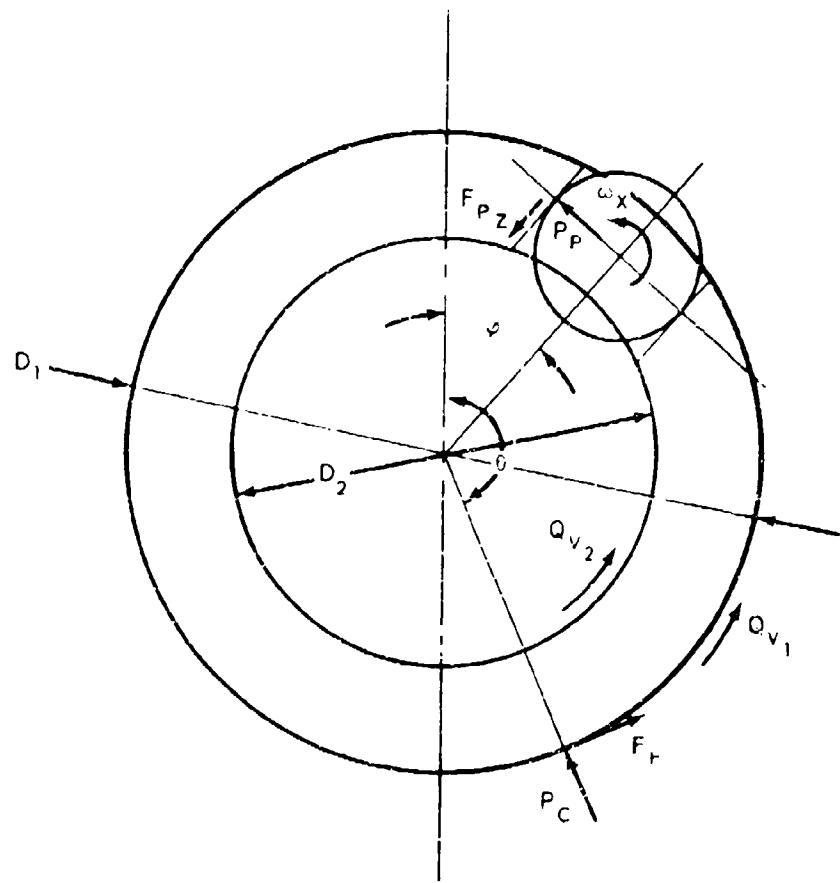


Figure 5. Forces and Moments Acting on Outer-Piloted Cage.

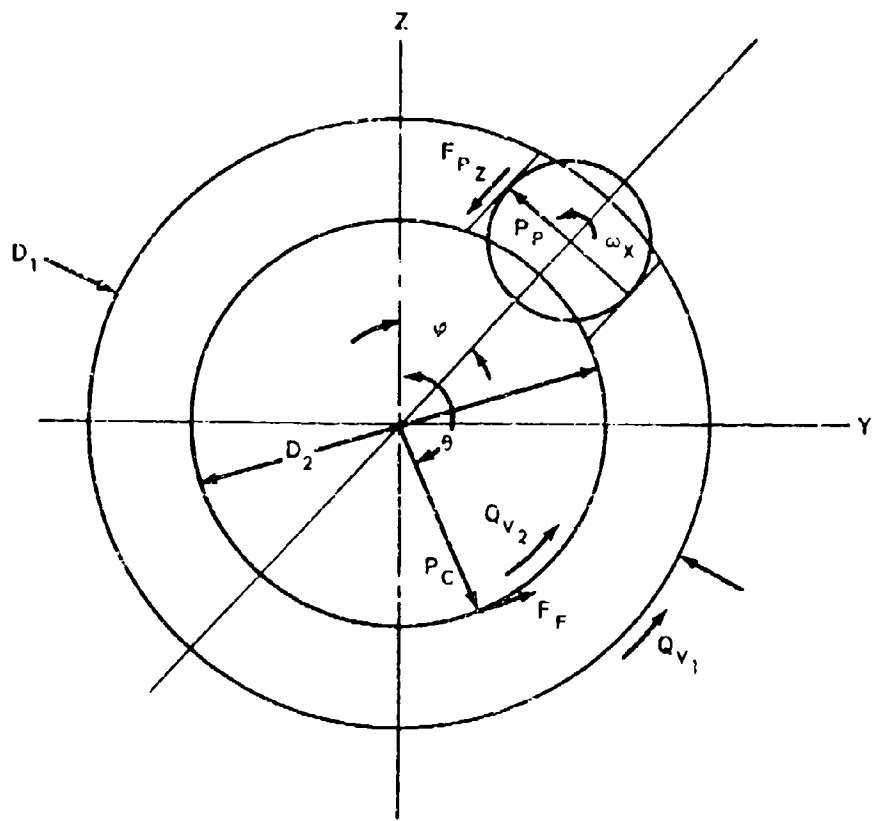


Figure 6. Forces and Moments Acting on Inner-Piloted Cage.

The requirements for equilibrium of the bearing and cage system may now be written:

$$F_x + \bar{F}_x = 0 \quad (46)$$

$$F_y = 0 \quad (47)$$

$$\bar{F}_z + \bar{F}_z = 0 \quad (48)$$

$$Q_{v_1} + Q_{v_2} + \frac{F_F D'}{2} + \frac{1}{2} \sum_{j=1}^n \left[ P_{P_j} E' + F_{P_z_j} d \right] = 0 \quad (49)$$

$D'$  is  $D_1$  for an outer-piloted cage and  $D_2$  for an inner-piloted cage.  $\bar{F}_X$  and  $\bar{F}_Z$  are external thrust and radial loads.

Equations (46) through (49) are nonlinear in the variables  $\delta_X$ ,  $\delta_Y$ ,  $\delta_Z$ , and  $\Omega_E$ . They are solved numerically by iterative procedures.

## ROLLER BEARING MATHEMATICAL MODEL

The determination of the forces on the cage of a high-speed roller bearing requires the evaluation of the internal load distribution, the friction forces in the EHD films at the race contacts, and the friction and normal forces in the roller to cage pocket contacts.

The calculation of individual roller loads is made without consideration of friction forces in the race contact film or in the pocket contact film. This procedure is valid since the tangential friction force of the roller against the pocket is small compared to the load at an outer-race contact.

For an assumed value of roller orbital speed (cage speed) the internal load distribution is obtained as follows. A first assumption of orbital speed is made close to the theoretical value for no slip.

$$\Omega_E = \frac{1}{2} \left[ \Omega_1 \left( 1 + \frac{d}{E} \right) + \Omega_2 \left( 1 - \frac{d}{E} \right) \right] \quad (1-S) \quad (50)$$

where  $\Omega_E$  = cage speed

$\Omega_1$  = outer ring speed

$\Omega_2$  = inner ring speed

$d$  = roller diameter

$E$  = pitch diameter

$S$  = a slip factor

A suggested value of  $S$  for the first pass is 0.001.

Figure 7 illustrates a typical radial roller bearing and shows the detail of the roller's profile.

Let  $\Delta_o$  be the approach of the roller to the race body measured at the midpoint of the roller's length. The approach is the same at all points of the cylindrical surface. The approach at a point on the crowned portion is less. At any location  $x$  along the roller's length, measured from the midpoint, the approach is

$$\Delta_x = \Delta_o \quad -f_F \leq x \leq f_F \quad (51)$$

$$\Delta_x = \Delta_o - \sqrt{R_c^2 - \frac{f_F^2}{4}} + \sqrt{R_c^2 - x^2} \quad \frac{f_F}{2} < |x| < \frac{f_F}{2} \quad (52)$$

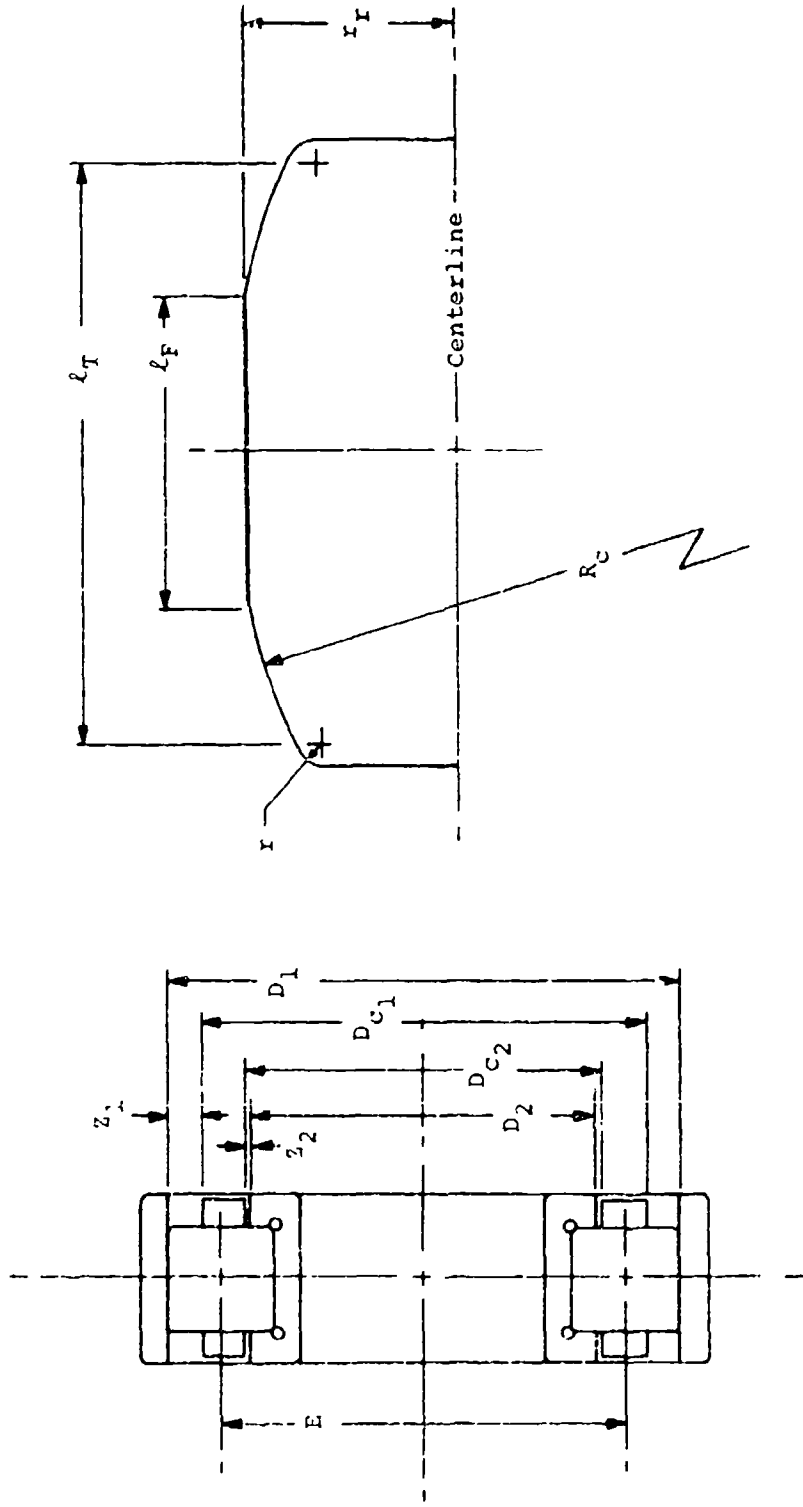


Figure 7. Bearing Details.

Lundberg, Reference 7, gives the relation between load and approach for a cylindrical roller of length  $\ell$  as

$$\Delta = \frac{(\vartheta_R + \vartheta_E) P}{2 \pi \ell} \left[ 1.8864 + \ln \left( \frac{\ell}{2b} \right) \right] \quad (53)$$

where  $\begin{cases} \vartheta_R \\ \vartheta_E \end{cases}$  = elastic constants for race and roller, respectively, and are of the form

$$\vartheta = \frac{4(1-m^2)}{E} \quad (54)$$

- $m$  = Poisson's ratio
- $E$  = modulus of elasticity
- $P$  = total force on the contact
- $b$  = semiwidth of the contact area
- $\ell$  = length of roller

Setting  $p_x$  as the lb/in. loading at point  $x$ , one may write

$$\Delta_x = \frac{(\vartheta_R + \vartheta_E)}{2 \pi} p_x \left[ 1.8864 + \ln \left( \frac{\ell'}{2b_x} \right) \right] \quad (55)$$

$b_x$  is given by

$$b_x = \left[ \frac{(\vartheta_R + \vartheta_E) p_x d (1 \pm \frac{d}{E})}{2 \pi} \right]^{1/2} \quad (56)$$

The upper sign is used for an outer-race contact and the lower for an inner-race contact.

$\ell'$  is the distance from the roller midpoint to the end of the contact area.

$$\ell' = \sqrt{R_c^2 - \left[ \sqrt{R_c^2 - \left( \frac{\ell_F}{2} \right)^2} - \Delta_o \right]^2} \quad (57)$$

If  $\ell'$  from Equation (57) is greater than  $\frac{\ell_T}{2}$ ,  $\ell'$  is set equal to  $\frac{\ell_T}{2}$ .

The contact force resulting from an approach  $\Delta_o$  is

$$P = 2 \int_0^{\ell} p_x dx \quad (58)$$

Equation (58) is evaluated numerically by Simpson's rule. In the process of evaluating the integral it is necessary to assume discrete values of  $x$  and to calculate the value of  $p_x$ . From Equations (55) and (56) with  $\Delta_x$  known,

$$\frac{d\Delta_x}{dp_x} = \frac{(\vartheta_R + \vartheta_E)}{2\Pi} \left[ 1.3864 + \ln \left( \frac{\ell}{2b_x} \right) \right] \quad (59)$$

An assumption of  $p_x$  is made and the corresponding  $\Delta_x$  calculated from Equation (55). An improved value of  $p_x$  is

$$p_x' = p_x - \frac{(\Delta_x' - \Delta_x)}{\left( \frac{d\Delta_x}{dp_x} \right)} \quad (60)$$

The process can be repeated until  $p_x'$  is to the desired accuracy.

Figure 8 shows a roller in contact with both races and acted upon by centrifugal force  $F_c$  and contact loads  $P_1$  and  $P_2$ .

Assuming that the shear forces due to the pocket contact are small with respect to  $P_1$ ,

$$- P_{1q} + P_{2q} + F_c = 0 \quad (61)$$

$$F_c = m_R \frac{E}{2} \Omega_E^2 \quad (62)$$

where  $m_R$  = mass of roller

$\Omega_E$  = orbital velocity of roller

$$\Delta_{o1} + \Delta_{o2} = \Delta_q \quad (63)$$

Figure 8. Roller Contact Forces and Roller Orientation Schematic.

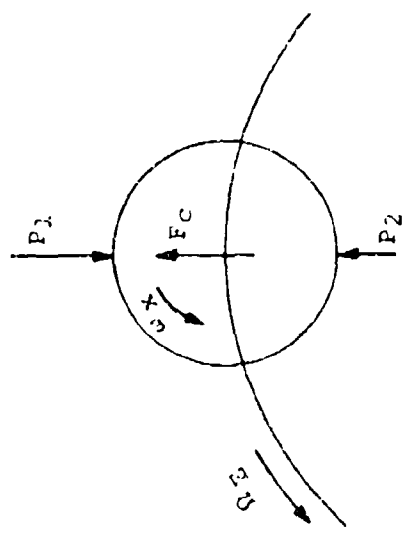
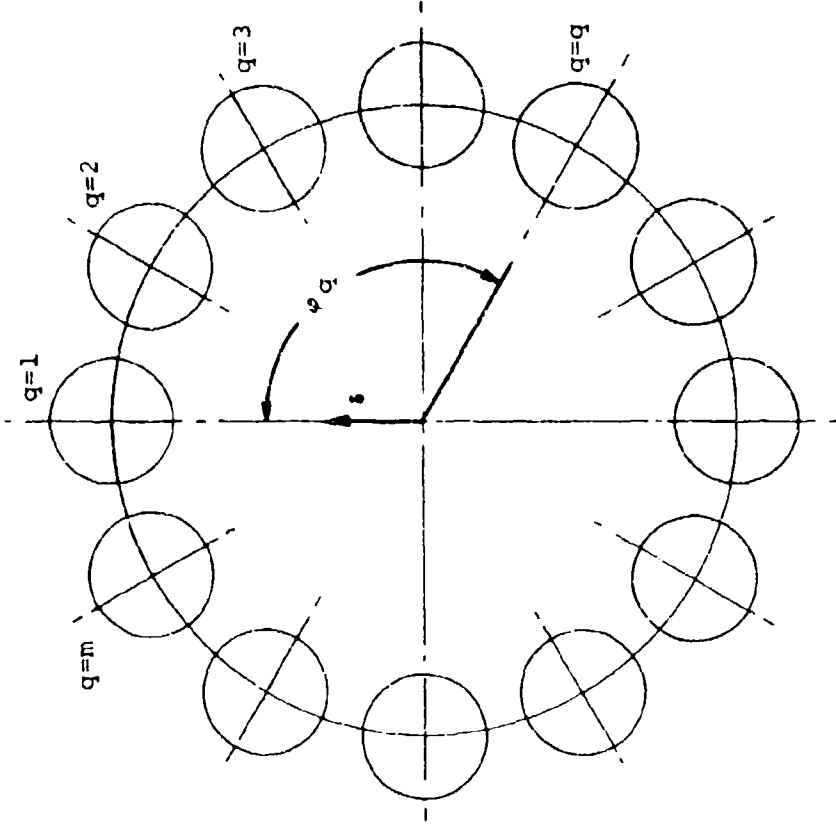


Figure 8 also shows the numbering scheme for the rollers in relation to the displacement  $\delta$  of the inner race with respect to the outer. The azimuth of the  $q^{\text{th}}$  roller is

$$\varphi_q = \frac{2\pi(q-1)}{n} \quad (64)$$

The total approach of inner race to outer at the  $q^{\text{th}}$  roller is

$$\Delta_q = \delta \cos \varphi_q - \frac{P_D}{2} \quad (65)$$

where  $P_D$  = operating diametral clearance of bearing

$\Delta_{o_1}$  = elastic approach of roller and race at outer contact

$\Delta_{o_2}$  = elastic approach of roller and race at inner contact

For an assumed value of bearing displacement  $\delta$ ,  $\Delta_q$  can be calculated. An estimate of  $\Delta_{o_1}$  is made and  $\Delta_{o_2}$  is given by Equation (63).  $P_{1q}$

and  $P_{2q}$  can be evaluated and substituted in Equation (61). In general,

Equation (61) will not be satisfied and the residue  $\psi$  exists.

$$\psi = -P_{1q} + P_{2q} + F_c \quad (66)$$

An improved value of  $\Delta_{o_1}$  is

$$\Delta'_{o_1} = \Delta_{o_1} - \left( \frac{\psi}{\frac{d\psi}{d\Delta_{o_1}}} \right) \quad (67)$$

$$\frac{d\psi}{d\Delta_{o_1}} = -\frac{dP_{1q}}{d\Delta_{o_1}} - \frac{dP_{2q}}{d\Delta_{o_2}} \quad (68)$$

The derivative of  $P$  with respect to the corresponding  $\Delta_0$  is of the form

$$\frac{\partial P}{\partial \Delta_0} = 2 \left( \frac{d_x}{\left( \frac{d \Delta_x}{d p_x} \right)} \right) \quad (69)$$

Repetition of the process leading to Equation (67) enables  $\Delta_{o_1}$  to be determined to any desired accuracy.

The reaction of the bearing to the displacement  $\delta$  is

$$F = \sum_{q=1}^n P_{2q} \cos \varphi_q \quad (70)$$

Equilibrium requires that

$$F - \bar{F} = 0 \quad (71)$$

where  $\bar{F}$  = external radial load

For an assumption of  $\delta$ , Equation (71) may not be satisfied. An improved value of  $\delta$  is

$$\dot{\delta} = \varepsilon - \frac{(F - \bar{F})}{\left( \frac{dF}{d\delta} \right)} \quad (72)$$

$$\frac{dF}{d\delta} = \sum_{q=1}^n - \frac{dP_{2q}}{d\Delta_{o2q}} \frac{d\Delta_{o2q}}{d\Delta_q} \cos^2 \varphi_q \quad (73)$$

Differentiating Equations (61) and (63) with respect to  $\delta_q$ ,

$$-\frac{dP_1}{d\Delta_{o1q}} \cdot \frac{d\Delta_{o1q}}{d\Delta_q} + \frac{dP_2}{d\Delta_{o2q}} \cdot \frac{d\Delta_{o2q}}{d\Delta_q} = 0 \quad (74)$$

$$\frac{d\Delta_{o1q}}{d\Delta_q} + \frac{d\Delta_{o2q}}{d\Delta_q} = 1 \quad (75)$$

From these is obtained

$$\frac{\frac{d\Delta_{o2q}}{d\Delta_q}}{\frac{d\Delta_{o1q}}{d\Delta_q}} = \frac{-\frac{dP_1}{d\Delta_{o2q}}}{-\frac{dP_1}{d\Delta_{o1q}} - \frac{dP_2}{d\Delta_{o2q}}} \quad (76)$$

Figure 9 shows the forces acting on the roller which arise from the lubricant effects. These are assumed small in comparison with  $P_j$ .

$\omega_1$  and  $\omega_2$  are the velocities of the outer and inner races with respect to the cage:

$$\omega_i = \Omega_i - \Omega_E \quad i = 1, 2 \quad (77)$$

where  $\Omega_i$  = angular velocity of a ring relative to ground

$\Omega_E$  = angular velocity of the cage relative to ground

The linear velocity of a race relative to the cage is

$$U_{y_i} = \frac{(E + C_i d)}{2} \omega_i \quad i = 1, 2 \quad (78)$$

where  $C_1 = +1$  for an outer contact

$C_2 = -1$  for an inner contact

The evaluation of the integral in Equation (58) by Simpson's rule requires the establishment of an odd number of stations over the contact length. The stress conditions and the sliding velocities of race on roll at these stations will be utilized in calculating the friction forces in the EHD film.

The maximum Hertz pressure at any location  $x$  within the pressure area is

$$S_{m_x} = \frac{2 p_x}{\pi b} \quad (79)$$

For stations within the cylindrical portion of the roll, the radius of the roll is

$$r_r = \frac{d}{2} \quad (80)$$

For stations within the crowned portion of the roll,

$$r_{rx} = \frac{d}{2} - \sqrt{r^2 - \left(\frac{f_F}{2}\right)^2} + \sqrt{R^2 - x^2} \quad (81)$$

The linear velocity of the roll at any station is

$$U_{R_{x_i}} = C_i r_{x_i} \omega_x \quad i = 1, 2 \quad (82)$$

where  $\omega_x$  is the angular velocity of roller about its center

The slip velocity of race on roll is

$$U_{S_{x_i}} = U_{y_i} - U_{R_{x_i}} \quad i = 1, 2 \quad (83)$$

The minimum film thickness at any station is\*

$$h_{x_i} = \frac{1.6 R_{x_i}^{.43} a^{.6} (\mu_0 |\bar{U}_{x_i}|)^7}{P_{x_i}^{.13} (E'')^{.03}} \quad i = 1, 2 \quad (84)$$

where  $R_{x_i}$  = the radius of a roll having the same conformity with regard to a flat plate that the actual contact has

$$\dot{R}_{x_i} = \frac{1}{\frac{2C_i}{(E + C_i d)} + \frac{1}{r_{x_i}}} \quad i = 1, 2 \quad (85)$$

$a$  = the pressure-viscosity coefficient of the lubricant

$\mu_0$  = the lubricant viscosity at inlet temperature

$\bar{U}_{x_i}$  = the average rolling velocity at the station

$$\bar{U}_{x_i} = \frac{1}{2} (U_{y_i} + U_{R_{x_i}}) \quad (86)$$

$$E'' = \frac{8}{\vartheta_R + \vartheta_E} \quad (87)$$

The friction or tractive force generated in the EHD film depends on the coefficient of friction at the various stations along the contact length.

---

\*Calculated as discussed under "Elastohydrodynamic Traction Coefficients"

A computer program provided by the Air Force Aero Propulsion Laboratory and Mechanical Technology, Inc. calculates the friction coefficient as a function of three parameters:  $G_1$ ,  $G_2$  and  $G_3$ .

$$G_{1x_i} = \frac{G_A |U_{S_{x_i}}|}{S_{m_{x_i}} h_{x_i}} \quad (88)$$

$$G_{2x_i} = G_B U_{S_{x_i}}^2 \quad (89)$$

$$G_{3x_i} = \alpha_3 S_{m_{x_i}} \quad (90)$$

where

$$G_A = \mu_3 \left( \frac{\alpha}{\alpha_3} \right)^{.6} \left( \frac{\mu_0}{\mu_3} \right)^{.7} \quad (91)$$

$$G_B = \frac{\mu_3 \beta}{1.728 K_F} \quad (92)$$

$$\alpha_3 = \frac{0 + 930 \alpha (T_1 - 86)}{546 (T_1 + 460)} \quad (93)$$

$$\mu_3 = \mu_0 e^{\beta} (T_1 - 86) \quad (94)$$

The tractive force is obtained by numerical integration of the following:

$$F_{T_1} = 2 \int_0^L f_{x_i} p_{x_i} dx \quad (95)$$

The derivative of  $F_{T_i}$  with respect to  $\omega_x$  will be required. These are obtained by calculating  $F_{T_i}$  values for  $\omega_x + \Delta\omega_x$  and  $\omega_x - \Delta\omega_x$  and substituting them in:

$$\frac{dF_{T_i}}{d\omega_x} = \frac{(F_{T_i})_{\omega_x + \Delta\omega_x} - (F_{T_i})_{\omega_x - \Delta\omega_x}}{2(\Delta\omega_x)} \quad (96)$$

Turning now to the pocket contacts, the following expressions for  $F_p$  and  $F_v$  are obtained\* (Figure 9 also shows a roller in a pocket and those forces acting on the roller from the cage):

$$F_{p_x} = \frac{2.447 \mu_o |\omega_x| \left(\frac{d_x}{2}\right)^2}{h_{p_x}} \quad (97)$$

$$F_{v_x} = \frac{.5482 \mu_o \omega_x \left(\frac{d_x}{2}\right)^{3/2}}{h_{p_x}^{1/2}} \quad (98)$$

Along the cylindrical portion, the film thickness is  $h_{p_x}$ . When  $x > \frac{l_F}{2}$  the film thickness is

$$h_{p_x} = h_{p_0} + \sqrt{R_c^2 - \left(\frac{l_F}{2}\right)^2} - \sqrt{R_c^2 - x^2} \quad (99)$$

The pocket forces are obtained by numerical integration of

$$F_p = 2 \int_0^{l_F} F_{p_x} dx \quad (100)$$

---

\*Calculated as described under "Analysis of Shear Forces on a Lubricated, High-Speed Bearing Retainer."

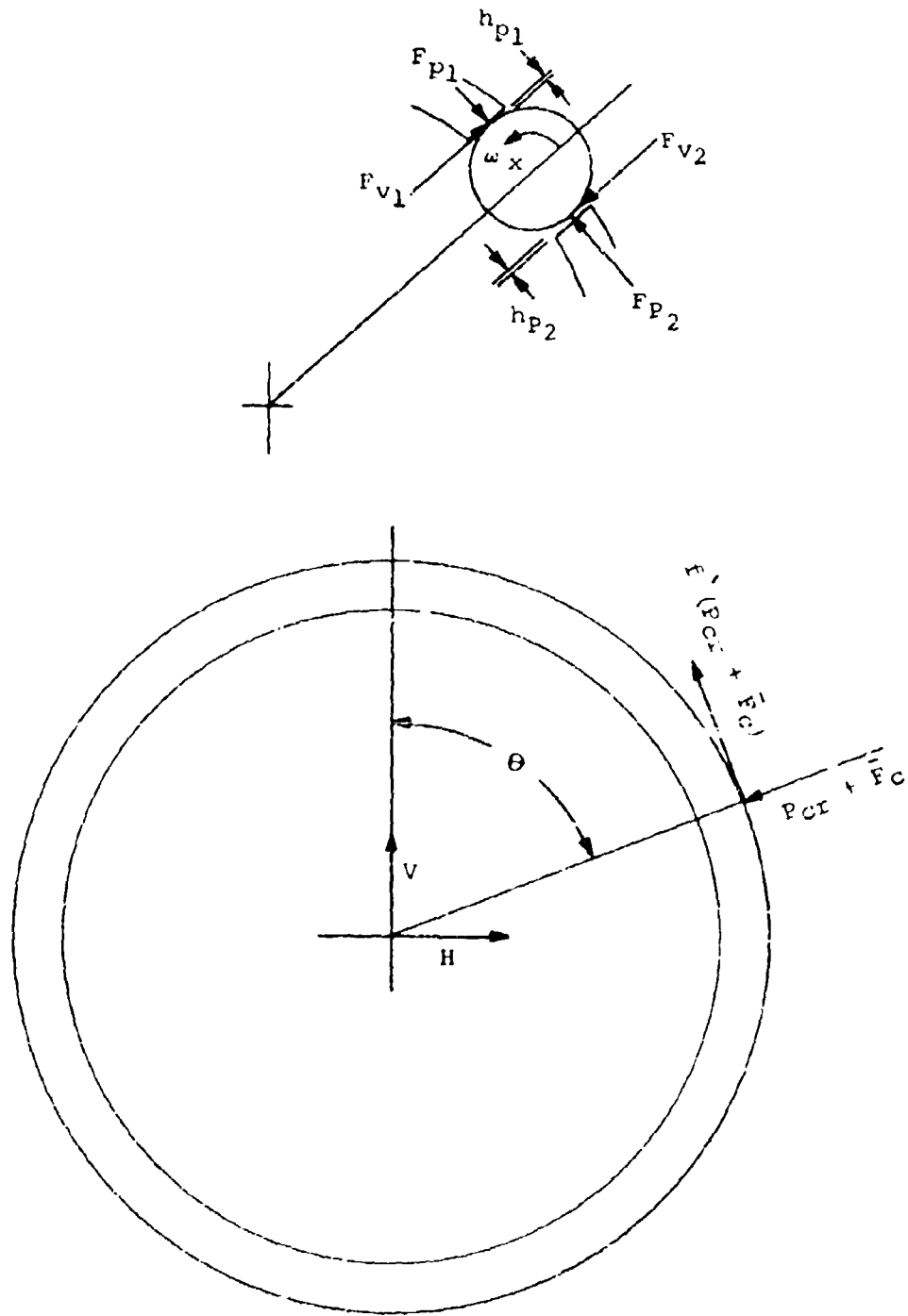


Figure 9. Roller Pocket Forces and Cage Whirl Forces.

and

$$F_v = 2 \int_0^T F_{v_x} dx \quad (101)$$

The derivatives of  $F_p$  and  $F_v$  with respect to  $\omega_x$  and  $h_o$  are required.

$$\frac{dF_p}{d\omega_x} = \frac{F_p}{|\omega_x|} \quad (102)$$

$$\frac{dF_v}{d\omega_x} = \frac{F_v}{\omega_x} \quad (103)$$

Differentiating Equations (97) and (98) gives

$$\frac{dF'_{p_x}}{dh_{p_x}} = \frac{-2.447 \mu |\omega_x| \left(\frac{d_x}{2}\right)^2}{h_{p_x}^2} \quad (104)$$

$$\frac{dF'_{v_x}}{dh_{p_x}} = \frac{- .2741 \mu \omega_x \left(\frac{d_x}{2}\right)^{3/2}}{h_{p_x}} \quad (105)$$

Then the required derivatives are

$$\frac{dF_p}{dh_{p_o}} = 2 \int_0^T \frac{dF'_{p_x}}{dh_{p_o}} dx \quad (106)$$

$$\frac{dF_v}{dh_{P_0}} = 2 \int_0^T \frac{dF'_{v_x}}{dh_{P_0}} dx \quad (107)$$

The viscous drag on a roller orbiting at high speed is\*

$$F_D = \frac{\rho f L}{64} \sum_{i=1}^2 z_i \left[ |D_i - D_{c_i}| \Omega_E \right]^2 \quad (108)$$

where  $\rho$  = lubricant density

$z_1$  = radial riding clearance at outer pilot surface

$z_2$  = radial riding clearance at inner pilot surface

$D_1$  = bore of outer ring

$D_{c_1}$  = outside diameter of cage

$D_2$  = outside diameter of inner ring

$D_{c_2}$  = bore of retainer

If  $z_1 > z_2$  the cage is inner-ring piloted. If  $z_1 < z_2$  the cage is outer-ring piloted.

From Figure 9, assuming the forces  $F_{v_1}$  or  $F_{v_2}$  are small in comparison with  $P_1$ , let

$$\Phi = F_{T_1} + F_{T_2} - F_D \quad (109)$$

---

\*Calculated as described under "Analysis of Shear Forces on a Lubricated, High-Speed Bearing Retainer."

If  $\Phi > 0$ , the roller contacts the leading wall of the pocket and drives the cage, and the value of an index, I, is 1.

If  $\Phi < 0$ , the roller contacts the trailing wall of the pocket and is driven by the cage. The value of the index is 2.

$F_p$  and  $F_T$  need be calculated only for the end of the pocket corresponding to I. The forces at the other end of the pocket are negligible due to the pocket clearance, which is large compared to the lubricant film at the I end.

Two modes of operation are recognized. In the first mode the roller is in contact with both outer and inner races. In the second the roller contacts the outer race only. In neither mode is the angular acceleration of the roller in orbit or about its own axis considered. In other words the transition from motion with contact at both races to steady-state motion with outer-race contact only is assumed to be instantaneous.

When the roller is in contact with both races,

$$F_{p_1} = |F_{T_1} + F_{T_2} - F_D| = 0 \quad (110)$$

Equation (110) is calculated using an assumed value of  $\omega_x$ . For the first pass,  $\omega_x$  is obtained from

$$\omega_x = \frac{(\Omega_1 - \Omega_E)(E + d)}{d} \quad (111)$$

Equation (110) is also evaluated using an assumed value of  $h_{p_{o_1}}$ , and

Equation (110) will probably have the residue  $\psi$ .

An improved value of  $h_{p_{o_1}}$  is

$$\hat{h}_{p_{o_1}} = h_{p_{o_1}} - \frac{\psi}{\left( \frac{d\psi}{dh_{p_{o_1}}} \right)} \quad (112)$$

where

$$\frac{d\Psi}{dh_{p_{o_1}}} = \frac{dF_{p_1}}{dh_{p_{o_1}}} \quad (113)$$

Repetition of the process yields  $h_{p_{o_1}}$  to desired accuracy.

Taking moments about the roll center,

$$(F_{T_1} - F_{T_2} - F_{v_1}) \frac{d}{2} = 0 \quad (114)$$

For the initial assumption of  $\omega_x$ , Equation (114) will not be satisfied and there will be the residue  $\Psi$ . An improved value of  $\omega_x$  is

$$\hat{\omega}_x = \omega_x - \frac{d\Psi}{\left(\frac{d\Psi}{d\omega_x}\right)} \quad (115)$$

$$\frac{d\Psi}{d\omega_x} = \frac{dF_{T_1}}{d\omega_x} - \frac{dF_{T_2}}{d\omega_x} - \frac{dF_{v_1}}{d\omega_x} - \frac{dF_{v_1}}{dh_{p_{o_1}}} \cdot \frac{dh_{p_{o_1}}}{d\omega_x} \quad (116)$$

where

$$\frac{dh_{p_{o_1}}}{d\omega_x} = - \frac{\left( \frac{dF_{p_1}}{d\omega_x} \right)}{\left( \frac{dF_{p_1}}{dh_{p_{o_1}}} \right)} \quad (117)$$

Repeated application of Equation (115) yields  $\omega_x$  to desired precision. After each pass the process returns to Equation (82).

The solution for the case of outer contact only is solved in a similar manner except that  $F_{y_2}$  and its derivatives are nonexistent.

The viscous drag force between retainer and ring is, from Reference 3,

$$F_{R_i} = .008 \rho^{3/4} \mu_0^{1/4} \sum_{i=1}^2 \frac{|U_i|^{7/4}}{Z_i^{1/4}} \frac{A_i U_i}{|U_i|} \quad (118)$$

where  $\rho$  = lubricant density

$\mu_0$  = lubricant viscosity

$U$  = sliding velocity of ring on cage

$A$  = total guiding area

$Z$  = 1.2 cage ring diametral clearance

$$U_i = \frac{(\Omega_i - \Omega_E) D_i}{2} \quad i = 1, 2 \quad (119)$$

The torque on the cage due to viscous drag is

$$Q_c = \frac{1}{2} \sum_{i=1}^2 F_{R_i} D_i \quad (120)$$

The total horizontal and vertical loads on the cage due to pocket forces are

$$H = \sum_{q=1}^n \left[ -C_{I_q} (F_{p_{I_q}} \cos \varphi_q + F_{v_{I_q}} \sin \varphi_q) \right] \quad (121)$$

$$V = \sum_{q=1}^n \left[ C_{I_q} (F_{P_{I_q}} \sin \varphi_q - F_{v_{I_q}} \cos \varphi_q) \right] \quad (122)$$

Figure 9 shows the reactions of the piloting surface on the cage. The radial force consists of a component,  $P$ , and a centrifugal force due to cage whirl with a rotating load. From Figure 9,

$$V + f (P + \bar{F}_c) \sin \Theta = (P + \bar{F}_c) \cos \Theta = 0 \quad (123)$$

$$H - f (P + \bar{F}_c) \cos \Theta = (P + \bar{F}_c) \sin \Theta = 0 \quad (124)$$

$$f = \frac{U_j}{|U_j|} f_r \quad (125)$$

where  $f_r$  = coefficient of sliding friction at the pilot interface

$J$  = 1 for an outer-piloted retainer and 2 for an inner-piloted retainer

$$\bar{F}_c = \frac{m_c Z_j \omega_w^2}{2} \quad (126)$$

$m_c$  = mass of cage

$\omega_w$  = speed of whirl

From Equations (120) and (121),

$$\tan \Theta = - \frac{(f V - H)}{(f H + V)} \quad (127)$$

$$P = \frac{H}{f \cos \Theta + \sin \Theta} - \bar{F}_c \quad (128)$$

The total torque on the cage may now be evaluated.

$$\ddot{Q} = \frac{1}{2} \sum_{q=1}^r \left[ C_{I_q} (F_{p_{I_q}} E + F_{v_{I_q}} D_p) \right] + \frac{i (P + \bar{F}_c)}{2} D_{c_J} + Q_v \quad (129)$$

The cage speed is now decremented and the value of  $\ddot{Q}$  recalculated. This is equivalent to returning to Equation (77) with the new value of  $\Omega_E$ .

The decrementing process is continued until  $\ddot{Q}$  changes sign. The method of false position is then applied to drive  $|Q|$  to a satisfactory minimum.

## ELASTOHYDRODYNAMIC FILM THICKNESS CALCULATION

The minimum EHD film thickness is calculated within the computer program by a subroutine provided by the Air Force Aero Propulsion Laboratory and Mechanical Technology, Inc., in accordance with Reference 11. The fundamental relationship employed is the Dowson and Higginson<sup>1</sup> equation as indicated below for cylindrical contacts. Ball and roller race contacts are reduced to equivalent contacts in the analysis by dividing the contact zones into strips.

$$h_0 = 1.6 R \frac{\left[ c_0 E'' \right]^{.6} \left[ \frac{u \mu_0}{E'' R} \right]^{.7}}{\left[ \frac{w}{E'' R} \right]^{.13}} \quad (130)$$

where  $\mu_0$  pressure coefficient of viscosity  $\left[ \frac{\text{in.}^2}{\text{lb}} \right]^2$

$$E'' = \left[ \frac{1-m_R^2}{2E_R} + \frac{1-m_E^2}{2E_E} \right] \left[ \frac{\text{lb}}{\text{in.}} \right]^2$$

$m$  Poisson's ratio (rolling element, race)

$E$  Young's modulus (rolling element, race)

$\mu_0$  viscosity at ambient pressure and film inlet temperature  $\left[ \frac{\text{lb}\cdot\text{sec}}{\text{in.}^2} \right]$

$u = \frac{1}{2} \left[ V_R + V_E \right]$  velocity term  $\left[ \frac{\text{in.}}{\text{sec}} \right]$

$R = \left[ \frac{1}{R_R} + \frac{1}{R_E} \right]^{-1}$  equivalent radius  $\left[ \text{in.} \right]$

$w =$  load per unit width of contact  $\left[ \frac{\text{lb}}{\text{in.}} \right]$

$h_0$  minimum film thickness

The application of this equation to ball bearings requires the establishment of various kinematic and geometric parameters that will be developed here. The general case of ball motion occurring in a high-speed angular contact ball bearing is represented in Figure 10. The case depicted is with the ball fixed in the plane of the paper with relative outer and inner ring speeds of  $\omega_1$  and  $\omega_2$ , respectively. As indicated, the ball is free to rotate about all three axes.

The operating contact angles at the inner and outer races are unequal owing to ball centrifugal forces and gyroscopic moments. As is evident, the relative motion between ball and race at each contact will be a combined rolling and spinning action. Proper calculation of the EHD film thickness in these contact areas must consider this combined motion. This was accomplished by dividing the contact area into a number of strips parallel to the y axis as shown in Figure 11. These strips are treated as individual cylindrical contacts rolling in the y direction.

Figure 11 represents the contact zone on the race, which has a velocity due to race rotation of

$$V_{YR_i} = \frac{\omega_i}{2} (E + C_i d \cos\beta_i) \quad (131)$$

where  $i = 1$  designates outer contact

$i = 2$  designates inner contact

$$\begin{aligned} C_1 &= +1 \\ C_2 &= -1 \end{aligned} \quad \left. \begin{array}{l} \text{sign terms} \\ \text{ } \end{array} \right.$$

and

$$\omega_i = \Omega_i - \Omega_e$$

where  $\Omega_1$  = oil ring speed

$\Omega_2$  = inner ring speed

$\Omega_e$  = retainer speed

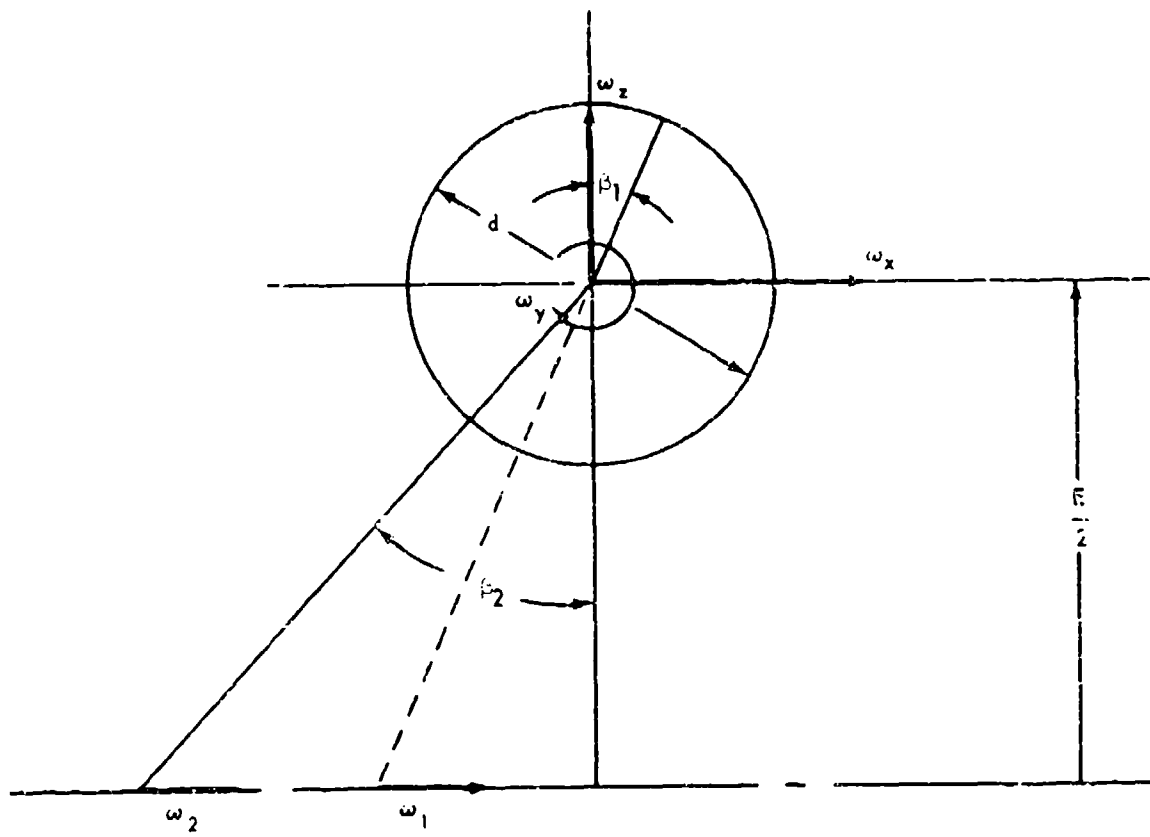
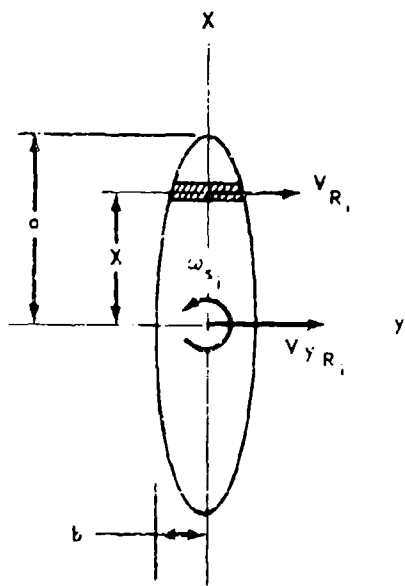
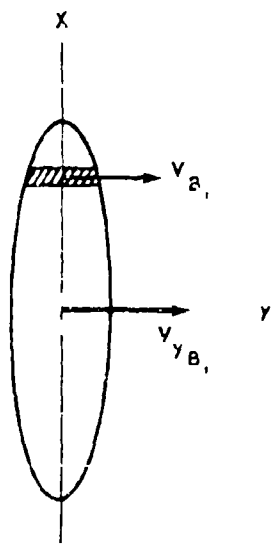


Figure 10. Ball Motion Occurring in High-Speed Angular-Contact Ball Bearing; General Case.



CONTACT AREA ON RACE



CONTACT AREA ON BALL

Figure 11. Contact Areas on Race and Ball.

and an angular spin velocity relative to the ball of

$$\omega_{s_i} = C_i \left[ (\omega_i - \omega_x) \sin\beta_i - \omega_z \cos\beta_i \right] \quad (132)$$

Combining these two velocity components, we can now calculate the velocity in the y direction of any point on the race contact by

$$V_{R_i} = V_{Y_{R_i}} - X \omega_{s_i} \quad (133)$$

The velocities within the contact zone on the ball as shown in Figure 11 in the Y direction can be calculated from

$$V_{B_i} - V_{Y_{B_i}} = \frac{C_i d}{2} (\omega_x \cos\beta_i - \omega_z \sin\beta_i) \quad (134)$$

The race radii of curvature in the plane of rolling required to calculate the equivalent radius of contact against a flat surface can be stated as

$$R_{R_i} = - \frac{C_i}{2} \left( \frac{E}{\cos\beta_i} + C_i d \right) \quad (135)$$

and the ball radius of curvature

$$R_{B_i} = \frac{d}{2} \quad (136)$$

Finally,  $w$ , the load per unit width of contact, can be found from

$$w = \frac{3P}{4a} \left( 1 - \frac{x^2}{a^2} \right) \quad (137)$$

The film thickness is calculated for each strip in the contact,  $-a < x < a$ , and the minimum value, all strips considered, is presented in the computer output as the minimum thickness for the contact.

The application of the Dowson and Higginson equation to cylindrical roller bearing contacts is treated in the same manner as in the above ball bearing method. The roller bearing case, however, is simpler because of the absence of spin velocities.

## ELASTOHYDRODYNAMIC TRACTION COEFFICIENTS

### Traction Model

The mechanics by which EHD oil films are generated in heavily loaded rolling element contacts such as those encountered in ball and roller bearings is well understood. The magnitude of the EHD film thicknesses can be accurately calculated using the Dowson and Higginson equation as indicated in the previous section. This is the case even though the analysis is predicated upon isothermal flow conditions, because the film thickness is determined primarily by the oil properties in the inlet region of the contact where the oil pressure is nearly ambient, and the oil temperature is approximately the same as that of the rolling surfaces.

Traction effects, however, present a more complicated picture to be analyzed in that the traction forces transmitted by the contacting surfaces are strongly influenced by the rheology of the fluid within the film. In the race contacts, high Hertz pressures are in effect accompanied by appreciable sliding with the attendant heating of the oil film. The rheological behavior of the lubricant film in the contact is strongly affected by these elevated pressures and temperatures. Currently, information regarding the shear properties of lubricant films under these high contact pressures and sliding velocities is incomplete, and sufficient understanding of the rheology of the lubricants in this regime is not available to produce analytical solutions.

The traction coefficients appearing within the computer programs were established with the use of computer program subroutines BALFTJ and TRAC provided by the Air Force Aero Propulsion Laboratory and Mechanical Technology, Inc. In these subroutines, sliding frictional coefficients were generated based upon the experimental data reported by Johnson and Cameron<sup>6</sup>. To apply this experimental data to a wide range of load, speed, and lubricant parameters, an analysis of friction similar to that developed by Crook<sup>4</sup> was conducted by Mechanical Technology, Inc., to identify the pertinent dimensionless parameters governing frictional behavior.

The results indicated that the friction coefficients are governed by three dimensionless parameters for a given inlet temperature and lubricant.

$$G_1 = \frac{\mu_o u_s}{P_{Hz} h_o}$$

$$G_2 = \frac{\beta_1^* \mu_o u_s}{8 K_f}$$

$$G_3 = \alpha_o P_{Hz}$$

where  $\mu_o$  = inlet viscosity  
 $u_s$  = sliding speed  
 $P_{Hz}$  = maximum Hertz pressure  
 $h_o$  = film thickness  
 $\beta_1^*$  = temperature viscosity coefficient based on the function used by Crook  
 $K_f$  = thermal conductivity of the lubricant  
 $\alpha_o$  = pressure viscosity coefficient based on the viscosity function used by Crook

Physically,  $G_1$  is a direct measure of the shear rate effects, whereas  $G_2$  and  $G_3$  measure the thermal heating effects and the pressure-viscosity effects respectively. With the use of these three parameters, Johnson's experimental frictional coefficients were plotted against  $G_1$  for a constant  $G_2$  with  $G_3$  as parameters. Typical graphs for a low and high value of  $G_2$  are given in Figures 12 and 13. Portions of the curves are extrapolations of Johnson's data to cover broader ranges of speed, load, and lubricant properties.

It is seen that at small values of  $G_1$ , all curves have a constant slope. This corresponds to the fact that at small sliding speeds the frictional coefficient varies linearly with sliding speed. In each graph, all curves merge at large values of  $G_1$  to a common value, which is the "ceiling" found by Johnson and Cameron and also by Plint.<sup>8</sup> The ceiling decreases with increasing  $G_2$ . The existence of a ceiling in friction suggests that there is a limiting shear stress in a lubricant film.

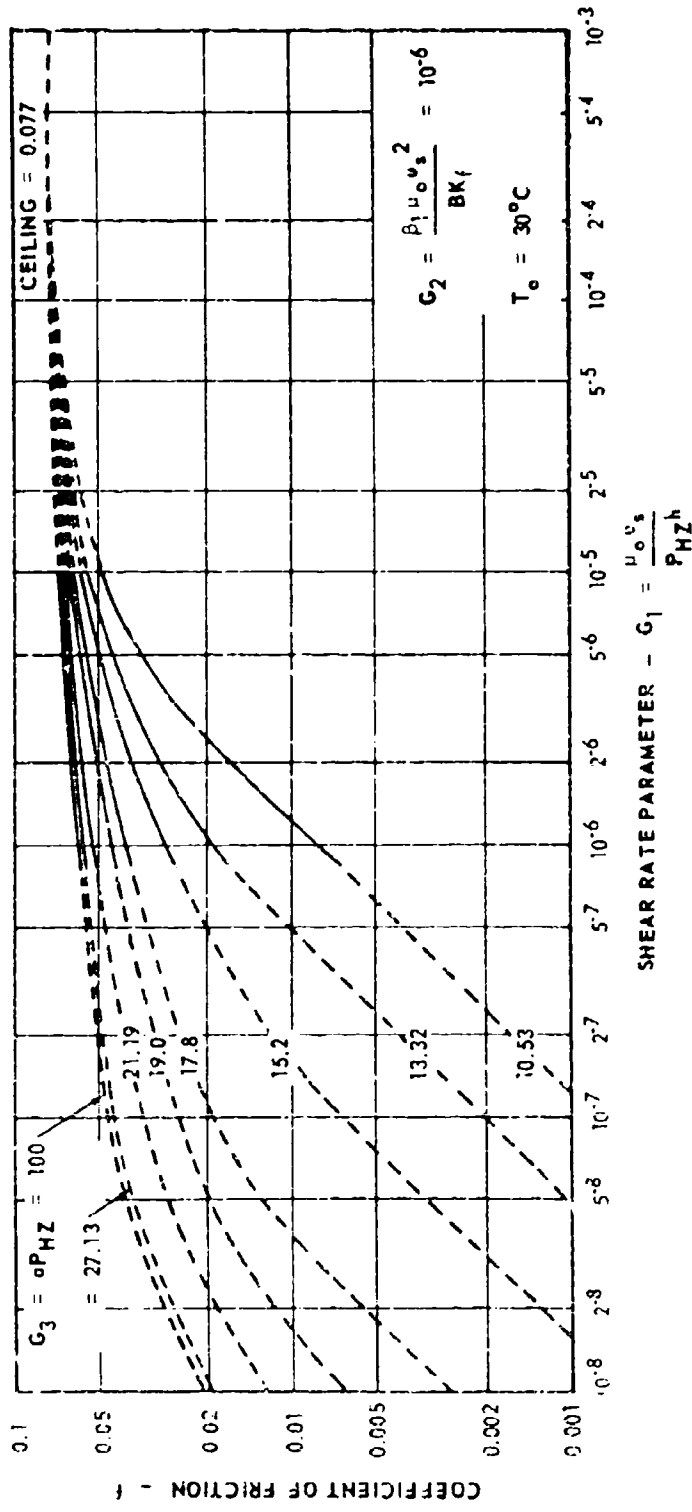


Figure 12. Coefficient of Friction Versus Shear Rate Parameter for Heating Parameter =  $10^{-6}$ . Reference (11), Figure 93.

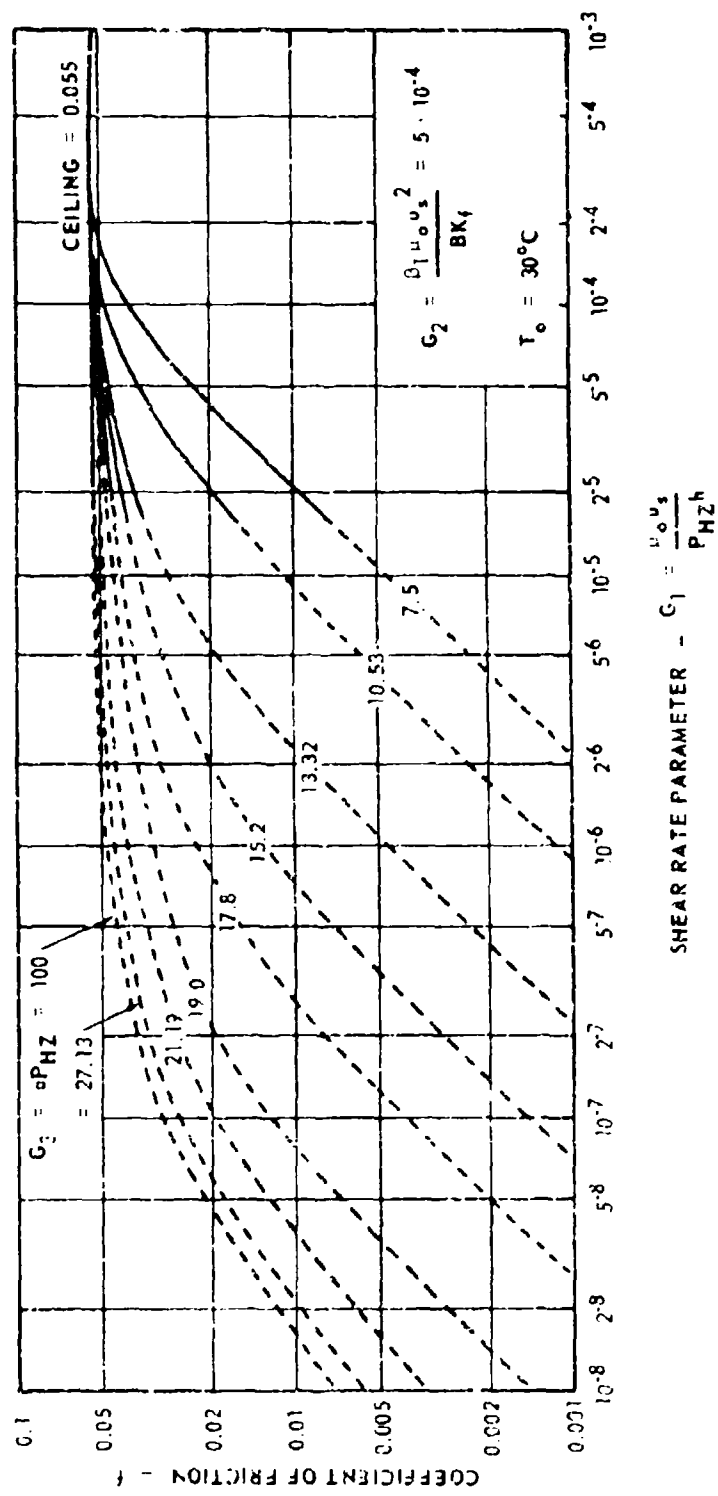


Figure 13. Coefficient of Friction Versus Shear Rate Parameter for Heating Parameter =  $5 \times 10^{-4}$ . Reference (11), Figure 97.

It should be noted that all the frictional coefficient graphs are for a given inlet lubricant temperature, 30° C. Change of inlet temperature affects the frictional coefficient due to the dependence of the limiting shear stress upon the inlet temperature. Johnson and Cameron and Plint investigated this inlet temperature effect. Pli's experiment shows that the variation of frictional coefficient with inlet temperature is approximately linear, and the slope does not seem to vary much with either rolling or sliding speed. The slope was found to be -0.001 per degree Fahrenheit. This relationship is used to predict frictional coefficients for inlet temperatures other than 30° C.

### Tractive Forces and Spin Torque

To facilitate the general kinematic solutions desired while accounting for gyroscopic slip and ball spin, it is necessary to calculate the tractive forces between the balls and races with the assumption of motion about all three ball axes. Figure 14 illustrates the velocity components active in the contact areas on the ball and race of a common contact. Each ellipse is divided into a number of strips parallel to the direction of rolling (Y axis). The dimensions  $a$  and  $b$  are the semimajor and the semiminor axes of the contacts, respectively. The sliding velocity in the Y direction at each strip can be found from Equations (133) and (134) and is

$$v_{s_y} = \left| v_{R_i} - v_{B_i} \right| \quad (138)$$

With this sliding velocity established and the Hertz stress, lubricant properties, and EHD film thickness known, the tractive coefficient  $f$  for the strip can be calculated with the procedure previously described. The tractive force acting on each strip in the y direction is

$$dF_y = 2 \tau_y^* y' dx \quad (139)$$

where  $y^*$  is the semistrip width dimension as shown in Figure 14 and

$$\tau_y^* = \frac{f_w}{2 y'} \quad (140)$$

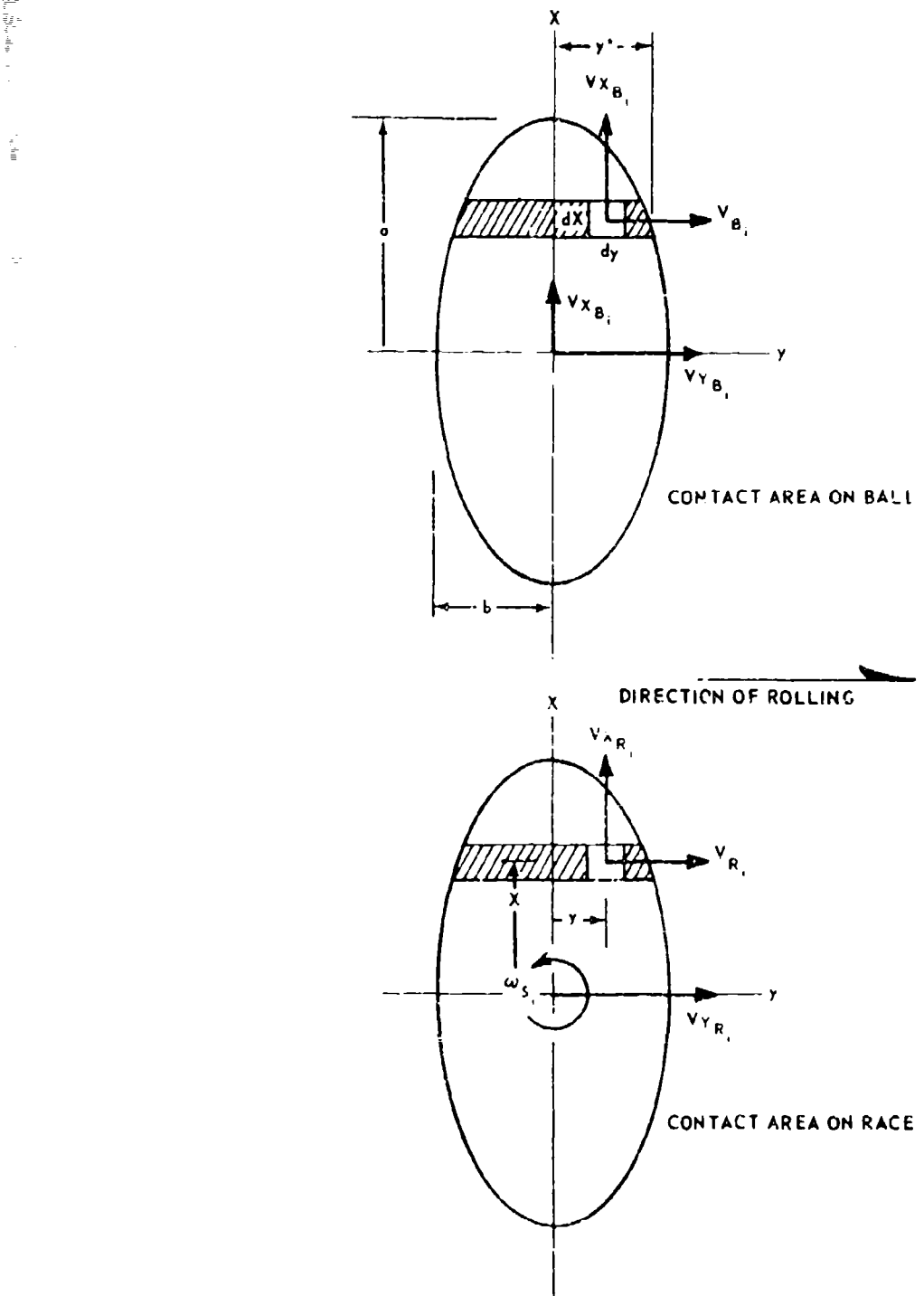


Figure 14. Velocity Components Active in Contact Areas.

The total tractive force for the contact at the y direction is the sum of the tractive forces within the individual strips, or

$$F_{y_i} = \int_{-a}^a 2\tau_y y^* dx = \int_{-a}^a f_w dx \quad (141)$$

The shear stress in the x direction is calculated with the assumption that the ratio of the two mutually perpendicular shear stresses is proportional to their shear rates. The previously defined strip is then further divided into differential elements to evaluate the velocity variations along the Y-axis as shown in Figure 14.

Therefore,

$$\frac{\tau_x}{\tau_y} = \frac{u_{s_x}}{u_{s_y}} \quad (142)$$

$$\frac{\tau_x}{\tau_y} = \left| \frac{v_{x_{R_i}} - v_{x_{B_i}}}{v_{K_i} - v_{B_i}} \right| \quad (143)$$

where

$$v_{x_{R_i}} = y \omega_{s_i} \quad (144)$$

is the velocity at each element on the race relative to the ball owing to ball spin and

$$v_{x_{B_i}} = -\frac{d}{2} \omega_y \quad (145)$$

is the velocity of the ball relative to the race resulting from gyroscopic precession of the ball. The velocity component  $\omega_y$  is the ball angular velocity about the axis dictated by the ball's gyroscopic movement and is one of the independent variables employed in the overall iterative bearing solution.

The total tractive forces in the x direction can be written

$$F_{x_i} = \int_{-a}^a \int_{-y'}^{y'} \tau_x dy dx \quad (146)$$

The spin torque normal to the contact ellipse can be expressed as

$$Q_{s_i} = \int_{-a}^a f_{wx} dx = \int_{-a}^a \int_{-y'}^{y'} \tau_x y dy dx \quad (147)$$

Each of these integrals, Equations (141), (146), and (147), was evaluated numerically in the subroutine BALFTJ to provide the tractive forces and moments along with their derivatives with respect to the velocity components and normal contact loads needed for the computer analysis.

Tractive forces and derivatives for the roller bearing contacts were calculated in the same manner in the subroutine ROLFTN subject to the simplification of zero spin velocity and torque.

#### Tractive Instability

The most significant difficulty encountered during the computer program development stems from the rheological behavior of the fluid and the resulting traction forces developed at high slip speeds. At high values of  $G_1$ , the slope of the traction curve in Figures 12 and 13 becomes progressively flatter, and finally reaches a zero slope at the ceiling, i.e., the limiting shear stress is reached. In this regime, changes in the sliding velocity do not strongly affect the tractive forces generated; consequently, all derivatives of forces and moments with respect to the velocity components are nearly zero. This behavior creates a breakdown within the iterative procedure because velocity changes are not then affecting bearing tractive forces, and the load adjustments with velocity changes required to achieve solutions are not forthcoming.

Another phenomenon that caused problems at high slip rates is illustrated in Figure 15, where tractive force is plotted against slip velocity directly. Note that at low slip rates the tractive forces increase with increasing slip rates, while at high slip rates the tractive forces decrease with increasing slip rates. This decrease in traction with increasing slip rate is primarily the result of heating of the oil film with an attendant temperature increase combined with a strong temperature dependence of the oil viscosity. In this regime, the heating effect overrides the increasing slip rate to produce a net decrease in traction.

This effect produces a surprising result when combined linear and spin slip velocities are superimposed on a race contact. In some cases, the computed reactive spin torque on the ball opposes the spinning velocity, as one would intuitively expect. However, in other cases, the reactive spin torque is in the same sense of the spinning velocity; i.e., the calculated reaction torque is in a direction so as to accelerate the spinning action of the ball. This anomaly can be explained by considering the two points A and B on the tractive curve, Figure 15. Point A is in the regime where shear rate predominates over tractive behavior, while point B is in the regime where thermal effects are predominant. Consider race contact as shown in Figure 16, with the ball sliding in the  $y$  direction with a sliding velocity  $V_y$ . The tractive force picture in the contact for this case would be as indicated in Figure 16. If angular velocity  $\omega$  is now superimposed, different tractive profiles are obtained as indicated in Figure 17, depending upon whether we were initially operating at point A or B. In this manner, the torque reaction to ball spin can either oppose or reinforce the ball spin velocities, depending on whether the dominant slip velocities are on the increasing or decreasing section of the traction curve. This phenomenon is not fully understood at this point, and it must be remembered that the base friction data have been obtained in cylindrical contacts in the absence of spin.

This traction behavior certainly implies that the ball motion would be unstable in these regimes and solutions are unattainable. This phenomenon hampers convergence not only when the desired solution is in the unstable regime, but also if these instabilities are encountered during intermediate passes through the iterative loop for a case which ultimately is stable.

To study this traction-slip behavior in depth, an auxiliary computer program was created. The program treats a single ball-race contact for which the linear and spinning slip velocities are introduced. The program first calculates the tractive forces and moments resulting from

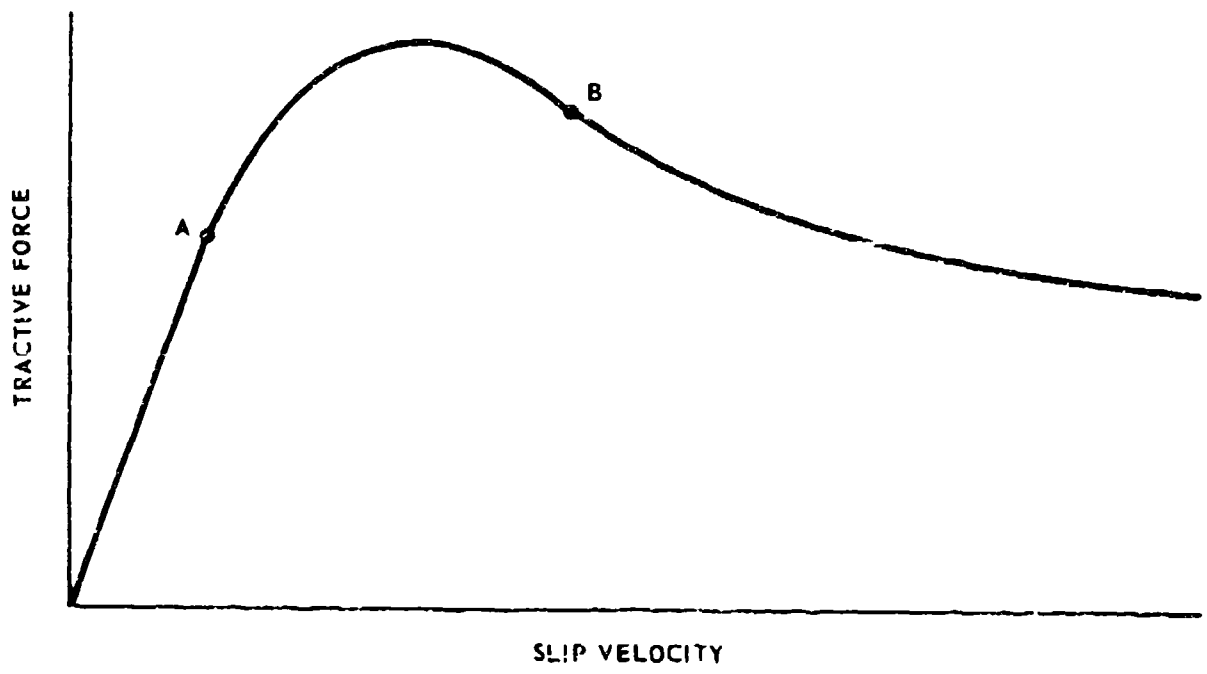
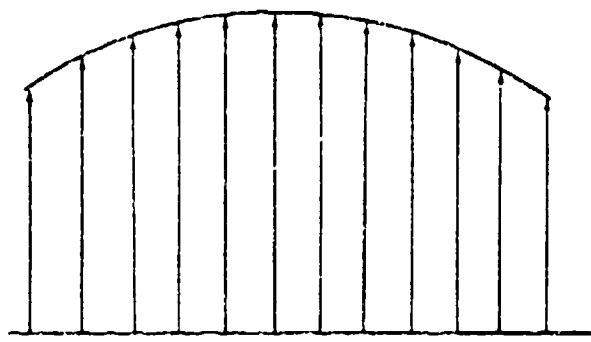
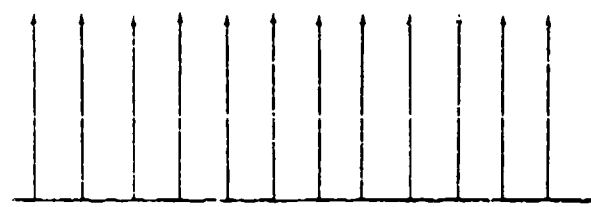


Figure 15. Tractive Force Versus Slip Velocity.

**TRACTIVE FORCE DISTRIBUTION**



**VELOCITY DISTRIBUTION**



**RACE CONTACT**

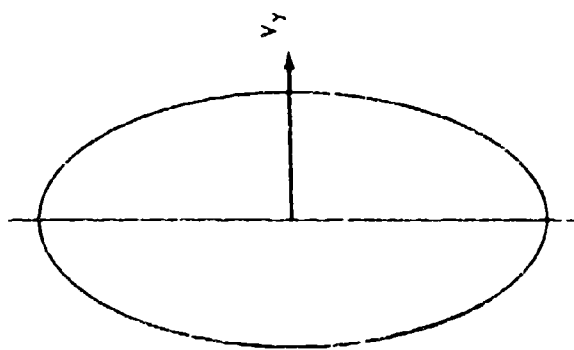


Figure 16. Race Contact, Velocity Distribution, and Tractive Force Distribution in a Ball-Race Contact.

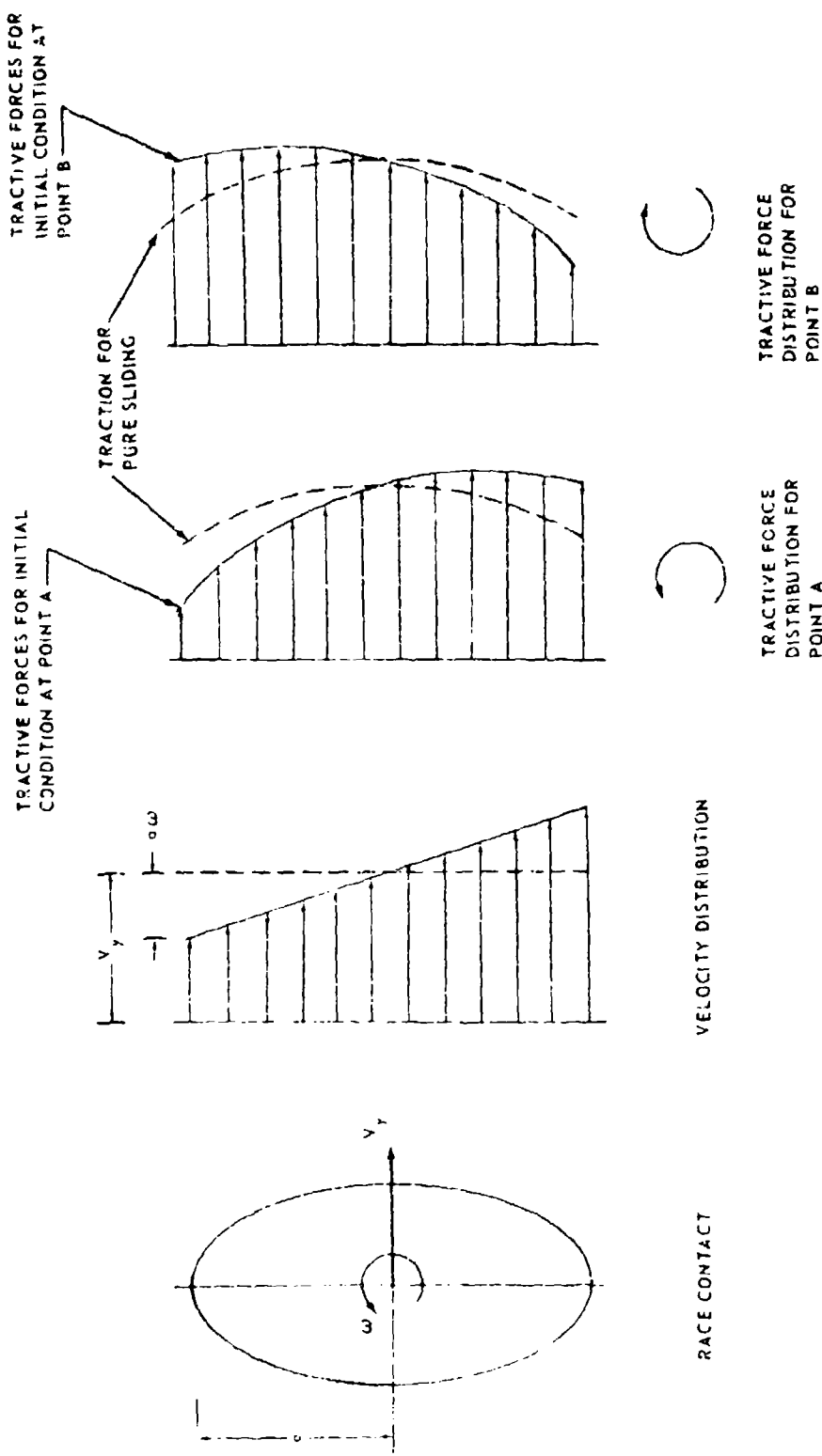


Figure 17. Sliding Velocity and Tractive Force Distribution in a Ball-Race Contact.

the input slip values, increments the input velocities a small amount, and then attempts to iterate back to the initial sliding velocities while knowing their corresponding tractive forces and moments. In this manner the areas of instability can be established as a function of linear and spin slip velocities.

The program incorporates three options to consider different traction versus slip relationships. The first relationship uses the aforementioned Johnson empirical data integrated into a table look-up/interpolation subroutine FRCTN written by Mechanical Technology, Inc. The second relationship is an analytical function that was derived to fit the FRCTN data by scaling and shifting of  $G_1$ ,  $G_2$ , and  $G_3$  terms. This smooth analytical function was formulated to eliminate any local numerical discontinuities that could creep into the table look-up interpolation procedure. The following analytical expression resulted:

$$\frac{.073 G_1 \left( \frac{G_1}{G_2} \right)^{-0.221}}{G_1 \left( \frac{G_1}{G_2} \right)^{-0.171} + 2.05 \left( e^{-7.4 \log_{10} G_3 + 2.4} \right)} \quad (148)$$

where

$$G_2 = 1 \times 10^{-5}$$

which represents, relatively well, the trends of the charts prepared by Mechanical Technology, Inc. However, the deviation in the absolute value of the traction coefficients can be relatively large. The third relationship is a general power law function of the type

$$f = C_1 G_1^e \quad (149)$$

Cases of combined linear and spin slip up to 10,000 inches per second and 1,000,000 rpm, respectively, were investigated. Tables I through IV present the results in a matrix of linear versus spin

slip velocity indicating the number of iterations required to achieve the back solution. The letter "D" that appears in some positions designates a divergence in the iterative process and is indicative of the tractive instability.

The test case used for the study is typical of ball bearing contacts with a semimajor axis of 0.050, a semiminor axis of 0.005, and a Hertz pressure of 150,000 psi.

Table I presents the stability picture for the FRCTN subroutine. As is evident, instabilities for the case studied occur at moderate and high spin slip velocities and do not seem to be as strongly influenced by linear slip. The constant divergence at 1,000 inches per second sliding velocity at all spin slip velocities does not seem to follow the general trend depicted.

Table II is the result when the smooth analytical function is used instead of the interpolation procedure for the same empirical data. The result is generally the same with an apparent slight improvement at higher linear slip velocities. The strong instability previously seen at 1,000 inches per second is not present. The nature of the stability maps indicates that, in general, as the slope of the curve (Figures 12 and 13) diminishes, the instability tendency increases; therefore, some further studies were conducted with various slopes. The subject curves being log-log plots of traction versus  $G_1$  implies that the slope of the curve is dictated by the exponent term  $e$  in Equation (149). Again referring to Figures 12 and 13, the slope of the straight-line portion of the curves at low values of  $G_1$  has an  $e$  equal to 1.0. As the slope becomes progressively flatter, while  $G_1$  is increasing, the value of  $e$  is decreasing and approaches 0. Tables III and IV give the results when the power law, Equation (149), is used with  $e$  values of 1/4 and 1/2 respectively. As is evident, the greater the value of  $e$  (greater slope), the greater the stability. In addition to investigating the effects of  $e$ , a number of numerical values for  $C_1$  were also run. Results indicated that stability of the system is not a function of  $C_1$ , which establishes the magnitude of the traction coefficient, but, as intuitively expected, is a strong function of the traction coefficient's relationship to the slip velocity.

#### Roller Bearing Tractive Instability

Difficulties encountered with nonconvergence of the ball bearing program were also present in the roller bearing program. As a result, the power law function for friction, developed previously for the ball bearing program, was adopted. The roller bearing program was thus developed and solutions for all cases inputted were realized.

TABLE I . STABILITY MAP - FRCTN SUBROUTINE \*

Linear Slip (in. /sec)	Spin Slip (rpm)						
	0	10	$10^2$	$10^3$	$10^4$	$10^5$	$10^6$
0	-	1	3	D	D	D	D
1	1	1	2	D	D	D	D
10	4	4	6	D	D	D	D
$10^2$	3	4	4	4	13	D	D
$10^3$	D	D	D	D	D	D	D
$10^4$	6	8	7	7	7	D	D

\* - Values indicate number of iterations required for solution

D - Divergence in iterative process

TABLE II . STABILITY MAP - ANALYTICAL FUNCTION  
FROM FRCTN SUBROUTINE \*

Linear Slip (in. /sec)	Spin Slip (rpm)						
	0	10	$10^2$	$10^3$	$10^4$	$10^5$	$10^6$
0	-	2	2	3	3	D	D
1	6	9	D	D	D	D	D
10	3	4	5	6	D	D	D
$10^2$	5	5	5	5	6	D	D
$10^3$	6	7	7	6	6	8	L
$10^4$	11	12	13	15	9	15	10

\* - Values indicate number of iterations required for solution

D - Divergence in iterative process

TABLE III. STABILITY MAP -  $f = C_1 G_1^{1/4}$  \*

Linear Slip (in./sec)	Spin Slip (rpm)						
	0	10	$10^2$	$10^3$	$10^4$	$10^5$	$10^6$
0	-	2	2	3	3	4	6
1	3	4	5	D	D	D	D
10	4	4	4	5	D	D	D
$10^2$	4	4	4	5	6	D	D
$10^3$	6	5	5	5	5	6	D
$10^4$	9	9	5	7	7	8	7

\* - Values indicate number of iterations required for solution  
D - Divergence in iterative process

TABLE IV. STABILITY MAP -  $f = C_1 G_1^{1/2}$  \*

Linear Slip (in./sec)	Spin Slip (rpm)						
	0	10	$10^2$	$10^3$	$10^4$	$10^5$	$10^6$
0	-	2	2	3	3	3	6
1	3	3	4	8	9	9	9
10	4	4	4	4	9	11	13
$10^2$	4	4	4	4	5	9	13
$10^3$	9	4	4	4	5	5	13
$10^4$	14	5	6	10	5	5	8

\* - Values indicate number of iterations required for solution

## ANALYSIS OF SHEAR FORCES ON A LUBRICATED, HIGH-SPEED BEARING RETAINER

Until recently, very little attention has been paid to the effects of the retainer on the operating characteristics of a ball or roller bearing assembly. A knowledge of the forces on the retainer is important with respect to both their effect on the dynamics of the other components of the bearing and their influence on the life of the retainer itself.

In this section, simplified analyses are developed to estimate the shear forces imposed on the retainer by retainer-rolling element and retainer-race interactions in a high-speed oil-lubricated bearing assembly. These analyses require geometry, speeds, lubricant properties, and normal loading as inputs, and are intended to provide relationships to be incorporated as subroutines in a bearing dynamics analysis. Consideration is given to ball and roller bearings.

### Traction and Load Analyses for Retainer-Ball Contact

Simplified relationships may be presented for predicting the shear forces on the retainer when in hydrodynamic contact with a ball. A schematic for a single ball in its pocket is shown in Figure 18. The ball imparts a normal load  $W$  to the retainer in the direction of orbital motion. For an angular contact bearing having angular velocity components  $\Omega_1$  and  $\Omega_2$  ( $\Omega_3$  is neglected) and a given lubricant and given geometry, it is desired to determine the relationship between the vertical and circumferential tractive forces  $F_1$  and  $F_2$  and the load  $W$ .

#### Development of Analysis

The analysis of the ball-retainer contact will start with a few basic assumptions:

1. Hydrodynamic forces at the contact can be described by Reynolds equation for steady, isoviscous, incompressible, laminar flow.
2. The radial clearance  $C$  is assumed large compared with the minimum film thickness  $h_0$  and small compared with the ball radius  $R_E$ .
3. The ball-retainer contact will be considered rigid as opposed to FHD.

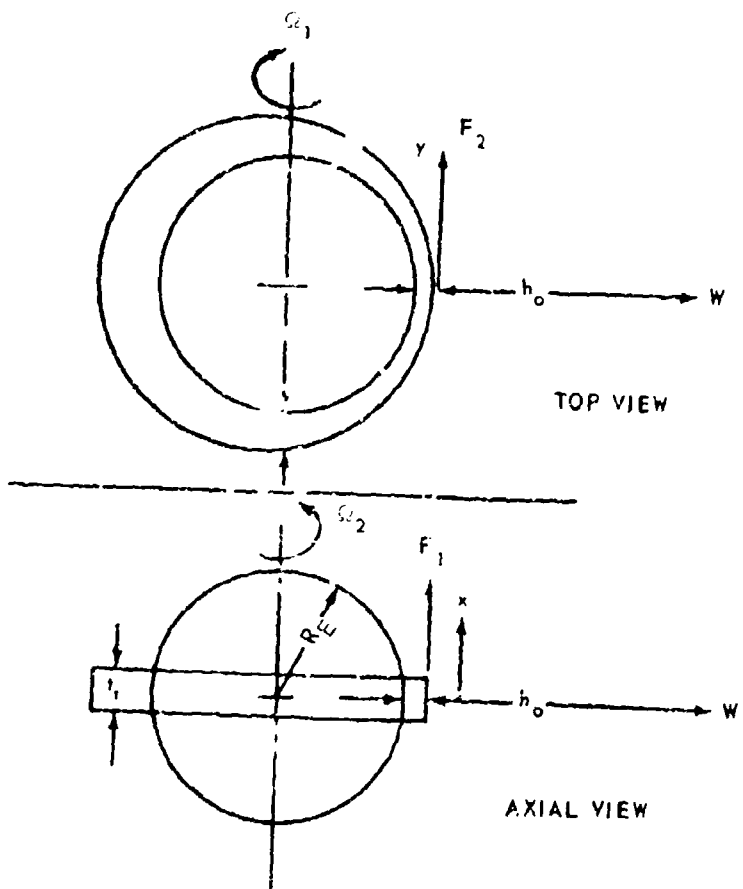


Figure 18. Analysis of Retainer-Ball Traction; Schematic.

The Reynolds equation for steady, isoviscous, incompressible flow is given by

$$\frac{\partial}{\partial x} \left( h^3 \frac{\partial p}{\partial x} \right) + \frac{\partial}{\partial y} \left( h^3 \frac{\partial p}{\partial y} \right) = 6\mu v_x \frac{\partial h}{\partial x} + 6\mu u_y \frac{\partial h}{\partial y} \quad (150)$$

If  $h_0/C < < 1$ , the load will be supported in a very small region in the neighborhood of the point of contact ( $x = y = 0$ ). Each of the surfaces can be represented by its quadratic approximation, thus giving a film thickness shape of the form

$$h = h_0 + \frac{x^2}{2R_E} + \frac{y^2}{2} \left( \frac{1}{R_E} - \frac{1}{R_E + C} \right)$$

or approximately,

$$h = h_0 + \frac{x^2}{2R_E} + \frac{y^2}{2R_E} \left( \frac{C}{R_E} \right) \quad (151)$$

The surface velocity  $u_y$  is given by  $u_y = R\Omega_2$ , and if  $h_0/C$  is small, the velocity  $u_y$  may be approximated by the constant value  $u_y = R\Omega_1$ .

Equations (150) and (151) may be put into convenient dimensionless form by substituting the dimensionless variables

$$\begin{aligned} \xi &= \frac{x}{\sqrt{2R_E h_0}} \\ \eta &= \frac{y}{\sqrt{2R_E h_0}} \sqrt{\frac{C}{R}} \\ p &= \frac{6\mu R\Omega_1}{h_0} \sqrt{\frac{2R_E}{h_0}} \tilde{p} \\ \tilde{h} &= h/h_0 \end{aligned}$$

for the respective dimensional quantities in Equations (150) and (151) to obtain the equation

$$\frac{\partial}{\partial \xi} \left( \tilde{h}^3 \frac{d\tilde{p}}{d\xi} \right) + \frac{C}{R_E} \frac{\partial}{\partial \eta} \left( \tilde{h}^3 \frac{d\tilde{p}}{d\eta} \right) = - \frac{d\tilde{h}}{d\xi} + \frac{\Omega_2}{\Omega_1} \sqrt{\frac{C}{R_E}} \frac{\partial \tilde{h}}{\partial \eta}$$

where

$$\tilde{h} = 1 + \xi^2 + \eta^2 \quad (152)$$

In accordance with assumption (2), terms of order  $\sqrt{C/R}$  are neglected to obtain the approximate form of Reynolds equation

$$\frac{d}{d\xi} \left( \tilde{h}^3 \frac{d\tilde{p}}{d\xi} \right) = - \frac{d\tilde{h}}{d\xi} \quad (153)$$

The usual downstream separation condition is imposed on Equation (153), which requires the pressure and pressure gradient to vanish simultaneously at some point downstream of the center of contact  $\xi = -\xi_1(\eta)$ . Hence,

$$p - \frac{dp}{d\xi} = 0 \quad (154)$$

at  $\xi = -\xi_1(\eta)$ .

We may now integrate Equation (153) with respect to  $\xi$  subject to the boundary condition given by Equation (154) to obtain the equation

$$\frac{d\tilde{p}}{d\xi} = \frac{\xi_1^2 - \xi^2}{(1 + \xi^2 + \eta^2)^3} \quad (155)$$

It can be seen that the pressure gradient dies out at  $1/\xi^4$  as  $\xi$  becomes large. The upstream edge of the retainer  $x = -t_r/2$  corresponds to a value of  $\xi = t_r / (2 \sqrt{2} R_h)$ , which will be much larger under the general range of conditions of interest than the value of  $\xi$  required for the pressure to approach its limiting value; hence, we may invoke the boundary condition

$$\lim_{\xi \rightarrow \infty} \tilde{p} = 0 \quad (156)$$

The results of this analysis will thus be independent of the width of the retainer. The two constraints imposed by Equations (154) and (156) are sufficient for determining the constant of integration associated with Equation (155), the separation point  $\xi_1(\eta)$ , and hence the pressure profile  $\tilde{p}(\eta)$ .

The pressure profile satisfying Equations (154) and (155) is given by

$$\tilde{p}(\xi, \eta) = \int_{-\xi_1(\eta)}^{\xi} \frac{\xi_1^2(\eta) - \xi^2}{(1 + \xi^2 + \eta^2)^3} d\xi \quad (157)$$

and  $\xi_1(\eta)$  is determined from Equation (156). The result is given below:

$$\xi_1(\eta) = 0.4751 \sqrt{1 + \eta^2} \quad (158)$$

#### Film Thickness-Load Relationship for Retainer-Ball Contacts

The dimensionless pressure profile at  $\eta = 0$  [ $\tilde{p}(\xi, 0)$ ] is shown graphically in Figure 19. It can be seen that the pressure dies out rapidly in the inlet region and at  $\xi = 3$  is 10 percent of its peak value. Hence the error in pressure introduced by our upstream boundary approximation will be small if  $t_r/(2\bar{R}h_o) > 3$ .

The pressure at any value of  $\eta$  is given by

$$\tilde{p}(\xi, \eta) = \frac{1}{(1 + \eta^2)^{3/2}} \tilde{p}(\xi, \sqrt{1 + \eta^2}, 0) \quad (159)$$

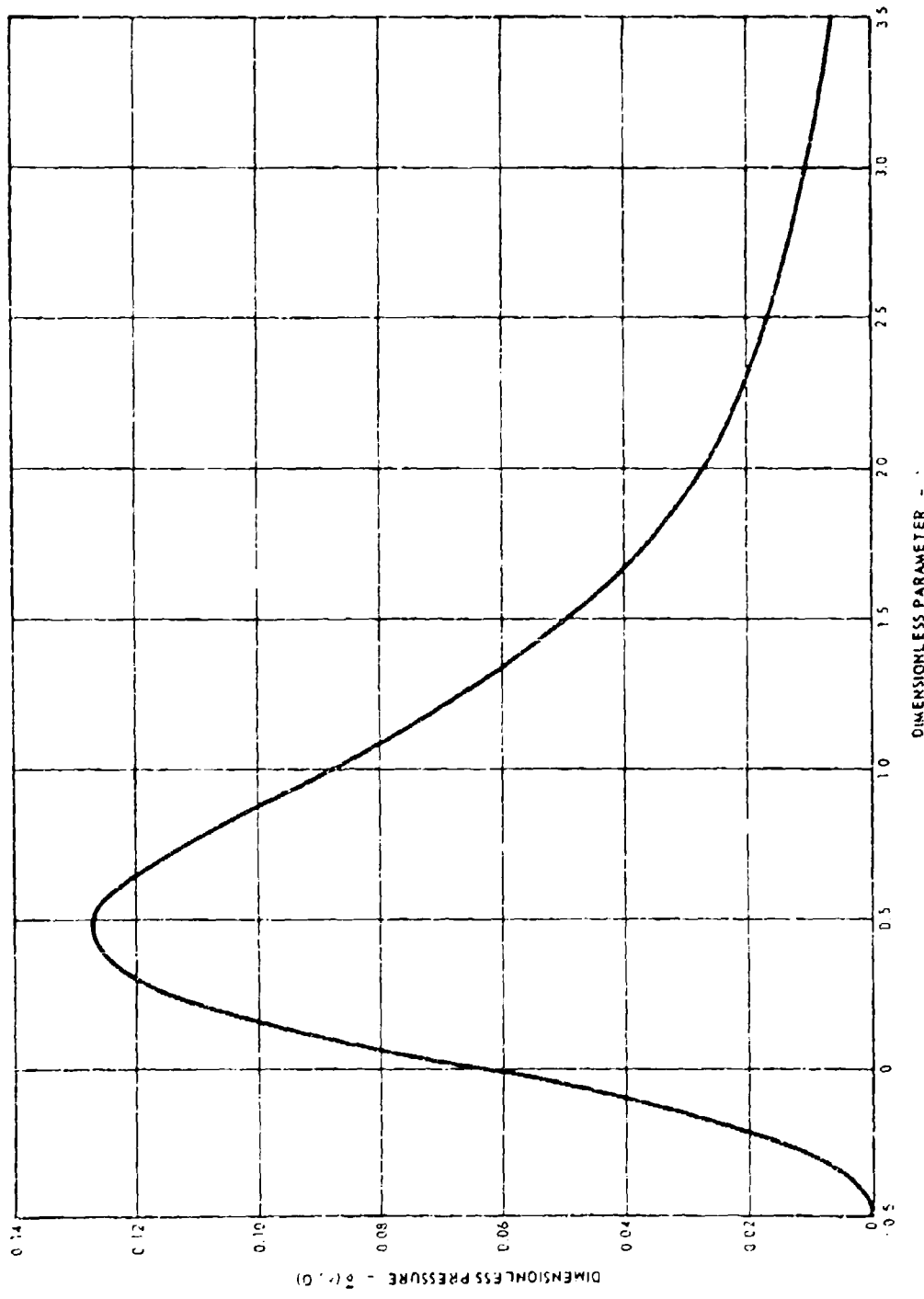


Figure 19. Dimensionless Pressure Profile for Ball-Retainer Contact ( $\eta = 0$ ).

Equation (159) may be integrated with respect to  $\xi$  over the interval  $-\xi_1 < \xi < \infty$  to obtain the dimensionless load per unit length  $\tilde{P}(\eta)$ , which is given by

$$\tilde{P}(\eta) = \int_{-\xi_1(\eta)}^{\infty} \tilde{p}(\xi, \eta) d\xi = 0.2040 (1 + \eta^2)$$

and the total dimensionless load  $\tilde{W}$  may be obtained by integrating  $\tilde{P}(\eta)$  over all  $\eta$  ( $-\infty < \eta < \infty$ ). It can be shown that the error introduced here will be of the order of  $\sqrt{h_o/C}$ .

The dimensionless load  $\tilde{W}$  is

$$\tilde{W} = \int_{-\infty}^{\infty} \tilde{P}(\eta) d\eta = 0.6407$$

and the load-film thickness relationship in terms of physical parameters is

$$W = \frac{\rho \Omega_1 R^3}{\sqrt{h_o C}} K_w$$

where  $K_w = 10.87$

(160)

#### Traction Relationships

The shear stress relationships on the retainer consistent with lubrication theory for isoviscous, incompressible flow are as follows:

$$\tau_{xz} = \frac{h}{2} \frac{dp}{dx} + \frac{\mu u_x}{h}$$

$$\tau_{yz} = \frac{h}{2} \frac{dp}{dy} + \frac{\mu u_y}{h}$$

The above equations may be put in their dimensionless form:

$$\tilde{\tau}_1 - \frac{h_0}{\mu R_E \Omega_1} \tau_{xz} = 3 \tilde{h} \frac{\partial \tilde{p}}{\partial \xi} + \frac{1}{\tilde{h}} \quad (161)$$

$$\tilde{\tau}_2 - \frac{h_0}{\mu R_E \Omega_2} \tau_{yz} = 3 \tilde{h} \frac{\sqrt{C}}{\sqrt{R_E}} \frac{\partial \tilde{p}}{\partial \xi} + \frac{1}{\tilde{h}} \quad (162)$$

The first term on the right side of Equation (162) is of the order  $\sqrt{C/R_E}$  and will be neglected. Equation (155) may be used to replace the pressure gradient appearing in Equation (161).

The resulting shear stress equations are

$$\tilde{\tau}_1 = 3 \frac{\xi^2 - \xi_1^2}{(1 + \xi^2 + \xi_1^2)^2} + \frac{1}{(1 + \xi^2 + \xi_1^2)} \quad (163)$$

and

$$\tilde{\tau}_2 = \frac{1}{1 - \xi^2 + \eta^2} \quad (164)$$

The shear stresses die out as the reciprocal of the square of the coordinate variables as they get large. If integrated over an infinite area, the tractions will diverge logarithmically. Rather than introduce new parameters into the system to limit the area that stresses act upon, it is convenient to define an effective length in the  $y$  direction and to consider variations in shear stress in the  $x$  direction only. In other words, an effective length will be used to treat the traction problem as one of lubricated line (rather than point) contact.

For the case of a roller bearing, line contact would actually occur and the effective length would be the flat portion of the roller.

An effective length for a ball bearing will be selected by examining the variation of the dimensionless load per unit length  $\tilde{P}$  with the dimensionless circumferential coordinate  $\eta$ , which is shown in Figure 20. An effective dimensionless length  $\eta_{eff}$  for calculating load can be defined such that  $\tilde{P}_{max} \eta_{eff} = \tilde{W}$ , which corresponds to a value of  $\eta_{eff} = \pi$  or an effective length of  $L_{eff} = \sqrt{2} \pi R \sqrt{h_0/C}$ .

This effective circumferential length is used to calculate the dimensionless tractive forces:

$$\tilde{F}_1 = \eta_{eff} \int_{-\xi_0}^{\xi_0} \tilde{\tau}_1 d\xi = 1.218$$

and

$$\tilde{F}_2 = \eta_{eff} \int_{-\xi_0}^{\xi_0} \tilde{\tau}_2 d\xi = 0.328$$

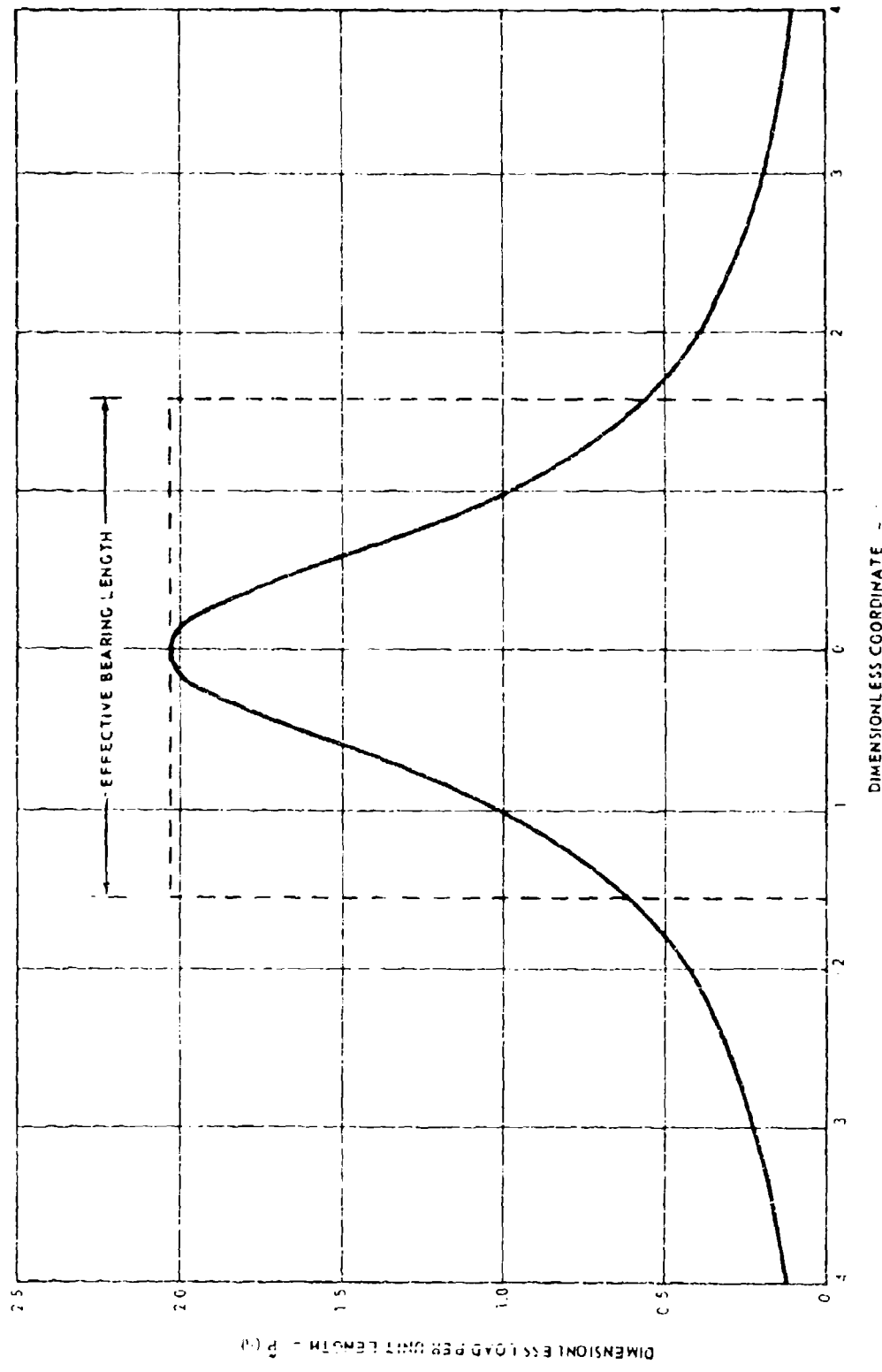


Figure 20. Dimensionless Load per Unit Length.

The hydrodynamic tractions may be expressed in terms of physical parameters as

$$F_i = \frac{\mu \Omega_i R_E^{5/2}}{C^{1/2}} K_i \quad i = 1, 2 \quad (165)$$

where  $K_1 = 2.436$  and  $K_2 = 12.66$ .

The traction formulas presented above are extremely simple to use for predicting hydrodynamic tractions. Some consideration should be given to the predicted film thickness and surface roughness to determine whether or not the contact is indeed hydrodynamic. Since the retainer ball contact is a concentrated contact, some consideration should also be given to the possibility of EHD effects. Further insight can be obtained here with the use of a numerical example.

Our numerical example will deal with a 0.5-inch-diameter ball spinning with an angular velocity of  $\Omega_i = 50,000$  rpm in a retainer pocket having a 5-mil radial clearance, lubricated with a 2-centipoise-viscosity oil. When EHD effects are considered, a pressure coefficient of viscosity of  $10^{-4}$  in.<sup>2</sup>/lb will be used and elastic properties will be taken to correspond to those of steel. Film thickness and peak pressure versus load relationships are shown in Figure 21 for rigid-hydrodynamic and EHD contacts.

The EHD results were obtained using Hertz contact and Grubin's film thickness relationships. Both pressure and film thickness are shown to vary much more rapidly with load for rigid contact. At low loads, hydrodynamic effects spread the load out over a larger area than the Hertz contact zone, and EHD effects will be small. At loads where the rigid hydrodynamic pressures are predicted to be much higher than EHD pressures, EHD effects will be dominant and the analysis presented here will not be valid. It can be seen, however, that the film thickness at that point as predicted by either theory will be of the same order of magnitude as the surface roughness, and it is quite likely that the tractions will more nearly approach those resulting from dry friction.

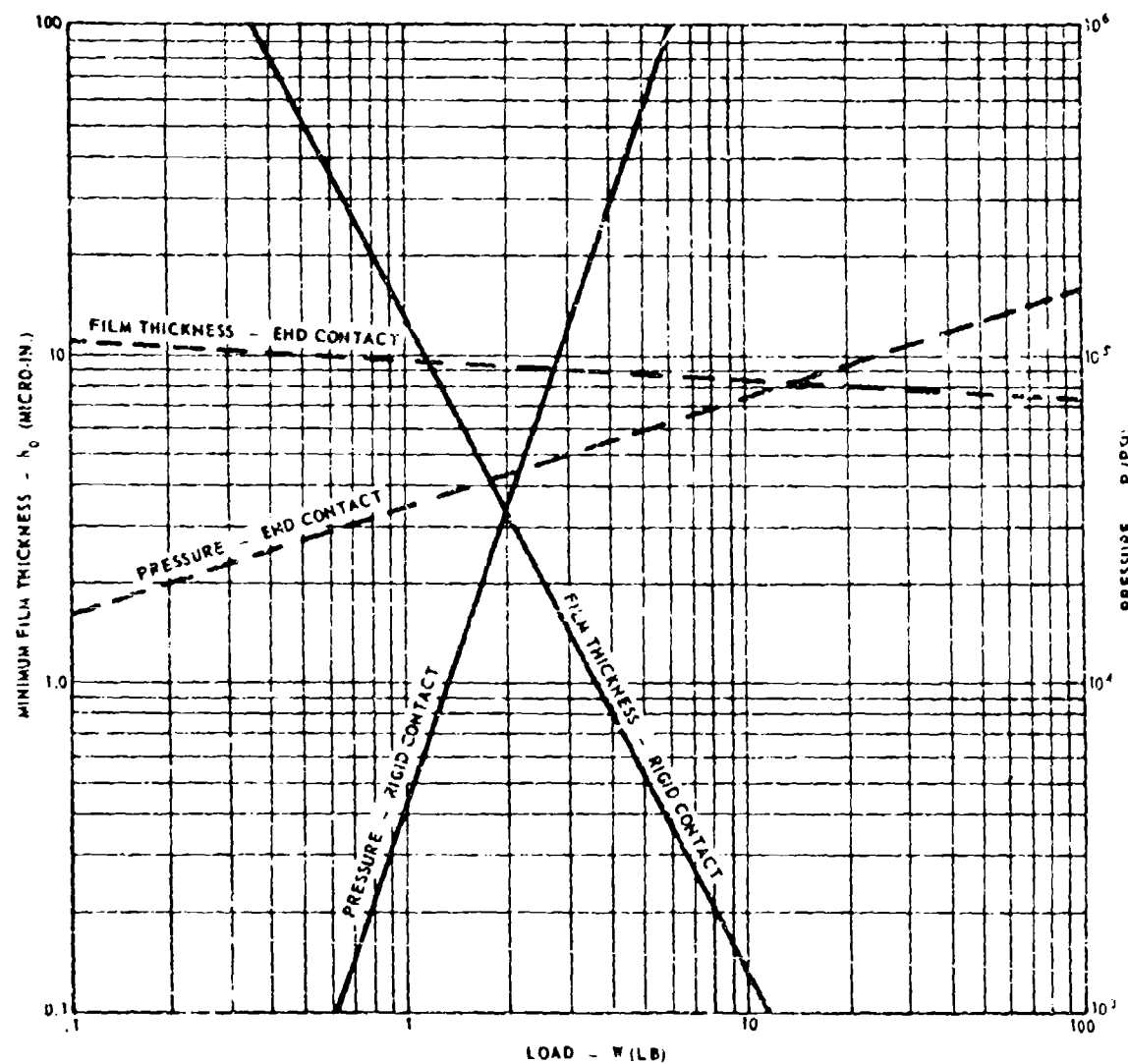


Figure 21. Film Thickness and Maximum Pressure for Retainer-Ball Contact.

The above arguments indicate that a reasonable result can be obtained by dividing the ball-retainer tractions into two regimes, rigid-hydrodynamic contact and dry friction, depending on the film thickness. A critical film thickness separating the two regimes may be determined from the surface roughness. We may define an effective surface roughness  $S_{eff}$  as

$$S_{eff} = \sqrt{S_R^2 + S_B^2}$$

where  $S_R$  and  $S_B$  refer to the RMS (root mean square) surface roughness of the retainer and ball respectively. When  $h_o/S_{eff} < 4$ , increased surface distress has been found to occur for bearings undergoing severe sliding. At a value of  $h_o/S_{eff} = 1.5$ , considerable surface distress is present as a result of asperity clashes. We will thus define our critical film thickness  $h_c$  for dry friction based on surface distress data as:

$$h_c = 1.5 S_{eff}$$

The resulting ball-retainer traction formulas are

$$\left. \begin{aligned} F_t &= \left\{ \frac{\mu(2)_R E}{C^{1.2}} \right\}^{5/2} K_1 h_o & h_o &= h_c \\ &\quad \times \frac{\Omega_1}{\sqrt{\frac{K_1 W}{V} + \frac{\Omega_1^2}{2}}} & h_o &= h_c \end{aligned} \right\} \quad (166)$$

$K_1 = 2,436, \quad K_2 = 12.66, \quad i = 1.2$

where  $K$  denotes coefficient of friction and  $h_o$  is calculated from Equation (160). A reasonable value for  $h_c$  is 10 microinches.

The variation of  $F_1$  with  $W$  for our numerical example is shown in Figure 22. Inspection of this figure indicates that for practical purposes there is essentially no friction until a threshold load for Coulomb friction is reached. The retainer dynamics will thus probably be much more sensitive to the film thickness formula, Equation (160), than the hydrodynamic traction formulas. It should be noted that the film thickness formula does not contain the effective line contact assumption that was used in developing the traction formulas and hence should be less prone to error.

#### Traction for Retainer-Roller Contact

The film thickness-load relationship and the traction relationship for the retainer-roller contact can be obtained from the formulas already presented for the retainer-ball contact. The pressures, shear stresses, and normal and tangential forces per unit length for the retainer-roller contact will be the same as those acting at  $y = 0$  for the retainer-ball contact. The forces for the retainer-roller contact are simply the forces per unit length for the retainer-ball contact at  $y = 0$  multiplied by the length  $\ell$  of the roller. The equations obtained in this manner are:

$$W = \frac{\mu \Omega_1 R_E^2 L}{h_0} K_w . \quad (167)$$

$$F_1 = \mu \Omega_1 R_E L \sqrt{\frac{R}{h_0}} K'_1 . \quad (168)$$

where  $K'_w = 2.447$ ,  $K'_1 = 0.5482$ .

Film thickness and peak pressure versus load relationships for a roller-retainer contact are shown in Figure 23. The lines are drawn in a manner analogous to those in Figure 21, and the input parameters are the same except for the additional input of the length of the roller  $\ell = 3/8$  inch. Comparison of Figures 21 and 23 indicates that the pressures

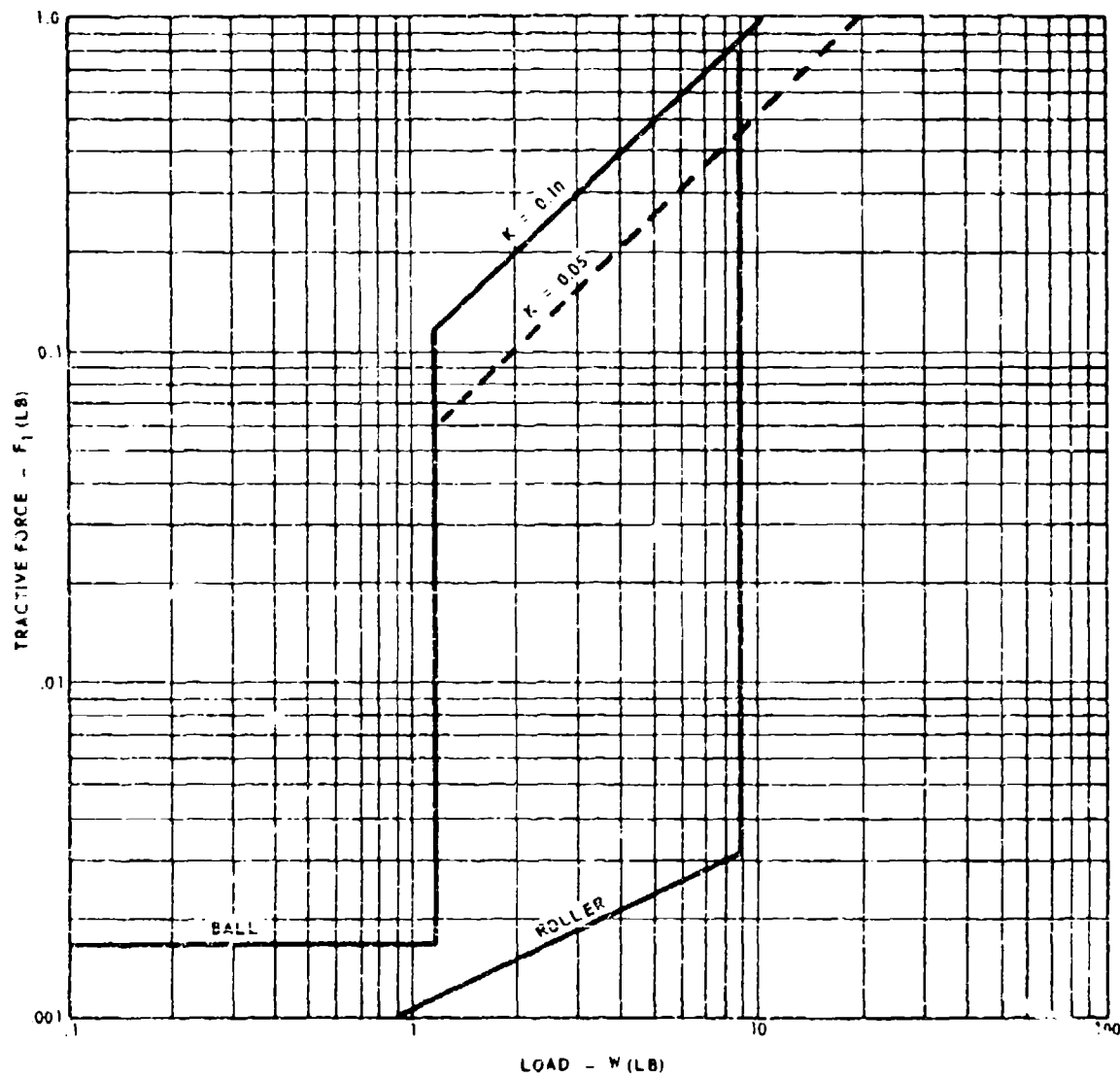


Figure 22. Traction Versus Load for Ball and Roller Contacts.

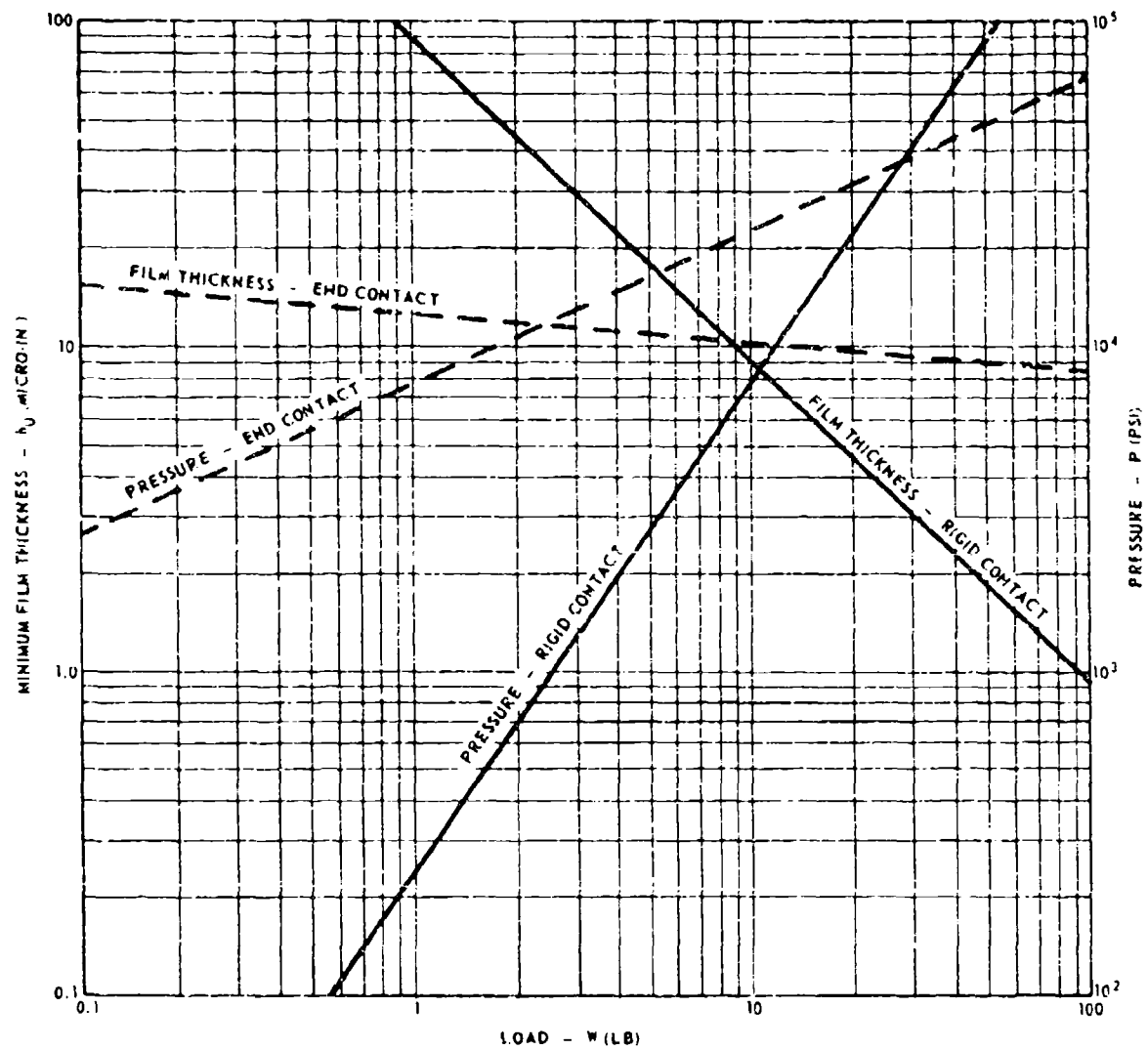


Figure 23. Film Thickness and Maximum Pressure for Retainer-Roller Contact.

will be lower and the retainer-roller contact will tend to be hydrodynamic at somewhat higher loads than in the retainer-ball contact. In other respects the two figures are qualitatively similar, and it should suffice to use the same criteria used in arriving at Equation (166) to obtain the relationship

$$F_1 = \begin{cases} \frac{\mu Q_1 R_E L}{h_o} \sqrt{\frac{R_E}{h_o}} K_1 & h_o > h_c \\ K_W & h_o < h_c \end{cases} \quad (169)$$

Tractions calculated from Equation (166) are shown in Figure 22.

#### Lubricant Drag Between Retainer and Race

A cross-sectional schematic of the retainer and races is shown in Figure 24. At the high speeds of interest here, the flow between the retainer and the races should be turbulent and the shear stress on either surface can be approximated by

$$|\tau_j| = \frac{1}{8} C_f \rho V_j^2 \quad j = 1, 2 \quad (170)$$

where  $\rho$  is the fluid density,  $V_j$  is the absolute value of the relative velocity between the retainer and race,  $j$ , and  $C_f$  is the friction factor for flow between the retainer and race,  $j$ . The friction factor will in general be a function of the Reynolds number  $R_j$ .

$$\beta_j = \frac{V_j H_j \rho}{\mu}$$

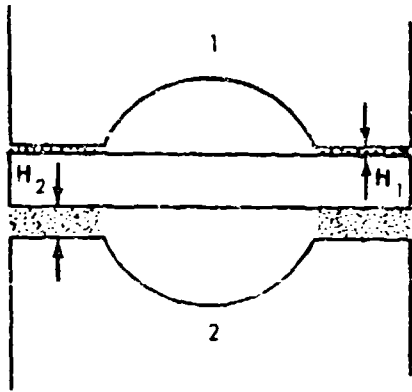


Figure 24. Geometry Used in Calculating Retainer-Race Tensions; Schematic.

It will be assumed that the spacing between the retainer and the guiding surfaces of each race is flooded with oil. We will use the friction factor relationship for Couette flow given by

$$C_f = \frac{0.064}{(R_{ij})^{1/4}} \quad (171)$$

The net drag force on the retainer in the grooved region should be small in comparison with the drag forces between the guiding surfaces, since the flow cross section is larger and the region will probably not be flooded. The drag force on the retainer will thus be calculated based on the area of the guiding surfaces ( $A_j$ ).

The net force on the retainer,  $F_R$ , is given by

$$|F_R| = 0.008 \cdot \left| \frac{v_1^2 A_1}{R_2^{1/4}} - \frac{v_2^2 A_2}{R_2^{1/4}} \right| \quad (172)$$

and will in general act in the direction of the relative velocity of the guiding race with respect to the retainer.

It should be noted that when the retainer is under load it will be operating with a high eccentricity with respect to the guiding race. It is doubtful that the retainer-race contact can support a significant amount of load hydrodynamically (as appears to be the case for the retainer-ball contact) because of the large clearances and resulting small area of effective contact. It is thus recommended that a tractive force due to Coulomb friction be added to  $F_R$  to obtain the total tractive force on the retainer.

### Drag on Ball/Roller

The accurate computation of viscous drag on the ball requires a somewhat more detailed knowledge of the flow field than is currently available. Drag formulas are available for unconfined motions of bodies of various shapes. The flow in a ball bearing assembly is highly confined; however, it is quite likely that both raceways are not flooded and the flow pattern will be quite complex.

Figure 25 shows the cross section to be considered in estimating drag for the case of a ball bearing. In general, conformity is such that the major open channel for flow will be that existing between the retainer and race 2 shown in the illustration. If we assume that all the flow past the ball occurs around the shaded region and treat this region as a cylinder, the drag force on the ball  $F_D$  will be given by

$$F_D = C_D A_3 \frac{\rho V_3^2}{2} \quad (173)$$

where  $A_3$  is the projected shaded region and  $V_3$  is the linear orbital velocity of area  $A_3$ . As a result of the highly approximate nature of these calculations, it will suffice to take  $A_3$  to be  $A_3 \sim 2R_E H_2$ ,  $V_3$  to be the orbital velocity of the ball  $V_C$ , and a characteristic drag coefficient of  $C_D = 1$  for flow past a cylinder to obtain the formula

$$F_D = \rho R_E H_2 V_o^2 \quad (174)$$

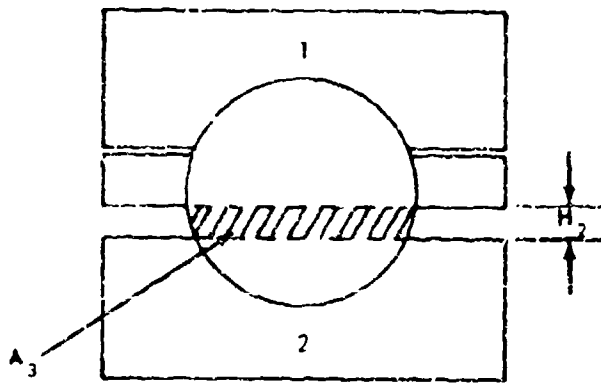


Figure 25. Section Used in Calculating Drag on Ball; Schematic.

## VERIFICATION TEST PROGRAM

### TEST RIG DESCRIPTION AND OPERATION

The test rig used in this program is shown in Figure 26. The rig simulates a 100-millimeter power turbine bearing and seal package, and it is capable of operating at speeds to 30,000 rpm with 1500° F air temperature and 250 psig air pressure outside the package. The test rig is driven by an 8-inch steam turbine rated at 100 horsepower at 30,000 rpm. A 2:1 speed increaser was installed between the turbine and the test rig. A picture of the test facility is shown in Figure 27. Photographs of the test rig are shown in Figures 28 and 29.

The test rig, Figure 26, incorporates the 100-millimeter bearing, a 100-millimeter radial load bearing, and a 55-millimeter support bearing package. When a roller bearing was installed in the test position, a ball bearing was used in the support position for axial positioning of the shaft.

The axial load for the ball bearing was applied during the test by creating an air pressure differential across the thrust load wheel. The magnitude of the axial load was accurately controlled by modulating the differential pressure across the wheel area. Axial thrust load as a function of air pressure differential is plotted in Figure 30. The radial load on the test bearing was obtained by applying a force to the load bearing. The housing of the load bearing is attached through a rod to a hydraulic piston. The housing is not restrained radially but is prevented from rotating by the loading rod, which is strain gaged to measure the applied radial load. The support bearing package of the test rig was adapted from existing engine hardware (T53-L-13, No. 2 bearing package).

In the main bearing test package, a carbon labyrinth was used to restrict the thrust wheel pressurization air from flowing into the bearing package. The load bearing was lubricated by one jet of 0.050 inch diameter, located on the forward side of the load bearing. The test bearing was lubricated by two jets of 0.035 inch diameter, one located on each side of the test bearing. The oil supply to the load and to the test bearings was controlled independently.

The oil used for the testing was MIL-L-23699, supplied by the Air Force Aero Propulsion Laboratory, oil code 0-64-2. Physical properties for this batch are listed in Table V.

The following parameters were measured and controlled during test rig operation:

1. Oil flow to the bearings, pph
2. Oil temperature in and out, °F } (test bearing)
3. Oil pressure in and out, psig }
4. Bearing cavity pressure, psig
5. Bearing cavity temperature, °F
6. Air temperature, °F } (outside test bearing package)
7. Air pressure, psig }
8. Inner and outer race temperatures, °F
9. Axial load, lb
10. Radial load, lb
11. Shaft speed, rpm
12. Vibration level (at test bearing housing)
13. Chip detection
14. Cage speed, rpm

The special instrumentation package for measuring retainer data was cantilevered off the rig housing (Figure 26). The retainer drives the instrumentation package, which consists of a multiplexer and mercury slip rings. The multiplexer bearings are oil mist lubricated and air cooled. The mercury slip ring bearings are self-contained and grease packed.

A schematic of the test rig facilities is shown in Figure 31. Typical data sheets are shown in Figure 32.

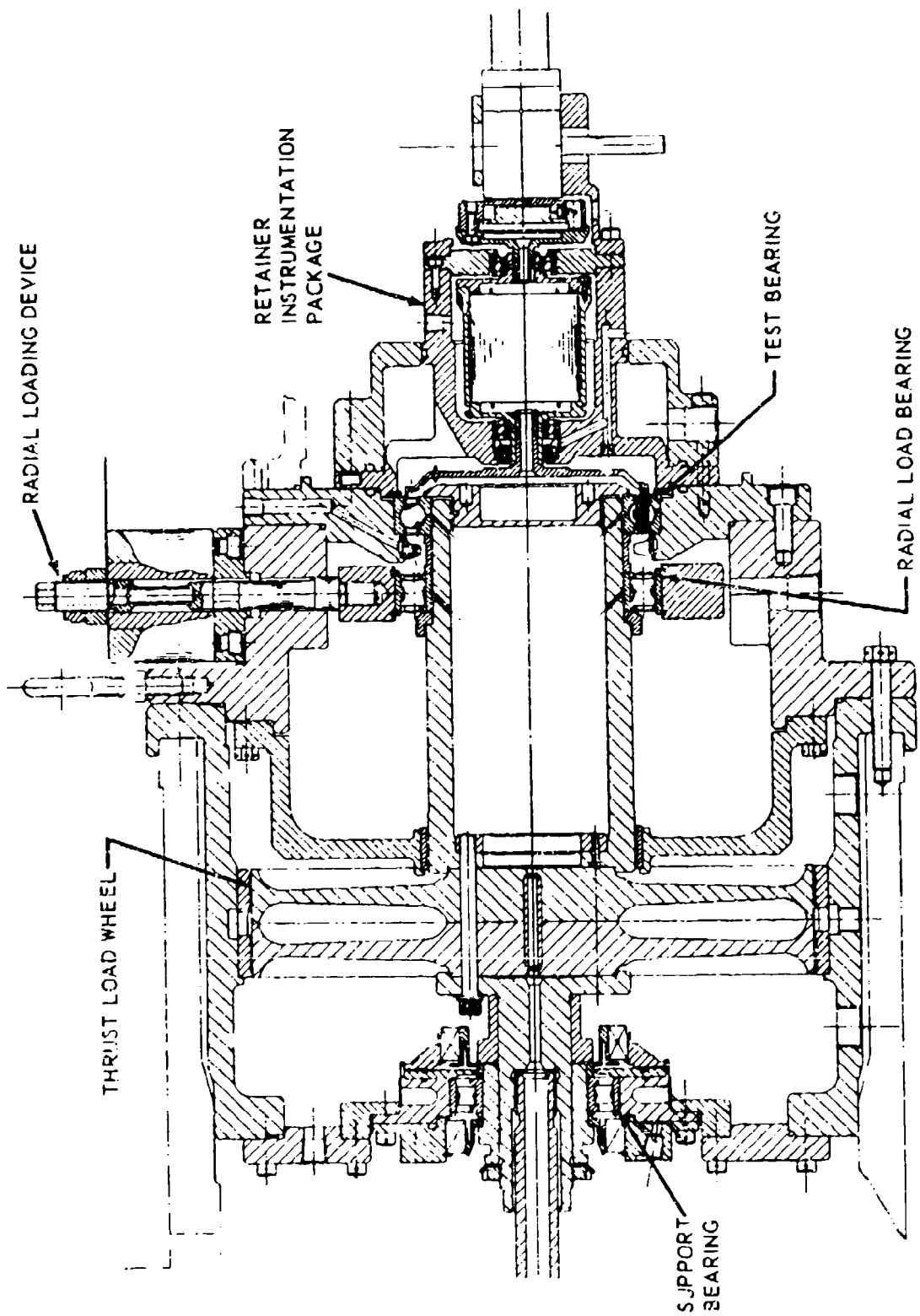


Figure 26. Bearing Test Rig; Cross-Sectional View.

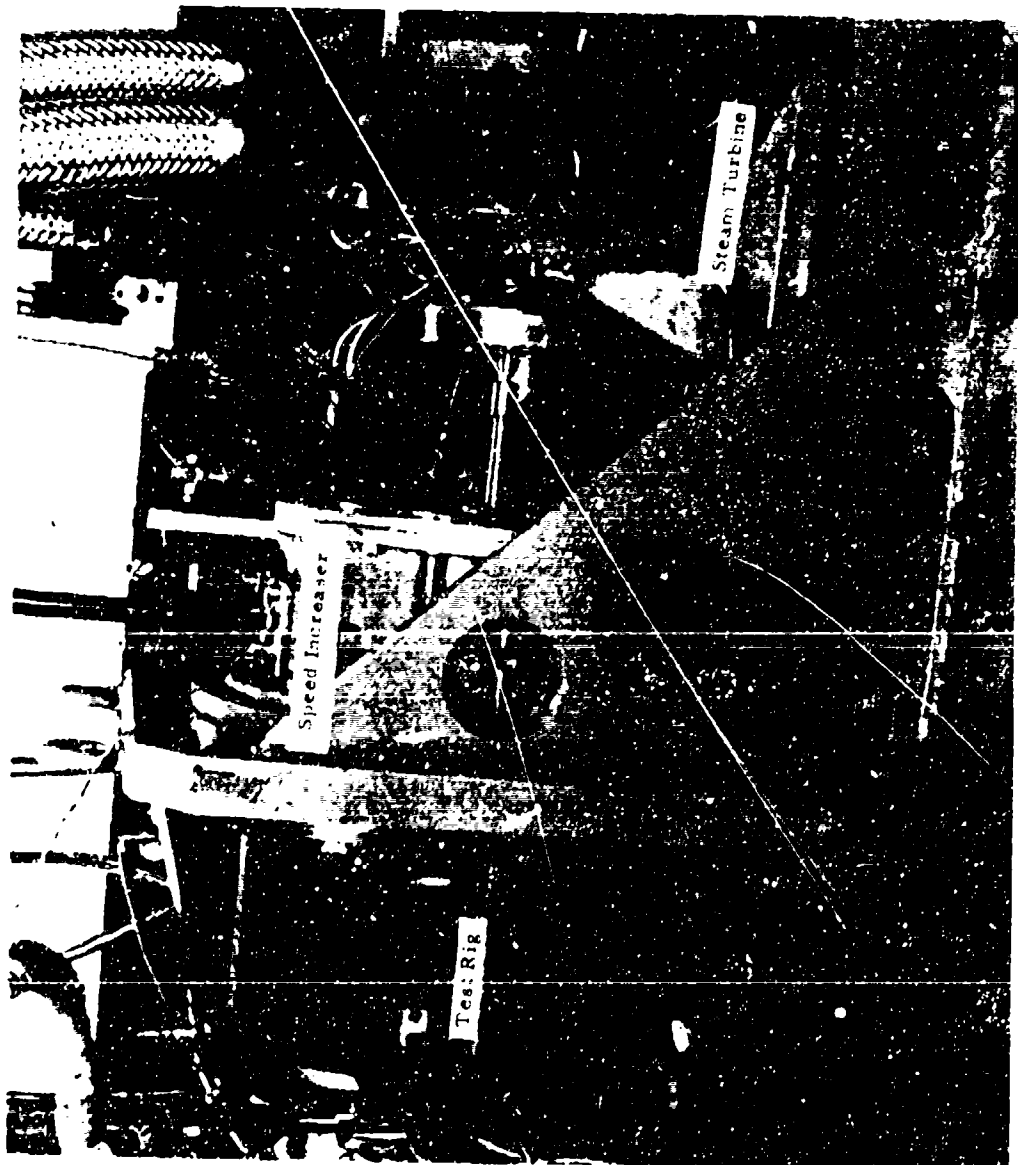


Figure 27. Bearing Test Facility.



Figure 28. Bearing Test Rig; Right Front View.

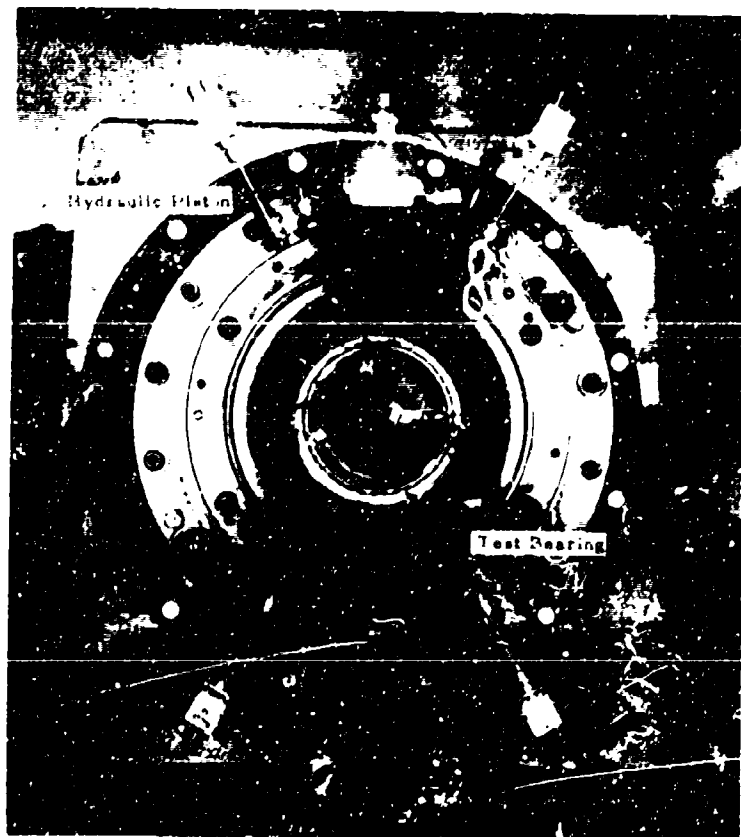


Figure 29. Bearing Test Rig; Front View.

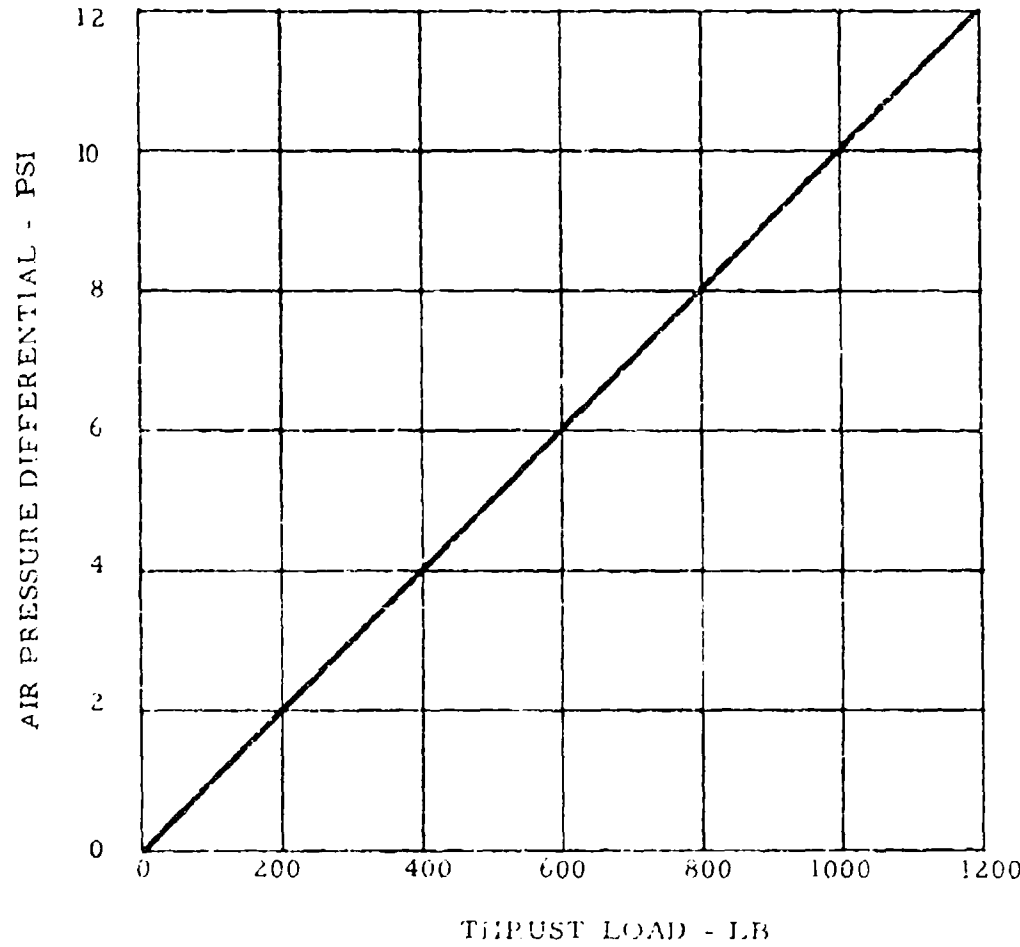


Figure 30. Air Pressure Differential Versus Bearing Thrust Load.

**TABLE V. PHYSICAL PROPERTIES OF MIL-L-23699 OIL,  
CODE 0-64-2**

**MATERIAL EXAMINATION REPORT**

MATERIALS LABORATORY

0-64-2

AVCO LYCOMING DIVISION

Lab No. \_\_\_\_\_

Lot No. \_\_\_\_\_

P.O. \_\_\_\_\_ R.R. \_\_\_\_\_ Quantity 1 qt Date 4/28/70

Batch No. \_\_\_\_\_ Mfr's Dsgn. \_\_\_\_\_ Date of Synthesis \_\_\_\_\_

Specification MIL-L-23699 Vendor \_\_\_\_\_

From \_\_\_\_\_ Condition \_\_\_\_\_

TEST	REQUIREMENTS	VENDOR	LYCOMING	DISP.
Viscosity at 100°	25 cs min		27.71	Accept
Viscosity at 210° F	5.0 to 5.5 cs		5.91	Reject
Flash Point, min	450° F		490	See Note
Pour Point, max	-65° F		L-65	
Evap. Loss, 400° F / 6 hr	10% max by wt		8.3	
Color, ASTM	Report		3	
Foam, max, 75° F	Volume/collapse			
200° F	25 ml/1 minute		15/45 sec	
75° F after 200° F	25 ml/1 minute		5/4 sec	
25 ml/1 minute			10/20 sec	
Visual	Transparent, Uniform No sediment, etc.		Clear	
Neutralization No.	0.50 max		.12	
"F" Rubber Swell, % 400° F/72 hr	+10 to +25		23.5	
Cracking Under Tension	None		None	
Trace Sediment	,005 ml		<.005	

By \_\_\_\_\_ Date 5/25/70

NOTE: Infrared indicates material to be similar to Mobil Jet II

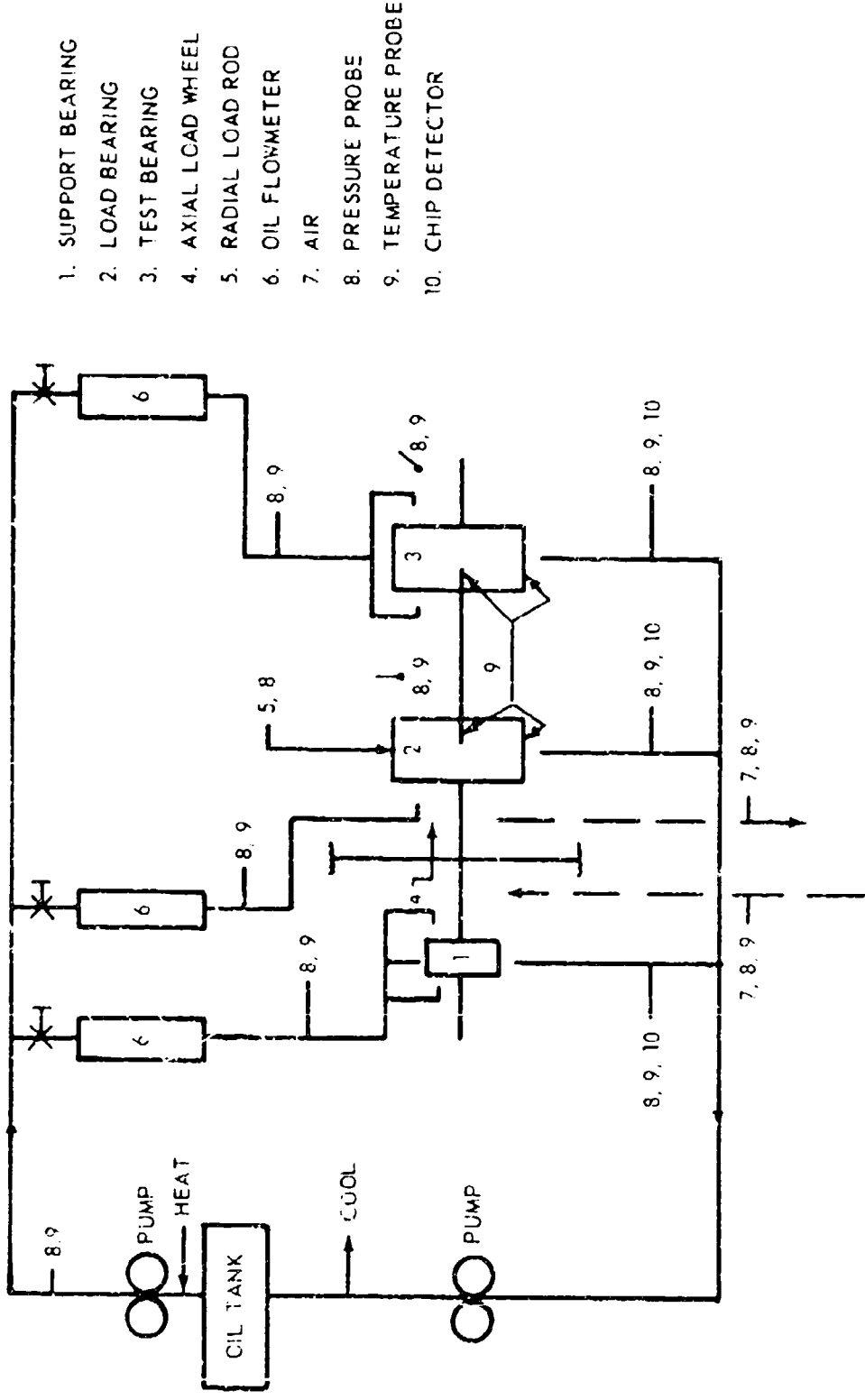


Figure 31. Test Rig Facilities; Schematic Diagram.

ENGINE N/A		CONFIGURATION Ball Brg		CONTRACT		DATE		TEST CELL 4	
TEST TITLE Bearing Retainer Analysis		Test Rig		OPERATOR		OBSERVER			
RUN NO.	TIME	Temperature		Oil		Oil			
		In	Out	Test	Sup	In	Out	Roller	Brg
		Brg	C. B.	Brg	Brg	Brg	Brg	Brg	Brg
		Output	Oil	Test	Rig	Oil	Oil	Oil	Oil
		C. B.	Out	Test	Retainer	Temp	Temp	Temp	Temp
		In	In	Retainer	Retainer	Retainer	Retainer	Retainer	Retainer
1									
2									
3									

ENGINE N/A		CONFIGURATION Ball Brg		CONTRACT		DATE		TEST CELL 4	
TEST TITLE Bearing Retainer Analysis		Test Rig		OPERATOR		OBSERVER			
RUN NO.	TIME	Pressure		Oil		Oil			
		Air	Gear Box	Oil In	Oil Out	Fwd Wheel	Aft Wheel	Vib. Turb	Vib. G. B.
		Mist	Mist	Test Oil	Test Oil	Thrust Brdg	Thrust Brdg	Dis/	Dis/
		Cav	Multi Sup	Brdg	Brdg	Load Press	Load Press	Vel	Vel
		Press	Plexe	19	20	23	24	25	26
		18	17						
1									
2									
3									

Figure 32. Typical Data Sheets.

## TEST BEARING DESCRIPTION

### Ball Bearings

The ball bearings used for the test program are typical of main shaft thrust bearing designs of aircraft gas turbine engines. The bearing design is of an angular contact, split inner ring configuration with a one-piece, machined, outer-land-piloted retainer. Complete design details are given in Figure 33 (PSK 18123). Some modifications to the test bearing were made to obtain desired inner and outer race surface texture.

One test bearing, S/N 003, was reworked to produce a race surface roughness of 5AA maximum; another, S/N 006, was reworked to produce a race surface roughness of 24AA maximum. This rework was done in order to evaluate the effect of surface texture/EHD film interaction upon bearing performance. Calculations indicate that the film thickness-to-composite surface roughness factor for the 5AA finish bearing at 100° F oil-in temperature and 20,000 rpm is greater than 4.0, and consequently the bearing would operate with full film separation of the contacting surfaces. In contrast, the bearing with the 24AA surface finish would have a film thickness-to-composite surface finish factor of less than 1.0 at 200° F oil-in and 20,000 rpm, and it should operate without full film lubrication, i.e., with boundary lubrication.

Modifications to the retainer were also required to facilitate the placement of strain gages for pocket load measurements. Undercuts were machined into three adjacent pockets as indicated in Figure 34 (PSK 17438). The undercuts provide a recess in the pocket to prevent contact of the strain gages with the ball, and also increase the flexibility of the cross beam section to produce measurable strain levels for load measurements under the anticipated force levels.

A complete pretest dimensional inspection of the test bearings was performed on critical dimensions and characteristics. Clearances, surface textures, groove radii, race runouts, etc., were measured and recorded, and are presented in Table VI and Figures 35 through 42.

### Roller Bearings

The roller bearings employed for the test program are also typical of main shaft gas turbine designs. The bearings incorporate cylindrical rollers in a one-piece, machined retainer that is piloted on inner ring shoulders. Bearing details are presented in Table VII.

Test retainer modifications similar to the ball bearing retainer modifications were required to provide for strain gage placement and suitable beam flexibility to facilitate measurement of the pocket loads, as depicted in Figure 43. Here, also, a complete pretest dimensional inspection was performed on the critical characteristics of the bearing. Results are presented in Figures 44 through 47.

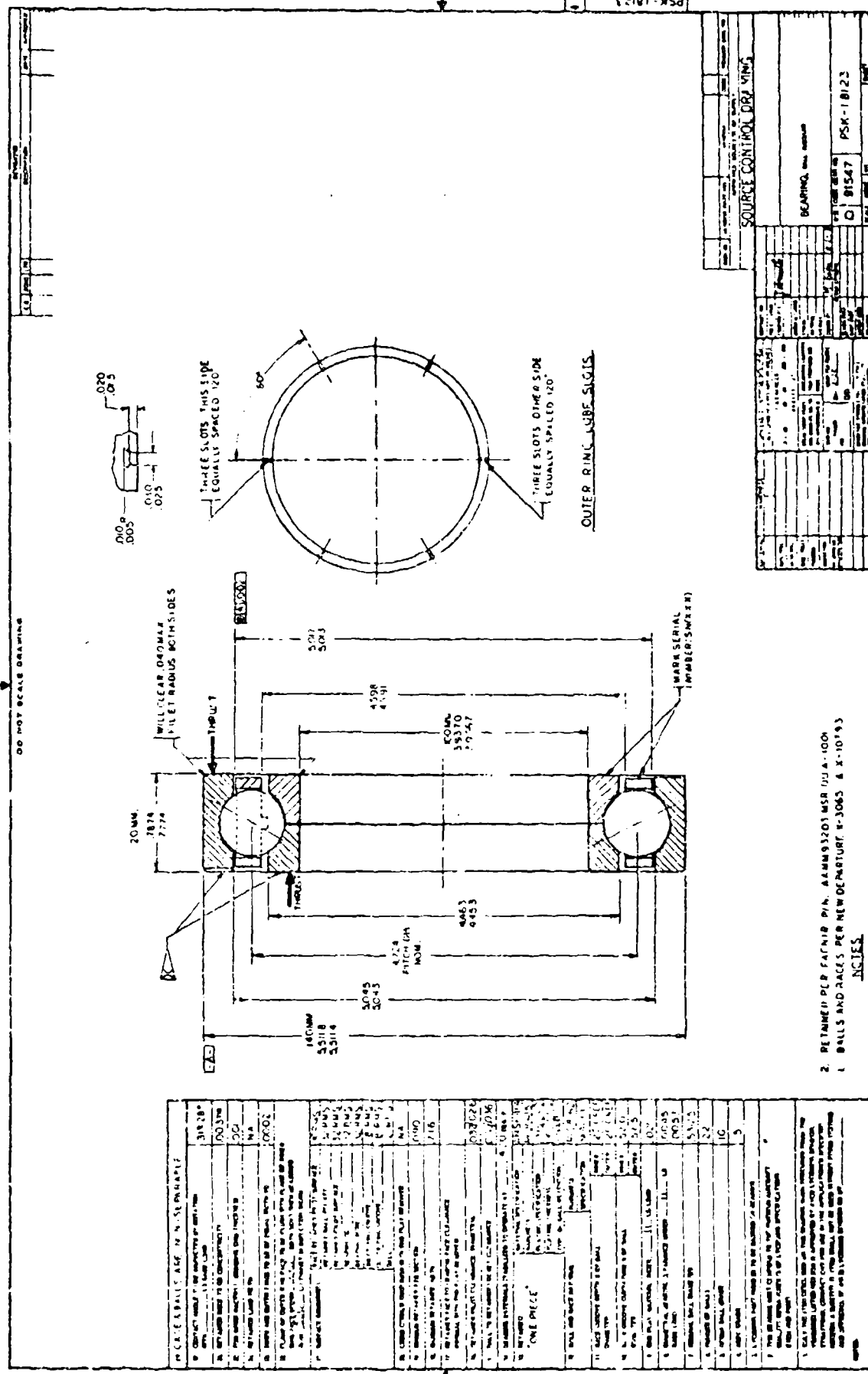
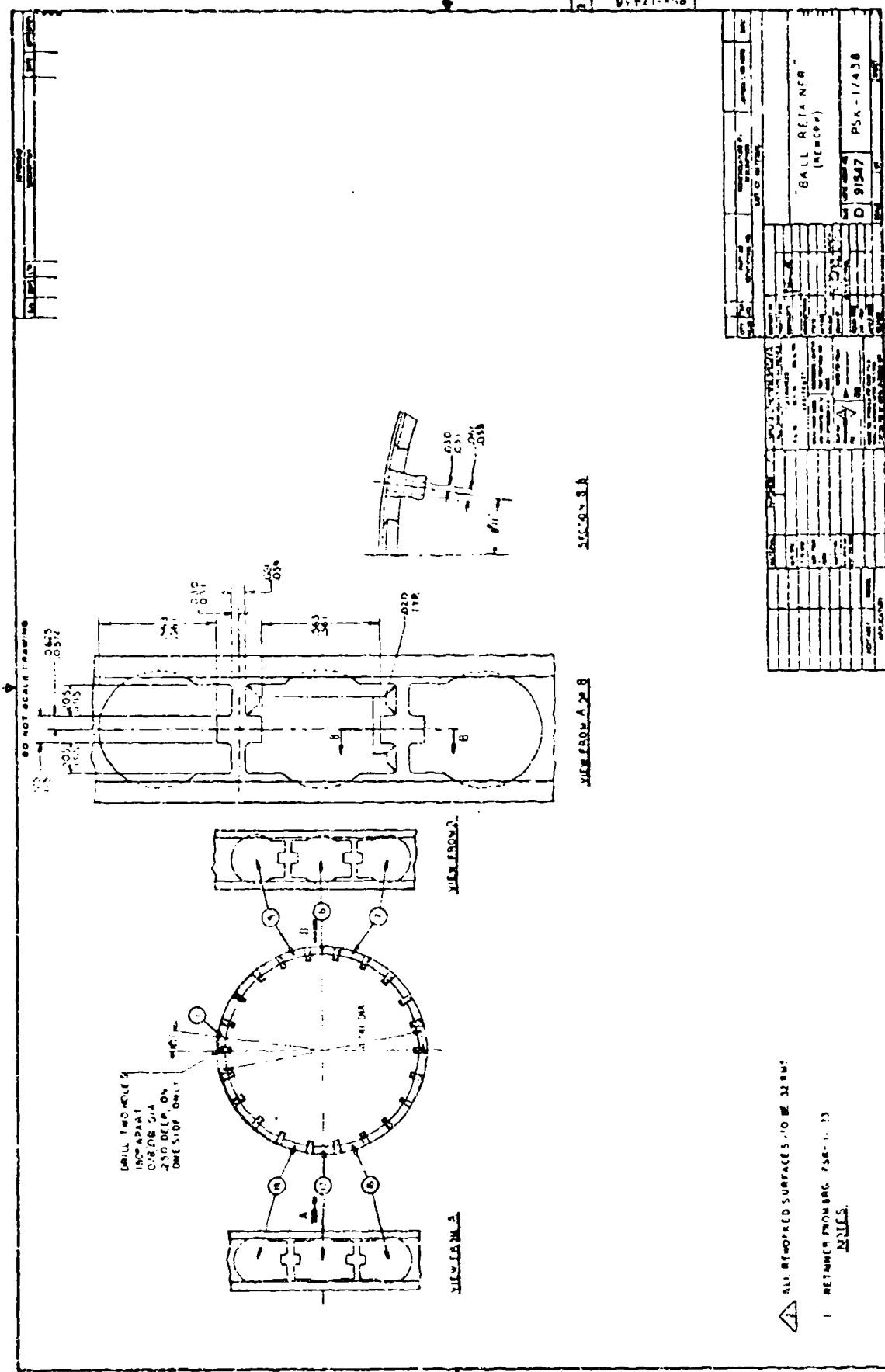


Figure 33: Ball Bearing P5K 13123.



**Figure 34:** Ball Retainer Rework ISK 17438.

Preceding page blank

TABLE VI. TEST BALL BEARING INSPECTION DATA,  
DETAIL INTERNAL GEOMETRY

	Bearing S/N	
	003	006
Outside Diameter (in.)	5.5110/5.5109	5.51163/5.51162
Inside Diameter (in.)	.9360/3.93596	3.9366, 3.93665
Ball Diameter (in.)	.53105	.53103
Inner Race Finish (AA)	4-5	30-35
Outer Race Finish (AA)	4-5	24
Ball Finish (AA)	2	2.5
Internal Clearance (in.)	.0050	.0045
Inner Race Groove Radius (thrust)	.2728	.27676
Outer Race Groove Radius	.2728	.2753
Inner Race Groove Radius (nonthrust)	.2741	.27676

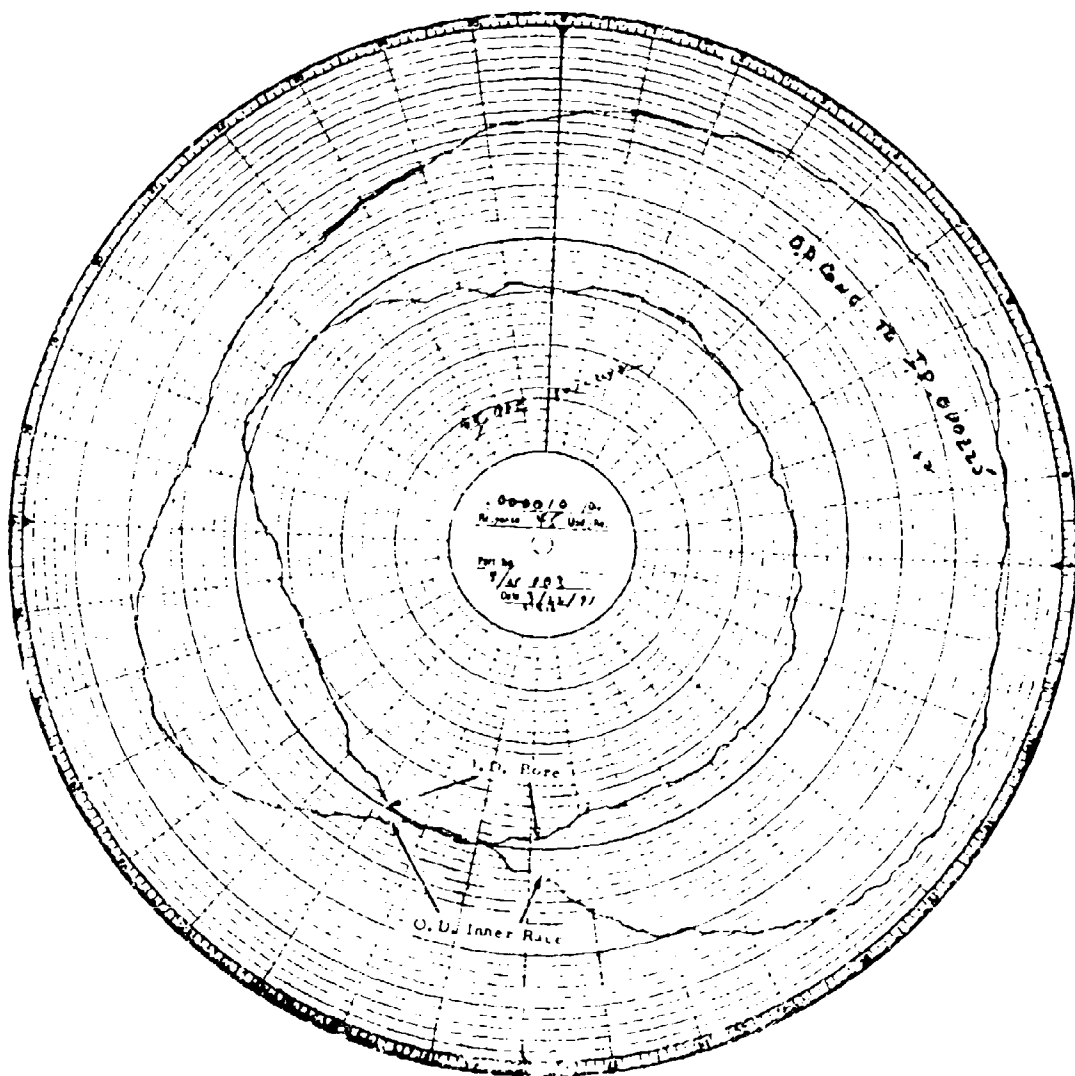


Figure 35. Ball Bearing S/N 003 Inner Race Roundness and Concentricity.

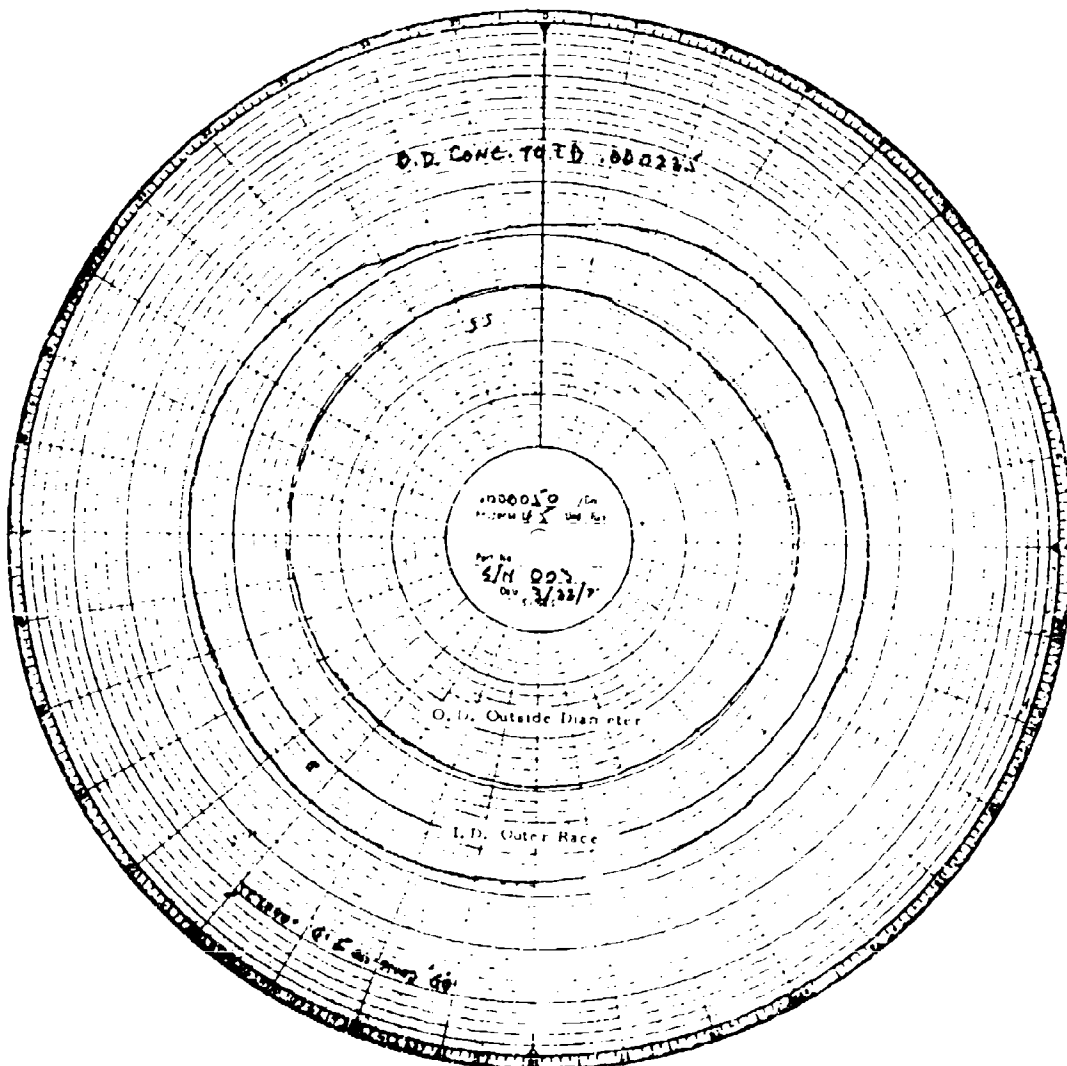


Figure 36. Ball Bearing S/N 003 Outer Race Roundness  
and Concentricity.

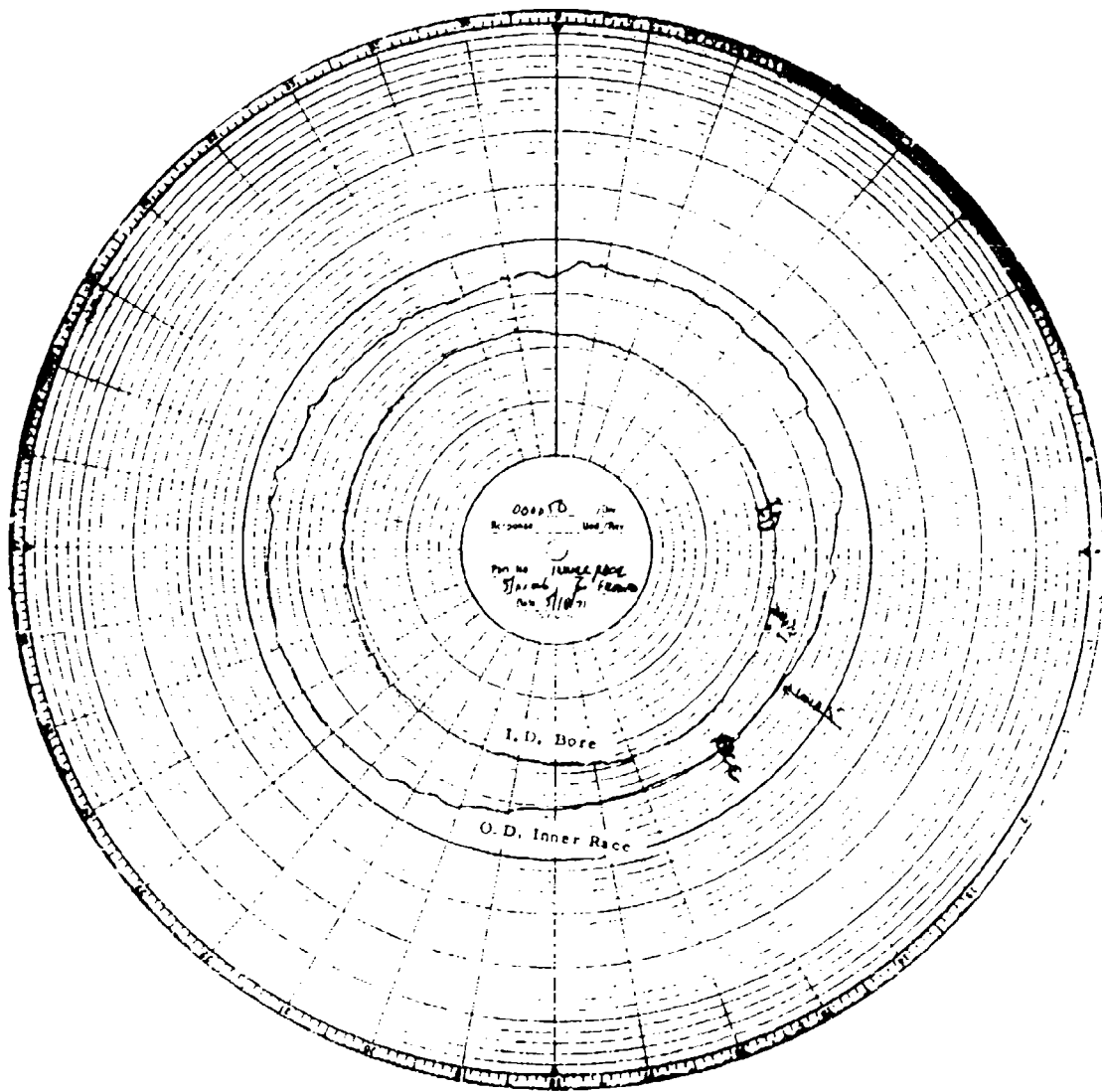


Figure 37. Ball Bearing S/N 006 Inner Race Roundness and Concentricity.

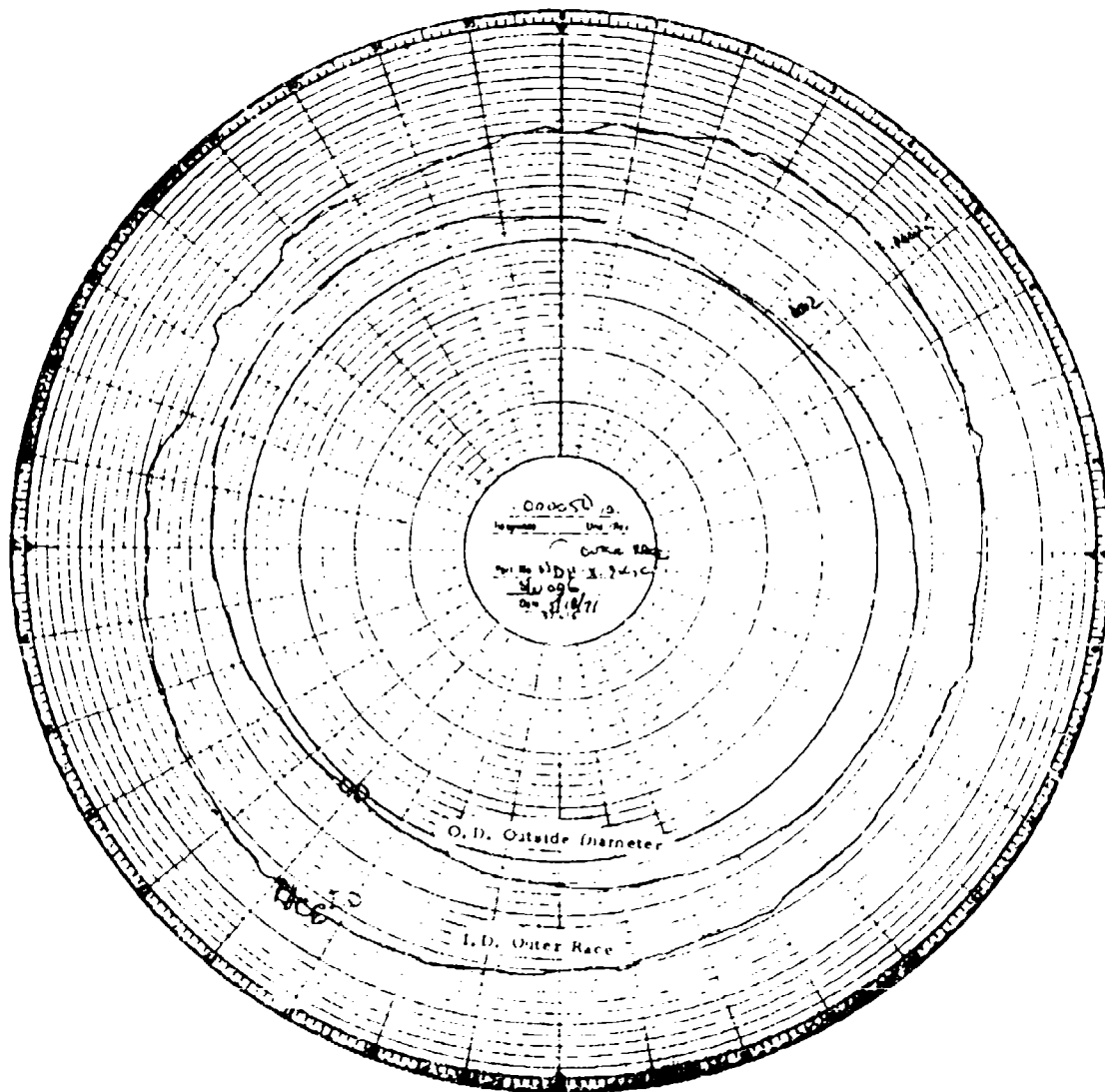


Figure 38. Ball Bearing S/N 006 Outer Race Roundness and Concentricity.

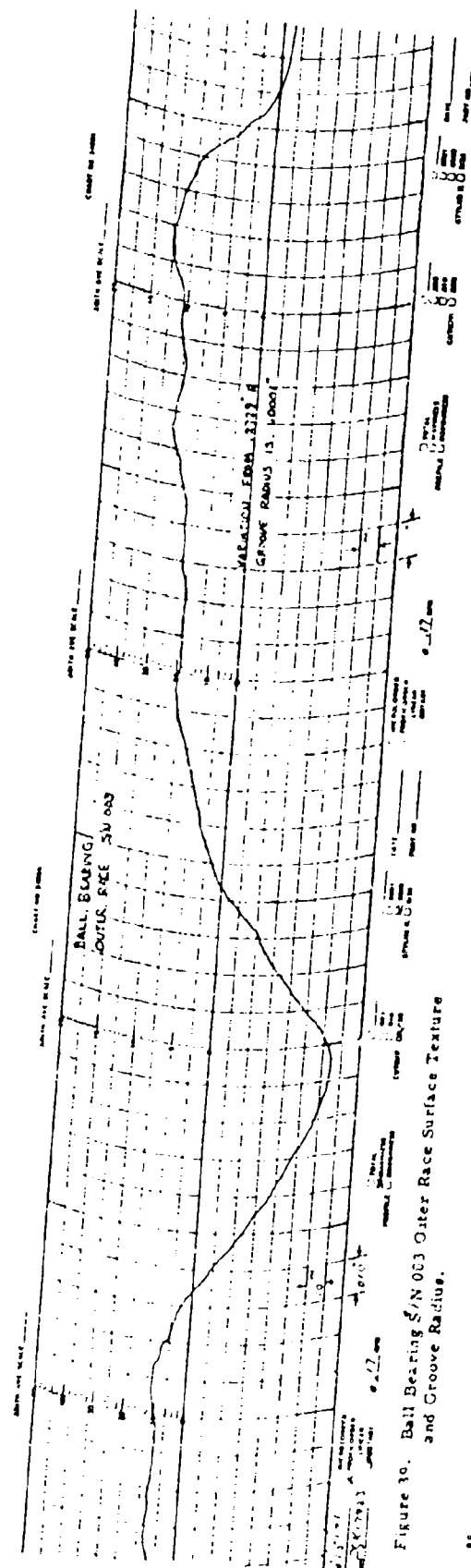
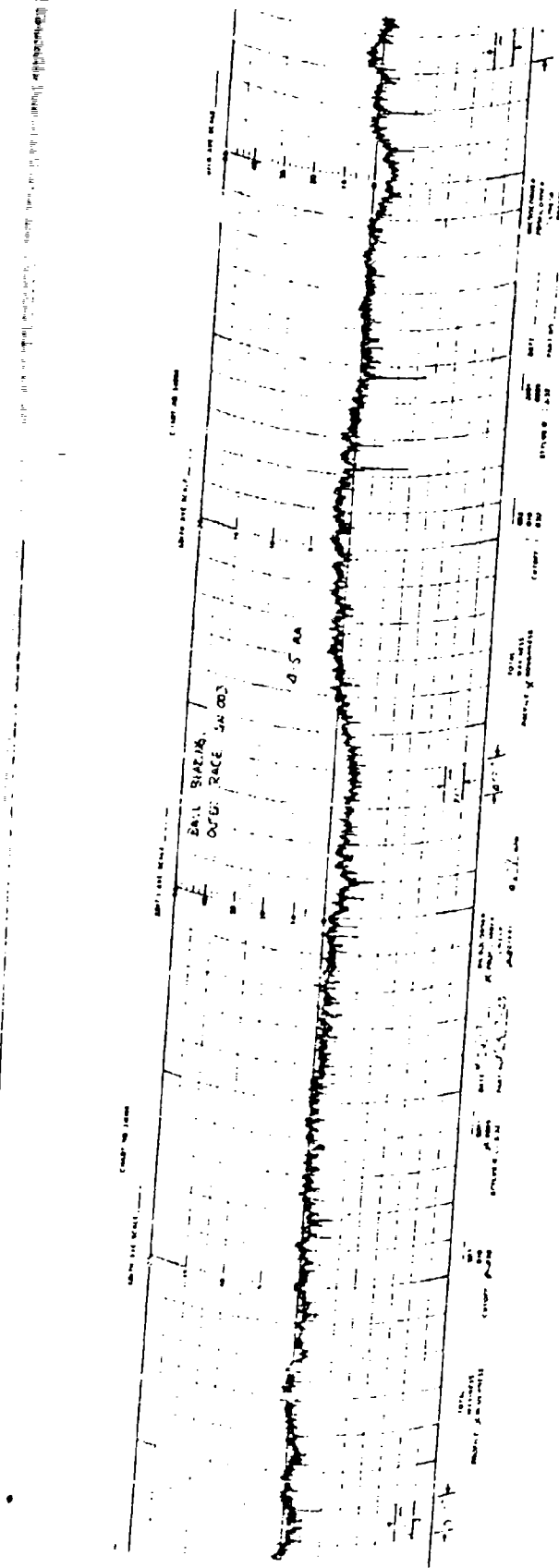


Figure 10. Ball Bearing S/N 003 Outer Race Surface Texture  
and Groove Radius.

Preceding page blank 1G5

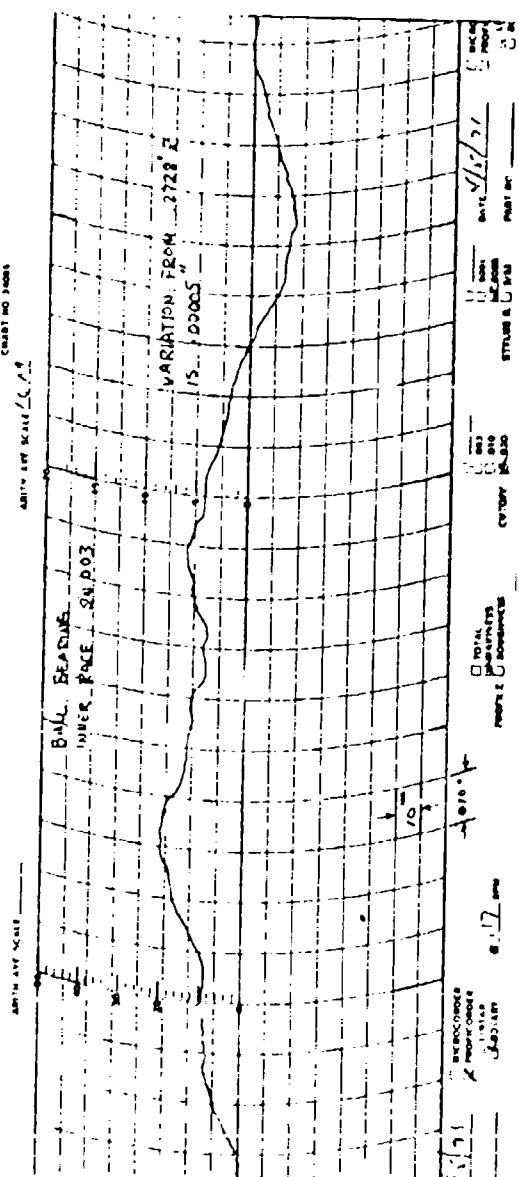
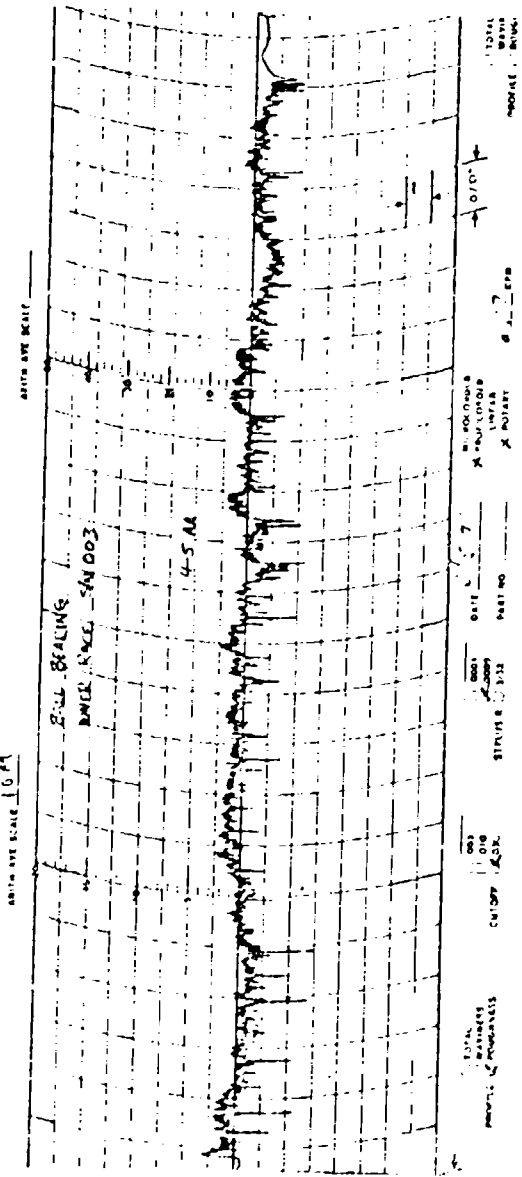


Figure 40. Ball Bearing S/N 003 Thrust Inner Race Surface Texture and Groove Radius.

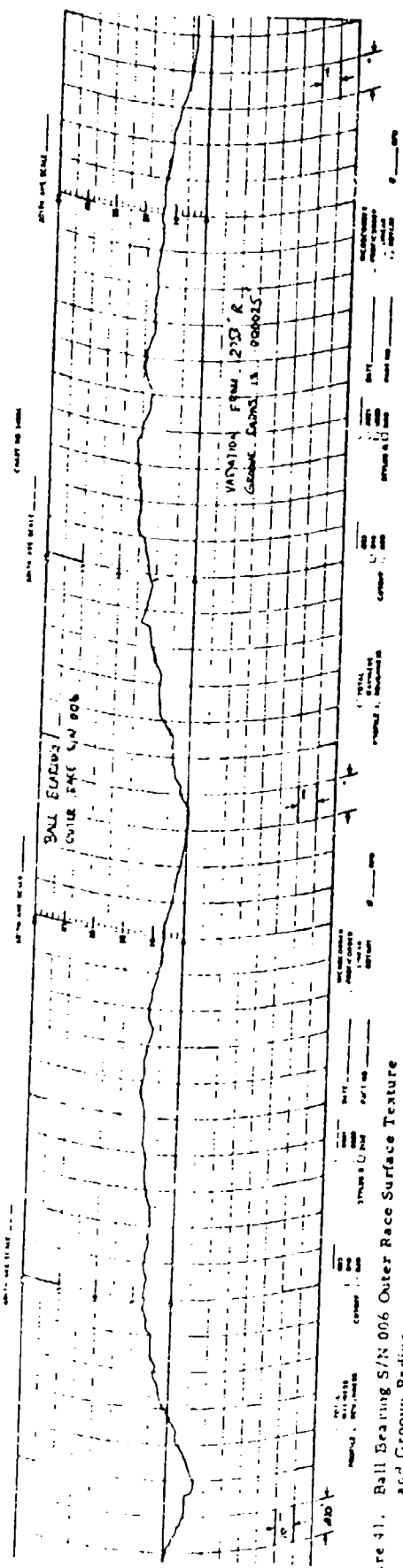
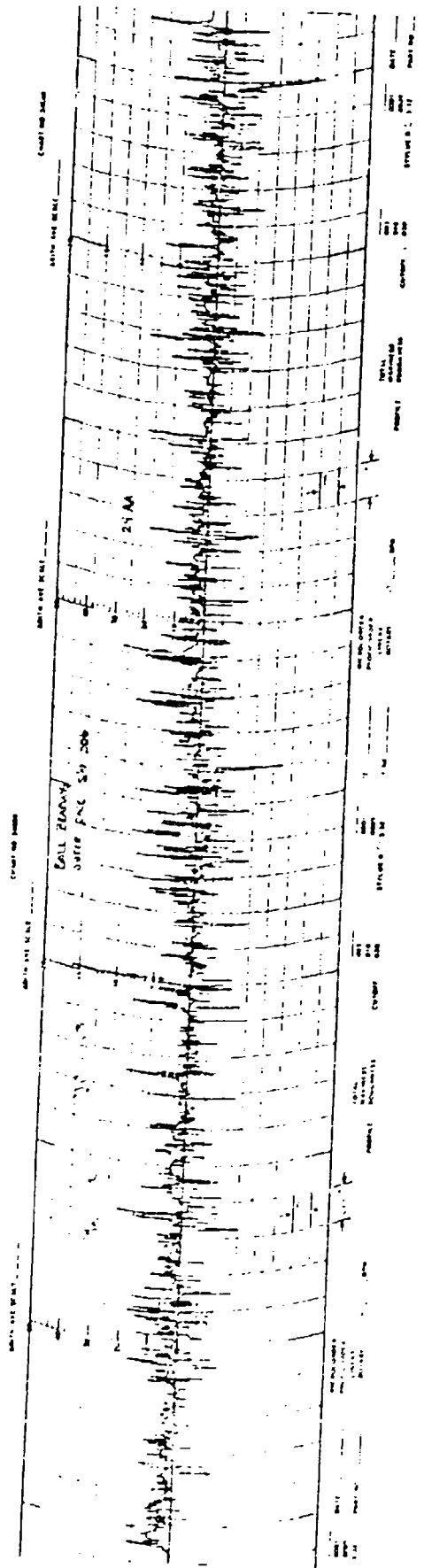


Figure 4. Ball Bearing S/N 006 Outer Race Surface Texture and Groove Radius.

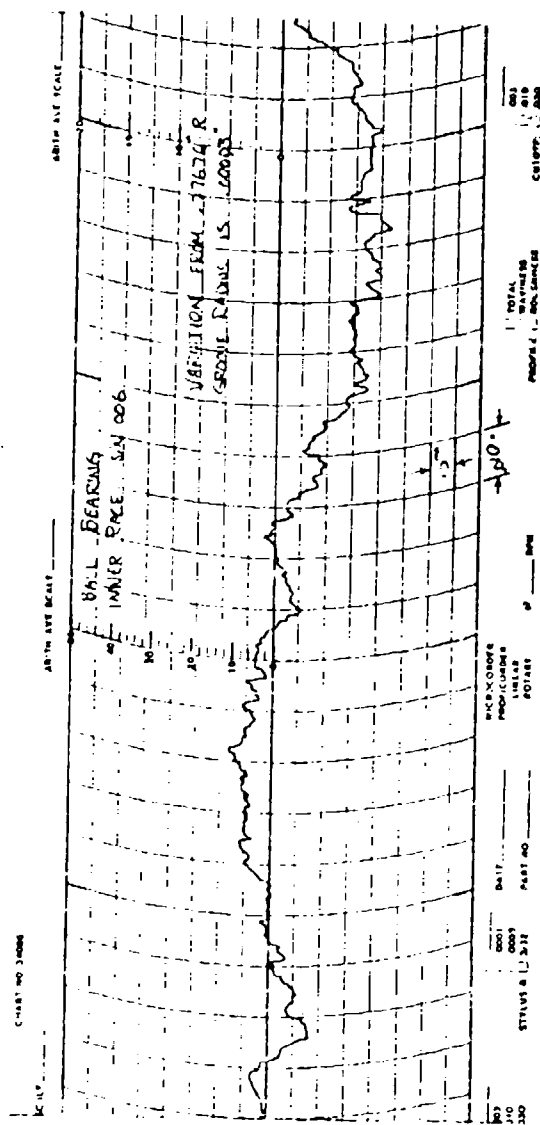
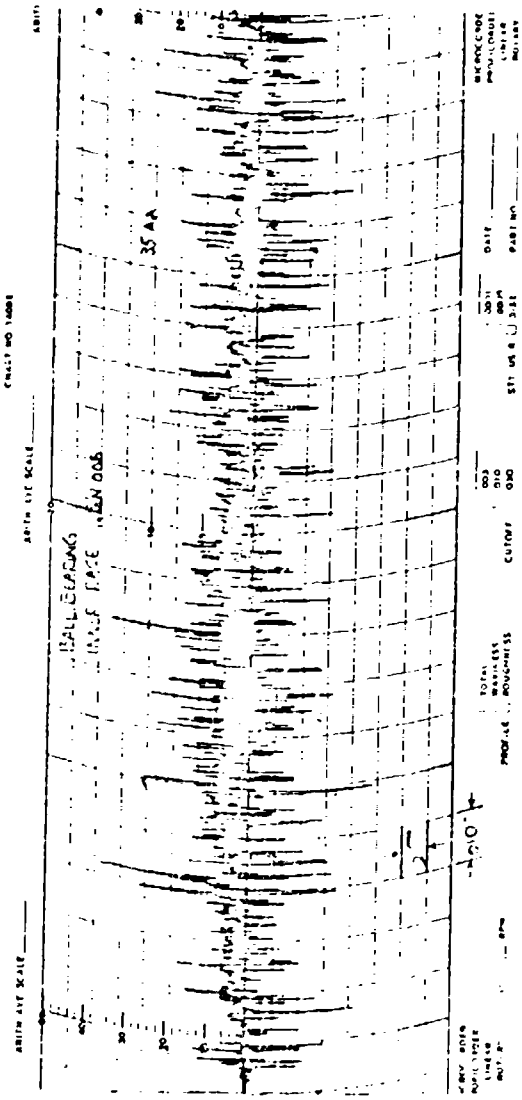


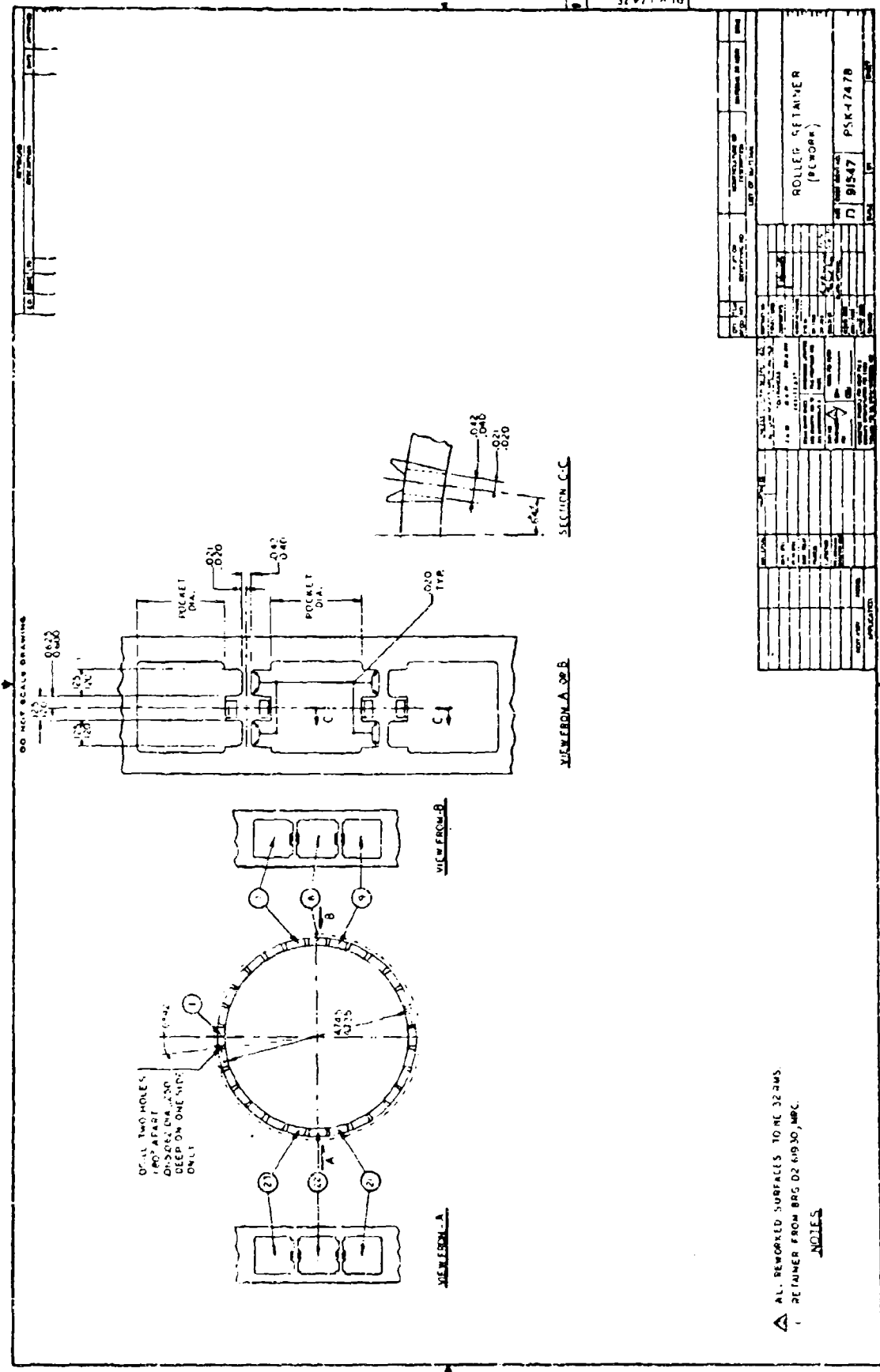
Figure 42. Ball Bearing S/N 006 Thrust Inner Race Surface Texture and Groove Radius.

TABLE VI. ROLLER BEARING ENGINEERING DATA

Lycoming Identification	MRC R-19 ZO-C
Bearing Application	Test Rig
Bearing Type	Straight Thru Outer
RBCG Grade	5
Bearing to Conform to Lycoming Specifications	P6903, E-1004
Bore	100 MM
Outside Diameter	140 MM
Width	20 MM
Number of Rollers	28
Roller Diameter	11 MM = .4331
Roller Length	11 MM = .4331
Roller Pitch Diameter	4.7244 Ref.
Roller Diameter Variation	$\pm .000025$
Roller Length Variation	$\pm .0001$
Roller End Radius	.030/.040
Roller Crown Radius	35.0
Roller Flat length	.144/.271
Roller Ends Square to Outside Diameter	.0001
Parallelism of Roller Active Surface	.000050
Diametral Clearance under 11-lb cage load	.0055
Inner Ring Shoulder Height, $\frac{1}{8}$ of Roller Diameter	22%
Outer Ring Shoulder Height, $\frac{1}{8}$ of Roller Diameter	NA
Inner Ring Shoulder Diameter	4.475/4.469
Outer Ring Shoulder Diameter	NA
Cross Corner Dimension	NA
Roller in Shoulders End Play	.0005
Raceway Surface Finish	6RMS
Roller Diameter Surface Finish	3RMS
Roller Ends Surface Finish	3RMS
Ring Pilot Surface Finish	16RMS
Retainer Pilot Surface Finish	20RMS

TABLE VII - Continued

Roller and Ring Material	SAE 52100 Steel
Roller and Ring Hardness	R <sub>c</sub> 58-62
Retsiner Material	Bronze
Retainer Hardness	
Retainer Plating	AMS 2412
Retainer Plating Thickness	.0005/.0015
Material Stabilized to Operate at	-65° to +350° F
Pilot Surface	Inner
Pilot Clearance (Total Diametral)	.025 - .035
Roller Axial Pocket Clearance	.010/.015
Roller Circumferential Pocket Clearance	.007/.012
Minimum Retainer Pocket Corner Radii	
Retainer Face to Bearing Face Clearance, Min. End Play Removed	
Roller Pocket Location in Retainer - Axially	.001 min
Roller Pocket Location in Retainer - Circumferentially	
Minimum Retainer Web Section	
Minimum Retainer Land Width	
Retainer Pilot Surface Runout	
Retainer O.D. to Bore Concentricity	
Type of Retention	SnapIn Type
Max/Min Diameter Over/Under Roller	
Minimum Roller Drop	.035 max
Runout of Outer Ring Shoulder Diameter	
Runout of Inner Ring Shoulder Diameter	
Note: Cage, Inner Race and Rollers are Nonseparable.	



**Figure 43.** Roller Retainer Rework PSK 17478.

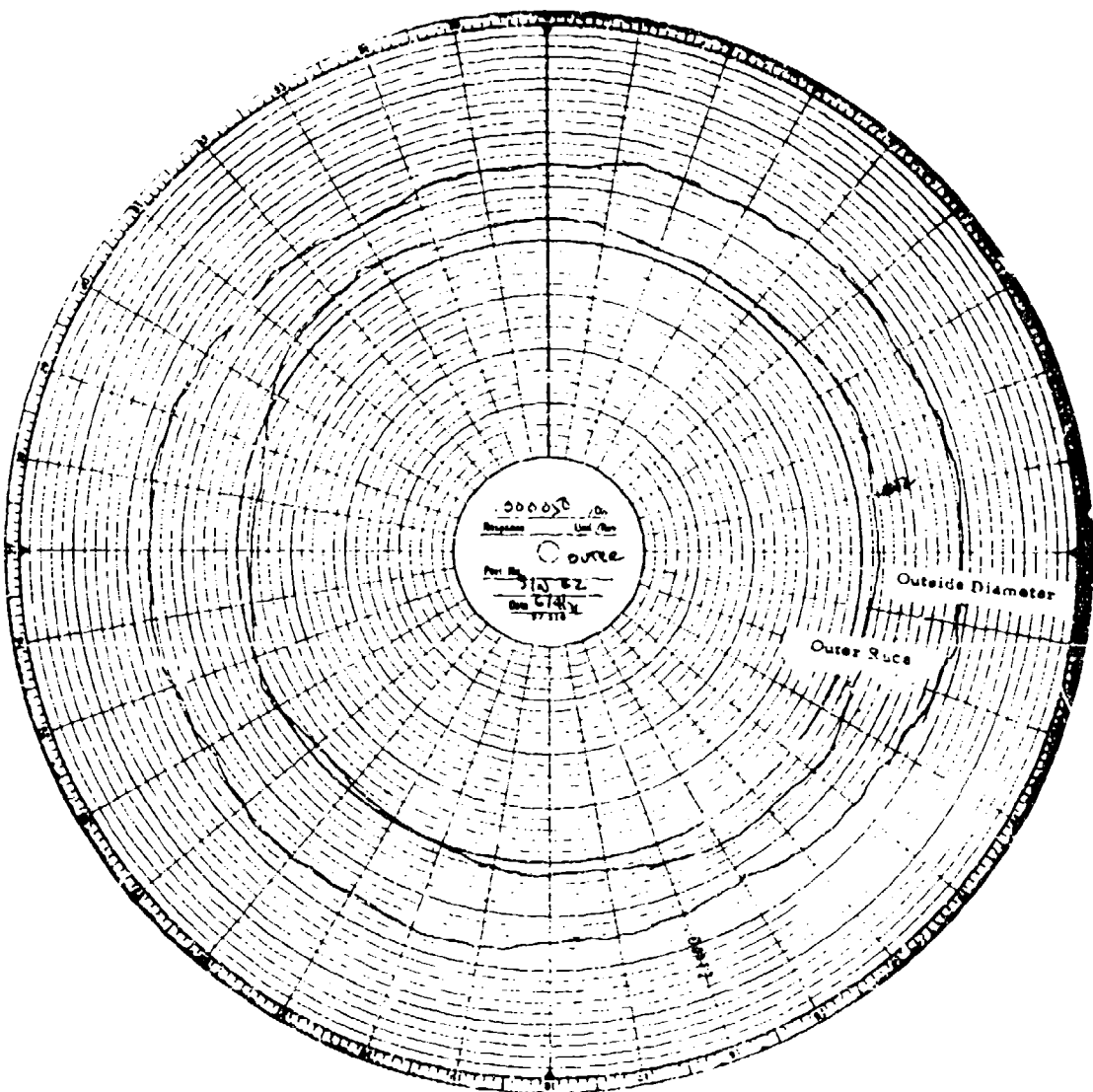


Figure 44. Roller Bearing Outer Ring Roundness and Concentricity.

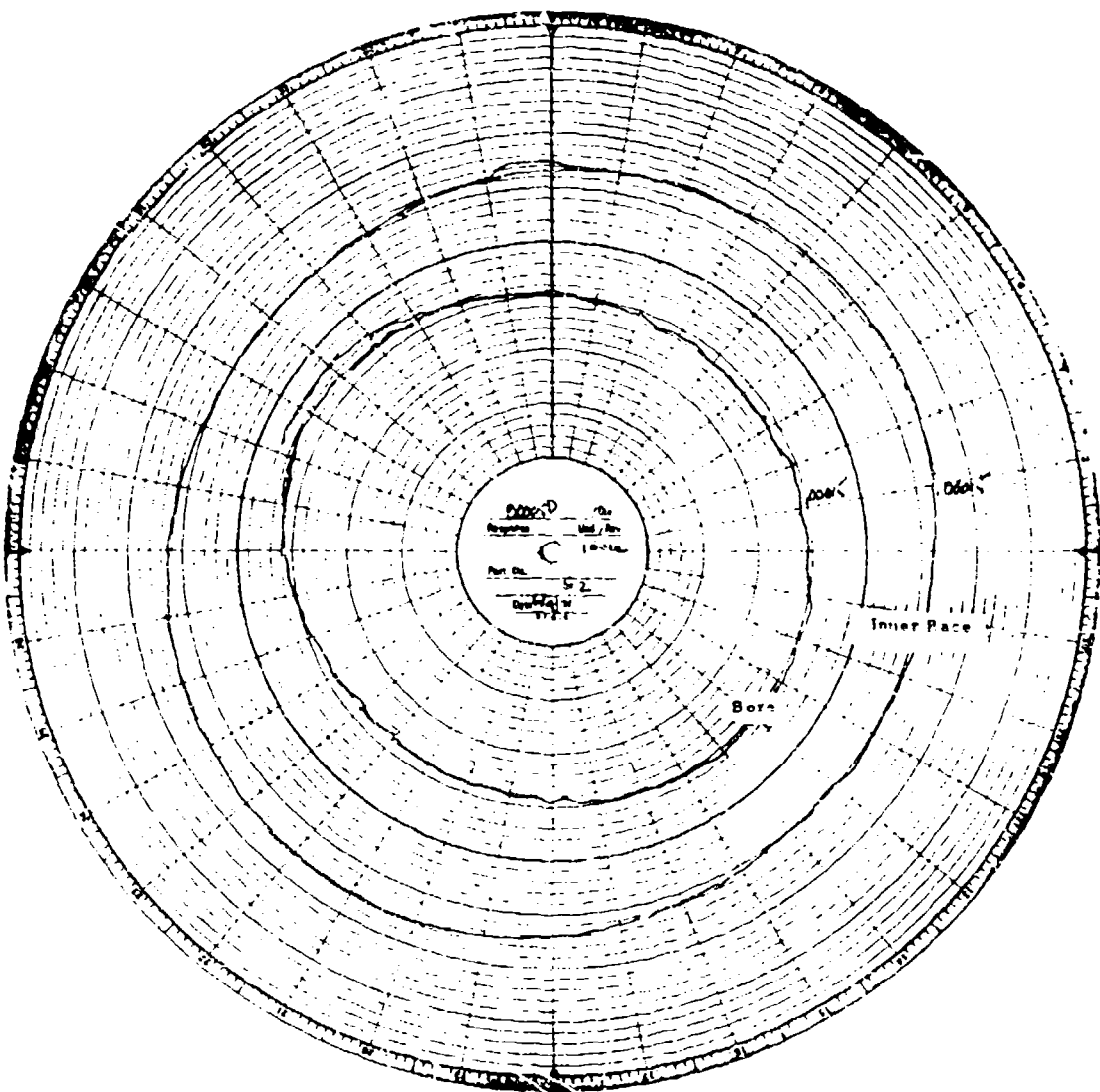


Figure 45. Roller Bearing Inner Ring Roundness and Concentricity.

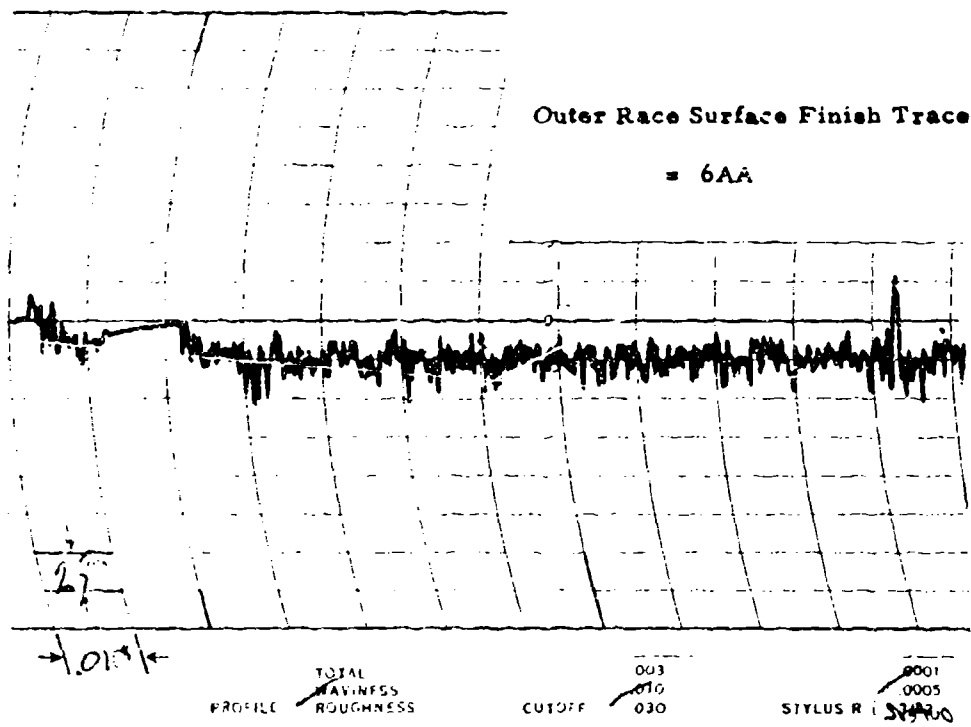


Figure 40. Roller Bearing Outer Race Surface Finish.

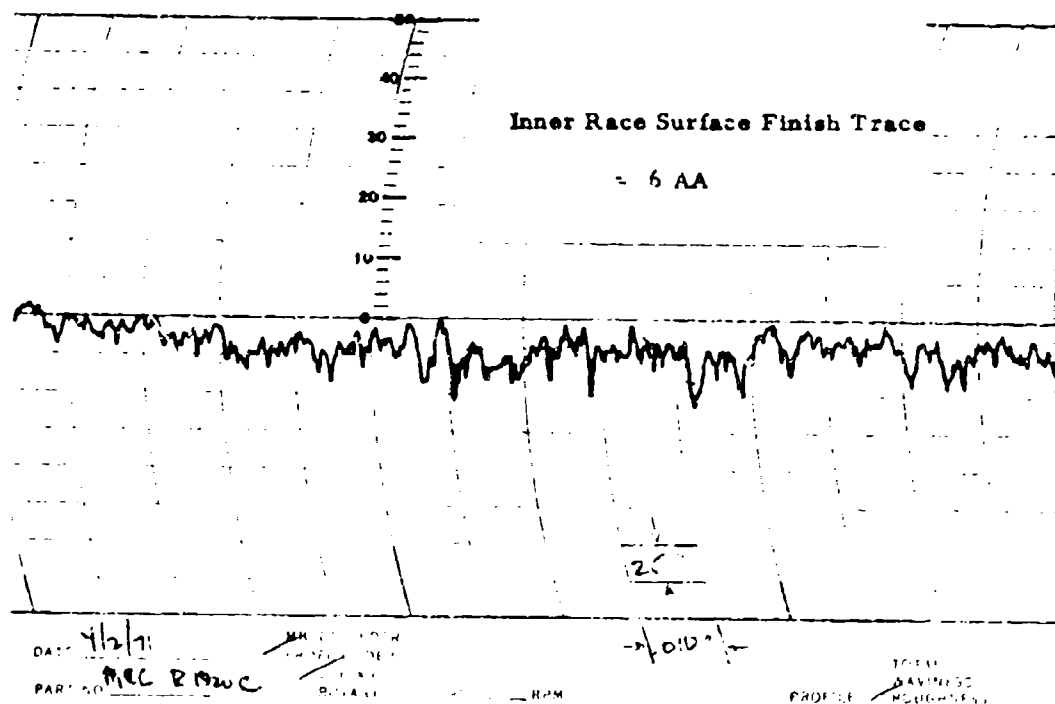


Figure 47. Roller Bearing Inner Race Surface Finish.

## INSTRUMENTATION

Instrumentation was incorporated in the bearing retainer test vehicle (F/N TE 21869), Figure 48, to measure the following key parameters:

1. Inner race temperature - °F
2. Outer race temperature - °F
3. Bearing retainer speed - rpm
4. Inner race speed - rpm
5. Radial load on bearing - lb
6. Force exerted by ball/roller on the bearing retainer pocket - lb
7. Ball attitude and three-axis rotational velocity (ball bearing test only)
8. Torque exerted on the retainer by slip ring drag and inertia - in.-lb
9. Bearing retainer and torque element temperature - °F

Items 1 through 7 were required to compare test results with the computer program output. Item 5 was a measurement duplication. Radial force was applied through a hydraulic ram with a known cross-sectional area with a known pressure. Item 7 was to provide an instantaneous ball attitude readout. Item 8 was to measure and divorce the effects of slip ring and associated hardware from the retainer data required by Item 6. Item 9 was to evaluate the effects of the retainer environment on Items 6 through 8.

A description of each item of instrumentation follows:

1. Inner Race Temperature - Inner race temperature measurement on both the bearing under study and the loading bearing was accomplished by embedding thermocouples in the shaft, which provided intimate contact between the thermocouples and the bearing inner race bore.
2. Outer Race Temperature - Outer race temperatures were measured using standard bayonet-type thermocouples in intimate contact with the outer race outer diameter.
3. Ball Retainer Speed - Speed was measured using a magnetic pickup sensing rotation of the slip ring shaft, which was directly coupled to the slip ring driving plate. The slip ring shaft was manufactured with five small lobes and one large lobe. This large lobe produced a magnetic pickup output greater than the other five. The angular relationship between the large lobe and the location of the instrumented

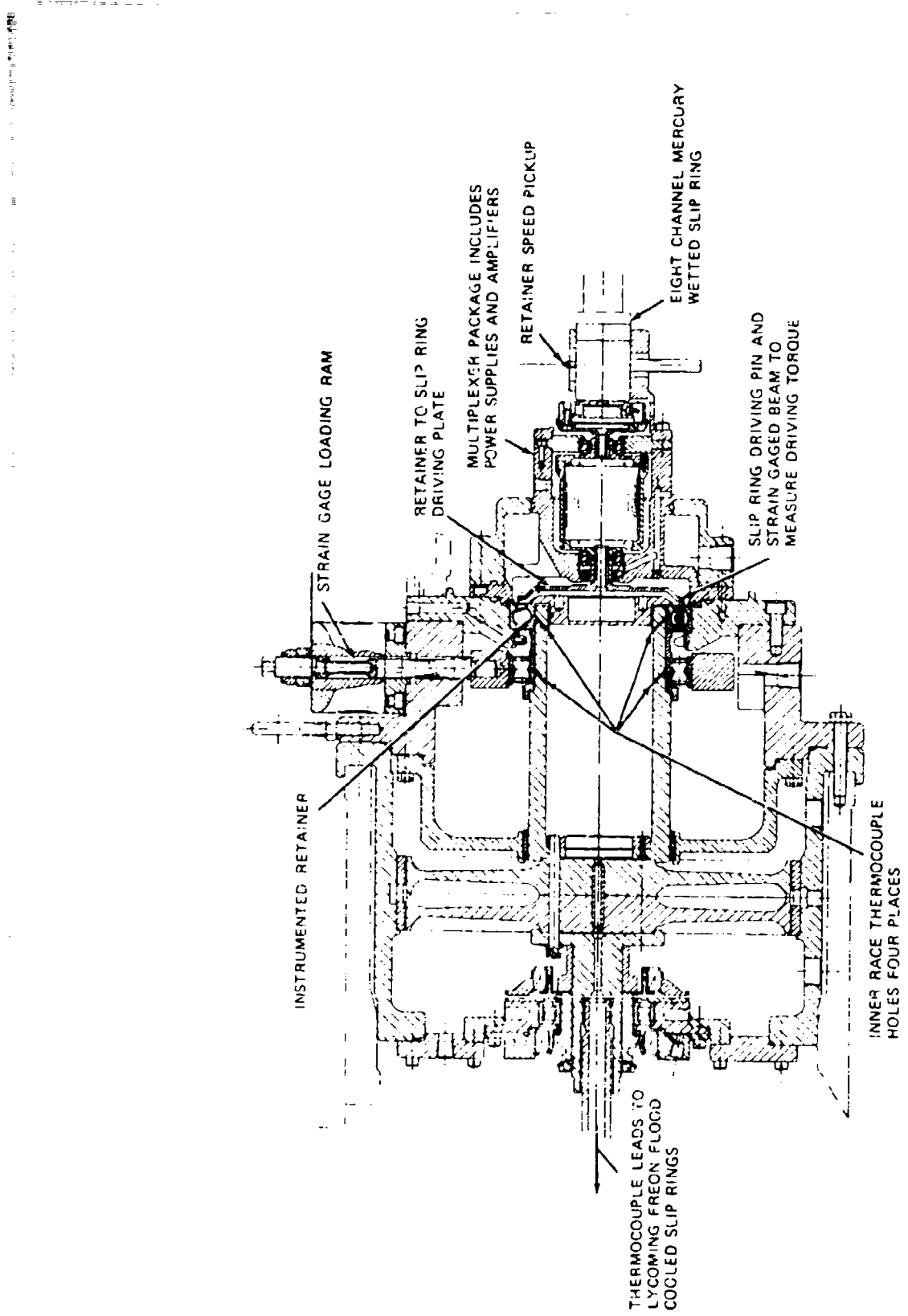


Figure 48. Instrumentation Location.

ball bearing pockets was known, as was the relationship between the stationary magnetic pickup and the point of application of the radial load. A means was thereby provided to relate the speed signal to the angular position of the retainer pockets under study and consequently the ball loading cycle. In the first tests, a strain gage was attached to the outer race to detect ball passing frequency, which is also a function of retainer speed.

4. Inner Race Speed - A magnet pickup was used to detect the speed of a gear directly coupled to the shaft supporting the rotating inner race.
5. Radial Load on Bearing - A hydraulic piston was used to apply radial loads to the bearing. The shaft between the piston loading bearing was instrumented with a four-active-arm strain-gage bridge and was deadweight calibrated. A pressure gage was installed in the line to the piston for cross checking the force on the loading bearing.
- 6a. Ball Force on Bearing Retainer - To measure the force exerted by the ball on the retainer web, two webs were reworked to accommodate the strain gages and increase the strain sensitivity. The two re-worked webs were strain gaged with two fully active four-arm bending bridges, Figure 49. The inside of the reworked web was chosen for strain gaging over the outside, as shown. A photoelastic model was used to determine the optimum location. The model showed the outside to be more cross sensitive to other cage loadings (i. e., a ball pushing axially on the cage would cause larger outputs at the outside of the web than at the inside). The strain gage bridges were calibrated. The first retainers were designed for a maximum strain sensitivity for a 50-pound ball load. At the time the retainer instrumentation was designed, accurate estimates of ball forces were not available, and 50 pounds was selected arbitrarily with the knowledge that the retainer could, if found too insensitive, be reworked and made more sensitive. Later retainers were modified for a maximum strain sensitivity at 25 pounds, based on preliminary results of retainer ball load measurements.
- 6b. Roller Force - The same type of strain gage instrumentation employed in the ball force measurements was used in the roller force measurement except that the rework to the retainer was only to accommodate the strain gages, not to increase its strain sensitivity, as the webs were already thin enough for good strain sensitivity.



Figure 44. Ball Bearing Retainer Strain-Gage Location and Rework.  
Top: Two additional strain gages are opposite the two shown, and the four gages are wired on a four-arm bending bridge.  
Bottom Left: View looking down through retainer ball pocket shows two instrumented retainer webs, each having a four-active-arm bending bridge. Bottom Right: Overall view of strain-gaged ball retainer pocket webs.

7. Ball Bearing Attitude - Each test ball bearing retainer was instrumented with two sets, three per set, of Hall generators (F. W. Bell Inc. Model 105-225). These generators were not standard. They were built for Lycoming in the smallest size practical (0.050 by 0.060 inch). The temperature resistance was also increased from 200° F for standard items to 248° F for this application. The vendor supplied the characteristics for each generator.

A Hall generator is a device whose voltage output is proportional to a current input and the magnetic field to which the Hall generator is subjected (see sketch below):

$$V_H \propto I_C B (\cos \phi)$$

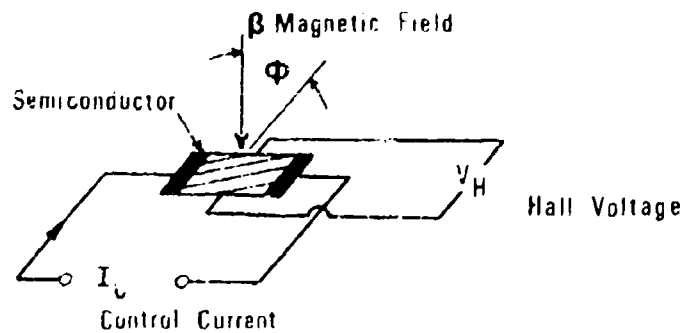
where  $V_H$  = Hall voltage

$I_C$  = Hall control current

$B$  = magnetic flux

$\phi$  = angle between  $I_C$  and  $B$

If the control current ( $I_C$ ) is held constant, the voltage ( $V_H$ ) is proportional to the magnetic field to which the Hall generator is subjected. Unlike generation of a voltage in a conductor through changing flux fields, the Hall requires no change in flux.



As originally proposed, three mutually perpendicular Hall generators would sense the magnetic field strength of a magnetized ball, making it possible to determine angular location at any instant in time. This was accomplished by producing magnetic poles at 90 degrees to one another. While more than one set of 90-degree poles is possible, it was believed that the resulting confusion and effort required to keep track of similar poles would not be justified. With this arrangement (one set of 90-degree poles), only about 25 percent of the surface of the ball has a field strength sufficient to be detectable by the Hall generators, using the planned generators and ball material. To increase the time during which the ball magnetic field could be sensed, the Hall generators were installed in line at the ball contact point on the retainer, in slightly recessed slots. With the Hall generator and ball bearing material used (M50), sensitivities were so low that the ball clearance had to be reduced to 0.005 inch. Figure 50 shows the Hall generators in place.

Prior to installing the instrumented retainer and magnetized balls in the test rig, each ball was mapped to describe the magnetic field in terms of a Hall generator output versus ball position (Figure 51). This mapping was to be transferred to a large three-dimensional model of the ball. Scale-model Hall generators could then be used to determine the angular position of the ball by rotating the model ball until three voltages obtained from testing matched the three model ball voltages. This position described by three voltages would be unique. It would describe the angular position of the ball with respect to the retainer. This process repeated at defined small time intervals over small azimuth angles would provide three-axis rotational velocities at these angles.

Preliminary static and low-speed laboratory tests indicated the idea to be feasible. In one test a magnetic ball was calibrated as outlined in Figure 51. The ball was spun in a lathe and the output was observed. The output was as expected. In another test the magnetic ball was placed in an instrumented retainer pocket and rotated slowly by hand using a Plexiglas rod bonded to the ball. The three resulting Hall voltages were observed on three oscilloscope channels.

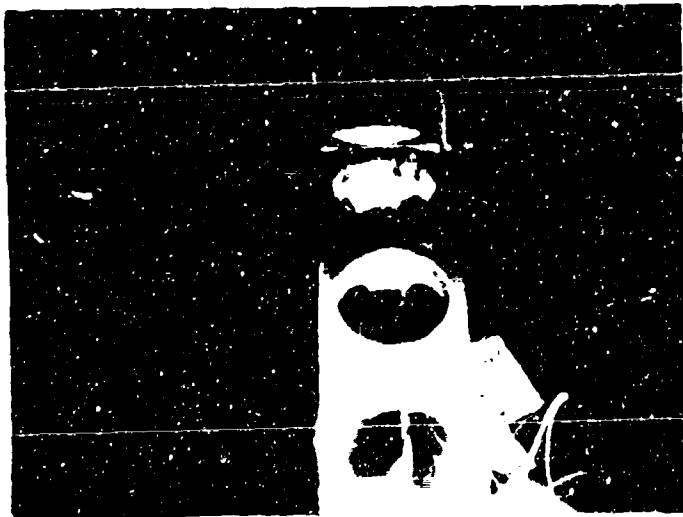
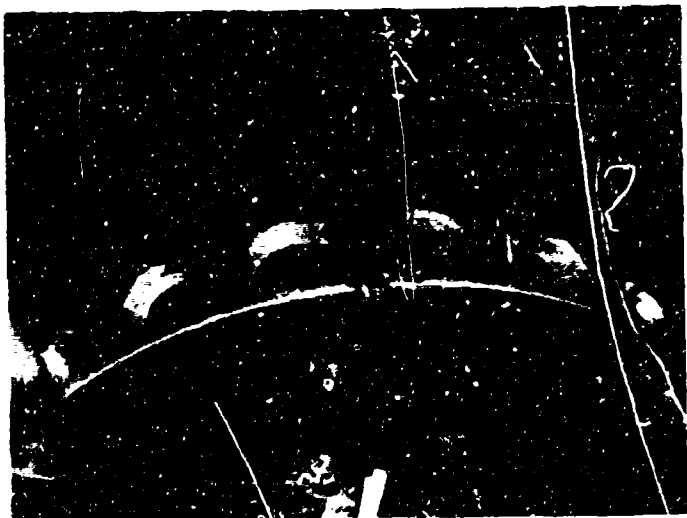


Figure 50. Hall Generators Installed in Ball Bearing Retainer Pockets.  
Top: Reworks and Hall lead wire routing. Bottom: Location of Hall generators.

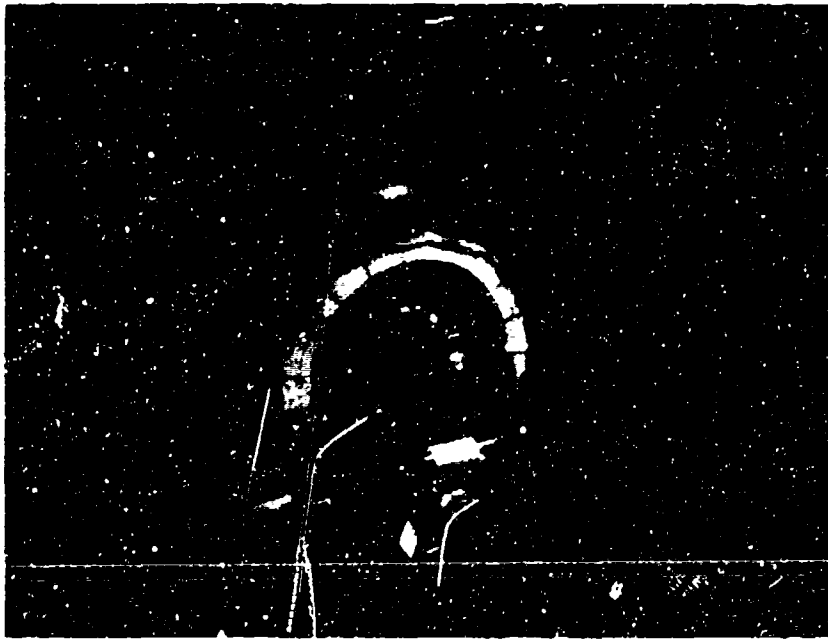


Figure 51. Ball Bearing Magnetic Field Mapping. The magnetic ball is bonded to a Plexiglas rod mounted in a lathe chuck. A Hall generator is mounted on a Plexiglas rod, held in the tool post. In the position shown, the ball is rotated 360 degrees in 20 degree increments. At each increment a reading from the Hall generator is taken. The tool post is then rotated 20 degrees and again the ball is rotated 360 degrees in 20-degree increments. The process is repeated until the mapping is complete.

8. Slip Ring Driving Torque - The bearing retainer would be driving a slip ring and multiplexer system, which it would not normally do. The torque required to drive the slip ring was measured by instrumenting the slip ring driving plate with two strain-gaged cantilever beams. The gaged beams were calibrated for torque and for temperature. The slip ring assembly and driving plate are shown in Figure 52.

The torque system was designed to read torque in one direction, but these tests showed that significant vibratory torques occur.

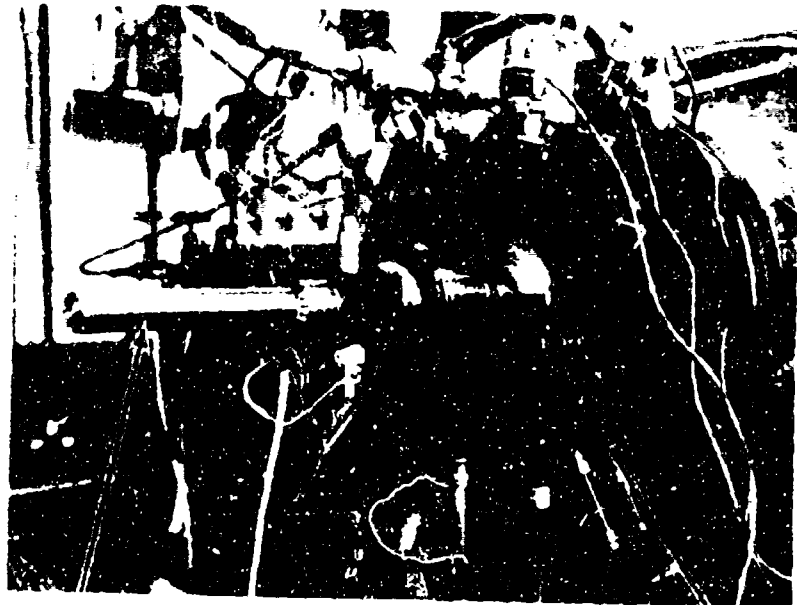
9. Retainer and Torque Element Temperature - To be able to compensate for temperature effects on the retainer strain-gaged bridges, torque element strain-gaged bridges, and Hall generators, thermocouples were installed at these locations.

## DATA ACQUISITION

### Retainer Data Transmission

The large number of signal leads from the retainer, 12 leads for the Hall generators, 8 leads from the ball force bridges, 4 leads from the torque bridge, and 6 leads from the thermocouples, would have required 30 slip ring channels. If common grounding were used, 26 channels would be required. Slip rings of this size would inherently have large drag characteristics. A mercury-wetted slip ring with 16 channels was proposed, but this is not a developed item and nonrecurring engineering cost would have been excessive. An eight-channel mercury-wetted slip ring was available, but if this were employed, data could not be taken simultaneously from Hall generators, ball force gages, and the torque driving plate. Simultaneous data acquisition was a goal. The problem of a large number of signals and the requirement for simultaneity suggested the use of a multiplexer.

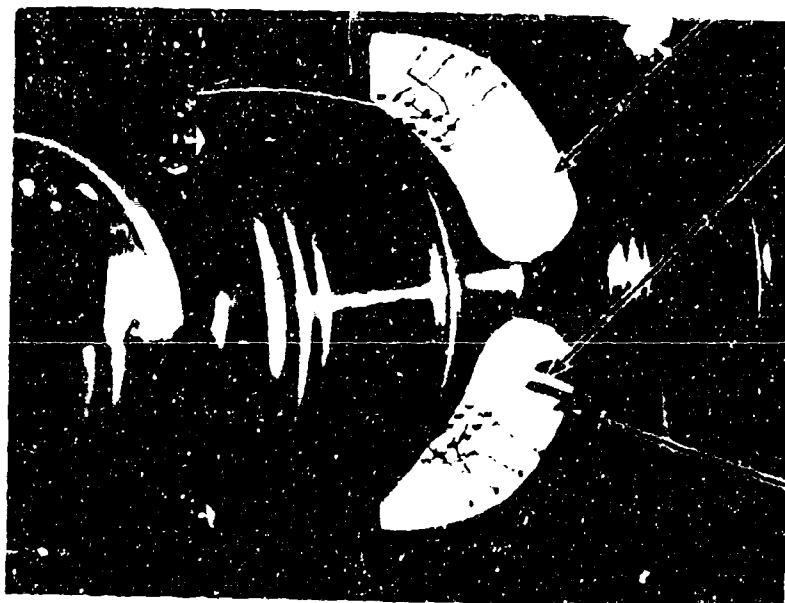
A multiplexer system, which was designed and built at Lycoming, incorporated constant-current power supplies for the Hall generators, constant-voltage power supplies for the strain-gaged bridges, compensating networks and cold-junction reference for the thermocouples, and buffer amplifiers with a gain of 100 for the output from all the previously mentioned channels. Coupled with an eight-channel mercury-wetted slip ring (Vibro-Meter SA Model MT8/A), this system provided close to the



Slip Ring

Driving Plate

Lead Wires From  
Bearing Retainer      Driving Plate



Instrumented Canti-  
lever To Measure Slip  
Ring Driving Torque

Driving Pin From  
Retainer - A  
Second Pin Is 180  
Degrees From One  
Shown

Figure 52. Slip Ring and Driving Plate. Top: Overall view.  
Bottom: Closeup of driving plate. Rotation is  
counterclockwise.

desired goal for obtaining simultaneous data from the rotating retainer instrumentation. The 30 leads were reduced to four through multiplexing, and three slip ring channels were required to power and sequence the multiplexer. The multiplexer was time divided, with the output from the Hall generators being multiplexed simultaneously, the output from the strain-gaged bridges being displayed simultaneously, and the output from thermocouples being displayed simultaneously. The switching rate of the multiplexer could be varied from 0.1 time per second to in excess of 10,000 times per second. Figure 53 shows typical outputs from the multiplexer.

#### Inner Race Temperature Data Transmission

The rotating inner race temperatures were transmitted through Lycoming-developed Freon flood-cooled slip rings coupled to the rear of the shaft supporting the test bearing inner race.

#### Recording

All signals except the inner race temperatures were recorded on magnetic tape. Lockheed tape recorder Model 417D was used. The frequency response of this system is 10,000 Hertz. Signals from the inner race were displayed on instrumentation in the test cell and were manually recorded.

#### Monitoring

During all testing, inner race speed, retainer speed, inner race speed ratio, ball force, radial load, and driving torque were monitored before and after magnetic tape recording. This procedure assured that the quality of the signals was maintained throughout the recording process.

#### Problem Areas

During this test program three bearing failures occurred which resulted in the loss of data and the elimination of certain instrumentation.

The first failure (a smooth-race ball bearing) was due to shaft unbalance. This failure also resulted in the loss of a Hall generator-instrumented retainer and multiplexer (Figure 54).

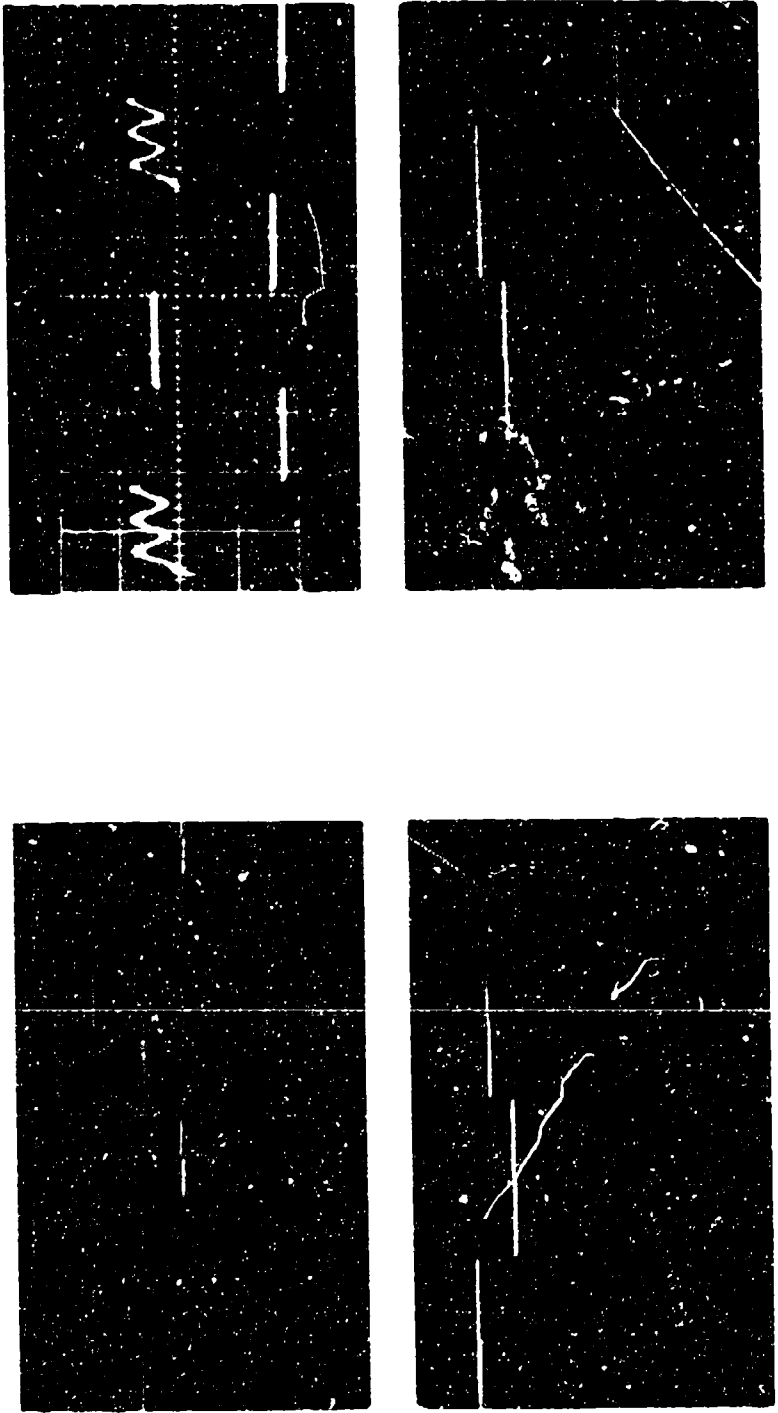


**Figure 53. Typical Multiplexer Outputs.** Top Left: Output from multiplexer when four different DC voltages are input to the four multiplex channels. Top Right: Output from multiplexer when (from left to right) a sine wave is input to the first channel, and a DC voltage is input to the second channel. Zero input to channel (to be used as a reference channel) and same voltage input to channel two is input to channel four. Bottom Left and Right: Outputs from multiplexer just prior to running. Note shift in output of channel four during calibration of one of the web force strain-gage bridges. The shift is approximately 0.2 volt and is equal to 9 pounds of force acting on the retainer pocket web.

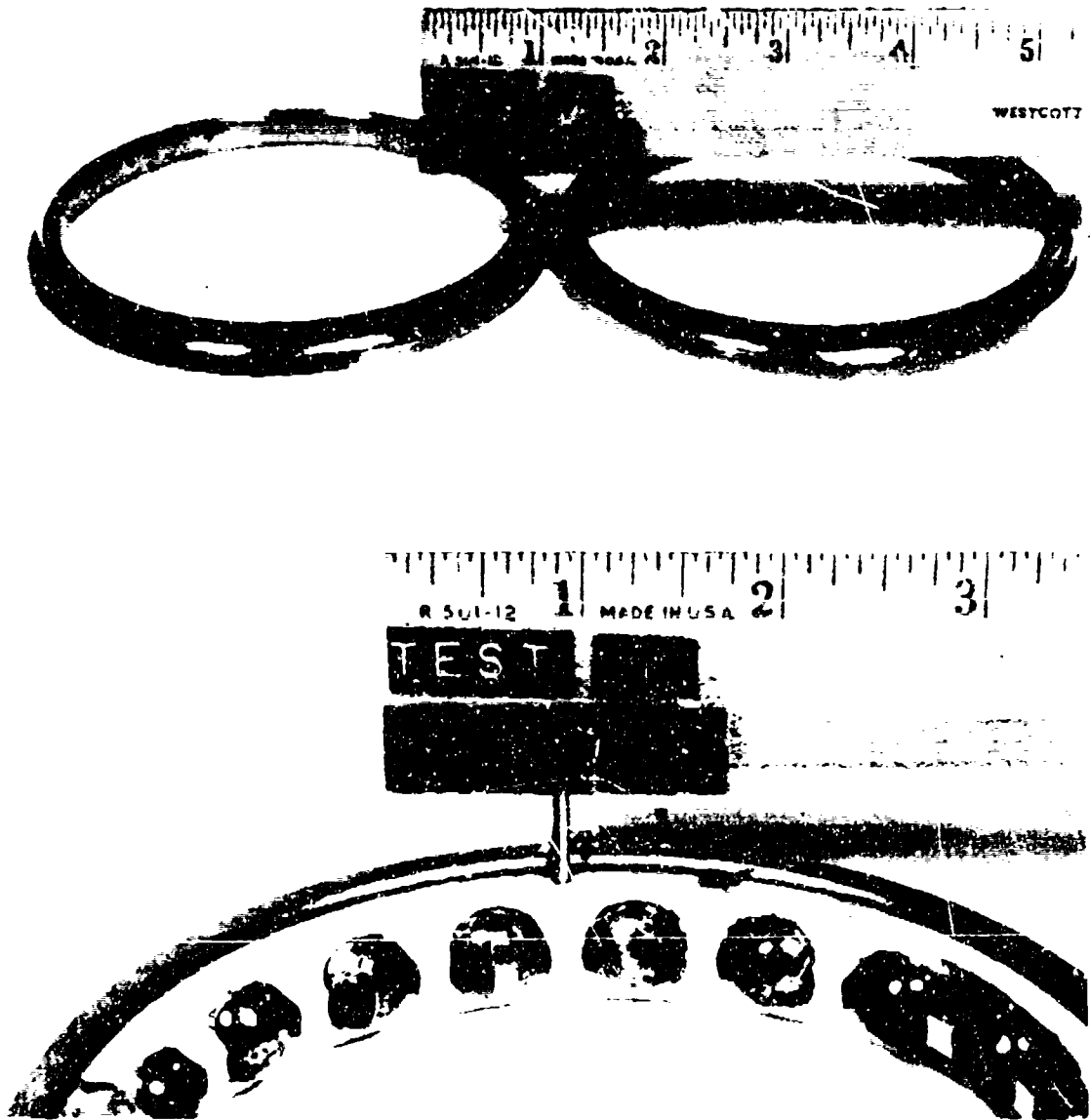


Figure 54. Build No. 2 Bearing Failure; Shaft Unbalance. Top: Inner races. Bottom: Cage, balls, and outer race.

The second failure (a smooth-race ball bearing) was the result of reducing the pocket clearance from 0.022 inch for the normal bearing to 0.005 inch to achieve the necessary Hall generator sensitivity. This failure is shown in Figure 55. When the Hall generators were eliminated to provide the necessary clearance, the multiplexer system was no longer required.

The third failure (a smooth-race roller bearing) was the result of excessive roller skewing during attempts to produce a skid map.

During early test runs, the wire routing from the retainer to the slip ring driving late was adequate; but during later runs, there were lead wire failures resulting in the loss of data, and improved techniques were devised. The original and the improved lead paths are shown in Figure 56.

#### TEST PROCEDURE

The test program was accomplished in four builds as follows:

<u>Build</u>	<u>Test Bearing</u>	<u>Lubrication Condition</u>
1	Ball	EHD
2	Ball	EHD
3	Ball	Boundary
4	Roller	EHD

A full EHD oil film was achieved by operating at high speed and moderate loads.

Boundary lubrication was achieved by utilizing races with poor surface finish (24 AA). Experience has shown that this degree of roughness allows metal-to-metal contact.

Load and speed test conditions for the ball and roller bearing tests are defined in Tables VIII and IX respectively.

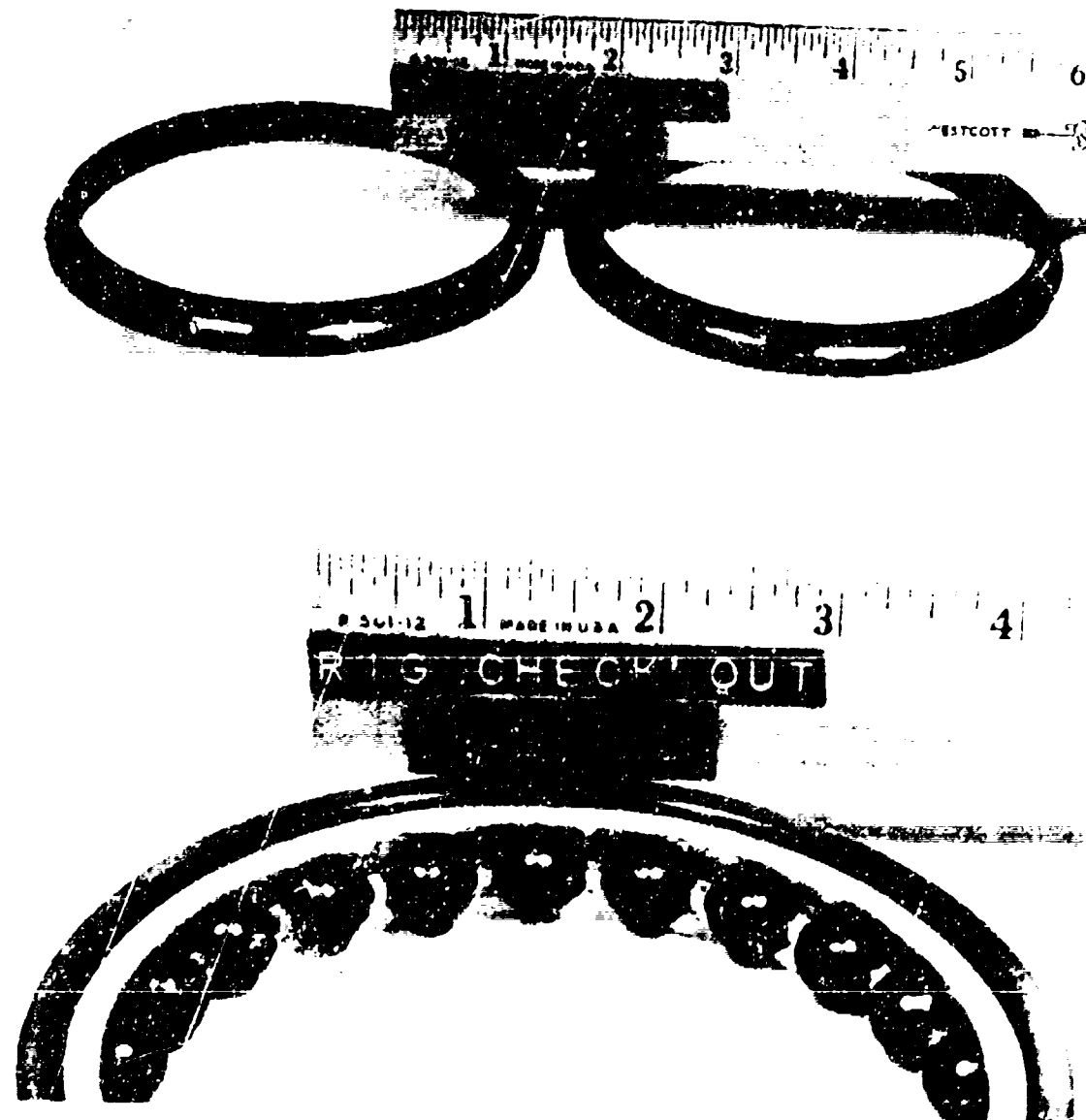


Figure 25. Build No. 2 Bearing Failure; Insufficient Pocket Clearance.  
Top: Inner races. Bottom: Cage, balls, and outer race.



Figure 56. Improved and Original Retainer to Driving Ring Strain Gage Lead Paths. Top: Improved lead path showing gage leads fixed to pins attached on retainer; leads are spot welded to plate riveted to driving plate, and the leads are larger than originally. Bottom: Original lead path, unsupported from retainer, epoxy bonded to driving plate.

TABLE VIII. BALL BEARING TEST CONDITIONS

Data Point	Inner Ring Speed (rpm)	Axial Load (lb)	Radial Load (lb)
1	16,000	1000	0
2	16,000	1000	500
3	16,000	500	500
4	16,000	100	0
5	20,000	1000	0
6	20,000	1000	500
7	20,000	500	500
8	20,000	100	0

TABLE IX. ROLLER BEARING TEST CONDITIONS

Data Point	Inner Ring Speed (rpm)	Axial Load (lb)	Radial Load (lb)
1	16,000	0	1000
2	16,000	0	600
3	16,000	0	200
4	16,000	0	~ 0
5	20,000	0	1000
6	20,000	0	600
7	20,000	0	200
8	20,000	0	~ 0

### Build No. 1, Rig Checkout

The objective of this build was to check out the test rig for the test program. Standard rig instrumentation was used. Retainer instrumentation and inner race temperature probes were not installed for this build. A standard ball bearing was installed in the test position.

The test rig was operated to 23,000 rpm. Oil flows to the test bearing and two support bearings were adjusted at various speed increments to note the effect on scavenge temperature. Radial and axial thrust loads were also varied at different shaft speed settings to determine load effects on vibration. The rig checkout was concluded with a 1-hour run at 23,000 rpm.

### Build No. 2, Smooth-Race Ball Bearing

The test rig was rebuilt with bearing instrumentation to take data on the ball bearing in the EHD region.

The oil-in temperature to the test bearing was maintained at  $100 \pm 5^{\circ}\text{F}$  during the test.

The rig was operated through all of the data points defined in Table VIII.

To generate a bearing skid map, the test rig was brought to 20,000 rpm, the radial load was reduced to zero, and the thrust (axial) load was reduced in increments until skidding occurred.

### Build No. 3, Rough-Race Ball Bearing

This build was the same as Build No. 2 except that the test bearing had a rough surface finish on the inner and outer races to promote boundary lubrication at the rolling contacts. The same data points defined in Table VII were evaluated. The oil-in temperature during the test was  $200 \pm 5^{\circ}\text{F}$ .

An attempt was made to produce a skid map, but skidding would not occur.

### Build No. 4, Smooth-Race Roller Bearing

The test rig was rebuilt with bearing instrumentation to take data on the roller bearing in the EHD region.

The oil-in temperature to the test bearing was maintained at  $100 \pm 5^{\circ}\text{F}$  during the test.

The eight data points to be evaluated during this build are defined in Table IX. The test rig was operated through all of these data points.

### TEST RESULTS

#### Build No. 1, Rig Checkout

This build resulted in successful operation of the test rig, without retainer or race instrumentation, to speeds of 23,000 rpm under test load conditions.

Disassembly and inspection of the test rig after checkout operation showed that both the test and facility bearings were in excellent condition.

#### Build No. 2, Smooth-Race Ball Bearing

The first ball bearing configuration tested was with a smooth-race surface finish (SAA). Test results are summarized in Table X, which includes test race temperatures, measured radial load, slip ring driving torque, radial load frequency, and retainer-to-inner race speed ratio.

These results show that radial load was composed of a steady and an oscillatory component. Retainer driving torque was found to be oscillatory also. When drag was introduced into the driving system by "holding back" the slip ring, torque was still oscillatory, which suggested that the cage motion was not steady but accelerated and decelerated once per revolution. Maximum torque required to drive the slip ring was measured at 7 inch-pounds steady load,  $\pm 7$  inch-pounds vibratory.

Samples of the outputs from both ball force strain gage bridges and the cage speed signal as a function of time are shown in Figures 57 through 64. These figures show large pulse-type forces being applied to the cage at a nonuniform amplitude and nonperiodic frequency. In addition, they show a small vibratory (approximately  $\pm 3$  to  $\pm 4$  pounds) force. This smaller vibratory signal is expanded five times and presented in Figures 65 through 72.

TABLE X. SUMMARY OF TEST RESULTS, BUILD NO. 2

Data Points (1)	Inner and Outer Race Temperatures			Radial Load <sup>(2)</sup> (lb)	Radial Load Frequency <sup>(3)</sup> (Hz)	Retainer to Ring Speed Ratio	Driving Torque <sup>(4)</sup> (in.-lb)
	Inner Race (°F)	Outer Race (°F)	ΔT (°F)				
1	320	209	-126	6 ± 100 0 ± 20	267 (5)	.46 .46	6 ± 3
2	-	295	-	470 ± 80 470 ± 120	281 254	.46 .46	6 ± 3
3	340	205	-135	470 ± 140 510 ± 130	279 (5)	.46 .46	5 ± 5
4	260	195	-65	6 ± 20 0 ± 20	(5) (5)	.31 (5) .45	5 ± 3
5	320	215	-75	0 ± 20 0 ± 20	(5) (5)	.46 .45	6 ± 6
6	250	230	-29	500 ± 120 480 ± 95	356 334	.45 .45	7 ± 7
7	300	225	-135	500 ± 120 480 ± 100	348 331	.45 .45	6 ± 6
8	260	220	-40	0 ± 20 0 ± 20	(5) (5)	.45 .46	3 ± 3

1. Each test was run twice (once with two web force strain gage bridges, once with one web force and one torque measurement); inner and outer race temperatures were determined during the second run only. Upper values are for test No. 1; lower values are for test No. 2.
2. From strain-gaged radial loading ring; static and dynamic components.
3. Frequency of oscillation of radial loading ring; caused by unbalance and/or eccentricity of shaft supporting bearing.
4. Vibratory component not sinusoidal during condition where torque goes to zero.
5. Ability to determine primary frequency limited by low-level dynamic component.
6. Indicate slip during first run but no slippage during second run; also shown in harmonic analysis.

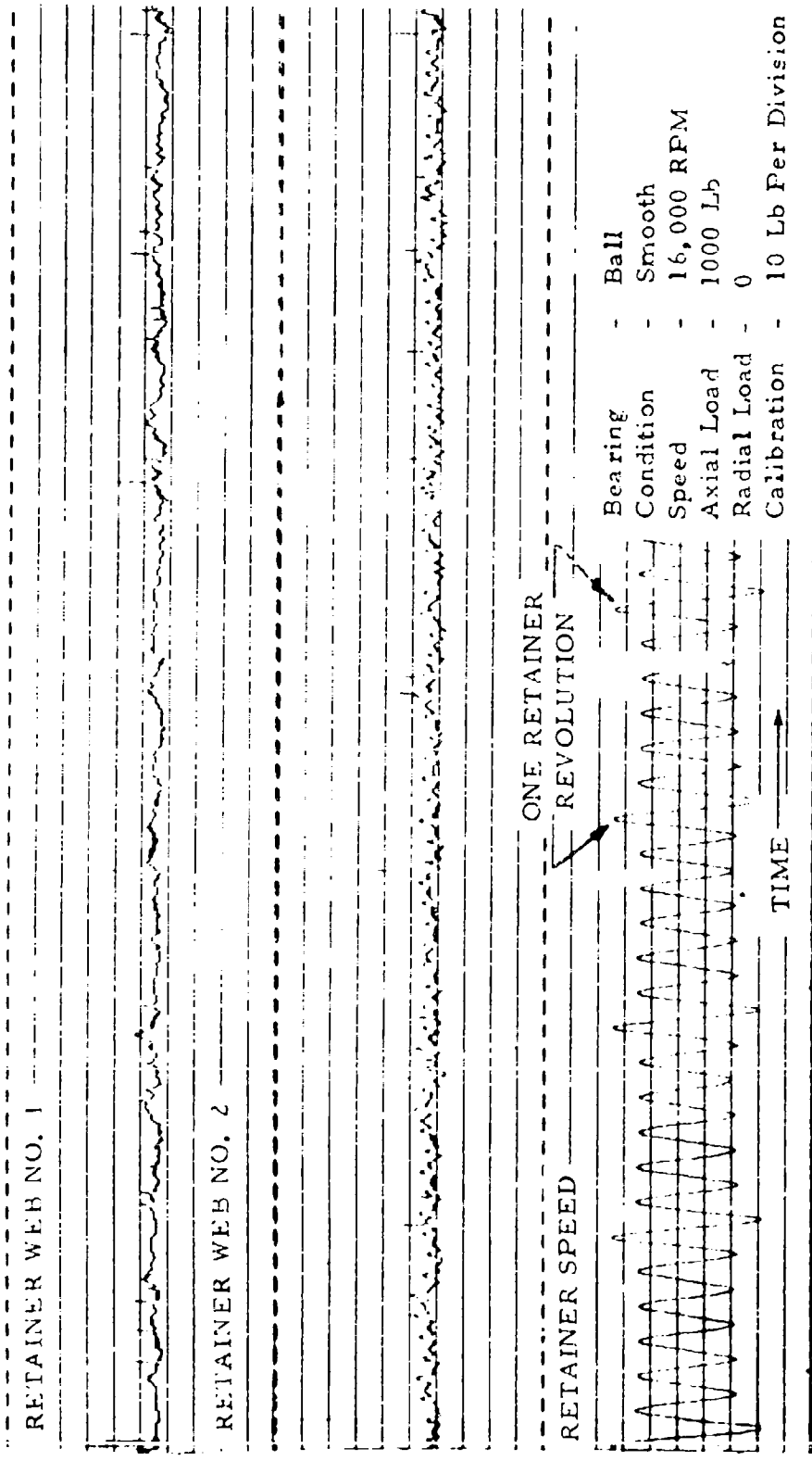


Figure 57. Retainer Web Force and Retainer Speed Versus Time, Showing Nature of Impact Loads.

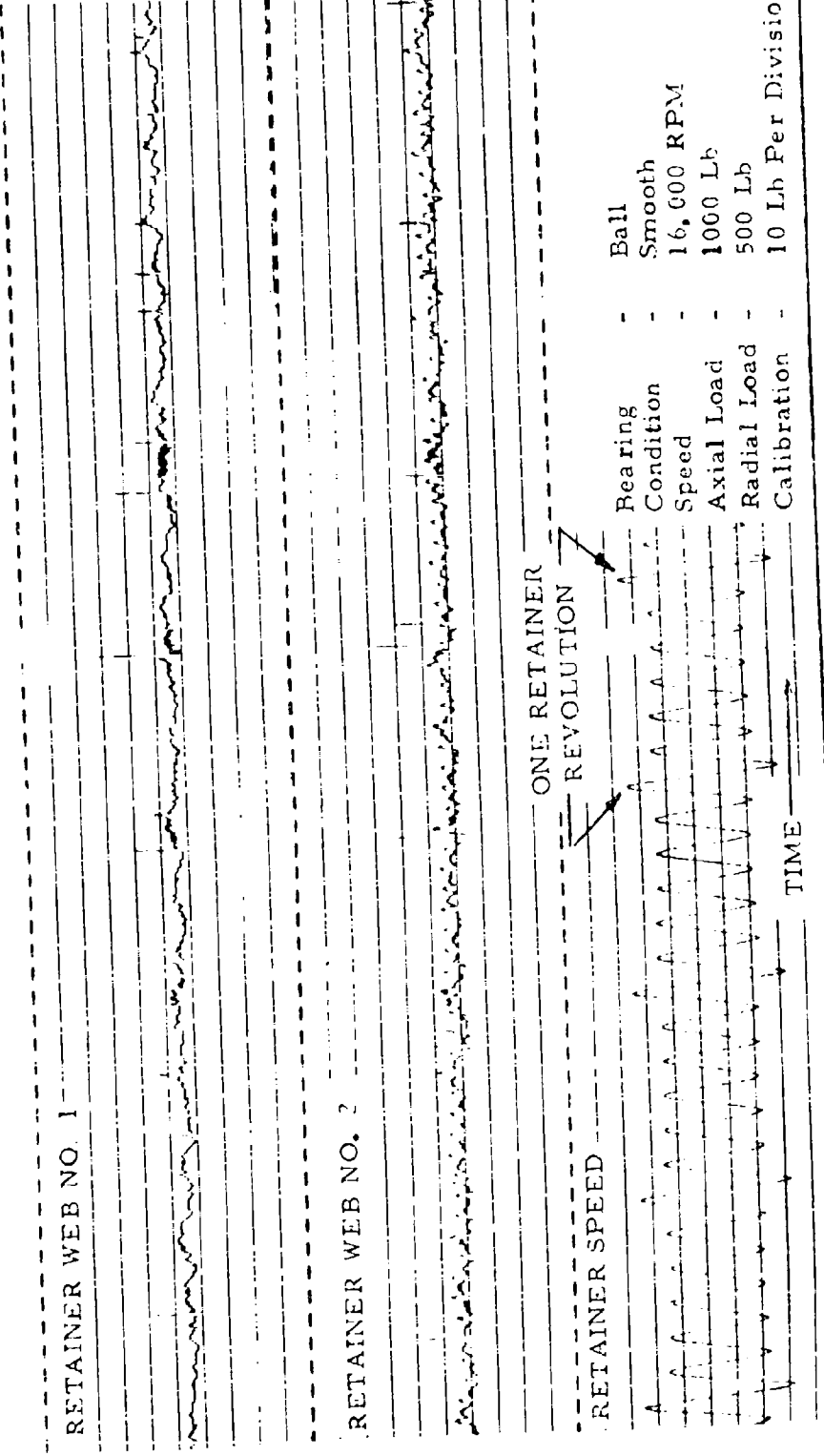


Figure 58. Retainer Web Force and Retainer Speed Versus Time, Showing Nature of Impact Loads.

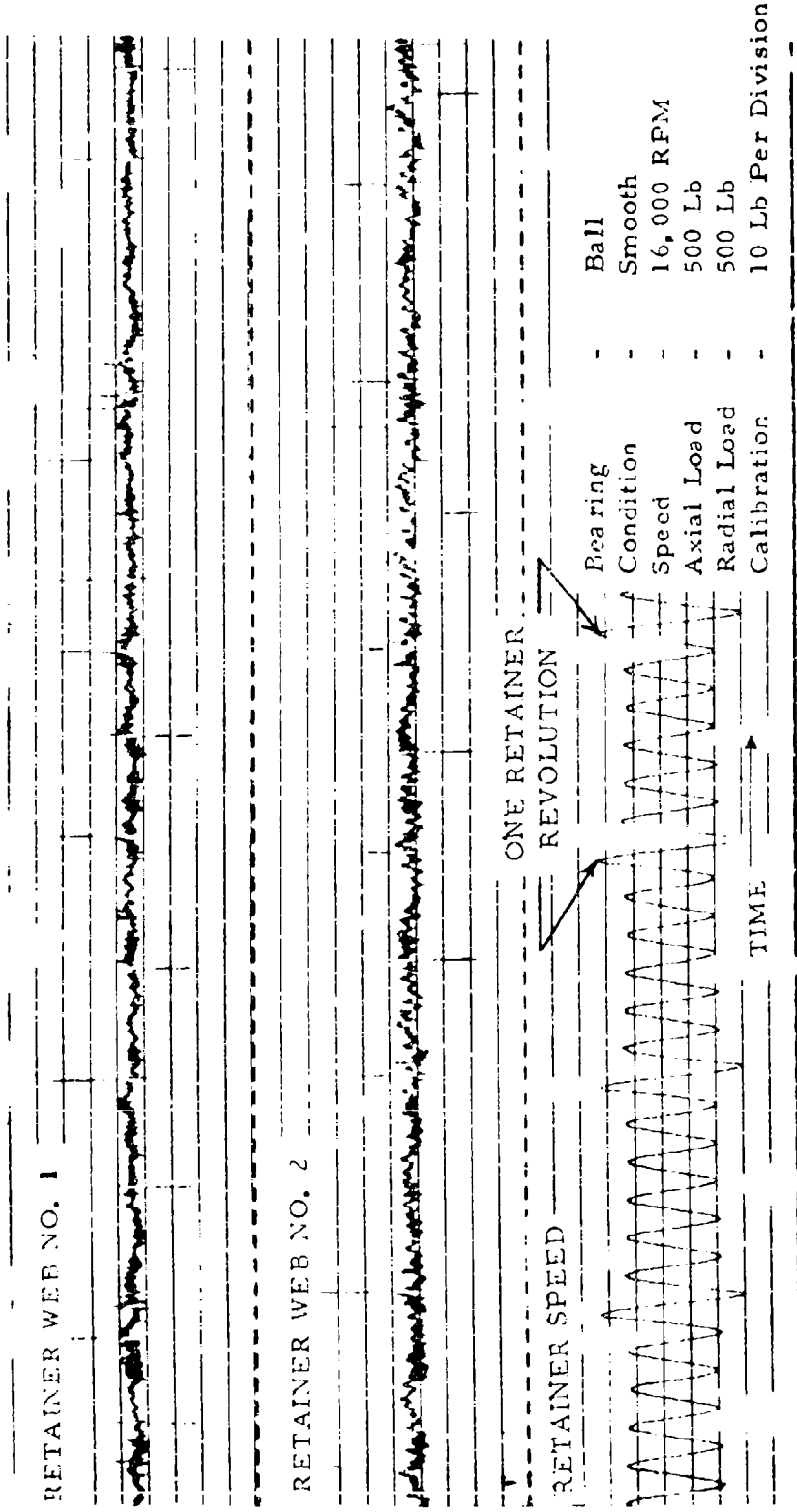
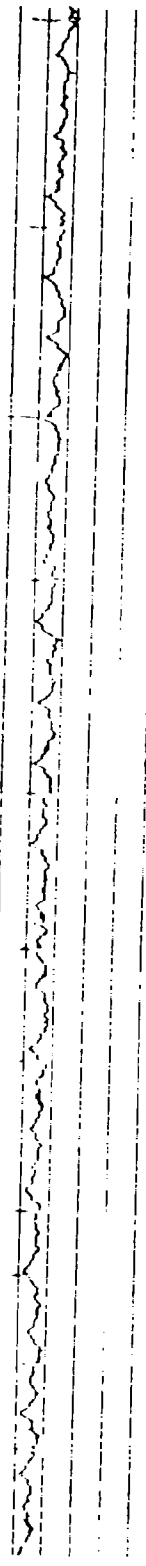


Figure 59. Retainer Web Force and Retainer Speed Versus Time, Showing Nature of Impact Loads.

RETAINER WEB NO. 1



RETAINER WEB NO. 2



ONE RETAINER  
RETAINER SPEED = REVOLUTION

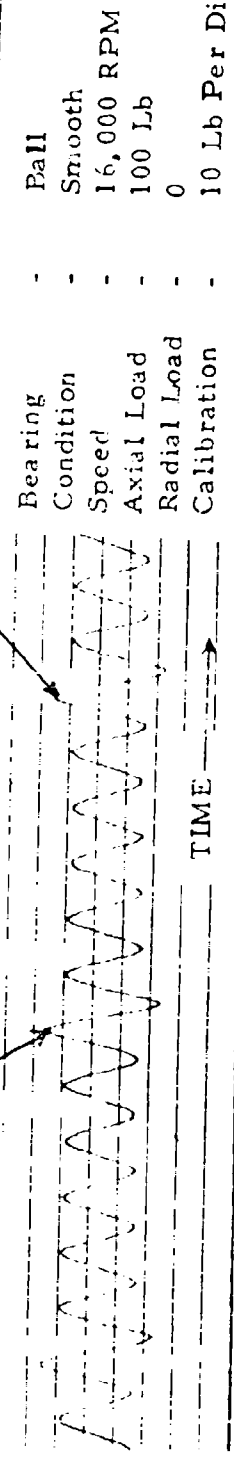


Figure 60. Retainer Web Force and Retainer Speed Versus Time, Showing Nature of Impact Loads.

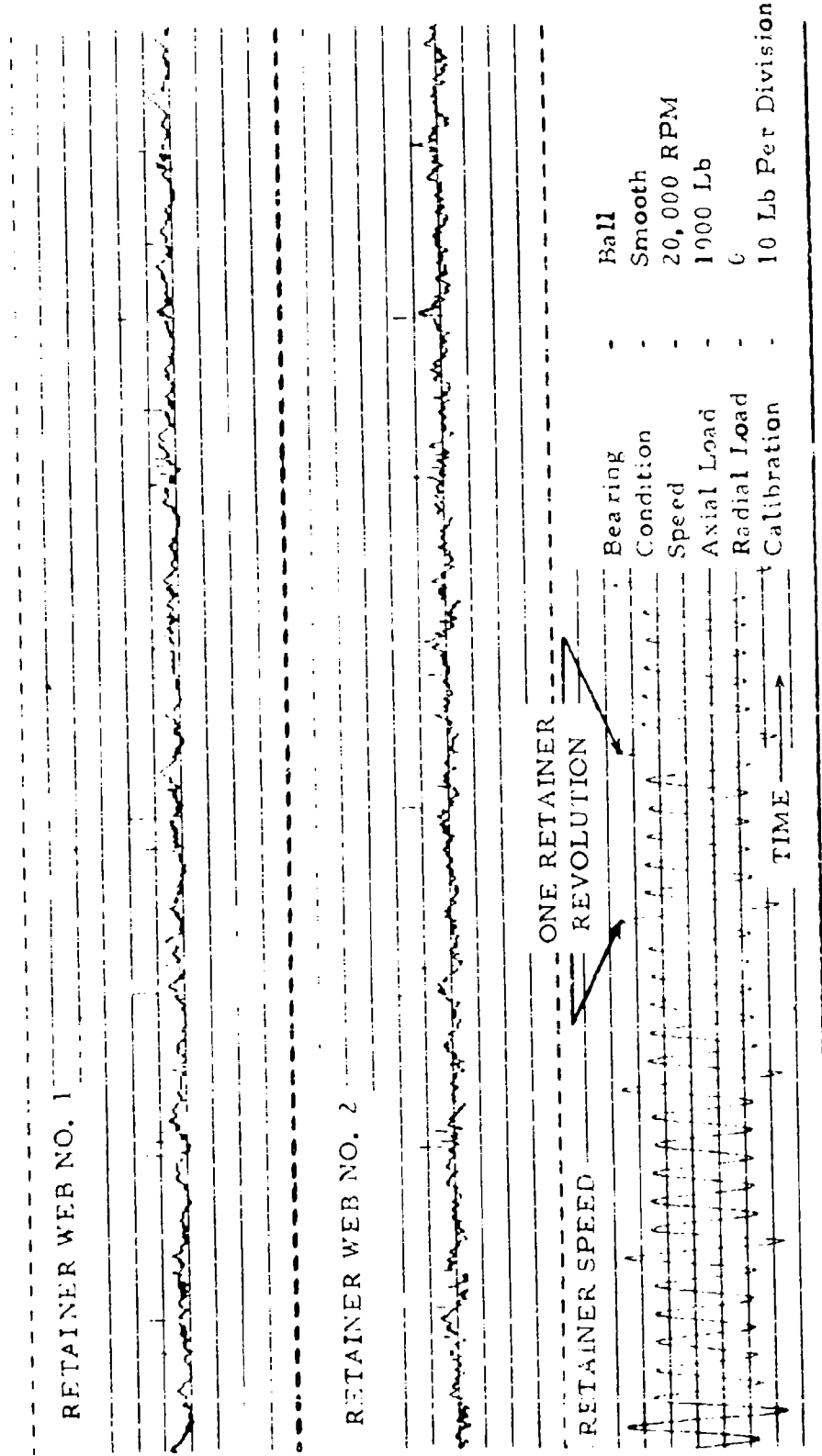


Figure 61. Retainer Web Force and Retainer Speed Versus Time, Showing Nature of Impact Loads.

RETAINER WEB NO. 1



RETAINER WEB NO. 2



147

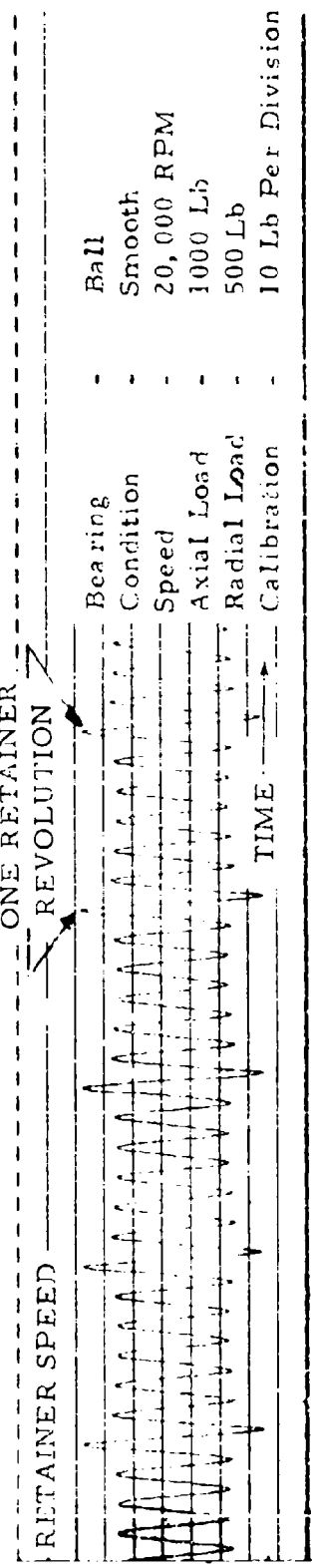


Figure 62. Retainer Web Force and Retainer Speed Versus Time, Showing Nature of Impact Loads.

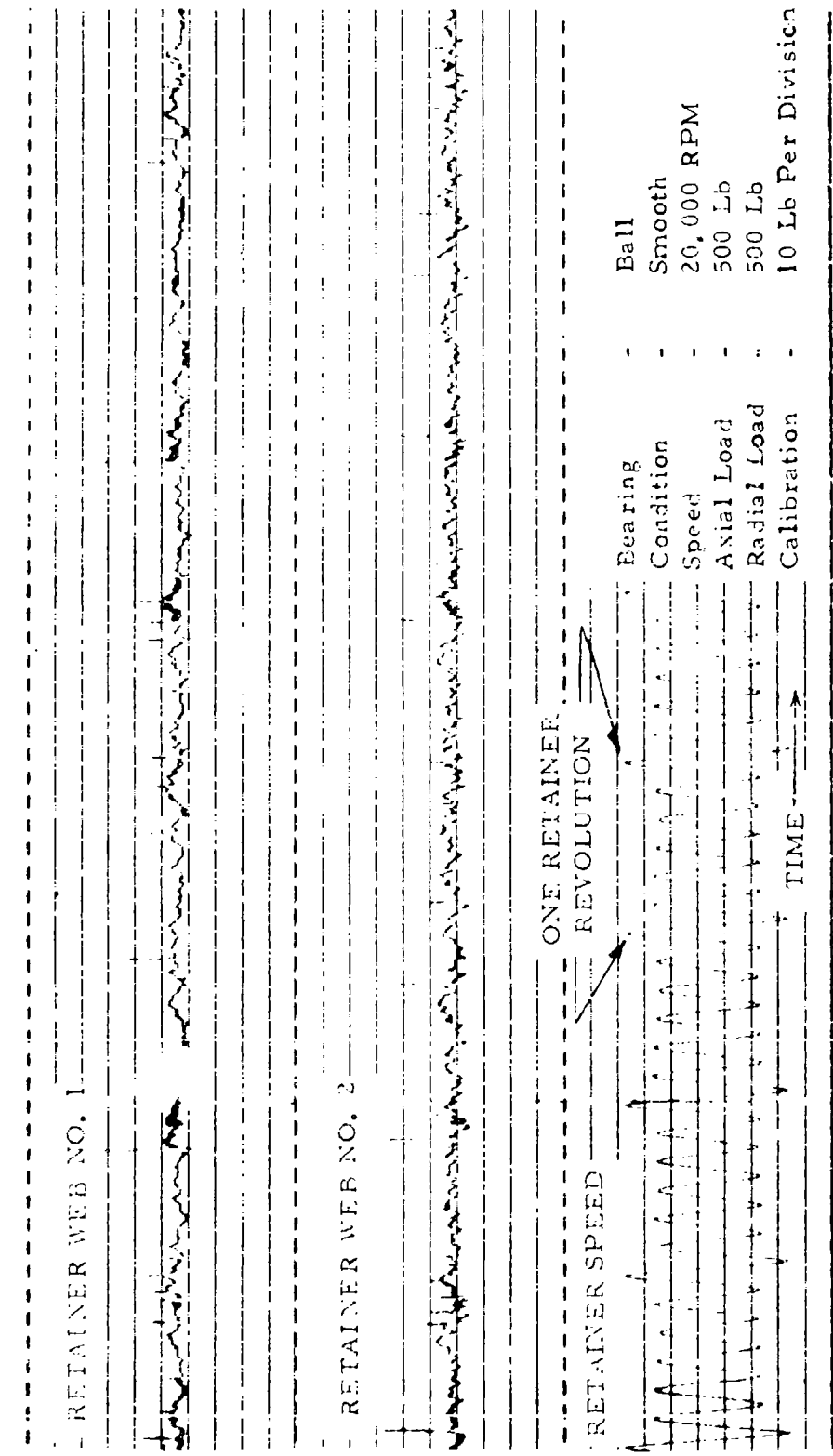
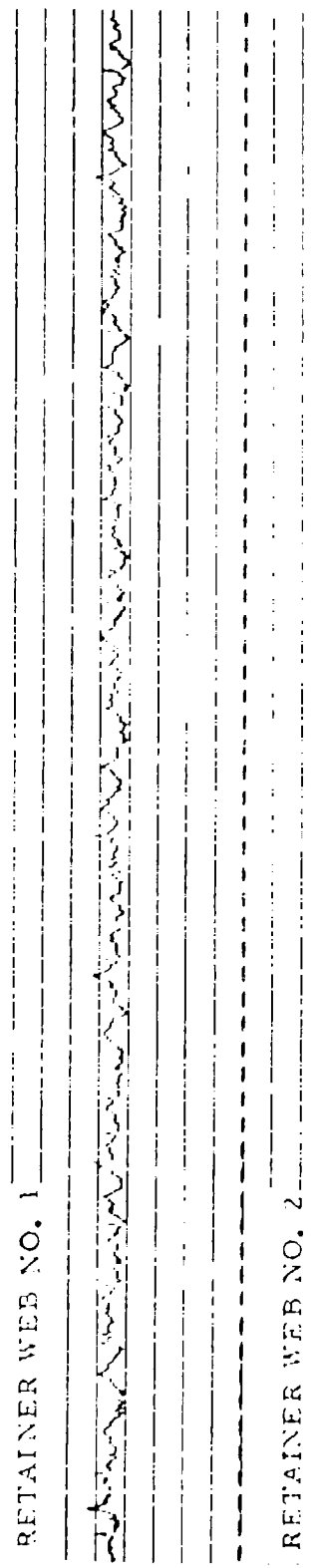


Figure 63. Retainer Web Force and Retainer Speed Versus Time, Showing Nature of Impact Loads.

RETAINER WEB NO. 1



RETAINER WEB NO. 2

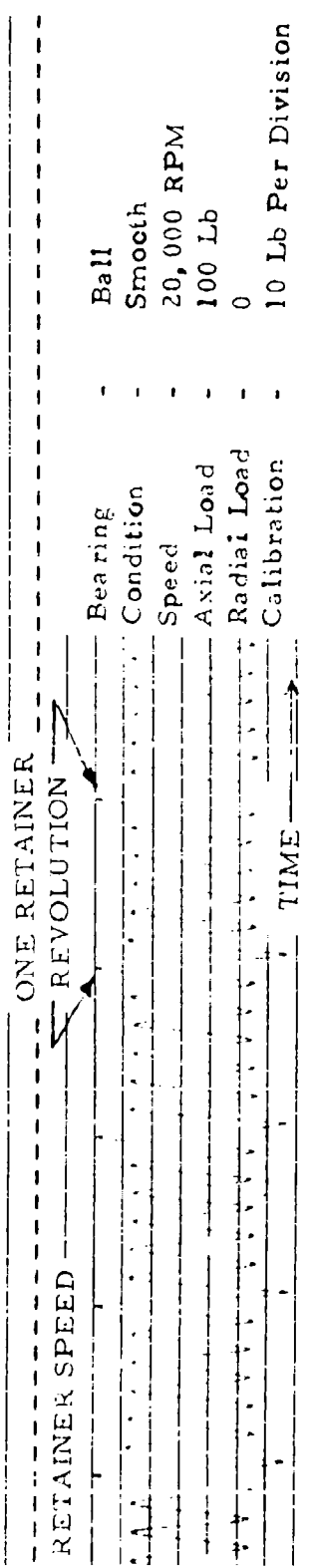
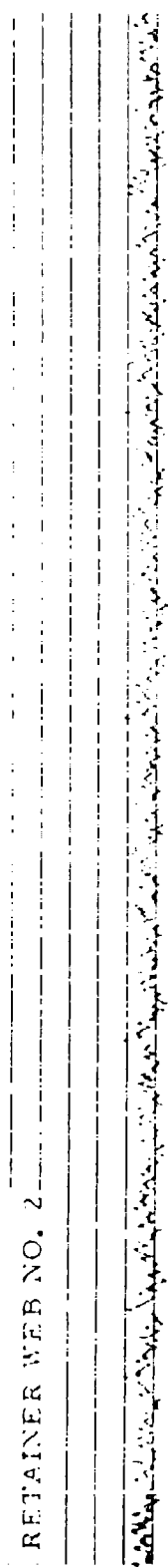


Figure 64. Retainer Web Force and Retainer Speed Versus Time, Showing Nature of Impact Loads.

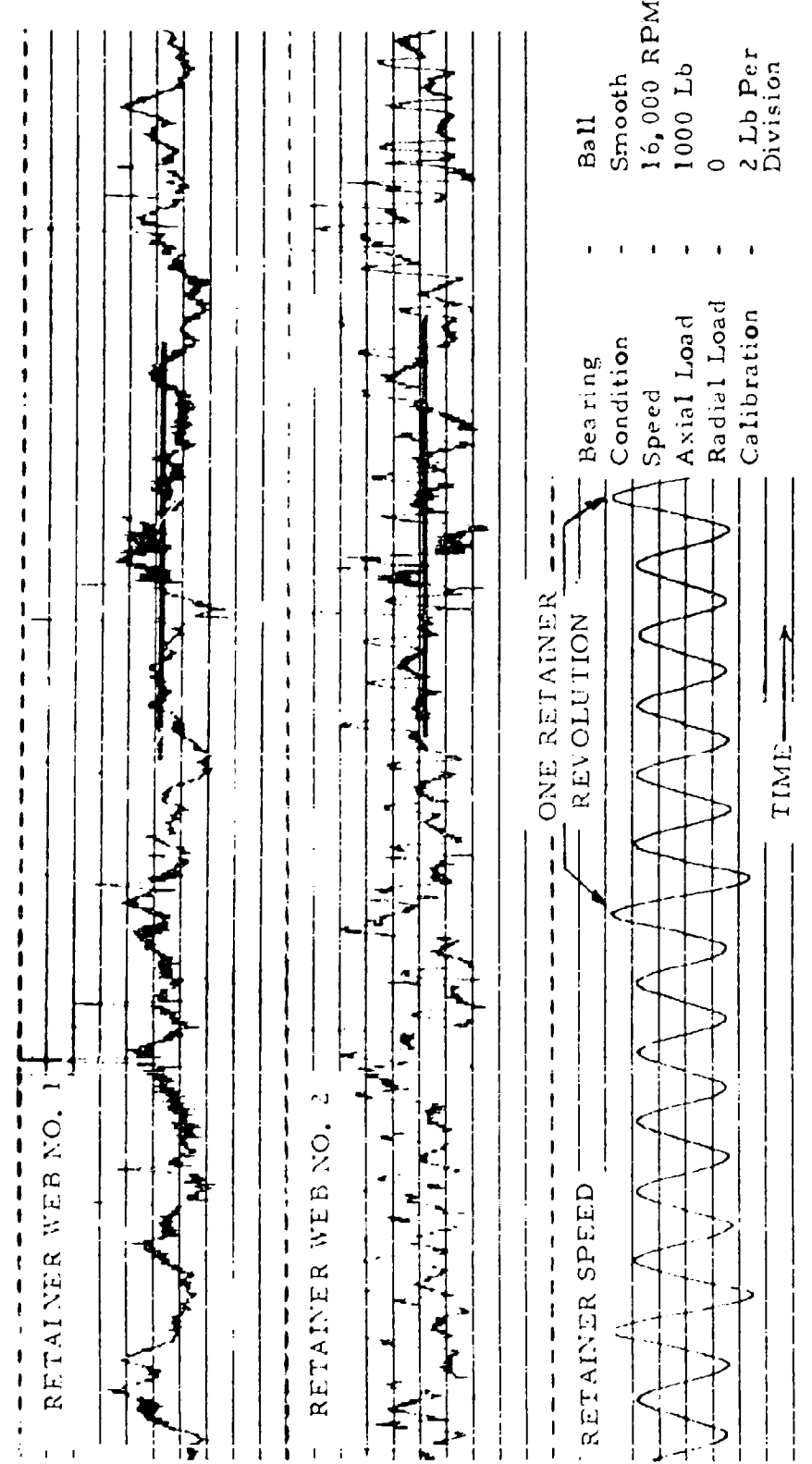


Figure 65. Retainer Web Force Expanded With Computed Web Force Superimposed.

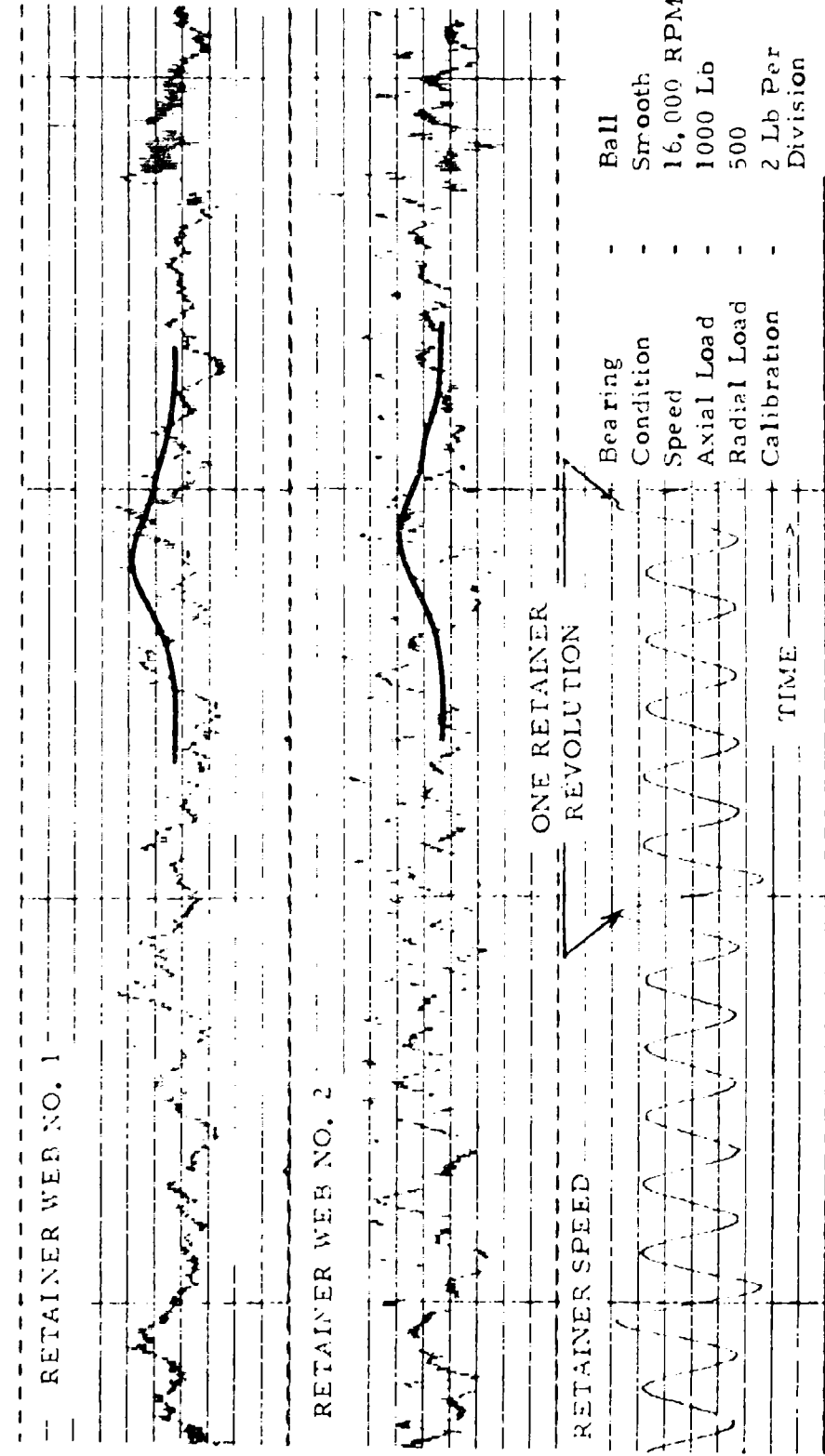


Figure 66. Retainer Web Force Expanded With Computed Web Force Superimposed.

RETAINER WEB NO. 1



RETAINER WEB NO. 2

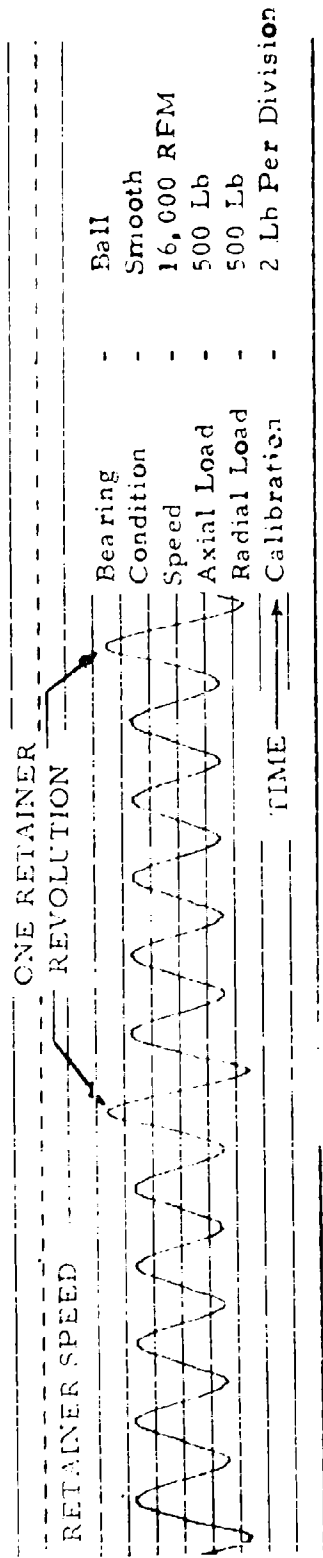


Figure 67. Retainer Web Force Expanded With Computed Web Force Superimposed.

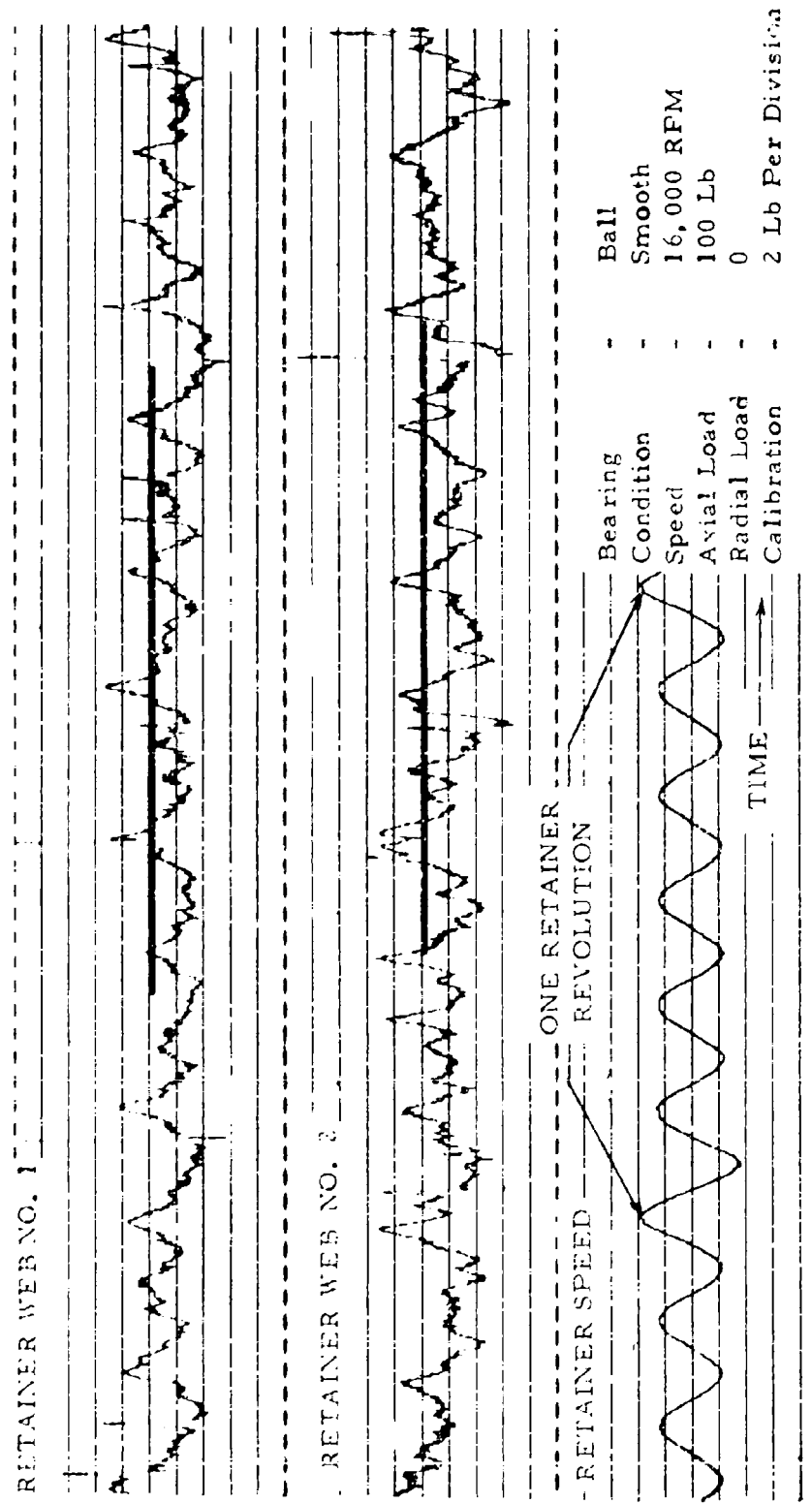


Figure 68. Retainer Web Force Expanded With Computed Web Force Superimposed.

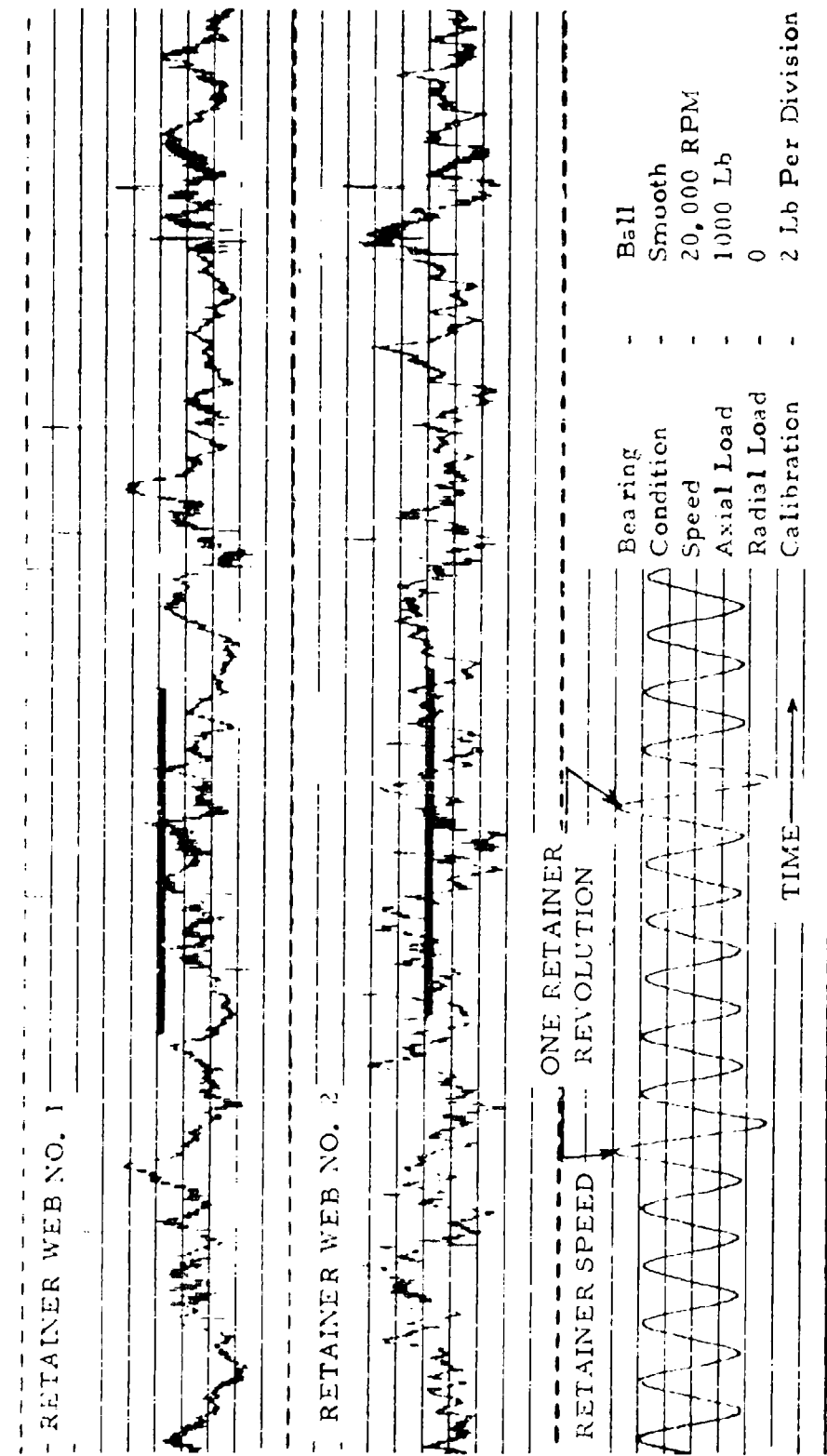


Figure 69. Retainer Web Force Expanded With Computed Web Force Superimposed.

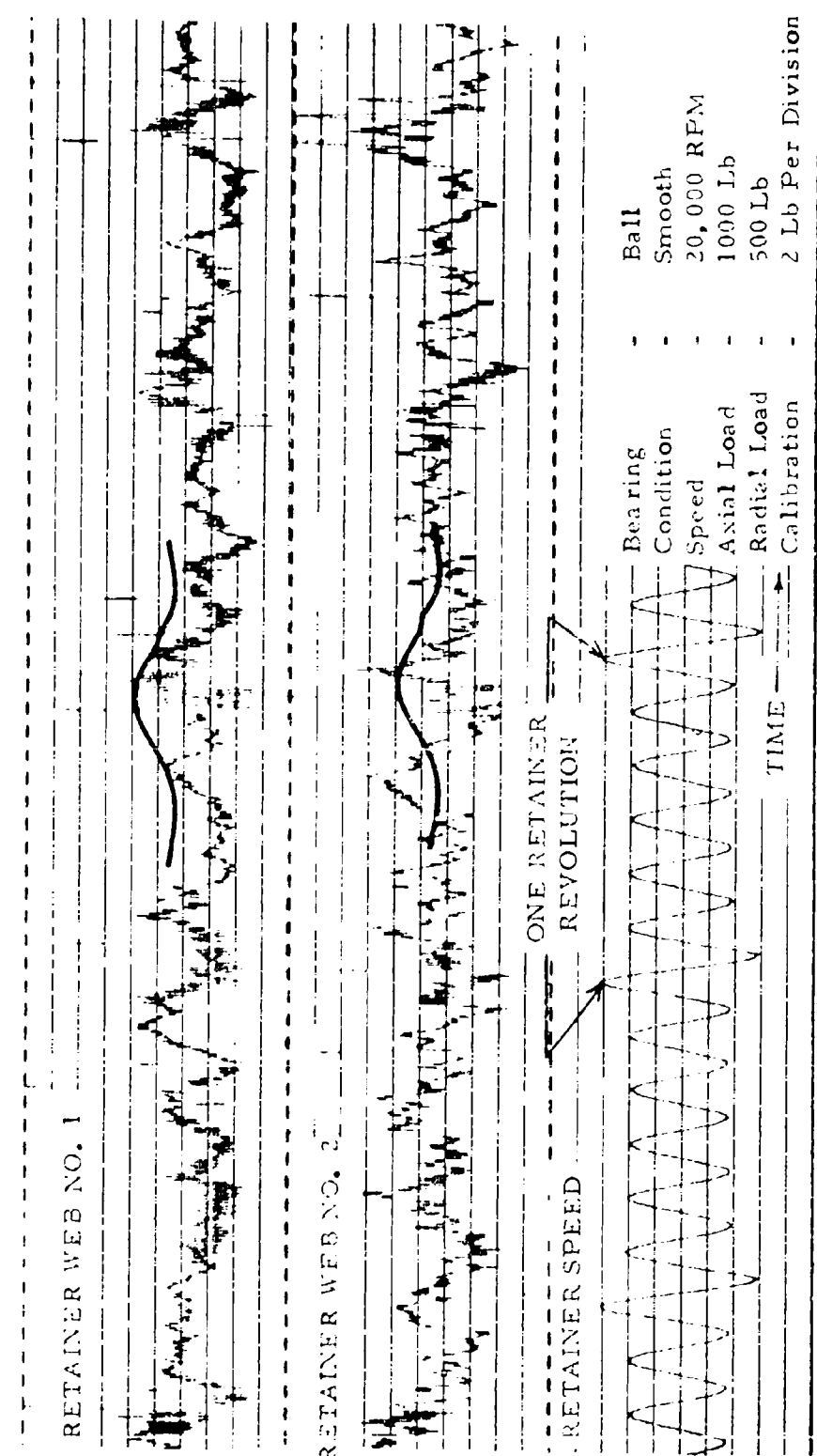


Figure 70. Retainer Web Force Expanded With Computed Web Force Superimposed.

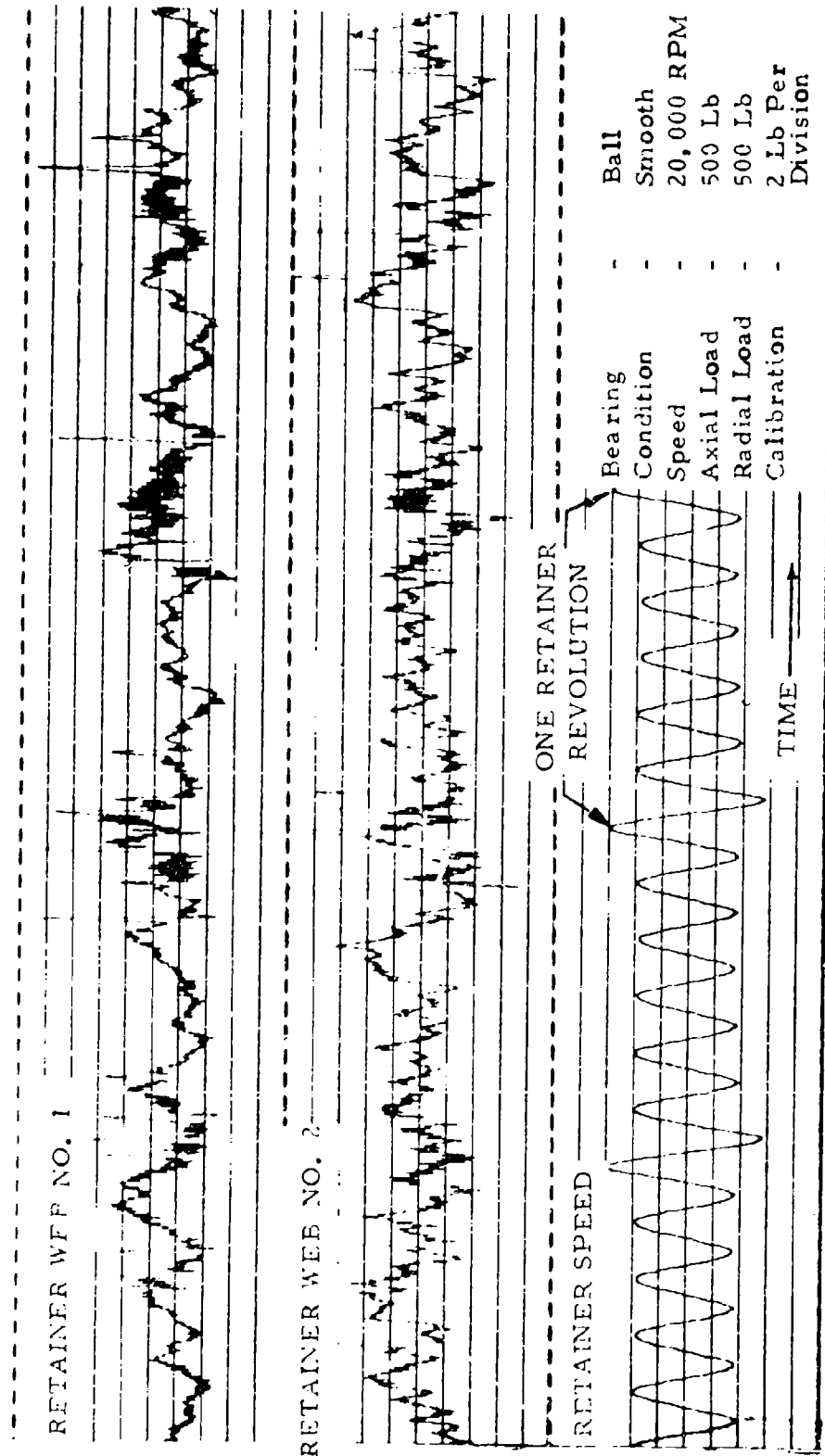


Figure 71. Retainer Web Force Expanded With Computed Web Force Superimposed.

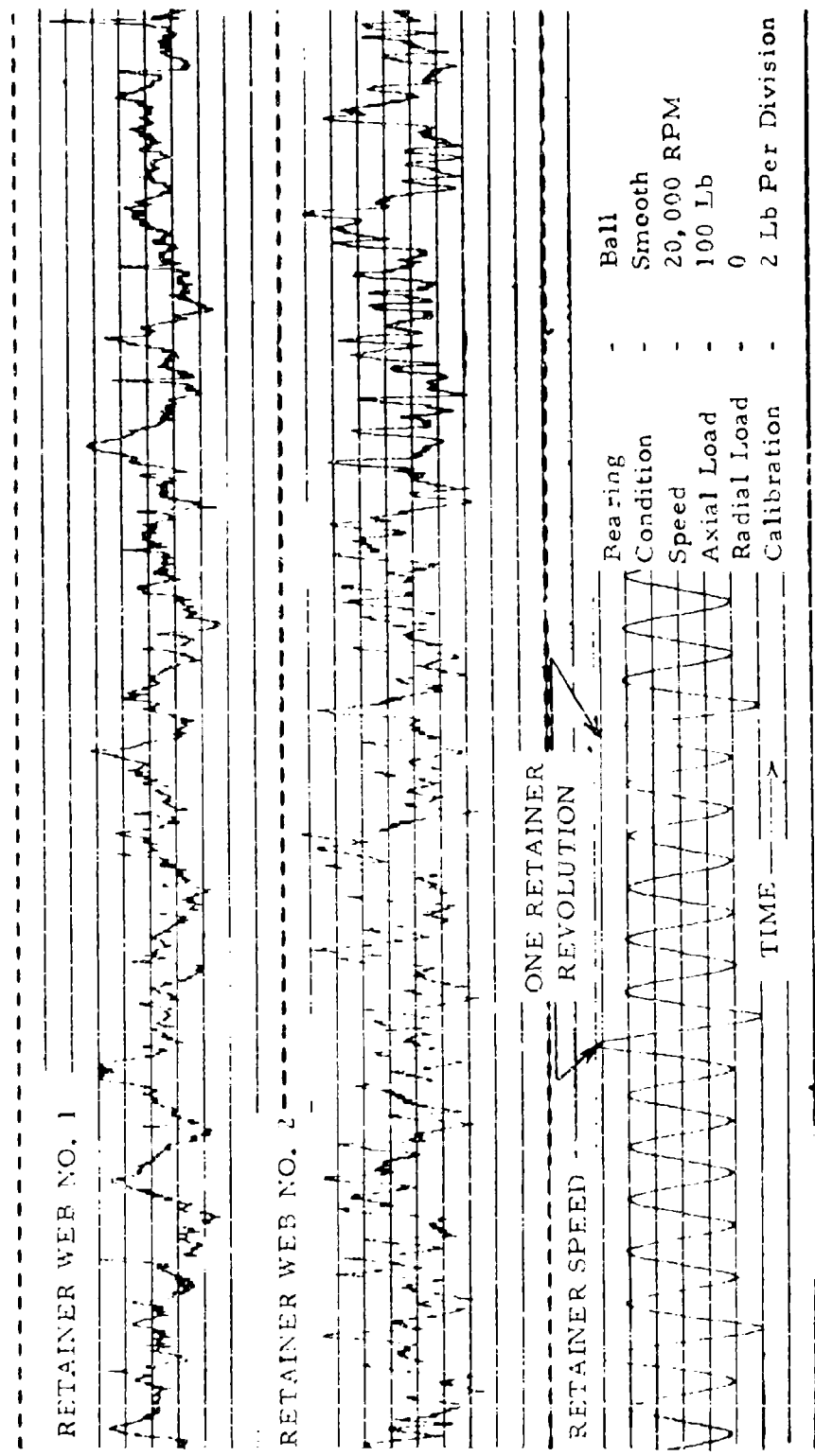


Figure 72. Retainer Web Force Expanded With Computer Web Force Superimposed.

The large, pulse-like force was later simulated in the laboratory by impact loading a ball against a retainer web. Results suggested the presence of dynamic ball/pocket forces resulting from accelerations of the ball within the pocket clearance or of the retainer itself. These dynamic effects were not predicted by the computer program.

With respect to the smaller vibratory signal, two approaches were taken in the analysis of the test data. First, ball azimuth versus retainer web force plots as determined by the computer program were superimposed on similar plots from the test program data (Figures 65 through 72). Second, a harmonic analysis of the computer-determined output was compared with similar analysis from the test data (Figures 73 through 75). Figure 75 shows the computer-determined harmonic analysis of the computed web force wave, and is normalized here to an arbitrary unit to compare ratios of harmonics rather than absolute values. Figures 73 and 74 show the average of 16 spectra obtained from experimental test tape recordings. Spectrum averaging was used to eliminate random signals that might be present in the experimental wave forces, since the harmonic analysis of any selected cycle could be distorted by random occurrences.

In the cases of pure thrust bearing loading (Figures 65, 68, and 69), where computed pocket force is a constant value of approximately 0.25 pound, the dynamic component determined experimentally (neglecting impact peaks) was between  $\pm$  3 and  $\pm$  4 pounds. It is suggested that the difference between the computed and measured force levels at these conditions, where the predicted force is nearly zero, is background or additional forces generated by conditions not considered in the computer analysis. Practically speaking, a 3- to 4-pound background force is of little consequence.

In the cases of combined thrust and radial loading (Figures 66, 67, and 70), the predicted and measured force levels are of the same magnitude, neglecting impact peaks. The computer program predicted approximately  $\pm$  1.5 to  $\pm$  2.0 pounds; the measured values were from  $\pm$  4 to  $\pm$  4.5 pounds. Note that the difference is not large in view of the background levels determined during pure thrust load tests.

Two of the test conditions, filtered and unfiltered, are shown in Figures 76 through 79. Frequencies higher than seven times retainer speed (seventh order) have been eliminated in the filtered wave.

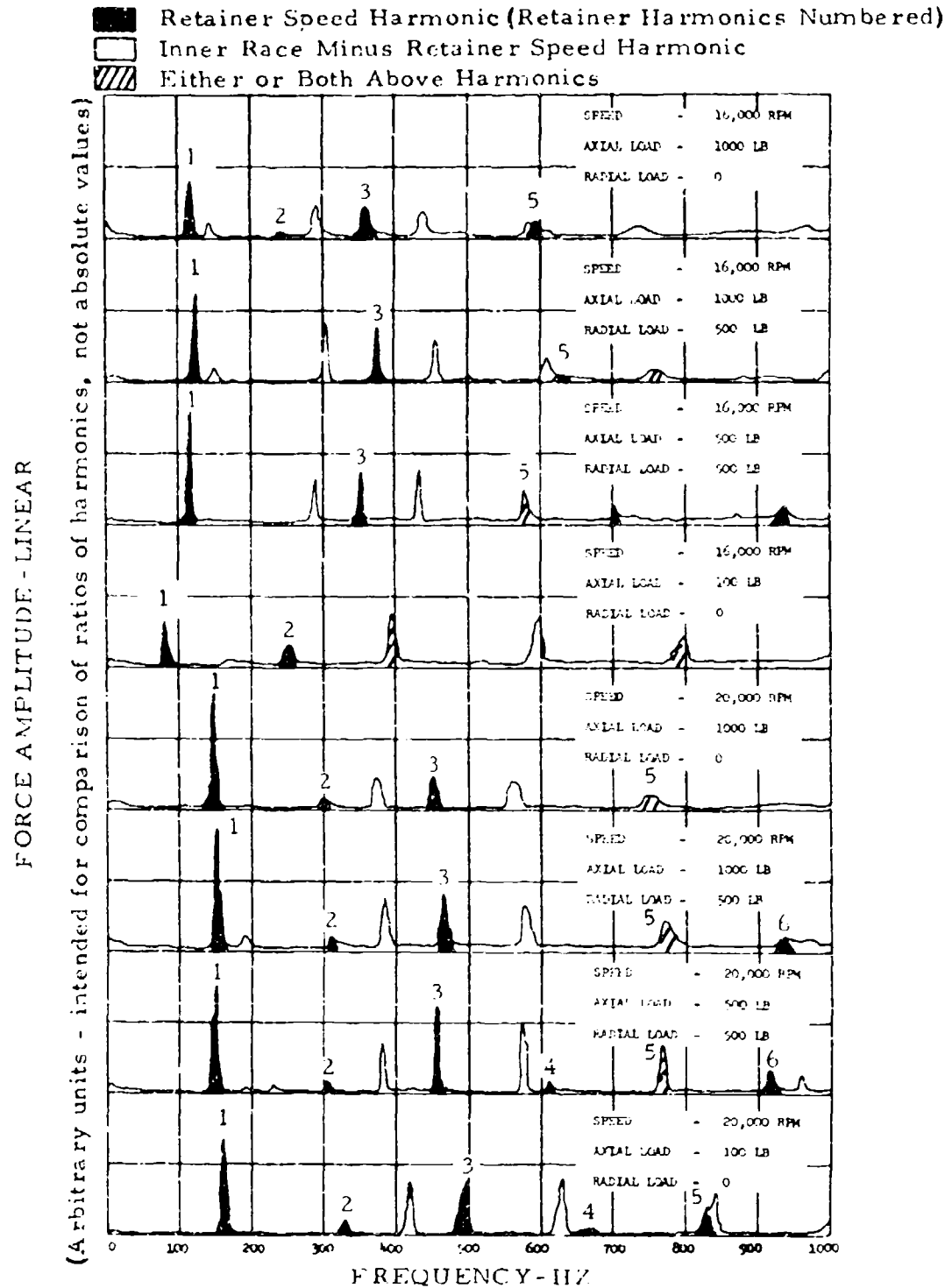


Figure 73. Harmonic Analysis of Experimentally Determined Retainer Web Force (Average of 16 Spectra) for Ball Bearing Smooth Race. Bearing Retainer Web No. 1.

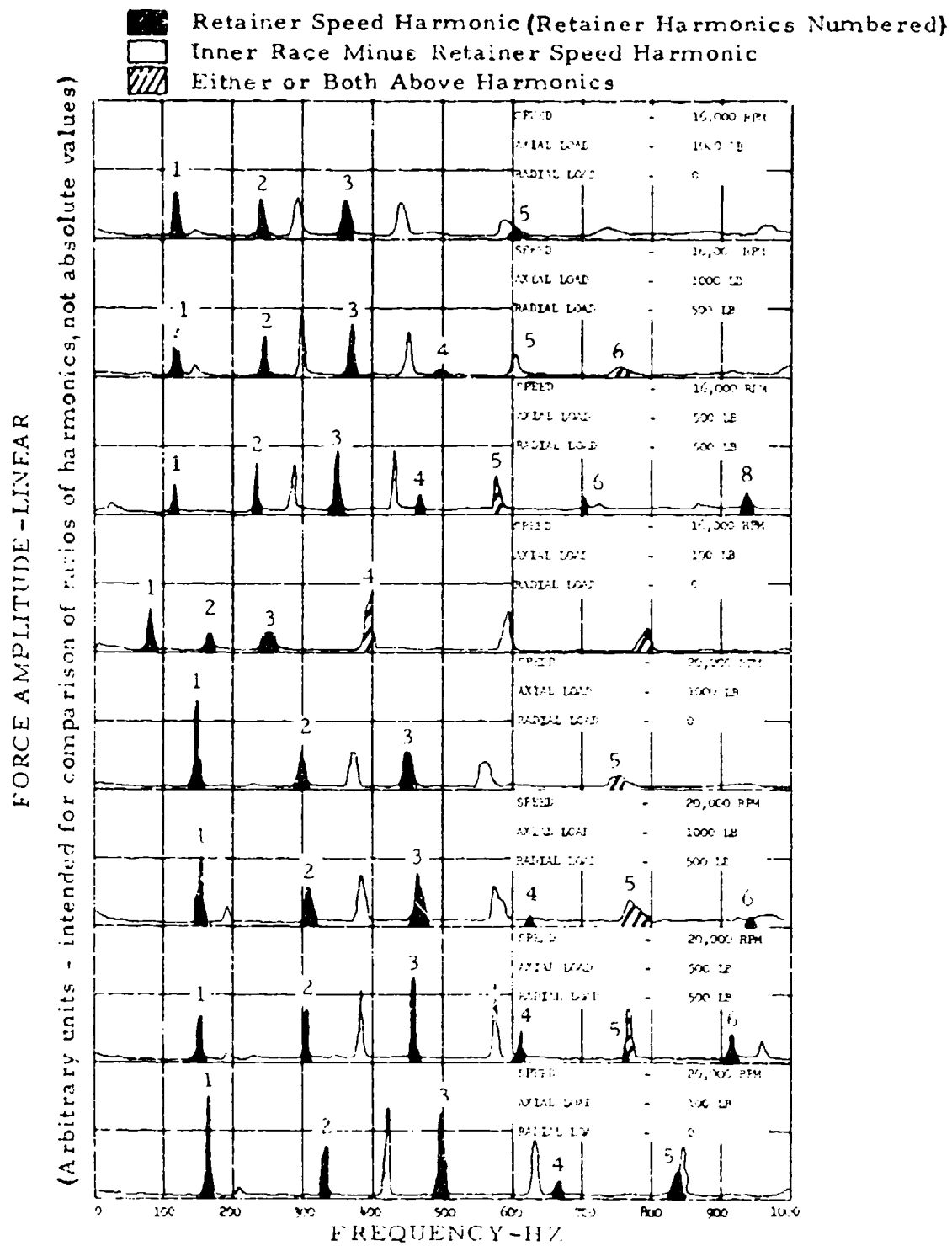


Figure 74. Harmonic Analysis of Experimentally Determined Retainer Web Force (Average of 16 Spectra) for Ball Bearing Smooth Race, Bearing Retainer Web No. 2.

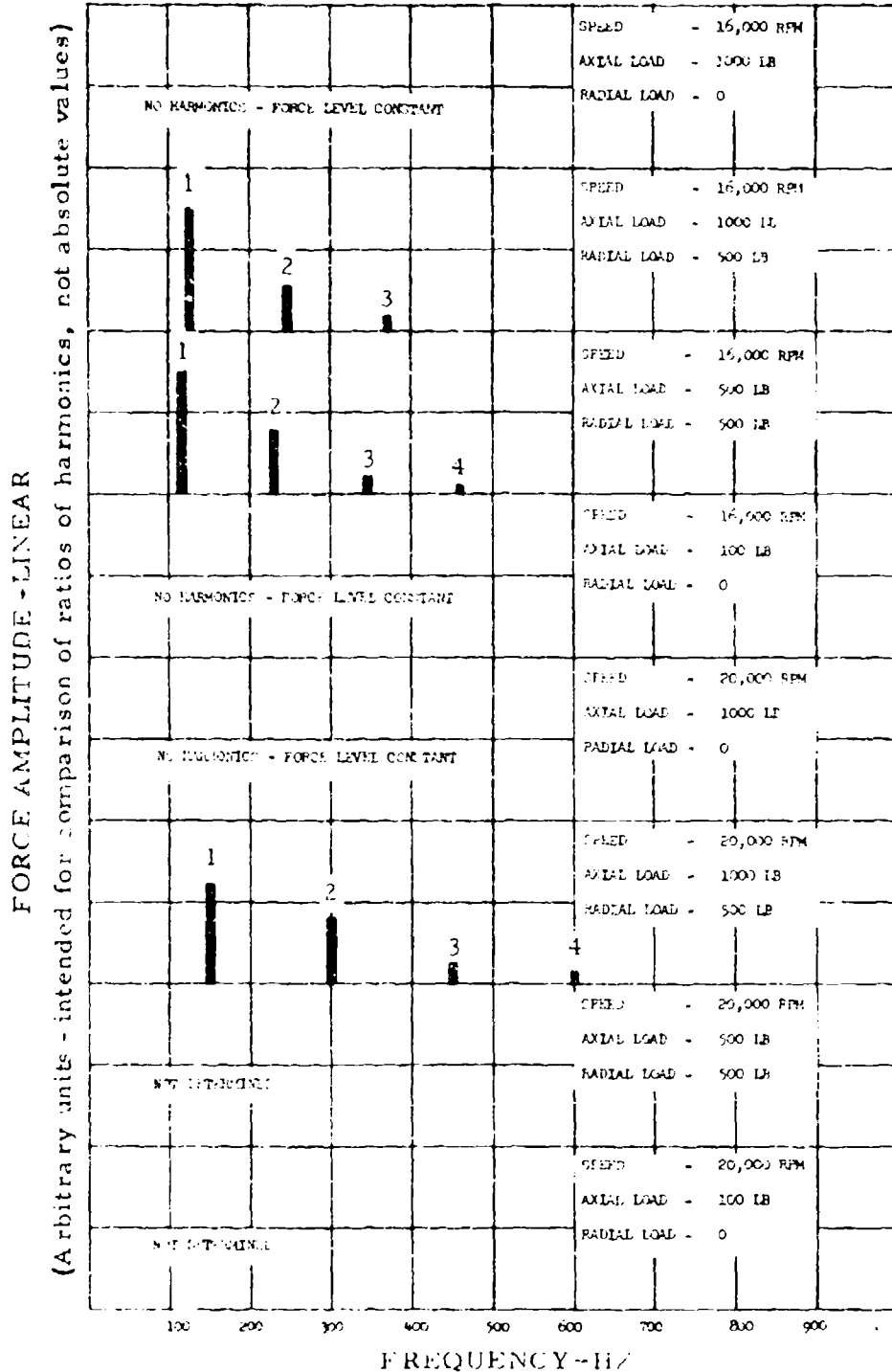


Figure 75. Harmonic Analysis of Computed Retainer Web Force for Ball Bearing Smooth Race.

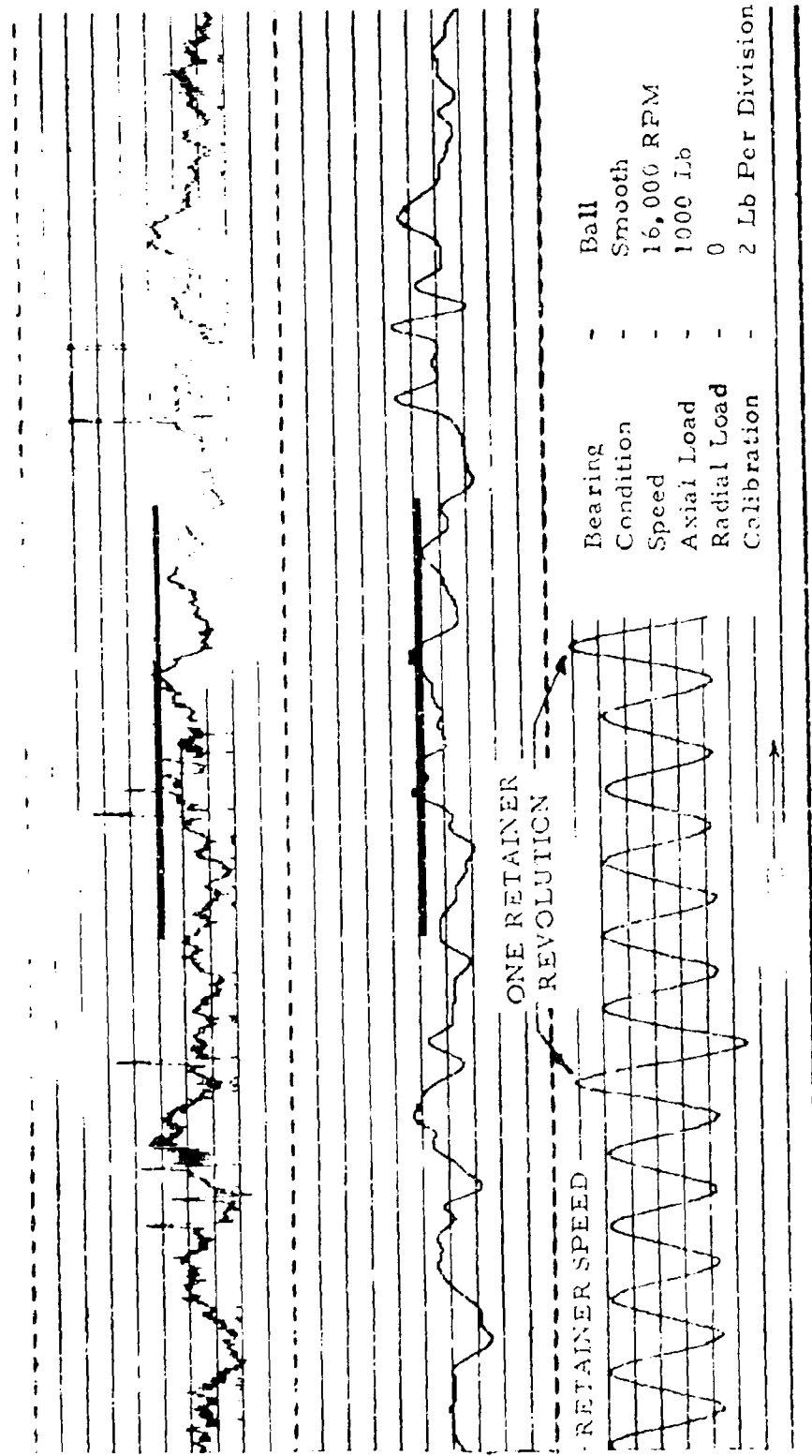


Figure 76. Retainer Web No. 1, Filtered and Unfiltered Retainer Force Wave Form With Computed Forces Superimposed. Frequencies Higher Than Seventh Order Retainer Speed Removed in Filtered Wave.

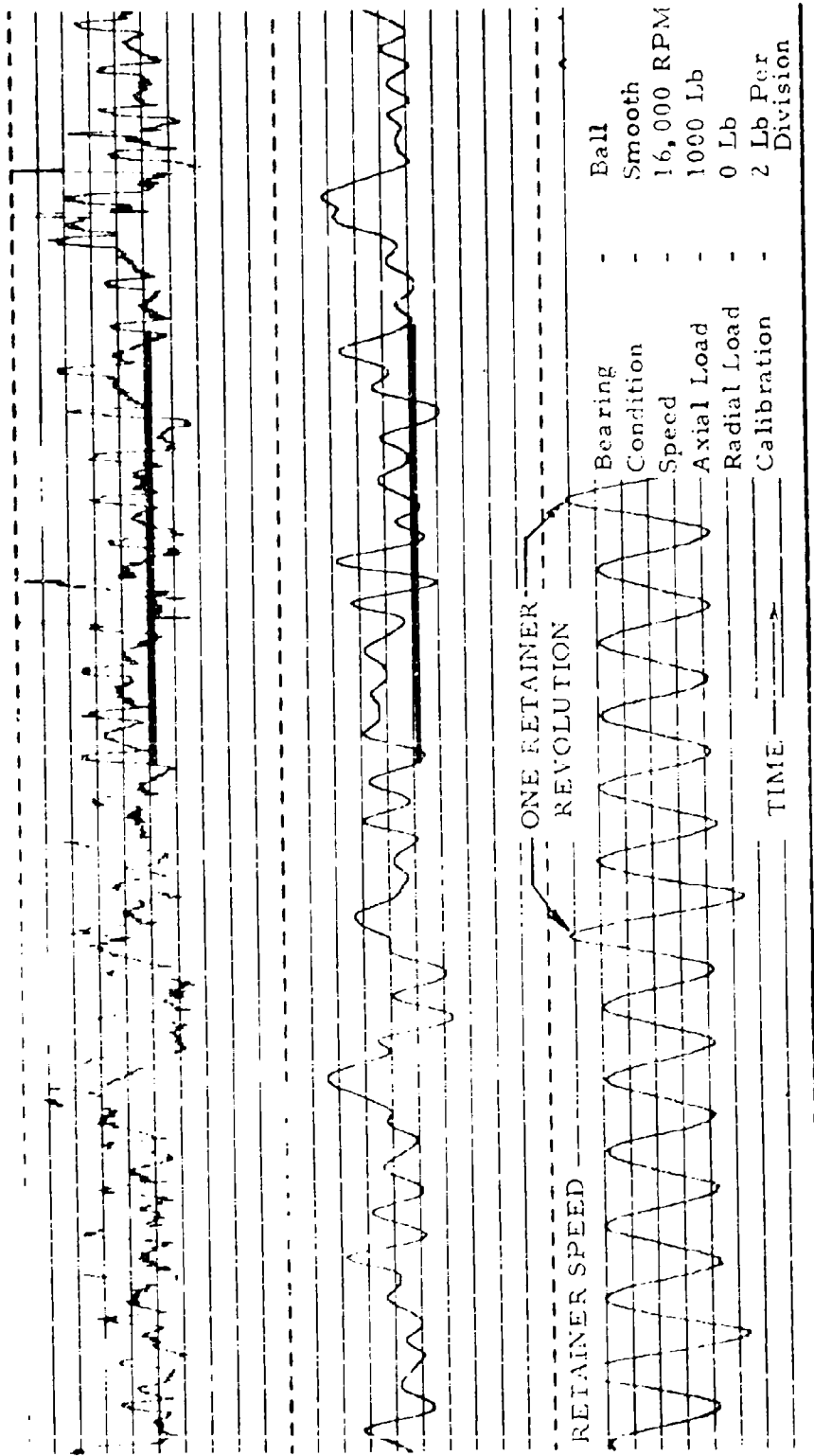


Figure 77. Retainer Web No. 2. Filtered and Unfiltered Retainer Force Wave Form With Computed Forces Superimposed. Frequencies Higher Than Seventh Order Retainer Speed Removed in Filtered Wave.

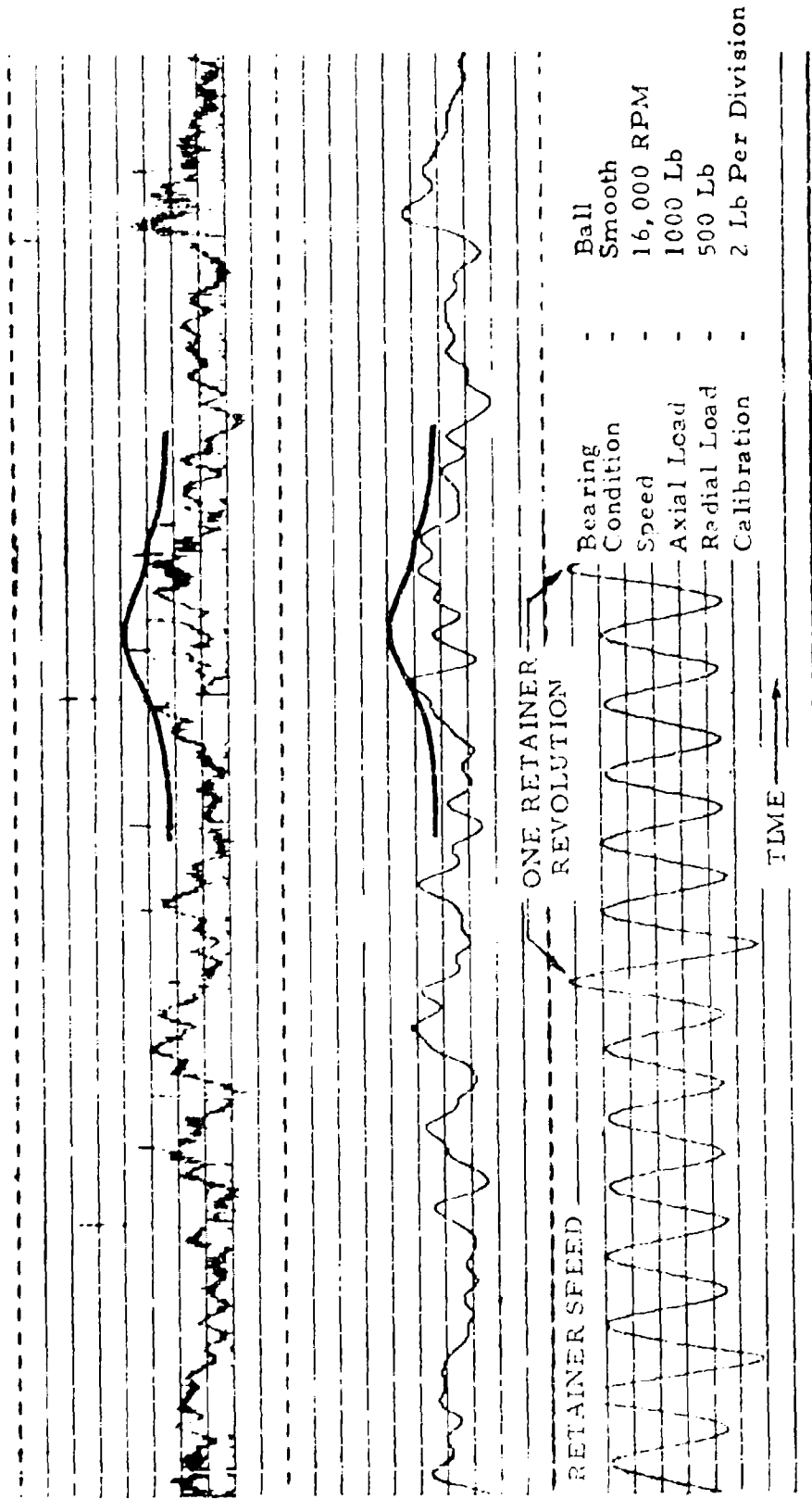


Figure 78. Retainer Web No. 1, Filtered and Unfiltered Retainer Force Wave Form With Computed Forces Superimposed. Frequencies Higher Than Seventh Order Retainer Speed Removed in Filtered Wave.

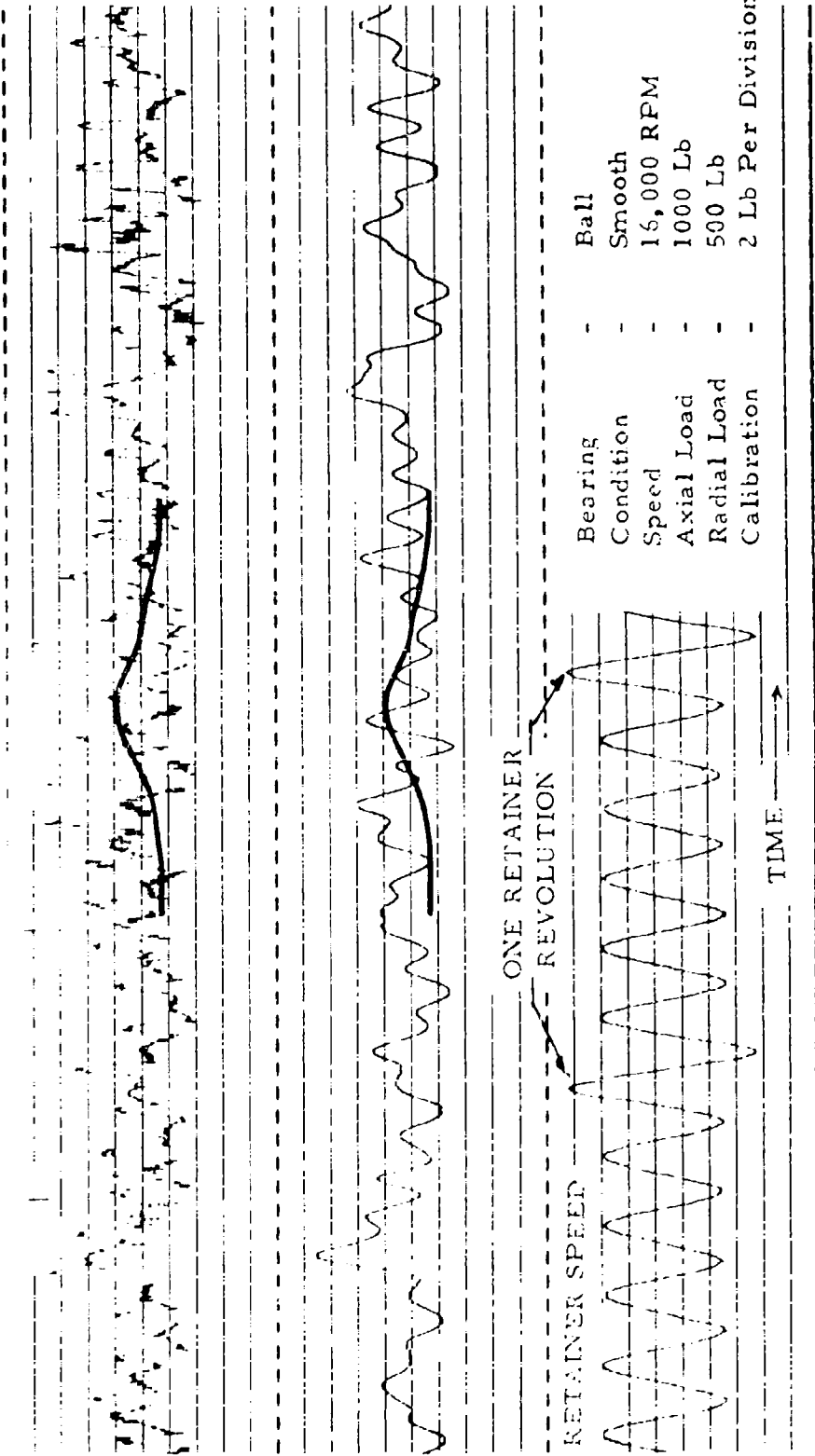


Figure 7a. Retainer Web No. 2, Filtered and Unfiltered Retainer Force Wave Form With Computed Forces Superimposed. Frequencies Higher Than Seventh Order Retainer Speed Removed in Filtered Wave.

Harmonic analysis (Figures 73 through 75) shows similar frequency components for computer and test results, but proportions of the harmonics are not comparable; in fact, two different retainer webs show different harmonic amplitudes. There are also more frequency components in the experimental data. Further experimentation and analysis are required to understand these differences between predicted and measured values and to explain the origin of the background force level described above.

A skid map is shown in Figure 80.

#### Build No. 3, Rough-Race Ball Bearing

Inner and outer race temperatures are summarized in Table XI. Ball force data from the rough bearing generally looked similar to that of the smooth bearing with pulse magnitudes reduced. Samples of data from the first two test points are shown in Figures 81 and 82. The distorted retainer speed signal is the result of magnetic tape saturation in one direction, but since the large peak is still discernible, the signal is still useful in establishing the time of a single ball cycle and the relationship between the location of the retainer and the leading zone. Figure 82 also shows the beginning of the deterioration of the No. 2 retainer-web strain-gage bridge.

#### Build No. 4, Smooth-Race Roller Bearing

Inner and outer race temperatures are summarized in Table XII.

Traces from the only functioning retainer-web strain-gage bridge for four test conditions are shown in Figures 83 through 86.

The roller force traces do not show the large pulse-like forces found in the ball force traces at the test conditions required for computer verification; however, these peaks were observed while sweeping to the test speed.

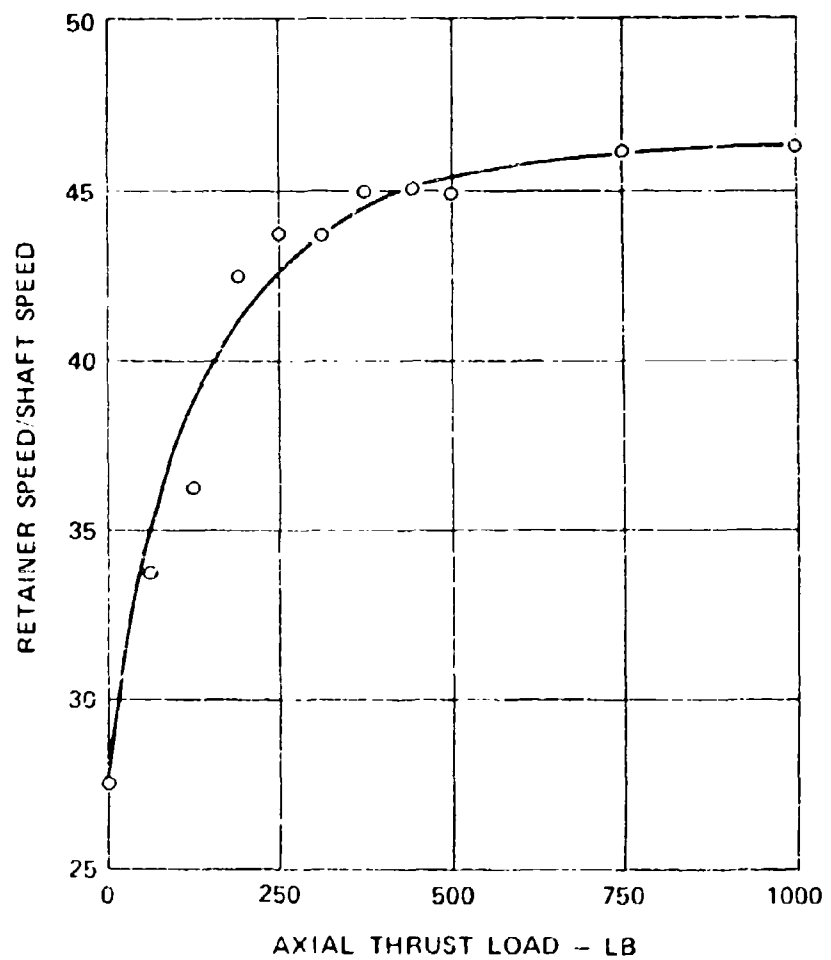
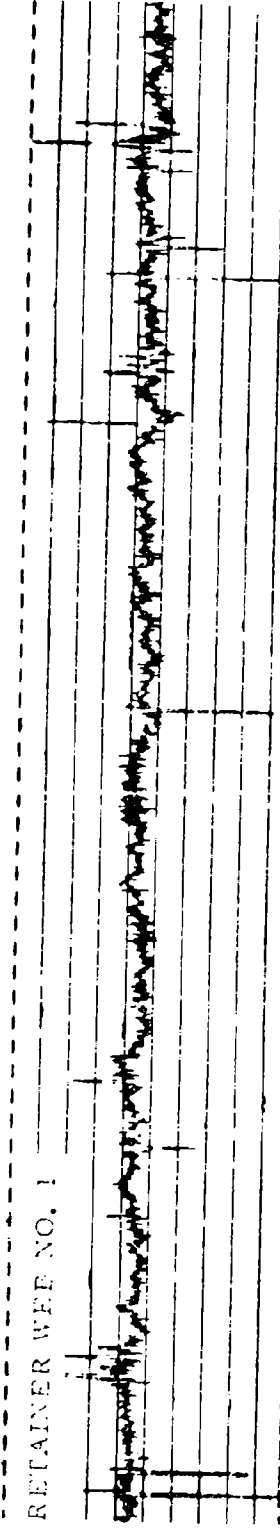


Figure 80. Retainer Speed Ratio Versus Axial Thrust Load.

TABLE XI. INNER AND OUTER RACE TEMPERATURES,  
BUILD NO. 3

Data Point	Inner Race (° F)	Outer Race (° F)	$\Delta T$ (° F)
1	275	250	-25
2	340	265	-75
3	20	260	0
4	290	265	-25
5	265	275	10
6	320	285	-35
7	300	285	15
8	-	275	-

RETAINER WEB NO. 1



RETAINER WEB NO. 2



169

ONE RETAINER  
REVOLUTION

RETAINER SPEED

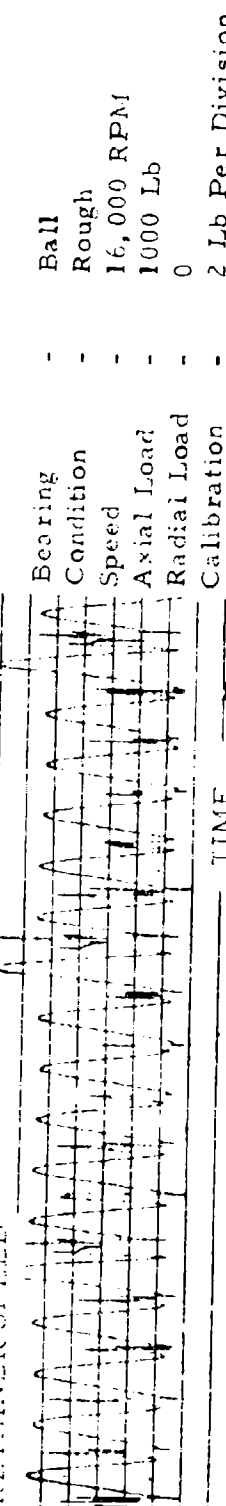


Figure 8i. Expanded Trace of Rough-Race Bearing Retainer Web Forces. Speed signal distortion is result of magnetic tape saturation.

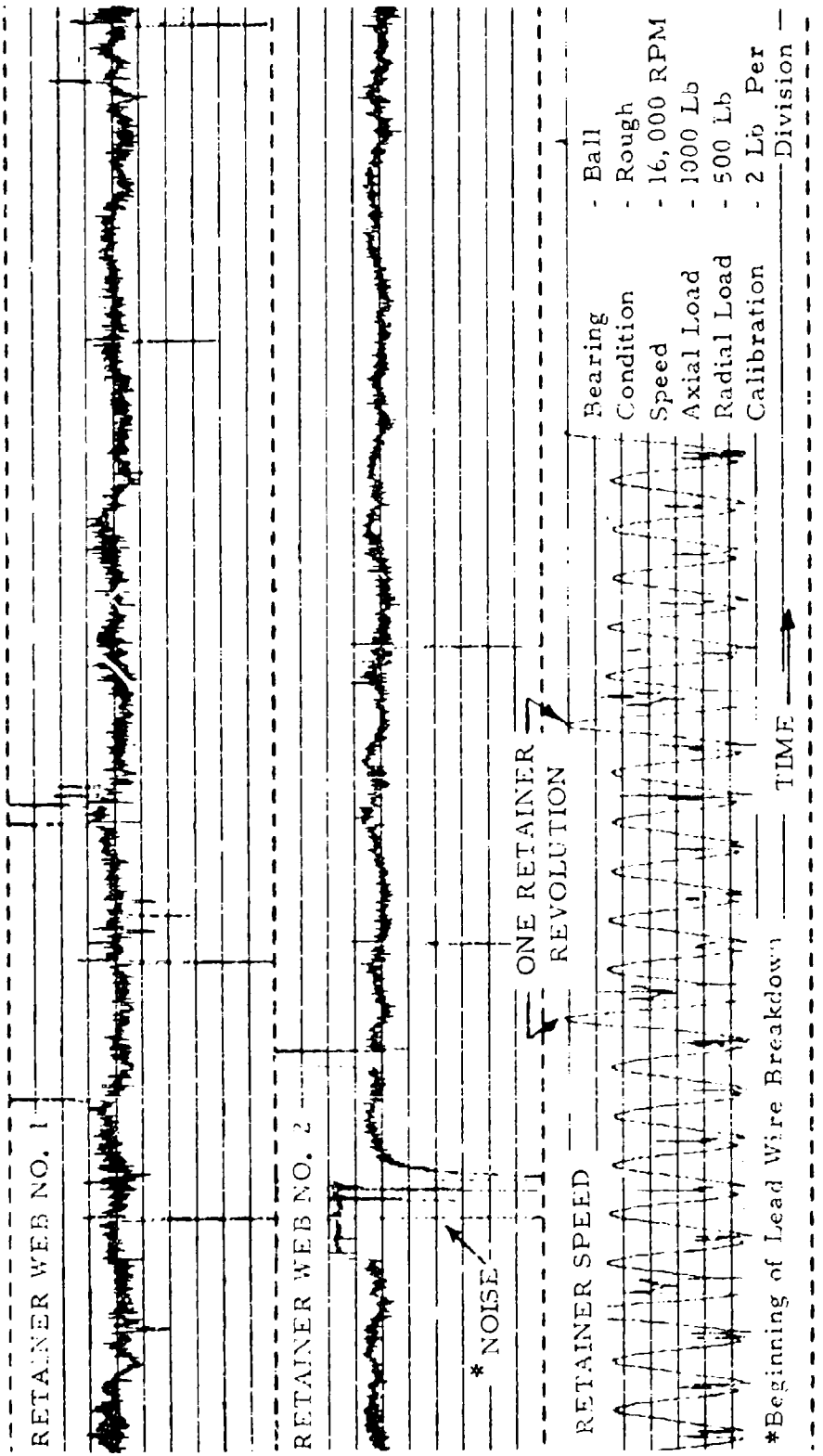


TABLE XII. INNER AND OUTER RACE TEMPERATURES,  
BUILD NO. 4

Data Point	Inner Race (° F)	Outer Race (° F)	$\Delta T$ (° F)
1	200	225	25
2	180	215	25
3	168	195	27
4	130	165	35
5	230	225	-5
6	245	245	0
7	180	255	75
8	140	265	125

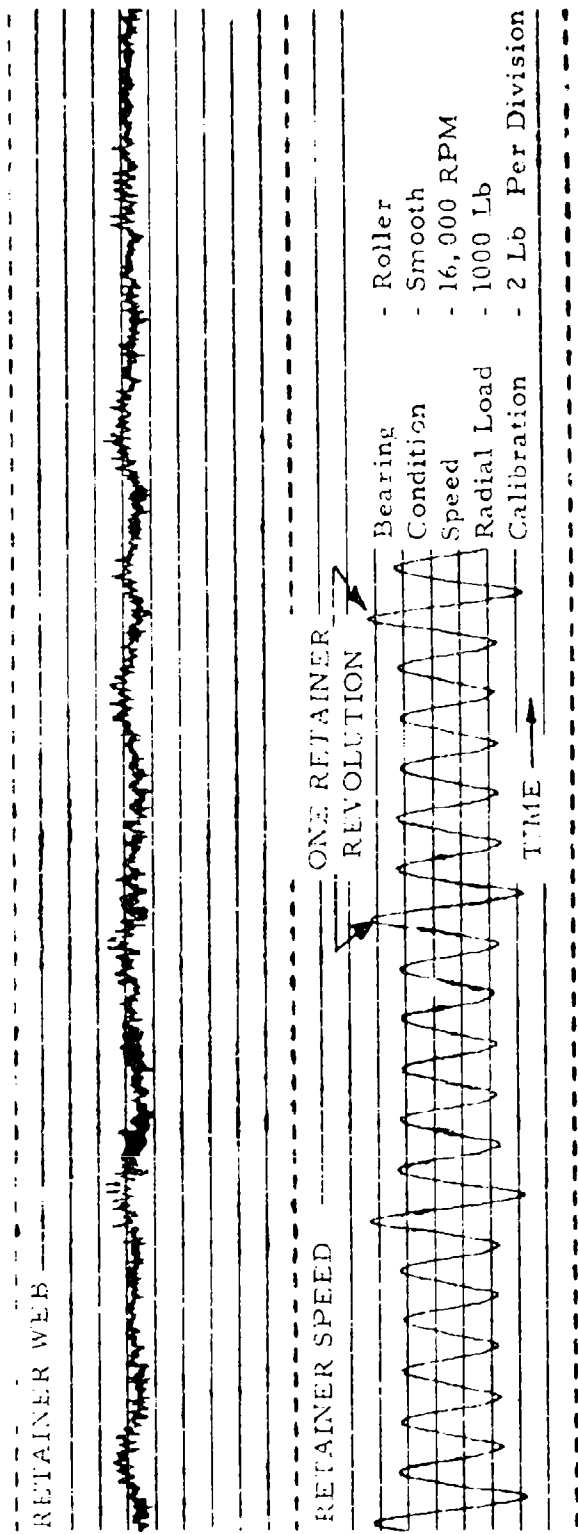


Figure 83. Bearing Retainer Web Force and Speed Versus Time.

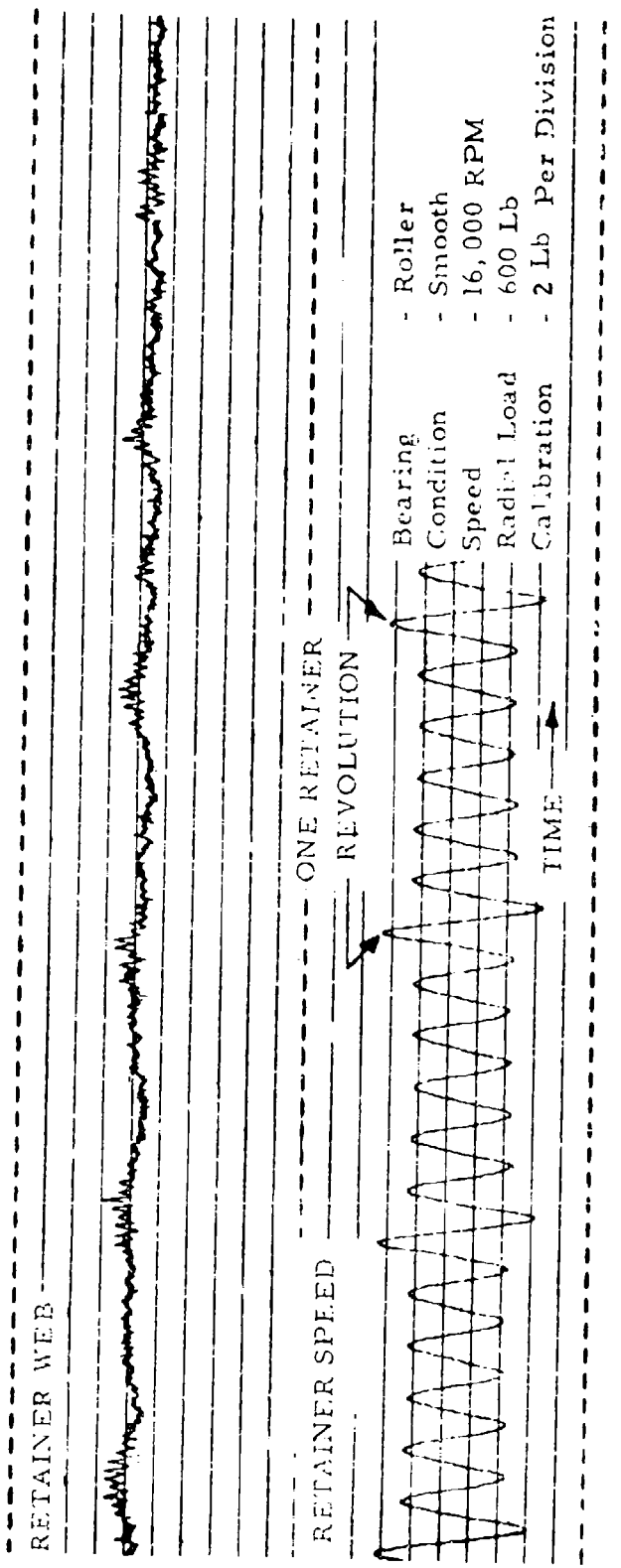


Figure 84. Bearing Retainer Web Force and Speed Versus Time.

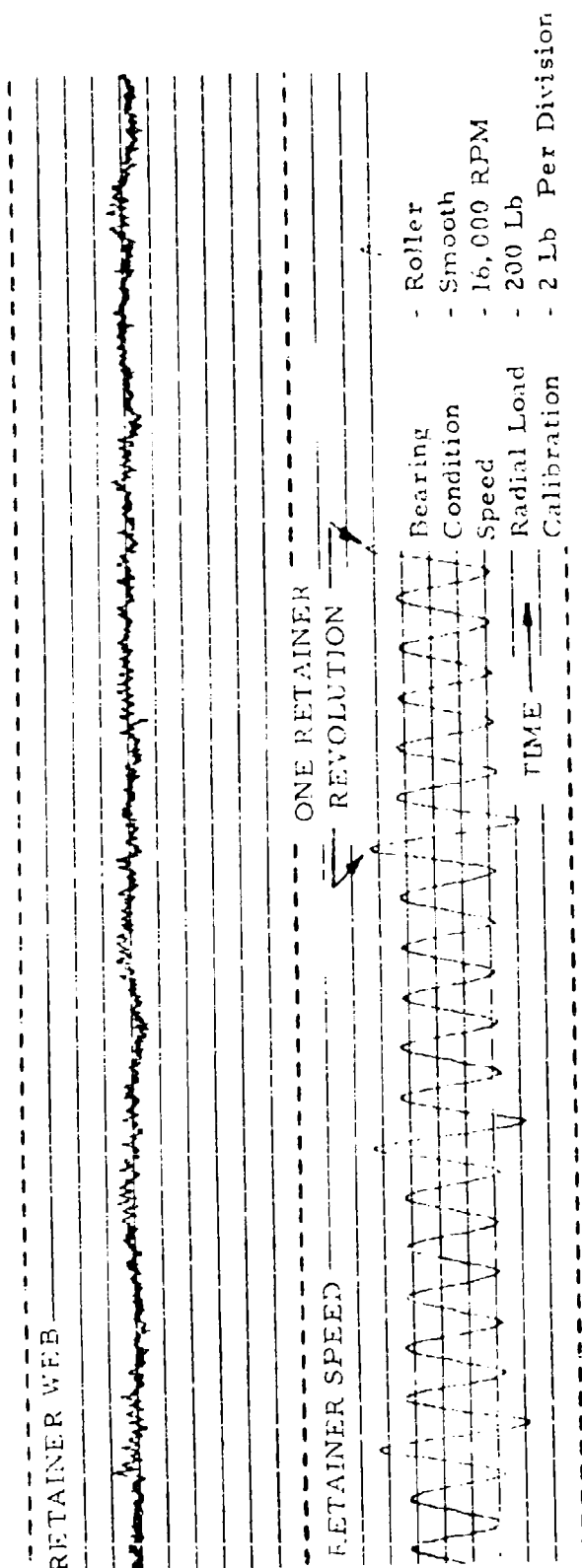


Figure 85. Bearing Retainer Web Force and Speed Versus Time.

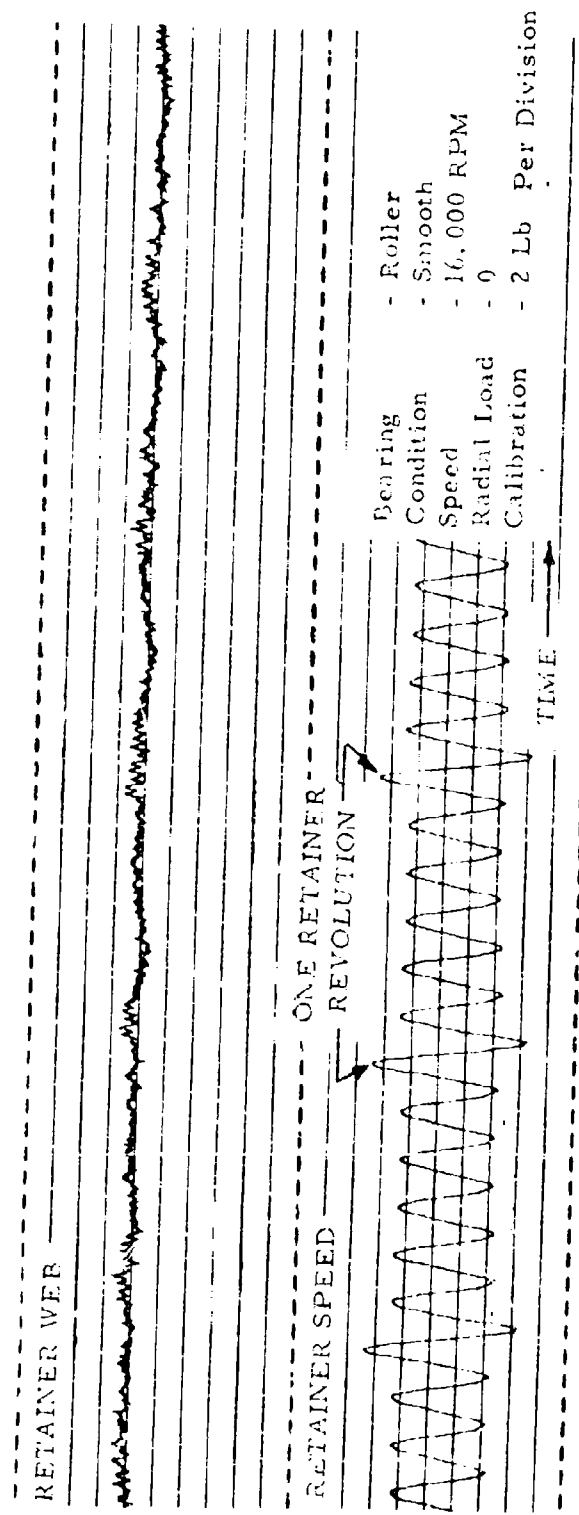


Figure 86. Bearing Retainer Web Force and Speed Versus Time.

## COMPUTER PROGRAM RESULTS

### BALL BEARING COMPUTER DECK

A listing of the ball bearing computer program FORTRAN source deck is presented in Appendix I. The program consists of a main section and eleven subroutines, each of which performs a specific function. This modular organization of the program facilitates the incorporation of alternate or improved mathematical models at a later date if revisions or modifications are indicated by future advances in the technology. For example, if it is desired to employ traction-slip data other than that reflected, only the subroutine FRCTN need be replaced.

The format for the input information required in the program is given in Appendix II. Cards signifying appropriate units for the input parameters and recommended values of convergence limits are included. Available options concerning the sequence of running numerous load cases with varying bearing definitions, lubricant descriptors, etc., are explained.

A typical problem with the input restated and the program output conveniently labeled for easy interpretation is presented in Appendix III.

### BALL BEARING TYPICAL RESULTS

#### Retainer Pocket Loading and Lubrication

To illustrate the results desired of the computer program, the bearing problem shown in Table XIII, based on the test bearing in the experimental program, was adopted.

The bearing is analyzed at a constant inner ring speed of 20,000 rpm ( $2.0 \times 10^6$  DN) and an axial thrust load of 1,000 pounds. Externally applied radial loads were varied to determine their effect on pocket loading and lubrication. The effects of applied radial loads on the ball pocket load distribution are shown in Figure 87.

A positive pocket force indicates that the ball is driving the retainer assembly; conversely, a negative pocket force indicates that the ball is retarding the rotation of the retainer assembly. The results clearly indicate, as intuition dictates, that ball pocket loading is strongly dependent upon the relationship between the thrust and the radial load when operating under combined axial and radial externally applied loads. This dependency occurs because the unconstrained orbital velocity of each ball

TABLE XIII. BEARING PROBLEM PARAMETERS

Number of Balls	22
Ball Diameter	.531 in.
Pitch Diameter	4.724 in.
Nominal Contact Angle	30 deg
Outer Race Curvature	.515
Inner Race Curvature	.520
Clearance Change	-.0015 in.
Pilot Clearance (outer)	.029 in.
Pocket Clearance	.031 in.
Pressure Viscosity Coefficient	$1.18 \times 10^{-4} \text{ in.}^2/\text{lb}$
Temperature Viscosity Coefficient	$1.53 \times 10^{-2} \text{ }^{\circ}\text{F}^{-1}$
Viscosity at Inlet	$3.86 \times 10^{-6} \text{ lb-sec/in.}^2$
Thermal Conductivity	$7.74 \times 10^{-2} \text{ Btu/}^{\circ}\text{F-hr/ft}$
Lubricant Density	$8.97 \times 10^{-5} \text{ lb-sec}^2/\text{in.}^4$

position would be different, owing to contact angle variations from position to position. Contact angle variations are strongly dependent on the magnitude of radial load relative to the axial load acting on the bearing. The calculated radial force acting between the pilot surface and the outer race land is shown as a parenthetic quantity in Figure 87. It is interesting to note the variation in this load component for the equal increments of externally applied radial loads. Note that for equal externally applied radial load increments from 500 to 750 pounds and from 750 to 1,000 pounds, the pilot surface contact force increase is 2.2 and 17.3 pounds, respectively. Additional cases were investigated with a thrust load of 500 pounds and a radial load of 1,000 pounds, and a pure radial load of 1,000 pounds with resulting pilot surface contact forces of 7.76 and 1.91 pounds, respectively. An axial-radial load ratio appears to exist (approximately 1:1) at which the pilot load is at a maximum value. This load component, in the case of an outer-piloted retainer, results in a retainer drag force; in the case of an inner-piloted retainer, it creates a retainer driving force. This effect might be theorized to be responsible for the skid recovery phenomenon often experienced on ball bearings at high speeds and extremely low thrust loads. Figure 88 illustrates the hydrodynamic ball-pocket film thickness as a function of azimuth angle for a thrust load of 1000 pounds and a radial load of 500 pounds. Also plotted on the same azimuth scale is the pocket loading to illustrate the strong dependence of film thickness upon load. For light loads, pocket film thicknesses are limited to pocket clearances in the analysis because often, with extremely light pocket loads, unrealistically large estimates will result.

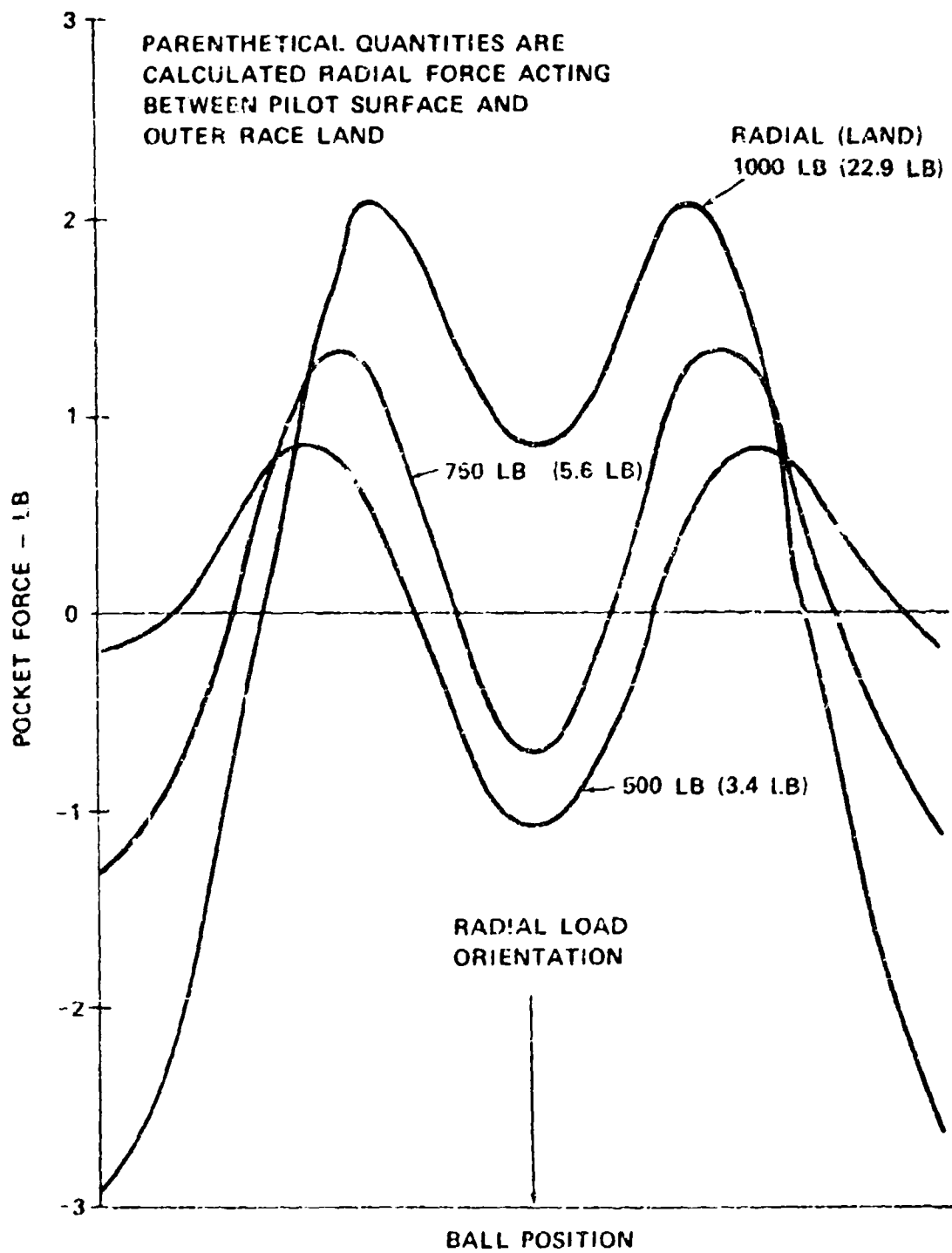


Figure 87. Pocket Loading Versus Radial Load (Axial Load = 1000 Pounds).

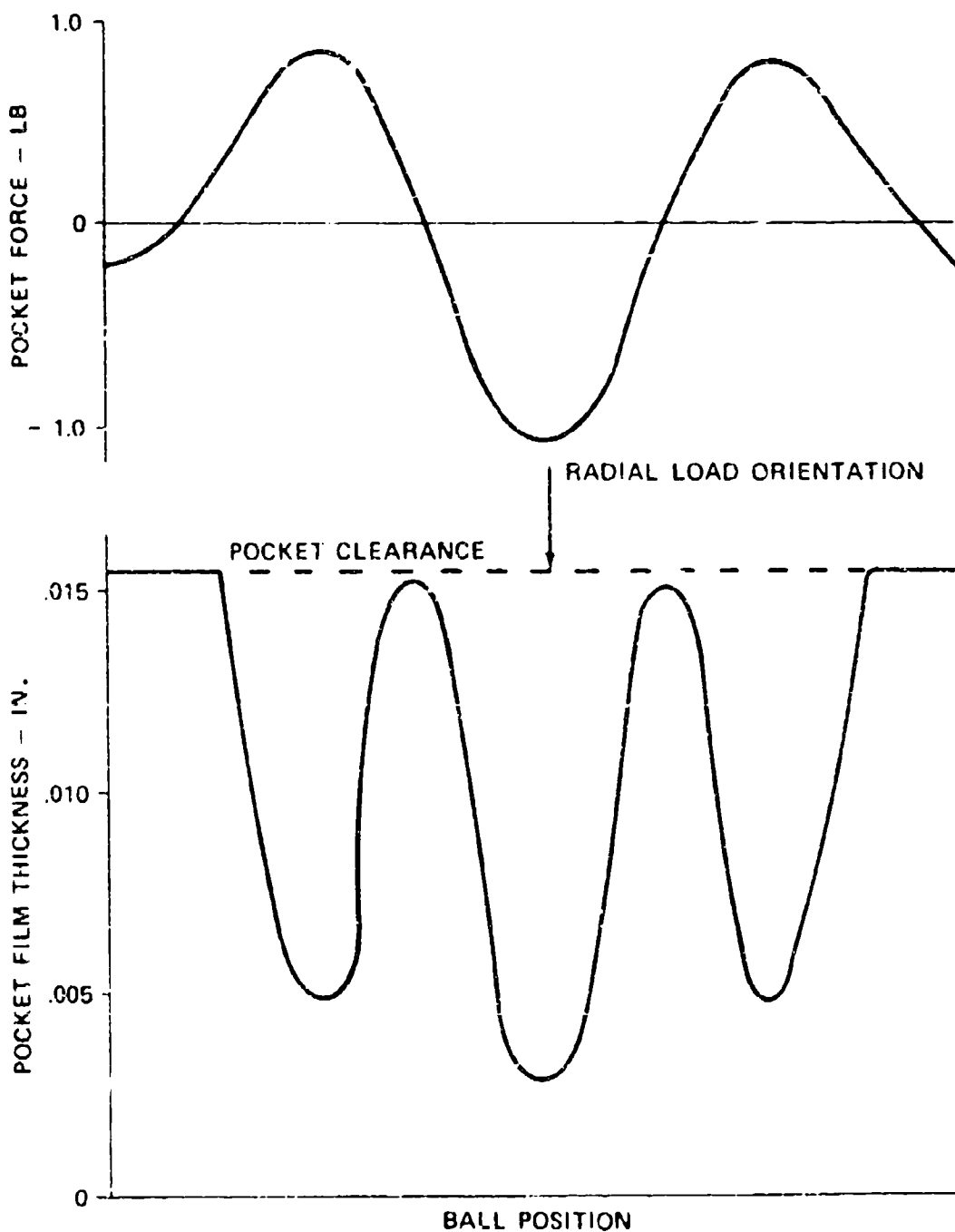


Figure 88. Pocket Film Thickness Versus Pocket Load  
(Axial Load = 1000 Pounds, Radial Load = 500  
Pounds).

### Retainer Speed Variations (Skidding)

An important spinoff benefit derived from the retainer analysis reported herein is the ability to predict retainer skidding as a function of externally applied loads for high-speed angular-contact ball bearings. Figure 89 compares retainer speed results derived from the computer program with data obtained during the verification program. Also shown are the retainer speeds calculated using the elastic analysis (no slip), which is extensively used for bearing design today throughout industry. The zone depicted between the dashed lines in the gross skid regime is indicative of retainer speed variations encountered. Unlike previous results,<sup>9</sup> retainer rotational velocities in this skid regime were not constant, and significant excursions were observed at constant thrust loads. This phenomenon is not considered to be of great importance from a design standpoint; what is significant is the break in the curve below which gross skidding occurs.

With respect to the difference between the elastic solution prediction and the EHD solution results, the difference in retainer speeds calculated at high thrust loads is predominantly the result of ball slip at the race contacts required to generate traction. Inner and outer race contact angles for this load case were essentially the same for the two different analytical solutions.

### Ball Kinematics

The kinematics of a ball in a high-speed angular-contact bearing has provided bearing engineers and analysts with a wide area for disagreement over the last decade. The reason is that in an angular-contact ball bearing, pure rolling cannot occur simultaneously at both inner and outer race contacts.<sup>2</sup> Consequently, assumptions were required concerned with the spin velocities prevalent at the race contacts and the distribution of tractive force components required to offset ball gyroscopic moments. The major controversy centers about the race control concept previously discussed under "Introduction."

This concept is based upon the supposition that all the spin occurs at the contact where the resistance to spin (spin torque) is minimum, and that all traction in the gyroscopic plane occurs at the race contact which exhibits pure rolling (no slip). For example, a bearing with outer race control would have zero spin at the outer contact with the inner contact operating at the geometrically required spin level, while all the required traction force to resist gyroscopic precession would be developed at the outer contact.

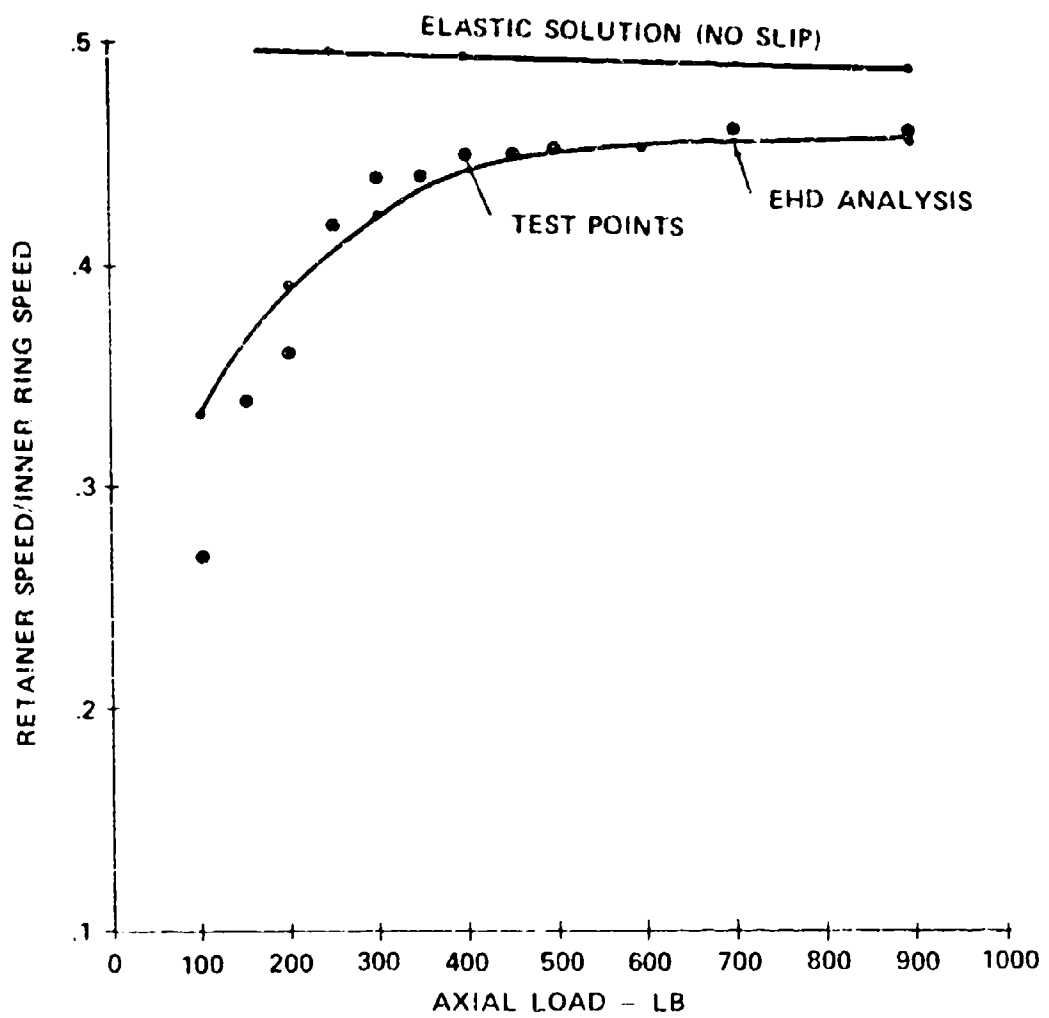


Figure 89. Retainer Speed Versus Axial Load.

The analysis developed herein is general and does not require these assumptions, and unbiased solutions can be obtained. Table XIV presents computer results pertaining to ball kinematics for varying thrust loads to explore this phenomenon in the skid regime and at high thrust loads. The cases studied are the same as those used for the skid curve, Figure 89. Also shown at the bottom of the table is the result of an elastic solution in which outer race control is assumed.

In Table XIV,  $\omega_x$ ,  $\omega_y$ , and  $\omega_z$  are the angular velocity components about the indicated axes. The angular velocity component  $\omega_y$  has a circumferential vectorial direction, i.e., gyroscopic precession.  $F_{X_1}$  and  $F_{X_2}$  are the tractive forces in the outer and inner contact areas, which are opposing the rotation  $\omega_y$ . The ratio  $F_{X_2}$  divided by  $F_{X_1}$  compares these two force components. Outer race control would have  $F_{X_2} = F_{X_2}/F_{X_1} = 0$ . The computer results do not rigorously substantiate this assumption, but  $F_{X_2}$  is significantly less than  $F_{X_1}$ , which indicates that the race control concept is, if not absolutely correct, practically useful from this standpoint. It is interesting to note that from a traction standpoint, bearings in the skid regime tend more toward race control than those that are operating at high thrust loads. Also, by comparing the 800-pound thrust load cases, it is seen that a greater value of  $\omega_y$  is predicted with the EHD analysis with a corresponding increase in gyroscopic moment and tractive force.

Another relationship that can be used to test the accuracy of the race control concept is the spin velocities at the race contact. Again, referring to Table XIV, it is evident that spin occurs predominantly at the inner contact as the control theory predicts. With regard to the behavior in the skid regime, values of  $\omega_{s_1}$  divided by  $\omega_{s_2}$  increase as gross skidding increases -- the opposite effect relative to race control behavior as observed with the tractive forces.

In general, kinematic behavior that is in relative agreement with the race control concept is not surprising, in that many successful bearings have been designed with the use of analytical techniques predicated upon its precepts.

TABLE XIV. BALL KINEMATICS; INNER RING SPEED = 20,000 RPM, RADIAL LOAD = 0

Thrust (lb)	$\omega_X$ (rpm)	$\omega_Y$ (rpm)	$\omega_Z$ (rpm)	$F_{X_1}$ (lb)	$F_{X_2}$ (lb)	$F_{X_2}/F_{X_1}$	$\omega_{S1}$ (rpm)	$\omega_{S2}$ (rpm)	$\omega_{S1}/\omega_{S2}$
100	-67,640	1,696	8,470	-3.78	-0.15	.013	-7,854	-39,753	.198
200	-78,834	1,960	10,030	-5.30	-0.15	.028	-7,764	-44,826	.173
300	-84,104	2,052	11,641	-6.32	-0.27	.043	-7,210	-46,953	.154
500	-88,447	2,075	13,930	-7.75	-0.59	.076	-5,945	-47,820	.124
800	-89,566	1,990	17,210	-9.29	-1.25	.135	-4,540	-45,800	.099
800 (Elastic Solution)	-94,800	0	12,600	-8.2	0	0	-52,669	0	

### ROLLER BEARING COMPUTER DECK

A listing of the roller bearing computer program FORTran source deck is presented in Appendix IV. The program is structured in a manner similar to the ball bearing deck and consists of a main section and nine subroutines. Four subroutines are inactive in this listing as a result of the convergence problems encountered with the COEFCT routine. They are included in this listing since they were part of the initial effort.

The format for the program input is given in Appendix V. Directions for exercising various program input options are also given. A particular input requirement for the roller bearing program is found on card 9, columns 41 through 50. This input item causes the program to execute the specific case for the cage slip inputted. It is therefore required that the user input an appropriate series of cases to achieve a desired solution. The solution is obtained when the "Torque on Cage" output value approaches zero.

A typical problem and corresponding output is presented in Appendix VI.

### ROLLER BEARING TYPICAL RESULTS

The bearing data shown in Table XV was used to illustrate the desired program output. This data represents the test roller bearing used during the experimental program.

The bearing was analyzed at an inner ring speed of 20,000 rpm, which results in a DN speed value of  $2 \times 10^6$ . Radial loads were varied to determine slip speeds of the cage and other bearing outputs. To arrive at the desired solution, various cage slip speed assumptions were inputted. Each output case yielded residual cage torques which were plotted as shown in Figure 90. The final solutions for slip are obvious and can be inputted to obtain final results for each load case. Final results for cage slip speeds as a function of radial loading are shown in Figure 91. The iterative procedure was pursued for the 200-pound load case, the solution for which is shown in Appendix VIII.

TABLE XV. ROLLER BEARING PROBLEM PARAMETERS

Number of Rollers	28
Roller Diameter - in.	.4331
Roller Length - in.	.4331
Pitch Diameter - in.	4.7244
Diametral Clearance - in.	.0025
Retainer Pilot Clearance (Inner) - in.	.030
Pocket Clearance - in.	.0125
Pressure Viscosity Coefficient - in. <sup>2</sup> /lb	$9.6 \times 10^{-5}$
Temperature Viscosity Coefficient - $^{\circ}\text{F}^{-1}$	$1.47 \times 10^{-2}$
Viscosity at Inlet - lb-sec/in. <sup>2</sup>	$7.35 \times 10^{-7}$
Thermal Conductivity - Btu/ $^{\circ}\text{F}\cdot\text{hr}/\text{ft}$	$7.40 \times 10^{-2}$
Lubricant Density - lb-sec <sup>2</sup> /in. <sup>4</sup>	$8.25 \times 10^{-5}$

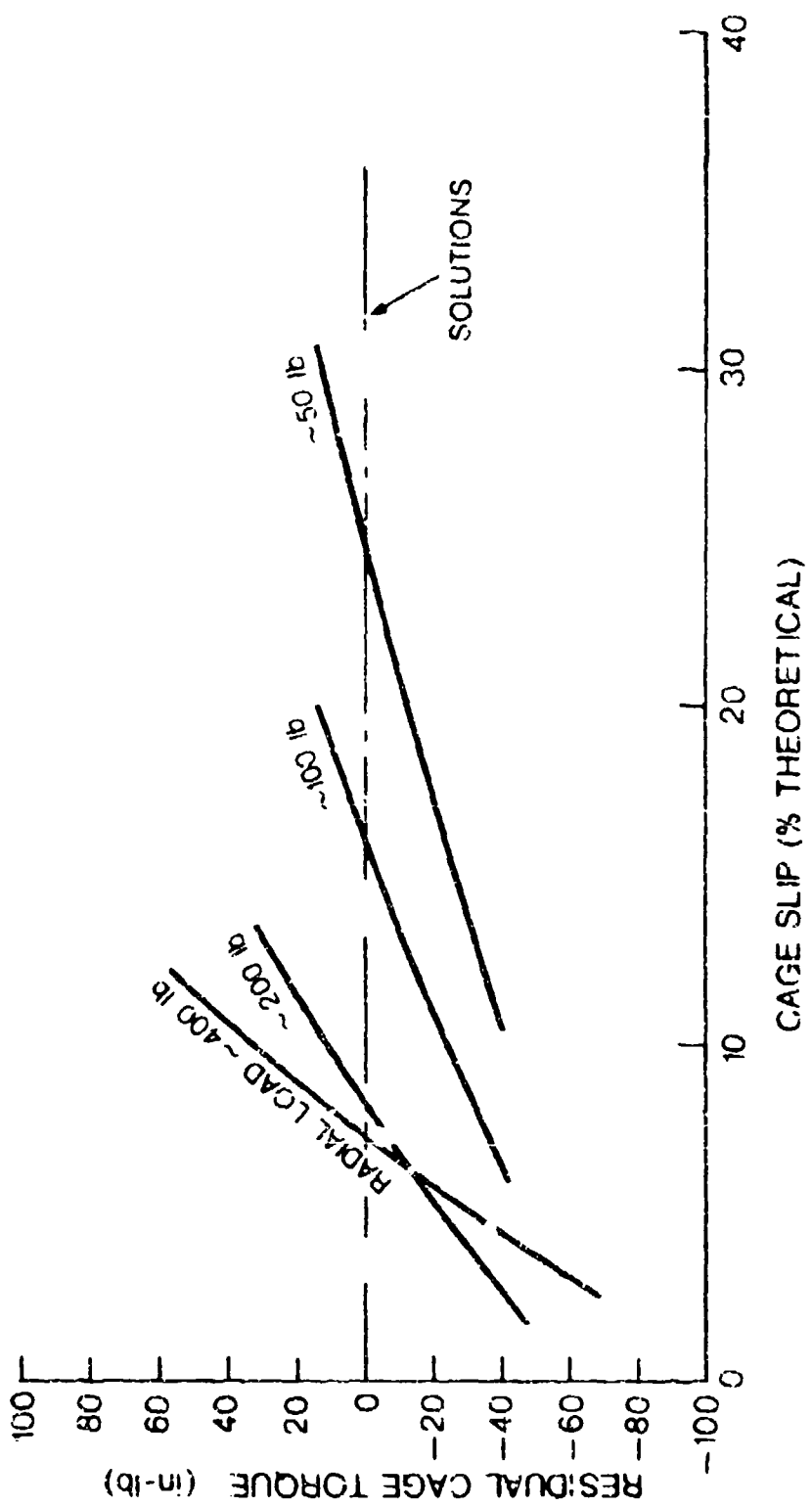


Figure 90. Roller Bearing Program Data: Residual Cage Torque Versus Cage Slip  
(Inner Race Speed = 20,000 RPM).

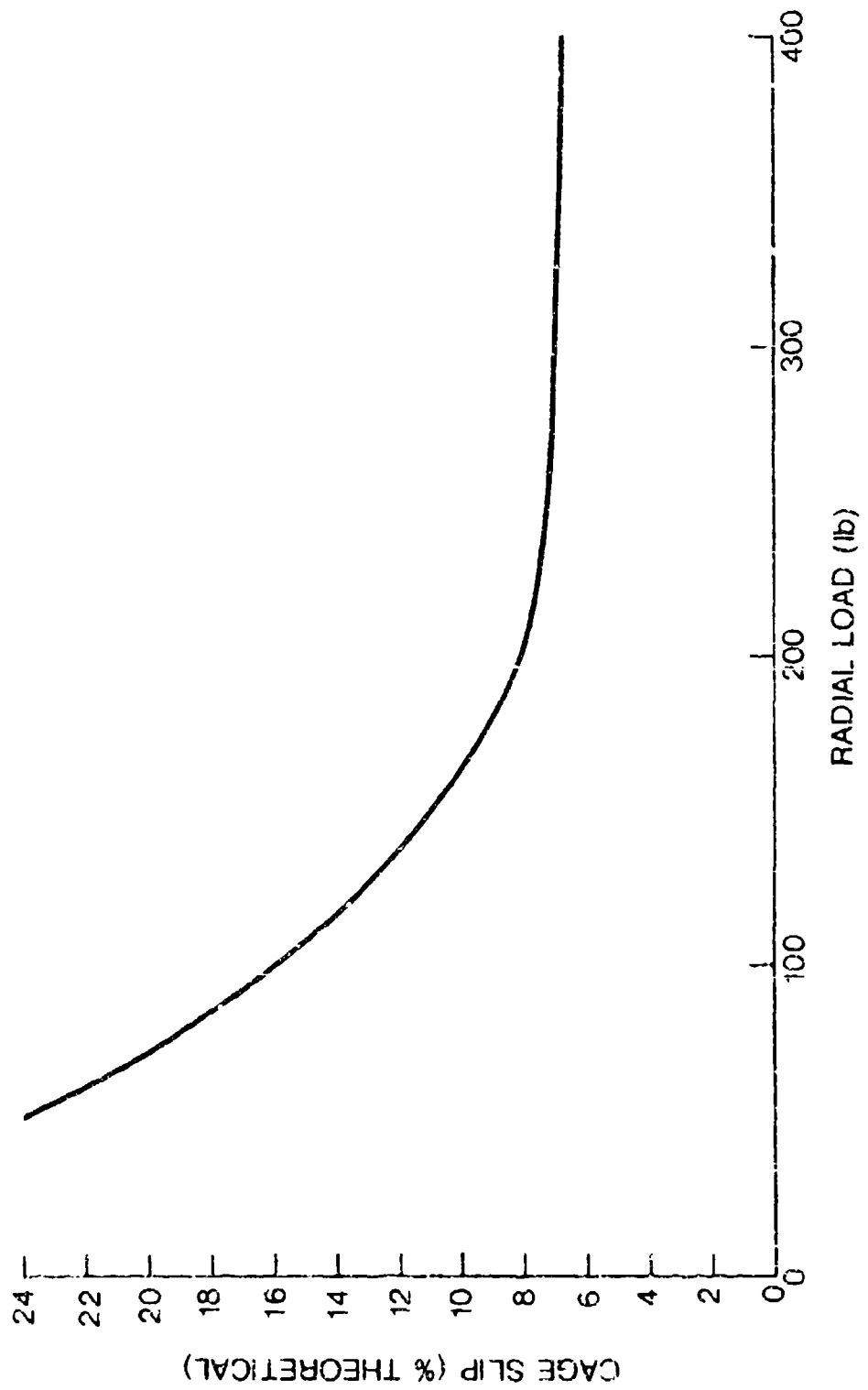


Figure 91. Roller Bearing Program Data; Cage Slip Versus Radial Load  
(Inner Race Speed = 20,000 RPM).

## CONCLUSIONS

1. Retainer pocket forces predicted by the computer analysis for the cases studied are small, approximately 5 pounds, and are in quantitative agreement with the basic pocket force cycles measured during the experimental test program. Existing differences between measured and predicted values can be attributed to dynamic shaft unbalance, imperfect bearing geometry, etc. However, superimposed upon these force levels are pulse-type forces that were measured at the retainer pockets. These forces were significantly larger than the former, on the order of 50 pounds, and are believed to be the result of impacts between the rolling elements and retainer pockets resulting from acceleration/deceleration of the rolling elements and/or retainer. Impact force levels dominate and constitute the major criteria in the establishment of the structural integrity of the high-speed retainer.
2. Lubricant film thicknesses developed at the rolling element-to-retainer pocket contacts are hydrodynamic in nature, and they are strongly dependent upon the contact force magnitudes.
3. Bearing kinematics resulting from the computer solutions that consider traction at the rolling element-to-race contacts are not widely different from analyses conducted hitherto that employ the race control assumptions. However, the new model does predict ball spin at both inner and outer contacts, gyroscopic precession, and resistance to gyroscopic precession at each of the inner and outer race contacts.
4. The computer analysis predicts regions of tractive ball instability at some load and speed conditions resulting from thermal effects in the EHD contact between balls and races.
5. Retainer slip at low-load conditions can be predicted by the computer program. Confirmation of the analysis for the test ball bearing employed during the program was obtained. Retainer pilot surface-to-race land contact force, which affects skidding characteristics, was found to be strongly dependent upon the ratio of the axial to radial loads applied to the bearing.

## RECOMMENDATIONS

1. It is recommended that further work conducted to achieve a better understanding of overall bearing operation address the rheological behavior of EHD lubrication with particular emphasis on traction.

The effects of lubrication upon bearing operating characteristics are central to the analysis of rolling element bearings. The dynamics and kinematics of bearing operation are well understood in comparison with the equally important effects of the rheological behavior of the lubricant. Much of the lubricant information drawn upon in the analysis is an extrapolation of empirical data obtained in different operating regimes. The development of more extensive and sophisticated bearing analyses based upon the relatively underdeveloped technology of EHD lubrication will not substantially increase our overall understanding of high-speed bearing performance, especially in the light of the convergence problems encountered with available data as described in "Tractive Instability," page 53.

2. Attention should be directed toward further investigation of the cage pocket impact forces observed. Tests should be conducted on a greater variety of bearing configurations and operating conditions to achieve a more general verification of the observed results.

### LITERATURE CITED

1. Dowson, D., and Higginson, G. R., ELASTOHYDRODYNAMIC LUBRICATION, Pergamon Press, Oxford, 1966.
2. Jones, A. B., THE MATHEMATICAL THEORY OF ROLLING-ELEMENT BEARINGS, Mechanical Design and Systems Handbook, Section 13, McGraw-Hill, New York, 1964.
3. Boness, R. J., THE EFFECT OF OIL SUPPLY ON CAGE AND ROLLER MOTION IN A LUBRICATED ROLLER BEARING, Journal of Lubrication Technology, Transactions of the ASME, Series F, Vol. 92, No. 1, 1970, pp. 39-53.
4. Crook, A. W., THE LUBRICATION OF ROLLERS. IV. MEASUREMENTS OF FRICTION AND EFFECTIVE VISCOSITY, Philosophical Transactions of Royal Society of London, Series A 255, 281.
5. Harris, T. A., AN ANALYTICAL METHOD TO PREDICT SKIDDING IN THRUST-LOADED ANGULAR-CONTACT BALL BEARINGS, Journal of Lubrication Technology, Vol. 93, No. 1, 1971, pp. 17-24.
6. Johnson, K. L., and Cameron, R., SHEAR BEHAVIOR OF ELASTOHYDRODYNAMIC OIL FILM AT HIGH ROLLING CONTACT PRESSURES, Proceedings of the Institution of Mechanical Engineers, 1967-1968, Vol. 182, p 307.
7. Lundberg, G., ELASTICHE BERÜHRUNG ZWEIER HALBRÄUME, VDI Forschung auf dem Gebiete des Ingenieurwesens, September-October 1939, Bd. 10, Nr. 5, pp. 201-252.
8. Plint, M. A., TRACTION IN ELASTOHYDRODYNAMIC CONTACTS, Proceedings of the Institution of Mechanical Engineers, 1967-1968, Vol. 182, p. 300.
9. Poplawski, J. V., and Mauriello, J. A., SKIDDING IN LIGHTLY LOADED HIGH-SPEED BALL THRUST BEARINGS, ASME Preprint 69-LUBS-20.
10. Walters, C. T., THE DYNAMICS OF BALL BEARINGS, Journal of Lubrication Technology, Vol. 93, No. 1, 1971, pp. 1-10.
11. McGrew, J. M., Gu, A., et al., ELASTOHYDRODYNAMIC LUBRICATION, Preliminary Design Manual, Technical Report AFAPL-TR-70-27, Mechanical Technology, Inc., November 1970.

**APPENDIX I**  
**BALL BEARING COMPUTER PROGRAM FORTRAN SOURCE DECK**

C	MAIN PROGRAM	10
	PFAL LURDEN	20
	COMMON HSO(40),HSI(40)	30
	COMMON ALPHA,AA(2),AMA(2,2,40),AMIN(2,40),APOCK(40), 1,0(2),B3(2),BPCCK(40), CAGEW, CRV12, CRAD, COSR,CPH,CTHET, 200PR(5),CR(2),CF,(2),CSP(2),COR(5), CLFARS(2),CLFARP, DP(2,5), 30G(2,2),DCF(5),D9(2,5),DEX(2),DROP,D,DENS,DDL(1),DFL(4),DTV(5,5), 40FTER,DFL(2),DNELEX(2,2),DXKOG(2),DFXVX(2),DFXY(2),DFXWS(2), 50FXP(2),DFYVX(2),DFYVY(2),DFYWS(2),DFYP(2),DGSVX(2),DOSVY(2),DOSWS 60(2),DQSP(2),DFX(2,5),DFY(2,5),DOS(2,5),DFPX(5),DFPZ(5),DOP(5),D4Y(5), 70DMZ(5),DPS(5,5),DPS(1,5,5),DBA(2),DDELA(2),DPA(2),DFXA(2),DFYA 80(2),DOSA(2),DFXOME(2),DFYOME(2),DOSOME(2),DFPXA(2),DFPZA(2),DOPA(2) 90,DVAR1(5),CVAR2(5),DVOME(5),DGA(2), E,EL	130
	COMMON FRR(5),E2,FSAVE(2), 1,FTAN,FFX(2,40),FFY(2,40), 2,HDR1,HDR2,HDR3,HDR4, 3,IPASS,LPASS,LURDEN,N, 4,TMS(2),TMFX(40),TMEY(40),TMFZ(40), 5,PR,PE,PC,PQ,PCKET,PHI,PILOT,PX(2),PSI(5),PL(2,40), 6,S(2),DOS(2,40), 7,SR(2),SO(2), 8,THICKR(2,40),THICKP(40), 9,VYB(2),VXR(2),VXP(40),VZP(40),VFC(5)	140
	COMMON X(5),XN,XF(4),XF(1,4),XK(2),XM1,XMY,XPH(140),XRF(2,40),XMS 1(2,40),XML,XMU1, YE,YR,YC,YNUM	150
	COMMON D2VYR,D2VK,D2WS,D2P2,XIN,XMASS	160
	C1MMON FX(2),FY(2)	170
	COMMON IC,CTL(40),LCTL,ICNT,LOOP,10(2),Y1,Y2,Y3,Y4,Y5,Y6,Y7,Y8,Y9 1,Y10,GAI(2,2),BA(2,2),DDELA(2,2),H(2),HH(2),H1(2),H2(2),SRAL(2), 2,CRAL(2),CMEGA,CMF(40),DCX(2),DPSIX(2,2),DGYA(2),PA(2,2),DPSIA(2), 3,XA(2),KONV,DADE(2,2),REFYA,DGYRD(2),CAL,SAL,A1,A2,DA,T1,T2,T3,T4, 4,FT,VM,XA(40),XA(40),ITPASS,REFVY(40),REFV(40)	180
	5,CAGFDI(2),RINGD(2),AREA(2), VFL(2),SDRAG(2),BDRAG,DSRAG(2,4), 6,EP/PA1,EP/PA2,EP/PA4,DRDRAG(4)	190
	COMMON/TSTCGM/TEST1,TEST2	200
	COMMON/RALTST/PLTEST	210
	COMMON/XTRAX/VDRAG(2),CDRAG(2),CFORCE	220
	CALL ZFRD(LPH),DRDRAG(4)	230
	GOTO 999	240
999	C INTINIE	250
	DAD(1,1)=1.	260
	DAD(2,1)=0.	270
	DAD(1,2)=0.	280
	RA(1,1)=0.	290
	RA(1,2)=0.	300
	REX(1)=0.	310
	REX(2)=0.	320
	DELA(1,1)=0.	330
	DELA(1,2)=0.	340
	H(2)=0.	350
	H1(1)=0.	360
	H1(1)=1.	370
	H1(2)=0.	380
	H2(1)=0.	390
	H2(2)=1.	400
	GA(1,1)=0.	410
	GA(1,2)=0.	420
	DCF(1)=0.	430
	DCF(3)=0.	440
	DCF(1)=0.	450
	DCF(2)=0.	460
	DCF(1)=0.	470
	DCF(2)=0.	480
	DCF(1,1)=0.	490
	DCF(1,2)=0.	500
	H(1)=0.	510
	H(2)=1.	520
	H(1)=0.	530
	H(2)=0.	540
	H(2)=1.	550
	GA(1,1)=0.	560
	GA(1,2)=0.	570
	DCF(1)=0.	580
	DCF(3)=0.	590

```

      DCF(4)=0.
      DCF(5)=0.
      C(1)=1.
      C(2)=-1.
  2 READ(5,80)
     WRITE(6,80)
     CALL INPT
     XMASS=1.3550691F-3*DENS*DE*3
     XIN=.1*XMASS* D**2
 10 READ(5,100)ALPHA,BETA,VIS,TI,FK,LUBDEN,D2VYR,D2VX
     LCASE=0
     IF(ALPHA<1.0)1
  9 WRITE(6,81)
     GO TO 2
 1  WRITE(6,3)
    FORMAT(1H /1H /1H /1H /1H /1H /23H0 LUBRICANT PROPERTIES)
    READ(5,1000)D2WS,D2P2,(TOL(K),K=1,9),CONST1,CONST2
    WRITE(6,4)ALPHA
    4 FORMAT(40H PRESSURE-VISCOSITY COEFFICIENT ,1P1E11.4)
    WRITE(6,5)BETA
    WRITE(6,6)VIS
    5 FORMAT(40H TEMPERATURE-VISCOSITY COEFFICIENT ,1P1E11.4)
    6 FORMAT(40H VISCOSITY AT INLET TEMPERATURE ,1P1E11.4)
     WRITE(6,7)TI
    7 FORMAT(50H INLET TEMPERATURE ,1P1E11.4)
     WRITE(6,8)FK
    8 FORMAT(40H THERMAL CONDUCTIVITY ,1P1E11.4)
     WRITE(6,9)LUBDEN
    9 FORMAT(40H LUBRICANT DENSITY ,1P1E11.4)
     WRITE(6,5000)XMU
 5000 FORMAT(40H PAUL POCKET FRICTION COEFFICIENT ,1P1E11.4)
     WRITE(6,5001)XMU1
 5001 FORMAT(40H CAGE PILOT FRICTION COEFFICIENT ,1P1E11.4)
 30 READ(5,1000)RFM(1),RPM(2),XF(1),XF(3),DOL(4),DOL(5),VCTR
     LCASE=LCASE+1
     CTL=VCTR
     IF(D2VYR.EQ.0.)D2VYR=.05
     IF(D2VX.EQ.0.)D2VX=.05
     IF(D2WS.EQ.0.)D2WS=.1
     IF(D2P2.EQ.0.)D2P2=.05
 1003 FORMAT(7H10.0,F9.0,1I)
     IF(VCTR.LE.0)CTL=1
     GGG=0.00058/F
     CMEGAF=.5*(RPM(1)*11.+GGG)+RPM(2)*(1.-GGG)
 4000 ZAPS=CMEGAF
 1000 FORMAT(8F10.0)
     IF((RPM(1)-RPM(2)).EQ.0.) GO TO 10
     WRITE(6,81)
     WRITE(6,8C)
     WRITE(6,71)LCASE
     WRITE(6,72)RFM(1)
     WRITE(6,73)RPM(2)
     WRITE(6,74)CMEGAF
     WRITE(6,75)XF(1)
     WRITE(6,76)XF(3)
     WRITE(6,77)DOL(4)
     WRITE(6,78)DOL(5)
     WRITE(6,79)VCTR

```

71	FORMAT(40H)	OPERATION DATA FOR LOAD CASE NUMBER	.12)	1190
72	FORMAT(4CH)	OUTER RACE SPEED	.1P1E11.4)	1200
73	FORMAT(4OH)	INNER RACE SPEED	.1P1F11.4)	1210
74	FORMAT(4OH)	THRUST LOAD	.1P1F11.4)	1220
75	FORMAT(4OH)	RADIAL LOAD	.1P1E11.4)	1230
76	FORMAT(4OH)	MISALIGNMENT	.1P1F11.4)	1240
77	FORMAT(4OH)	INITIAL AXIAL DEFLECTION	.1P1E11.4)	1250
78	FORMAT(4OH)	INITIAL RADIAL DEFLECTION	.1P1E11.4)	1260
79	FORMAT(4OH)	RACE CONTROL INDEX	.1P1E11.4)	1270
80	FORMAT(71H)			1280
1				1290
81	FORMAT(1H1)			1300
82	FORMAT(4OH)	THEORETICAL CAGE SPEED	.1P1E11.4)	1310
83	FORMAT(1P3F11.4)			1320
	OMEGA_E=1.0471976*OMEGA_E			1330
	IF(ABS(DDI(1))+ABS(DDI(3))+ABS(DDI(4))>13,13,14			1340
13	DDI(1)=DDI(1)			1350
	DDI(3)=DDI(3)			1360
	DDI(4)=DDI(4)			1370
14	N=XN			1380
	IF(TOL(1).EQ.0.)TOL(1)=1.E-6			1390
	IF(TOL(2).EQ.0.)TOL(2)=1.E-6			1400
	IF(TOL(3).EQ.0.)TOL(3)=10.			1410
	TOL(3)=TOL(3)*.1047198			1420
	IF(TOL(4).EQ.0.)TOL(4)=1.			1430
	TOL(4)=TOL(4)*.1047198			1440
	IF(TOL(5).EQ.0.)TOL(5)=5.			1450
	TOL(5)=TOL(5)*.1047198			1460
	IF(TOL(6).EQ.0.)TOL(6)=1.E-6			1470
	IF(TOL(7).EQ.0.)TOL(7)=1.E-6			1480
	IF(TOL(8).EQ.0.)TOL(8)=1.E-6			1490
	IF(TOL(9).EQ.0.)TOL(9)=.5			1500
	TOL(9)=TOL(9)*.1047198			1510
	CINST1=2			1520
	CONST2=1.			1530
	DO 34 K=1,4			1540
34	DRAG(K)=DDI(K)			1550
	KINV=0			1560
	RPM(1)=RPM(1)*.10471976			1570
	RPM(2)=RPM(2)*.10471976			1580
	PL=4.*((1.-PE**2)/YE*(1.-PC**2)/YC)			1590
	DO 43 J=1,N			1600
43	CTL(J)=LCTL			1610
48	CONTINUE			1620
	DO 15 ITER=1,15			1630
	RTFST=0.0			1640
	DO 481 K=1,4			1650
481	SORAG(K)=0.			1660
	ITPASS=ITER			1670
	TEMP1=.3CA*LUBDEN**.75*SORT(SORT(VIS))			1680
	DO 400 K=1,2			1690
	VFL(K)=(PPM(K)-OMEGA_E)*CAGFD(K)**.5			1700
	SORAG(K)=TEMP1*AREA(K)*ABS(VEL(K))**1.75/CLFARS(K)**.25*.5*CAGFD(K)			1710
	SORAG(K)=SIGN(SORAG(K))*VFL(K)			1720
400	VDRAG(K)=SORAG(K)			1730
	BDRAG=LUBDEN*D*(CLFARS(1)+CLFARS(2))+(E*OMEGA_E)**2*.002			1740
	BDRAG=SIGN(BDRAG,OMEGA_E)			1750
	DO 16 K=1,4			1760
				1770

```

16 XF1(K)=0. 1780
 01 17 K=1,4 1790
 02 17 L=1,4 1800
17 DIV(L,K)=0. 1810
 03 17 M=0. 1820
 04 17 N=0. 1830
 05 17 VERT=0. 1840
 06 17 MPR1=0. 1850
 07 17 MPR2=0. 1860
 08 17 MPR3=0. 1870
 09 17 MPR4=0. 1880
 10 17 VRT1=0. 1890
 11 17 VRT2=0. 1900
 12 17 VRT3=0. 1910
 13 17 VRT4=0. 1920
 01 19 J=1,N 1930
 02 19 NJM=0 1940
 03 19 TONT=0 1950
 04 19 LUDP=0 1960
 05 19 IPASS=J 1970
 06 19 DMF(J)=0. 1980
 07 19 XJ=J 1990
 08 19 IF(K>N)152,62,53 2000
51 19 IF((T1+4-1)>2,55,52 2010
55 19 Y(3)=PFYX(J) 2020
 09 19 X(4)=0. 2030
 10 19 Y(5)=4*VZ(J) 2040
52 19 0.41+6.29319*3*(X,I-1,5/XN) 2050
 01 19 SPH=SPH(V(I)) 2060
 02 19 CPH=CPH(PHT) 2070
 03 19 DAD(2,2)=CPH 2080
 04 19 CALL BALL(CCNST1,CCNST2,FP7,0VX) 2090
 05 19 IF(TEST1,F0,0.0) GO TO 2054 2100
 06 19 WRITE(6,2042)TEST1 2110
2052 19 FORMAT(1X,3H TEST1 N ,VS,1) 2120
 01 19 GO TO 30 2130
2054 19 CONTINUE 2140
 02 19 IF(P(2,J)>18,18,54 2150
54 19 FPR(4)=FPR(4)+PPC(J)*.5*E2+FPZ*,5*0 2160
 03 19 IF(PLTFST,F0,1.0)TEST=1.0 2170
18 19 CONTINUE 2180
 04 19 IF(K>N)44,44,45 2190
44 19 DFT=DTV(1,1)*DTV(2,2)-DTV(2,1)*DTV(1,2) 2200
 05 19 FPR(1)=XF1(1)+XF(1) 2210
 06 19 FPR(3)=XF1(3)+XF(3) 2220
 07 19 CORR(1)=(FPR(1)*DTV(2,2)-FPR(3)*DTV(1,2))/DFT 2230
 08 19 CORR(3)=(DTV(1,1)*FPR(3)-DTV(2,1)*FPR(1))/DFT 2240
 09 19 IF(APS(CORR(1))-TOL(1))46,1515,1515 2250
45 19 IF(ABS(CORR(3))-TOL(3))47,1515,1515 2260
1515 19 CONTINUE 2270
 01 19 DFL(1)=DFL(1)-CORR(1) 2280
 02 19 DFL(3)=DFL(3)-(DPR(3)) 2290
 03 19 GO TO 19 2300
46 19 FPR(1)=XF1(1)+XF(1) 2310
 04 19 FPR(2)=XF1(2) 2320
 05 19 FPR(3)=XF1(3)+XF(3) 2330
 06 19 IF(MPR12,F0,0.0)MPR12=.01 2340
 07 19 IF(VRT4,F0,0.0)VRT=0.01 2350
 08 19 MP2=SORT(DMP17*92+VRT*42) 2360

```

```

CFOFCE=TEMP2          2370
KPLT=PILOT+.1         2380
DO 402 K=1,2           2390
DO 403 L=1,4           2400
403 DSORG(K,L)=0.      2410
IF(K,NE,KPLT)GOTO 1402 2420
TEMP=.5*XHUI1*CAGED1(K)*TEMP2
CDRAG(K)=SIGN(TEMP,VFL(K))
SDRAG(K)=SDRAG(K)+CDRAG(K)
TEMP=XHUI1*CAGED1(K)/THMP?
TEMP=SIGN(TEMP,VFL(K))
DSORG(K,1)=(HCR1Z*HOR1+VERT*VRT1)*TEMP
DSORG(K,2)=(HCR1Z*HOR2+VERT*VRT2)*TEMP
DSORG(K,3)=(HCR1Z*HOR3+VERT*VRT3)*TEMP
DSORG(K,4)=(HCR1Z*HOR4+VERT*VRT4)*TEMP
TEMP=CAGED1(K)**2*TEMP1*ARFA(K)*ARS(VFL(K))**.75*.4175/CLEARSK** 2520
1.25
TEMP=SIGN(TEMP,VFL(K))
DSORG(K,4)=DSORG(K,4)+TEMP
1402 CONTINUE          2530
EPR(4)=EPR(4)+SDRAG(K) 2540
402 CONTINUE          2550
TEMP=ATAN2(HCR1Z,VRT1) 2560
SNT1=SIN(TEMP)          2570
CSTH=COS(TEMP)          2580
TMPL=SNT1*XHUI1*CSTH   2590
TMPL2=CSTH*XHUI1*SNTH   2600
TMPL3=CSTH*XHUI1*SNTH   2610
TMPL4=-SNT1*XHUI1*CSTH  2620
AY=-TEMP*TMPL1          2630
AZ=-TEMP2*TMPL3          2640
TMPL21=(HCR1Z*HOR1+VERT*VRT1)/TEMP2
TMPL22=(HCR1Z*HOR2+VERT*VRT2)/TEMP2
TMPL23=(HCR1Z*HOR3+VERT*VRT3)/TEMP2
TMPL24=(HCR1Z*HOR4+VERT*VRT4)/TEMP2
DAY1=-TEMP2*TMPL2*(VERT*HOR1-HOR1Z*VRT1)/(VERT*CSTH)**2-TMP1*TMPL21 2680
DAY2=-TEMP2*TMPL2*(VERT*HOR2-HOR1Z*VRT2)/(VERT*CSTH)**2-TMP1*TMPL22 2690
DAY3=-TEMP2*TMPL2*(VERT*HOR3-HOR1Z*VRT3)/(VERT*CSTH)**2-TMP1*TMPL23 2700
DAY4=-TEMP2*TMPL2*(VERT*HOR4-HOR1Z*VRT4)/(VERT*CSTH)**2-TMP1*TMPL24 2710
DA1=-TEMP2*TMPL4*(VERT*HOR1-HOR1Z*VRT1)/(CSTH*VERT)**2-TMP1*TMPL21 2720
DA2=-TEMP2*TMPL4*(VERT*HOR2-HOR1Z*VRT2)/(CSTH*VERT)**2-TMP1*TMPL22 2730
DA3=-TEMP2*TMPL4*(VERT*HOR3-HOR1Z*VRT3)/(CSTH*VERT)**2-TMP1*TMPL23 2740
DA4=-TEMP2*TMPL4*(VERT*HOR4-HOR1Z*VRT4)/(CSTH*VERT)**2-TMP1*TMPL24 2750
DO 404 K=1,4           2760
404 DTV(4,K)=DIV(4,K)+DSORG(1,K)+DSORG(2,K) 2770
IF(KPLT-2)33,42,33
42 XFI(2)=XFI(2)+AY 2780
XFI(1)=XFI(3)+AY 2790
DTV(2,1)=DTV(2,1)+DAY1 2800
DTV(2,2)=DTV(2,2)+DAY2 2810
DTV(2,3)=DTV(2,3)+DAY3 2820
DTV(2,4)=DTV(2,4)+DAY4 2830
DTV(3,1)=DTV(3,1)+DA1 2840
DTV(3,2)=DTV(3,2)+DA2 2850
DTV(3,3)=DTV(3,3)+DA3 2860
DTV(3,4)=DTV(3,4)+DA4 2870
33 NN=4
CALL SIMULT(DTV,NN,EPR,COPR,IQUIT)
IF(IQUIT)24,24,25 2880

```

```

25 WRITE(6,26)                                2960
26 FORMAT(14HOSTAT 25, MAIN)
27 GO TO 30
24 DO 27 K=1,3                               2970
27 DFL(K)=DFL(K)-CORR(K)                   2980
28 OMEGAF=OMEGA-E-CORR(4)                  2990
29 DO 28 K=1,6                               3000
30 IF (ABS(CORR(K))-TOL(K+5))>8,15,15    3010
31 CONTINUE                                     3020
32 GO TO 31                                     3030
33 CONTINUE                                     3040
34 WRITE(6,29)                                 3050
35 29 FORMAT(1X,21'RETAINER LOOP FAILURE')
36 STOP                                         3060
37 CALL OUTPT                                  3070
38 IF (RTFST.EQ.1.0) WRITE(6,131)             3080
39 131 FORMAT(1X,17F      B-L)
40 GO TO 30                                     3090
41 KJNY=1
42 IF (OMEGAF)>8,48,48
43 VK=0.
44 XMEGA=0.
45 DO 50 J=1,N                               3100
46 IF (P(J).EQ.0) GO TO 50,51
47 YK=VK+1.
48 YMEGA=XMEGA+CMF(J)
49 CMF(2)=XMASS*CMEGAE**2
50 CONTINUE                                     3110
51 CMEGAF=XMEGA/VK
52 CMF(2)=XMASS*CMEGAF**2
53 GO TO 48
54 299 CALL ZER0(K,XMEGA)
55 GO TO 999
56 2992 FORMAT(1P11E12.4)
57 END

```

```

SUBROUTINE BALL(CONST1,CONST2,FPZ,RX1)          BALL 10
REAL LUBDEN
COMMON HSC(4,1),HS(140)
COMMON ALPHA,AA(2),AAJ(2,40),AMIN(2,40),APOCK(40),
     1,B(2),BB(2),BFOCK(40), CAGEH, CRV(2), CRAD, CDSR,CPH,CTHET, BALL 40
     2,CCR(5),CR(2),CF,C(2),CSP(2),COR(5), CLEARS(2),CLFARP, DP(2,5), BALL 50
     3,DG12,21,DCF(5),DB(2,5),DEX(2),DROP,D,DENS,DL(4),DFL(4),DVS(5,5), BALL 70
     4,DF(TP,DFL(2),DDESLX(2,2),DXKDC(2),DFXVX(2),DFXVY(2),DFXWS(2), BALL 80
     5,DFXP(2),DFYVX(2),DFYVY(2),DFYWS(2),DFYP(2),DQSVX(2),DQSVY(2),DQSWS, BALL 90
     6(2),DQSP(2),DFX(2,5),DFY(2,5),DQS(2,5),DFPX(5),DFP(5),DQP(5),DHY(BALL 100
     75),DMZ(5),DPS(15,5),DPS(15,5),DBA(2),DDEL(2),DPA(2),DFXA(2),DFYABALL 110
     8(2),DQSA(2),DFXME(2),DFYMF(2),DQSOME(2),DFPXA(2),DFPA(2),DQPA(2BALL 120
     91,DVAR1(5),DVAR12(5),DVOME(5),DGAL2). E,EL BALL 130
COMMON ERR(5),F2,FSAVF(2),
     1,FTAN,FFX(2,40),FFY(2,40),
     2,          HORIZ,HORI,HOR2,HOR3,HOR4, FLAT,F(2),FK,FRAD, RALL 140
     3JPASS, LPASS,LUBDEN, N, OMEGA,F,OMY,OMX, BALL 150
     4,OMZ,OMS(2),OMFX(40),OMFY(40),OMFZ(40), PR(1)(40),PL,BALL 160
     5PK,PE,PC,PD,POCKET,PHI,PILDT,PX(2),PSI(5),P(2,40), QMV,BALL 170
     6PS(2),DPS(2,40), P,RP(2), SINP,SPH,STHFT, RALL 180
     7SP(2),SP(2), TOTL,T1,THFT,TOL(11),TCRV,TSAVE(2), BALL 190
     8THICKR(2,40), THICKP(40), .,S,VERT,VRT1,VRT2,VRT3,VRT4,VYR(2), BALL 200
     9YYB(2),VXB(2),VXP(40),VZP(40),VEC(5) BALL 210
COMMON X(5),XA,XF(4),XF(4),X(2),XMZ,YXY,XPH(40),XHET(2,40),XOMSRALL 220
     1(2,40),XMU,YMU, YE,YR,YL IUM BALL 230
COMMON D2VYR,D2VX,D2WS,D2P2,XIN,XMASS BALL 240
COMMON FX(2),FY(2) BALL 250
COMMON IC,CTL(40),LCTL,ICNT,LOOP,TD(2),YL,Y2,Y3,Y4,Y5,Y6,Y7,Y8,Y9BALL 260
     1,Y10,GA(2,2),BA(2,2),DELA(2,2),H(2),HH(2),H1(2),H2(2),SRAL(2), BALL 270
     2,SRAL(2),OMEGA,OME(40),DCX(2),DPSIX(2,2),DGYA(2),PA(2,2),DPSIA(2), BALL 280
     3,KA(2), KUNV,DA(2,2),REFV,B,DGYR0(2),CAL,SAI,A1,A2,DN,T1,T2,T3,T4, BALL 290
     4,FT,NUM,XA1(40),XA(40),ITPASS,REFVX(40),REFVZ(40) BALL 300
     5,CAGFD(2),RINGD(2),ARFA(2), VEL(2),SDRAG(2),DRAG,DSORG(2,4), BALL 310
     6,DPZDA1,DPZDA2,DPZDME,DRDRAG(4) BALL 320
DIMENSION BDR(2) BALL 330
COMMON/TSTCOM/TTEST1,TTEST2 BALL 340
COMMON/RAL1ST/RALTEST BALL 350
TEST1=0.0 BALL 360
I=JPASS BALL 370
DPIC(J)=0. BALL 380
DPCK(J)=0. BALL 390
APCK(J)=0. BALL 400
DXW=0. BALL 410
FPZ=0. BALL 420
DSP=0. BALL 430
VXP(J)=0. BALL 440
VZP(J)=0. BALL 450
DFPWXZ=0. BALL 460
DFPWXY=0. BALL 470
DFPZWX=0. BALL 480
DFPZWY=0. BALL 490
DQSPP=0. BALL 500
DQSPWX=0. BALL 510
DQSPWZ=0. BALL 520
DQSPHY=0. BALL 530
DX(1)=0. BALL 540

```

```

-- -- X(2)=0.
    0) 52 K=3,5          BALL 600
    0) 52 L=1,2          BALL 610
    0) (L,K)=0.          BALL 620
52  D8(L,K)=0.          BALL 630
    D8X(1)=0.            BALL 640
    D8X(2)=2.            BALL 650
    612 A1=TCRV*SINA +DFL(1)+9* DFL(4)*CPH          BALL 660
    12=TCPV*COSB+DFL(3)*CPH+DFL(2)*SPH-.5*PD          BALL 670
C   IF(KINV<4C9,4C9,90          BALL 680
C80  X1<0XA12JC          BALL 690
C   X2<0XA22JC          BALL 700
C   G) TO 8              BALL 710
4C9  TEMP=A;             BALL 720
    A1A2=A1*`2+A2**2          BALL 730
    ART=SORT(A1A2)           BALL 740
    IF(LRS(A1)=1,E-6)1,1,2          BALL 750
2   IF(A113,3,4          BALL 760
3   TAG=-1.              BALL 770
G1  TO 5              BALL 780
1   IF(A2-TCPV-1.E-8)9,9,7          BALL 790
7   X(1)=0.              BALL 800
    X(2)=.55*(A2-TCPV)+CPV(1)          BALL 810
G1  TO 17             BALL 820
4   TAG=1.              BALL 830
5   IF((A2-CPV(1))**2<A1**2-(CPV(2))**2,9,9,10          BALL 840
9   NOLNAD=NOLNAC+1          BALL 850
    ?(2,J)=0.          BALL 860
    RETURN              BALL 870
10  A1=APSEAL1          BALL 880
    TA=A1/A2          BALL 890
    IF(ART-TCRV(1),12,13          BALL 900
12  AX=A1*CPV(1)/APT          BALL 910
    AV=A2*CPV(1)/APT          BALL 920
16  XX=(AX+TA+AY-A2)/TB          BALL 930
    IF(XX>14,14,15          BALL 940
15  X(1)=(XX-.5*(AX-XX))+TAG          BALL 950
    X(2)=A2-.5*(A2-AY)          BALL 960
17  A1=TEMP          BALL 970
G1  TO 3              BALL 980
21  CLAM=(CRV(1)**2+A1A2-CPV(2)**2)/(2.*CPV(1)*ART)          BALL 990
    A1M=ATAN(SORT(1.-CLAM**2)/CLAM)          BALL1000
    R1=ATAN(TP)-ALAM          BALL1010
    AX=CRV(1)*SIN(P1)          BALL1020
    AY=SORT(CRV(1)**2-AX**2)          BALL1030
G2  TO 16             BALL1040
14  X(1)=.6*AX+TA          BALL1050
    Y(2)=AY+.4*AX*TH          BALL1060
G2  TO 17             BALL1070
13  G) 1B L=1,?          BALL1080
    G=D*SQRT(1./(L.+TB**2))*C(L)/E          BALL1090
    T1=1./F(L)-2.*G/(1.+G)          BALL1100
    T2=.4.-2./F(L)*T1          BALL1110
    CALL FILPIN(T1,T2,FE,FK,CSE2,100IT)          BALL1120
    IF(100IT)1A,18,19          BALL1130
19  CONTINUE          BALL1140
    TEST1=19.C          BALL1150
    RETURN              BALL1160
19  XK(L)=L+.847711/CL+SQRT(FE*D/(ER**3*CSE2*T2))          BALL1170
                                BALL1180

```

```

1 APIN=(ART-TCRV)/(1.+(XK(2)/XK(1))+.66666667)          BALI1190
2 APD=ART-TCRV-APIN                                     BALI1200
3 AX=(CRV(1)+APC)*TR/SORT(1.+TR**2)                   BALI1210
4 AY=SORT((CRV(1)+APD)**2-AX**2)                      BALI1220
5 G3 TO 26                                              BALI1230
6 CVRG2=0.                                              BALI1240
7 2000.FORMAT1X.1P10E12.41                               BALI1250
8   DO 21 IT=1,15                                       BALI1260
9     XMY=X1N*CMFCDE*X(5)                                BALI1270
10    YMZ=-X1N*CMFCDF*X(4)                                BALI1280
11    CVRG2=CVRG2+CONST1                                BALI1290
12    IF(CVRG2-CONST2)>22,22,23                         BALI1300
13    CVRG2=CONST2                                     BALI1310
14    A(1)=ATAN(X(1)/X(2))                            BALI1320
15    B(2)=ATAN((A1-X(1))/(A2-X(2)))                  BALI1330
16    DO 24 K=1,2                                         BALI1340
17      SR(K)=SIN(B(K))                                 BALI1350
18    CR(K)=COS(B(K))                                 BALI1360
19    DB(1,1)=CBL(1)**2/X(2)                           BALI1370
20    DB(1,2)=-X(1)*CBL(1)/X(2)                        BALI1380
21    DB(2,1)=-CBL(2)**2/(A2-X(2))                    BALI1390
22    DB(2,2)=-DB(2,1)*(A1-X(1))/(A2-X(2))           BALI1400
23    E2=E+2.*EM(2)-CRV(1)*COSB1                     BALI1410
24    DEL(1)=SORT(X(1)**2+X(2)**2)-CRV(1)             BALI1420
25    DEL(2)=SORT((A1-X(1)**2+(A2-X(2)**2))-CRV(2))  BALI1430
26    DO 25 K=1,2                                         BALI1440
27    IFIDEL(K)=L-E-719.25,25                          BALI1450
28    CONTINUE                                           BALI1460
29    DO 26 K=1,2                                         BALI1470
30    G2(K)=D*CR(K)/F2                                  BALI1480
31    SG(K)=1.+C(K)*G2(K)                                BALI1490
32    T1=1./F(K)-2.*C(K)*G2(K)/GG(K)                  BALI1500
33    T2=4.-2./F(K)+T1                                    BALI1510
34    CALL ELTPIN(T1,T2,EE,EK,CSE2,1QUIT)              BALI1520
35    IF11QUIT128,2E,29                                  BALI1530
36    CONTINUE                                           BALI1540
37    TEST1=29.0                                         BALI1550
38    RETURN                                              BALI1560
39    CSEP=SORT(CSE2)                                   BALI1570
40    CSPI(K)=CSEP                                      BALI1580
41    ESAVE(K)=EE                                       BALI1590
42    SNEP=SORT(1.-CSE2)                                BALI1600
43    TSAVE(K)=T2                                       BALI1610
44    YK(K)=11.847711/FL*SORT(D*EE/(FX**2+CSE2*T2))  BALI1620
45    SD(K)=XK(K)*SORT(DEL(K))                          BALI1630
46    DDELX(K,1)=C(K)*SR(K)                            BALI1640
47    DDELX(K,2)=C(K)*CR(K)                            BALI1650
48    CYAU=T1/T2                                         BALI1660
49    STAU=SQRT(1.-CTAU**2)                            BALI1670
50    DTDG=2.*((T2-T1)*C(K)/(1.(T2*GG(K))**2*STAU))  BALI1680
51    DKDEP=(FE-EK*CSE2)/(SNEP*CSEP)                 BALI1690
52    DEDEP=(EE-EK)/SNEP*CSEP                         BALI1700
53    DEDTAU=(EE*SNEP**2*STAU*.5/(CSEP**2*(EK-FF))/SNEP*(FF*DKDEP-  BALI1710
54    1.EK*DEDEP1*CSEP))                                BALI1720
55    DXKDEP=5.9238555*SQR(D/(T2*EE*EK**51.L/|ELOCSE2|*(EK*DEDEP-3.*EE*BALI1720
56    1.EK*DEP1*CSEP+2.*EK*FE*SNEP))                  BALI1740
57    DXKDZ2=-XK(K)**.5/T2                             BALI1750
58    DXKG(K)=DXKDEP*DEDTAU*DTDG-DXKDZ2*2.*C(K)/GG(K)**2  BALI1760
59    DO 31 L=1,2                                         BALI1770

```

```

LPASS=!
PK(L)=DEL(L)*SC(L)
PL,J1=P(X(L))
RR(L)=1.23473261*FSAVE(L)*CSP(L)*EL*P(X(L))*D/TSAVE(L)*2.3333333
AA(L)=RR(L)/CSP(L)
DO 32 K=1,2
DG(L,K)=-D/E2**2*(E2+SB(L)*DB(L,K)+CB(L)*DEX(K))
32 DP(L,K)=1.5*SC(L)*DDFLX(L,K)+DEL(L)*SORT(DFL(L))+DXNG(L)*DG(L,K)
TF(KONV) 31,3,403
403 VYR(L)=(PBM(L)-CMGAE)*.5*(F2+C(L)*D*CR(L))
VYB(L)=.5*C(L)*D*(X(3)*CR(L)-X(5)*SR(L))
VXR(L)=-.5*D*X(4)
OMS(L)=C(L)*(IPM(L)-OMFGAE-X(3)*SB(L)-X(5)*CR(L))
RG=-F(L)*D
CF=XMASS*CHECAE**2*.5*E2
CALL RALFTJ(RG)
31 CONTINUE
TF(KONV) 404,404,405
404 CALL BALL1
DO 406 K=1,2
TF(ARS(COR(K))-5.E-6) 406,406,21
406 CONTINUE
XA1(J)=X(1)
XA2(J)=X(2)
407 CALL BALL2
TF(NIM) 408,408,409
408 OME(J)=CMGAE
RETURN
409 PPOC(J)=FY(1)+FY(2)-BDRAG
RGH(L)=R(L)*57.2358
RJH(2)=B(2)*57.2958
TF(PPOC(J)) 36,38,36
36 T1=2.*D/POCKET
T2=4.-T1
CLFAHP=.5*(POCKET-D)
VZP(J)=X(3)*.5*D
VXP(J)=-X(5)*.5*D
CALL ELIPEN(T1,T2,FF,EK,CSF2,1QUIT)
TF(1QUIT) 33,23,34
34 CONTINUE
TEST1=35.0
RETURN
13 PPOCK(J)=1.23473261*FF*SORT(CSF2)*PL*ARS(PPOC(J))*D/T2**.33333333BALL2200
1POCK(J)=PPCK(J)/SORT(CSF2)
THICKP(J)=(V15*X(3)+.125*0**2+10.87/PPOC(J))*2/CLEARP
TF(THICKP(J))-10.F-61401,402,402
402 FPX=V15*X(5)+.5*0**2+.5*12.56/SORT(CLEAP)
FPZ=V15*X(3)+(.5*0**2+.5*2.436/SORT(CLEAP))
DFPXP=0.
DFPZD=0.
DFPXWK=0.
DFPZK=0.
DFPXY2=FPX/X(5)
DFPZY2=FPZ/X(3)
GO TO 38
401 TEMP=XMH/SORT(X(3)**2+X(5)**2)
FPX=TEMP*X(5)*PPOC(J)
FPZ=TEMP*X(3)*PPOC(J)
TEMP1=TEMP*PPOC(J)/(X(3)**2+X(5)**2)

```

```

DEFPX4X=-TEMP1*X(3)*X(5).                                RALL2370
DEFPKWZ=TEMP1*X(3)**2.                                    RALL2380
DEFXPX=TEMP*X(5).                                         RALL2390
DEFQZWX=TEMP1*X(5)**2.                                    RALL2400
DEFP2HZ=-T4P1*X(3)*X(5).                                 RALL2410
DEFP2P=TEMP*x(3).                                         RALL2420
38.  DS1(1)=-DX(1)+SB(1)+PX(2)*SB(2)+FX(1)*CB(1)-FX(2)*CB(2)-FPX   RALL2430
    DS1(2)=-PX(1)*CA(1)+PX(2)*CB(2)-FX(1)*SH(1)+FX(2)*SR(2)+CF+FPZ   RALL2440
    DS1(3)=(FY(1)*CB(1)-FY(2)*CB(2)-FPZ)*D*.5+QS(1)*SB(1)-DS(2)*SB(2) RALL2450
    DS1(4)=(FX(1)+FX(2))*D*.5+XMY-DSP.                         RALL2460
    DS1(5)=(-FY(1)*SB(1)+FY(2)*SB(2)-FPX)*D*.5+2S(1)*CB(1)-DS(2)*CB(2)RALL2470
    1+X47
    - 00 42 K=1,2.                                         RALL2480
    - 00 43 L=1,2.                                         RALL2490
    - DEF(X(K,L))=DEFXP(K)+D*(K,L)+.5*(RP4(K)-OMEGA)*((DEF(X(L))-C(K)*D*SR(K)*DB(K))ALL2510
    1*(K,L))+DEFXVY(K)+.5*C(K)*D*(X(3)*SA(K)+X(5)*CB(K))+DEFXVY(K)*DB(K,L)ALL2520
    21+C(K)*(PPM(K)-OMEGA*-K(3)*CB(K)+X(5)*SB(K))*DEFWS(K)*DB(K,L)          RALL2530
    - DEF(Y(K,L))=DEFY(K)+D*(K,L)+.5*(RP4(K)-OMEGA)*((DEF(X(L))-C(K)*D*SR(K)*DB(K))ALL2540
    1*(K,L))+DEFYVY(K)+.5*C(K)*D*(X(3)*SB(K)+X(5)*CB(K))+DEFYVY(K)*DB(K,L)ALL2550
    21+C(K)*(PPM(K)-OMEGA)*((CH(K)+X(5)*SP(K))*DEFWS(K)*DB(K,L))          RALL2560
43.  DS2(K,1)=DOSV(K)*PP(K,L)+.5*(RP4(K)-OMEGA)*((DEX(L))-C(K)*D*SB(K)*DB(K,L))ALL2570
    1*(K,L))+DOSVY(K)+.5*C(K)*D*(X(3)*SH(K)+X(5)*CB(K))+DOSVY(K)*DB(K,L)ALL2580
    21+C(K)*(PPM(K)-OMEGA*-X(3)*CB(K)+X(5)*SB(K))*DOSHS(K)*DB(K,L)          RALL2590
    - DEF(X(K,5))=-C(K)*D*(K)+D*CP(K)*DEFXVY(K)+SA(K)*DEFXWS(K))           RALL2600
    - DEF(Y(K,3))=-C(K)*D*(K)+D*CP(K)*DEFYVY(K)+SB(K)*DEFYWS(K))           RALL2610
    - DS2(K,3)=-C(K)*D*(K)+D*CP(K)*DOSVY(K)+SA(K)*DOSWS(K))              RALL2620
    - DEF(Y(K,4))=-.5*D*DEFYVX(K)                                           RALL2630
    - DEF(X(K,4))=-.5*D*DEFXVX(K)                                           RALL2640
    - DS2(K,4)=-.5*D*DOSVX(K)                                              RALL2650
    - DEF(X(K,6))=C(K)*(.5*D*SP(K)*DEFXVY(K)-CB(K)*DEFXWS(K))             RALL2660
    - DEF(Y(K,5))=C(K)*(.5*D*SP(K)*DEFYVY(K)-CB(K)*DEFYWS(K))             RALL2670
    - DS2(K,5)=C(K)*(.5*D*SP(K)*DOSVY(K)-CB(K)*DOSWS(K))                  RALL2680
    - DEF(X(1))=DEFXP*(DEFY(1,1)+DEFY(2,1)).                               RALL2690
    - DEF(X(2))=DEFXP*(DEFY(1,2)+DEFY(2,2)).                               RALL2700
    - DEF(X(3))=DEFXP*(DEFY(1,3)+DEFY(2,3))+DEFPXW.                         RALL2710
    - DEF(X(4))=DEFXP*(DEFY(1,4)+DEFY(2,4))+DEFPXW.                         RALL2720
    - DEF(X(5))=DEFXP*(DEFY(1,5)+DEFY(2,5))+DEFPXW.                         RALL2730
    - DEFZ(1)=DEFZP*(DEFY(1,1)+DEFY(2,1)).                               RALL2740
    - DEFZ(2)=DEFZP*(DEFY(1,2)+DEFY(2,2)).                               RALL2750
    - DEFZ(3)=DEFZP*(DEFY(1,3)+DEFY(2,3))+DEFZW.                           RALL2760
    - DEFZ(4)=DEFZP*(DEFY(1,4)+DEFY(2,4))+DEFZW.                           RALL2770
    - DEFZ(5)=DEFZP*(DEFY(1,5)+DEFY(2,5))+DEFZW.                           RALL2780
    - M(1)=DOSPR*(DEFY(1,1)+DEFY(2,1)).                               RALL2790
    - M(2)=DOSPR*(DEFY(1,2)+DEFY(2,2)).                               RALL2800
    - M(3)=DOSPR*(DEFY(1,3)+DEFY(2,3))+DOSPRW.                         RALL2810
    - M(4)=DOSPR*(DEFY(1,4)+DEFY(2,4))+DOSPRW.                         RALL2820
    - M(5)=DOSPR*(DEFY(1,5)+DEFY(2,5))+DOSPRW.                         RALL2830
    - MY(1)=0.                                                               RALL2840
    - MY(2)=0.                                                               RALL2850
    - MY(3)=0.                                                               RALL2860
    - MY(4)=0.                                                               RALL2870
    - MY(5)=XIN*OMEGA*AF.                                         RALL2880
    - M(1)=0.                                                               RALL2890
    - M(2)=0.                                                               RALL2900
    - M(3)=0.                                                               RALL2910
    - M(4)=XIN*OMEGA*AF.                                         RALL2920
    - M(5)=0.                                                               RALL2930
    - CF(1)=0.                                                               RALL2940
    - CF(2)=XIN*SE*NS*AF**2.                                         RALL2950

```

```

      DCE(3)=0.                                RALL2960
      DCE(4)=0.                                RALL2970
      DCE(5)=0.                                RALL2980
      DO 40 K=1,5
      DPSI(1,K)=PX(1)*CB(1)*DB(1,K)-SB(1)*DP(1,K)+PX(2)*CB(2)*DB(2,K)+ RALL3000
      ISB(2)*DP(2,K)-FX(1)*SC(1)*DR(1,K)+CR(1)*DFX(1,K)+FX(2)*SB(2)*DR(2,K) RALL3010
      ZK1-CR(2)*DFX(2,K)-DFPX(K)                                RALL3020
      DPSI(2,K)=PX(1)*SB(1)*DB(1,K)-CB(1)*DP(1,K)-PX(2)*SB(2)*DB(2,K)+CB(1)*DB(2,K) RALL3030
      +(2)*DP(2,K)-FX(1)*CR(1)*DB(1,K)-SB(2)*DFX(1,K)+FX(2)*CB(2)*DB(2,K) RALL3040
      +SB(2)*DFX(2,K)+DFPZ(K)+DCE(K)                                RALL3050
      DPSI(3,K)=(-FY(1)*SB(1)*DB(1,K)+CB(1)*DFY(1,K)+FY(2)*SB(2)*DB(2,K)) RALL3060
      -CR(2)*DFY(2,K)-DFPZ(K))*+.5*DOS(1)*CR(1)*DB(1,K)+SB(1)*DOS(1,K)- RALL3070
      20S(2)*DB(2,K)-SB(2)*DB(2,K)+DOS(2,K)                                RALL3080
      DPSI(4,K)=(FX(1,K)+DFX(2,K))*+.5*DOS(DY(K)-DOP(K))                                RALL3090
      40 DPSI(5,K)=(-FY(1)*CR(1)*DB(1,K)-SB(1)*DFY(1,K)+FY(2)*CR(2)*DB(2,K)) RALL3100
      +SH(2)*DFY(2,K)-DFPX(K))*+.5*DOS(1)*SA(1)*DB(1,K)+CR(1)*DOS(1,K)+ RALL3110
      20S(2)*SA(2)*CE(2,K)-CB(2)*DOS(2,K)+DMZ(K)                                RALL3120
      C DPSI(7),2<#DPSI#7,2<6XMASS+DMEGAE#4#2                                RALL3130
      NN#5                                RALL3140
      DO 53 K=1,5                                RALL3150
      DO 53 L=1,5                                RALL3160
      53 DPSI(1,L,K)=DPSI(L,K)
      CALL SIMULT(DPSI,NN,PST,COR,QUIT)
      IF(QUIT)44,44,45                                RALL3170
      44 CONTINUE                                RALL3180
      TEXTI=45.0                                RALL3190
      RETURN                                RALL3200
      44 47 K=1,5                                RALL3210
      X(K)=X(K)-COR(K)*CPV02                                RALL3220
      DO 48 K=1,5                                RALL3230
      IF(ABS(COR(K))-TOL(K))48,21,21                                RALL3240
      48 CONTINUE                                RALL3250
      HOMI1=HOMI2-PPOC(J)*CPH*EPZ+SPH,
      VFAT=VERT+, POC(J)*SPH-FPZ*CPH                                RALL3260
      BLTEST=0.0                                RALL3270
      GO TO 54                                RALL3280
      21 CONTINUE                                RALL3290
      BLTEST=1.0                                RALL3300
      54 DBA(1)=CP(2)**2/(A2-X(2))
      DBA(2)=-(A1-X(1))*(CP(2)/(A2-X(2)))**2                                RALL3340
      DSA(1)=-D*DBA(1)*SB(2)/E2                                RALL3350
      DSA(2)=-D*(FA(2)*SB(2)/E2)                                RALL3360
      DDELA(1)=SB(2)                                RALL3370
      DDELA(2)=0.0                                RALL3380
      V1=-PX(2)*CB(2)-FX(2)*SB(2)                                RALL3390
      V2=PX(2)*SB(2)-FX(2)*CB(2)                                RALL3400
      V3=-.5*D*FY(2)*SH(2)+OS(2)*CB(2)                                RALL3410
      V4=-.5*D*FY(2)*CB(2)-OS(2)*SB(2)                                RALL3420
      JKOUNT=0                                RALL3430
      XPHI(J)=2.1*57.295780                                RALL3440
      DMEX(J)=X(3)/.10471975                                RALL3450
      DMEM(J)=X(4)/.10471976                                RALL3460
      DMEZ(J)=X(5)/.10471976                                RALL3470
      DO 60 K=1,2                                RALL3480
      PI(K,J)=PX(K)
      XHET(K,J)=B(K)*57.295780                                RALL3490
      AMAJ(K,J)=AA(K)*2.0                                RALL3500
      AMIN(K,J)=BB(K)*2.0                                RALL3510
      FFX(K,J)=FX(K)                                RALL3520
      RALL3530
      RALL3540

```

```

      FFY(K,J)=FY(K)
      DOS(K,J)=OS(K)
      XOMS(K,J)=OMS(K)/.10471276
      DPA(K)=1.5*SO(2)*DPLA(K)+PX(2)*DXNKG(2)*DGA(K)/XK(2)
      DFXA(K)=DFXP(2)*DPA(K)-.5*D*(-(RPM(2)-OMEGA-E(X(3)))*SH(2)+X(5)*CR(BALL 3590
      121)*DFXYV(2)+(IRPM(2)-OMEGAF-X(3))*CR(2)*X(S)*SR(2))*DFXWS(2)*DRARALL3600
      2(K)
      DFYAK(K)=DFYP(2)*DPS(K)-.5*D*(-(RPM(2)-OMEGA-E(X(3)))*SR(2)+X(5)*CR(BALL 3620
      121)*DFYVV(2)+(IRPM(2)-OMEGA-E(X(3)))*CB(2)+X(S)*SB(2))*DFYHS(2)*DRARALL3630
      2(K)
      DQSA(K)=DQSP(2)*DPA(K)-.5*D*(-(RPM(2)-OMEGA-E(X(3)))*SR(2)+X(5)*CR(BALL 3650
      121)*DQSVD(2)+(IRPM(2)-OMEGAF-X(3))*CR(2)+X(S)*SR(2))*DQSNS(2)*DRARALL3660
      2(K)
      DFXOME(K)=-E2+C(K)*D*CR(K)+.5*DFXYV(K)-C(K)*SR(K)*DFXWS(K)
      DFYOME(K)=-E2+C(K)*D*CR(K)+.5*DFYVV(K)-C(K)*SB(K)*DFYWS(K)
      DQSCMF(K)=-E2+C(K)*D*CR(K)+.5*DQSVD(K)-C(K)*SR(K)*DQSWs(K)
      DFPXA(K)=DFPXP*DFYA(K)
      DFPZA(K)=DFPZP*DFYA(K)
      DQPA(K)=DQSP*DFYA(K)
      DF2DME=DFYOME(1)+DFYOME(2)
      XMYCME=XIN*X(S)
      XMZOME=-XTN*X(4)
      VEC(1)=V1*DRA(1)-SR(2)*DPA(1)+CB(2)*DFXA(1)+DFPXA(1)
      VFC(1)=V2*DRA(1)-CR(2)*DPA(1)-SB(2)*DFXA(1)-DFPZA(1)
      VEC(3)=V3*DRA(1)+.5*D*CR(2)*DFYA(1)+SR(2)*DQSA(1)+.5*D*DFPZA(1)
      VEC(4)=-.5*D*DFXA(1)+DPA(1)
      VEC(5)=V4*DRA(1)-.5*D*SB(2)*DFYA(1)+CR(2)*DQSA(1)+.5*D*DFPXA(1)
      M 66 K=1,5
      DVARA1(K)=0.
      M 66 I=1,5
      66 DPSI(L,K)=DPSI1(L,K)
      CALL SIMULT(DPSI,NN,VFC,DVARA1, IQUIT)
      KOUNT=KOUNT+1
      IF(IQUIT)61,61,62
      62 CONTINUE
      TEST1=62.0
      RETURN
      61 VFC(1)=V1*DRA(2)-SR(2)*DPA(2)+CB(2)*DFXA(2)+DFPXA(2)
      VFC(2)=V2*DRA(2)-CR(2)*DPA(2)-SB(2)*DFXA(2)-DFPZA(2)
      VFC(3)=V3*DRA(2)+.5*D*CR(2)*DFYA(2)+SR(2)*DQSA(2)+.5*D*DFPZA(2)
      VFC(4)=-.5*D*DFXA(2)+DPA(2)
      VEC(5)=V4*DRA(2)-.5*D*SB(2)*DFYA(2)+CR(2)*DQSA(2)+.5*D*DFPXA(2)
      M 67 K=1,5
      DVARA2(K)=0.
      M 67 L=1,5
      67 DPSI(L,K)=DPSI1(L,K)
      CALL SIMULT(DPSI,NN,VFC,DVARA2, IQUIT)
      KOUNT=KOUNT+1
      IF(IQUIT)64,64,62
      64 VEC(1)=-CR(1)*DFXOME(1)+CR(2)*DFXOME(2)+DFPXP*(DFYOME(1)+DFYOME(2))
      VFC(2)=SP(1)*DFXOME(1)-SB(2)*DFXOME(2)-XMASS*F2*OMEGAF-DFPZP*(DFYOME(1)+DFYOME(2))
      VFC(3)=-.5*D*(CR(1)*DFYOME(1)-CR(2)*DFYOME(2))-SB(1)*DQSOME(1)+SB(1)*BALL 4080
      12)*DQSOME(2)+.5*D*DFPZP*(DFYOME(1)+DFYOME(2))
      VFC(4)=-.5*D*(DFXOME(1)+DFXOME(2))-XMYOME+DOSPP*(DFYOME(1)+DFYOME(2))
      VFC(5)=.5*D*(DFYOME(1)*SB(1)-DFYOME(2)*SR(2))-CR(1)*DQSOME(1)+CR(2)*BALL 4120
      11)*DQSOME(2)-XMZOME+.5*D*DFPXP*(DFYOME(1)+DFYOME(2))

```

```

-- 2D_6R K=1,5
DOVDMF(K)=0.
DO 68 L=1,5
50 DPSI(L,K)=DPSI1(L,K)
CALL SIMULT(DPSI,NN,VEC,DVOME,IQUIT)
KOUNT=KCUNT+1
IF(IQUIT.EQ.5,62
65 DH2CA1=DPA(1)*DVAPA1(1)*DB(2,1)+DVARA1(2)*DR(2,2)
DH2DA2=DPA(2)+DVAPA2(1)*DR(2,1)+DVARA2(2)*DB(2,2)
DR2DMF=DVOME(1)*DH(2,1)+DVOME(2)*DR(2,2)
DP2CA1=DPA(1)*DVARA1(1)*DP(2,1)+DVARA1(2)*DP(2,2)
DP2DA2=DPA(2)+DVARA2(1)*DP(2,1)+DVARA2(2)*DP(2,2)
DP2DMF=DVCME(1)*DP(2,1)+DVCME(2)*DP(2,2)
DFPA1=DFY(1,1)+(DFY(1,1)+DFY(2,1))*DVAPA1(1)+(DFY(1,2)+DFY(2,2))*DVAPA1(2)+DFY(1,3)+DFY(2,3))*DVARA1(3)+(DFY(1,4)+DFY(2,4))*DVARA1(4)+DFY(1,5)+DFY(2,5))*DVARA1(5)
DFPA2=DFY(1,2)+(DFY(1,1)+DFY(2,1))*DVARA2(1)+(DFY(1,2)+DFY(2,2))*DVARA2(2)+(DFY(1,3)+DFY(2,3))*DVARA2(3)+(DFY(1,4)+DFY(2,4))*DVARA2(4)+(DFY(1,5)+DFY(2,5))*DVARA2(5)
DFPOME=DFPCME+(DFY(1,1)+DFY(2,1))*DVOME(1)+(DFY(1,2)+DFY(2,2))*DVOME(2)+(DFY(1,3)+DFY(2,3))*DVOME(3)+(DFY(1,4)+DFY(2,4))*DVOME(4)+DVOME(5)-2.*DFPAG*(2.*DMEGAF*DOME(2)+E2)/(E2*BALL4350
3*DMEGAF)
FPZDA1=DFPZP*DFPA1+DFPZ(1)*DVARA1(3)
FPZCA2=DFPZP*DFPA2+DFPZ(3)*DVARA2(3)
FPZCME=DFPZP*DFPOME+DFPZ(3)*DVOME(3)
HORA1=-DFPA1*CPH-FPZDA1*SPH
HORA2=-DFPA2*CPH-FPZDA2*SPH
HOROME=-DFPCME*CPH-FPZOME*SPH
VRTA1=DFPA1*SPH-FPZDA1*CPH
VRTA2=DFPA2*SPH-FPZCA2*CPH
VRTOME=DFPCME*SPH-FPZOME*CPH
HTR1=HTR1+HORA1
HTR2=HTR2+HORA2*SPH
HTR3=HTR3+HORA2*CPH
HTR4=HTR4+HTR3*SPH
VRT1=VRT1+VRTA1
VRT2=VRT2+VRTA2*SPH
VRT3=VRT3+VRTA2*CPH
VRT4=VRT4+VRTCME
XF1(1)=XF1(1)+PX(2)*SR(2)-FX(2)*CR(2)
XF1(2)=XF1(2)+(PX(2)*CR(2)+FX(2)*SR(2))*SPH-FY(2)*CPH
XF1(3)=XF1(3)+(PX(2)*CH(2)+FX(2)*SR(2))*CPH+FY(2)*SPH
XF1(4)=XF1(4)+(R*PX(2)*SR(2)-FX(2)*(R*CR(2)-F(2)*D))*CPH+FY(2)*F(2)BALL4570
1*SR(2)*SPH
DXA(1)=DXXA(1)+DVARA1(1)*DFX(2,1)+DVARA1(2)*DFX(2,2)+DVARA1(3)*
1DFX(2,3)+DVARA1(4)*DFX(2,4)+DVARA1(5)*DFX(2,5)
DFXA(2)=DFXA(2)+DVARA2(1)*DFX(2,1)+DVARA2(2)*DFX(2,2)+DVARA2(3)*
1DFX(2,3)+DVARA2(4)*DFX(2,4)+DVARA2(5)*DFX(2,5)
DFXOME(2)=DFXCE(2)*DVOME(1)*DFX(2,1)+DVOME(2)*DFX(2,2)+DVOME(3)*
1DFX(2,3)+DVOME(4)*DFX(2,4)+DVOME(5)*DFX(2,5)
DFYA(1)=DFYA(1)+DVAPA1(1)*DFY(2,1)+DVAPA1(2)*DFY(2,2)+DVAPA1(3)*
1DFY(2,3)+DVAPA1(4)*DFY(2,4)+DVAPA1(5)*DFY(2,5)
DFY(2,3)=DVARA2(1)*DFY(2,1)+DVARA2(2)*DFY(2,2)+DVARA2(3)*
1*DFY(2,3)+DVARA2(4)*DFY(2,4)+DVARA2(5)*DFY(2,5)
DFYOME(2)=DFYOME(2)+DVOME(1)*DFY(2,1)+DVOME(2)*DFY(2,2)+DVOME(3)*
1DFY(2,3)+DVOME(4)*DFY(2,4)+DVOME(5)*DFY(2,5)
A1=-V1*FPZDA1*SR(2)*DP2DA1-CR(2)*DFXA(1)
A2=-V1*DP2CA2*SR(2)*DP2DA2-CR(2)*DFXA(2)

```

```

-- A3=V1*DP2OME+SB(2)*DP2OME+CRL2)*DFXOME(2) . . .
DTV(1,1)=DTV(1,1)+A1
DTV(1,2)=DTV(1,2)+A2*SPH
DTV(1,3)=DTV(1,3)+A2*CPH
DTV(1,4)=DTV(1,4)+A3
A1=-V2*DP2CA1+CRL2)*DP2DA1+SB(2)*DFXAL(1)
A2=-V2*DP2DA2+CB(2)*DP2DA2+SB(2)*DFXAL(2)
A3=-V2*DP2OME+CRL2)*DP2OME+SB(2)*DFXOME(2)
DTV(2,1)=DTV(2,1)+A1*SPH-DFYAL(1)*CPH
DTV(2,2)=DTV(2,2)+A2*SPH**2-DFYAL(2)*SPH*CPH
DTV(2,3)=DTV(2,3)+A2*SPH*CPH-DFYAL(2)*CPH**2
DTV(2,4)=DTV(2,4)+A3*SPH-DFYOMF(2)*CPH
DTV(3,1)=DTV(3,1)+A1*CPH+DFYAL(1)*SPH
DTV(3,2)=DTV(3,2)+A2*CPH*CPH+DFYAL(2)*SPH**2
DTV(3,3)=DTV(3,3)+A2*CPH**2+DFYAL(2)*SPH*CPH
DTV(3,4)=DTV(3,4)+A3*CPH+DFYOMF(2)*SPH
DTV(4,1)=DTV(4,1)+.5*(DFPA1*E2+FPZDA1*D1)+DQVXWX*DVARA1(3)
DTV(4,2)=DTV(4,2)+1.5*(DFPA2*E2+FPZDA2*D1)+DQVXWX*DVARA2(3))*SPH
DTV(4,3)=DTV(4,3)+1.5*(DFPA2*E2+FPZDA2*D1)+DQVXWX*DVARA2(3))*CPH
DTV(4,4)=DTV(4,4)+.5*(DFPOME*(2+FPZOMF*D1)+DQVXWX*DVMFE(3))
RETURN
END

```

```

-- SUBROUTINE ELIPIN(TERM1,TERM2,EE,EK,CSE2,IER)
CTAU=TERM1/TERM2
SNES=.00005
TER=0
D1=1 I=1,30
SNES=5 SNES
CSE2=1.-SNES
IF(CSE2>3,.4)
3 WRITE(6,5)
5 FORMAT(9H0ELIPIN-1)
IER=1
RETURN
4 CTE2=CSE2/SNES
XLG=ALOG(1./CSE2)
EE=1.+CSE2*(.444792040+CSE2*(.085099193+CSE2*.060005094))+CSE2*(.2ELIP 150
149597940+CSE2*(.091502240+CSE2*.0139299901)*XLG ELIP 160
EE=1.3B529436+CSE2*(.097932891+CSE2*(.054544609+.032024666*CSE2))ELIP 170
1+1.5+CSE2*(.124750742+CSE2*(.060118519+.010944912*CSE2))XLG ELIP 180
EUK=EK/EE
CIR=(1.-CIR-2.*EUK-1.)*CTE2*SNES*SNF/((R,-4.*SNES)*EUK-2.*CSE2*ELIP 200
1EUK**2-6.1 ELIP 210
SNF=SNF-(CIR
1 ABS(CIR)-5.E-7)2,1,1
CONTINUE
WRITF(6,6)
6 FORMAT(9H0ELIPIN-2)
IER=1
2 RETURN
END

```

```

-----SUBROUTINE TAPT-----  

  REAL LUBDEN  

  REAL BW1,W2,WORD  

  COMMON HS0(40),HS1(40),  

    COMMON ALPHA,AA(2),AMAJ(2,40),AMIN(2,40),APOCK(40),  

    1,BR(2),BR(2),BPCCK(40), CAGEW, CRV(2), CRAD, COSB,CPR,CTHET, INPT 10  

    INPT 20  

    INPT 30  

    INPT 40  

    BET,RETAINP  

    INPT 50  

    INPT 60  

    INPT 70  

    INPT 80  

    INPT 90  

    INPT 100  

    INPT 110  

    INPT 120  

    INPT 130  

    INPT 140  

    E,EL INPT 140  

    FLAT,F(2),FK,FRADINPT 150  

    GAGE,G2(2),GG(2),INPT 160  

    INPT 170  

    INPT 180  

    INPT 190  

    INPT 200  

    INPT 210  

    INPT 220  

    INPT 230  

    INPT 240  

    INPT 250  

    INPT 260  

    INPT 270  

    INPT 280  

    INPT 290  

    INPT 300  

    INPT 310  

    INPT 320  

    INPT 330  

    INPT 340  

    INPT 350  

    INPT 360  

    INPT 370  

    INPT 380  

    INPT 390  

    INPT 400  

    INPT 410  

    INPT 420  

    INPT 430  

    INPT 440  

    INPT 450  

    INPT 460  

    INPT 470  

    INPT 480  

    INPT 490  

    INPT 500  

    INPT 510  

    INPT 520  

    INPT 530  

    INPT 540  

    INPT 550  

    INPT 560  

    INPT 570  

    INPT 580  

    INPT 590

```

```

    R=.5*F+CRV(2)*COSA          INPT 600
    DIA=F*2.*C(K)*D-CRV(K)*COSB1   INPT 610
    DEPTH=APS(DIA-RINGD1(K))*.5    INPT 620
    DEPTH=SQRT(F(K)*D**2-(F(K)*D-DEPTH)**2)*2.  INPT 630
    AREA(K)=3.14159*CAGED1(K)*(CAGFW-WOTH)  INPT 640
    41 .CLEARSIK)=ABS(RINGD1(K)-CAGED1(K))*0.5  INPT 650
    PILOT=1.                      INPT 660
    IF(CLEARSI<2).LT.CLEARSI1)PILOT=2.        INPT 670
    21 WRITE(6,181)                  INPT 680
    18 FORMAT(12H BEARING DESIGN DATA)       INPT 690
    WRITE(6,191)                  INPT 700
    INPT 710
    19 FORMAT(129HO NO. OF ELEMENT PITCH CONTACT RAINPT 720
    1CF CURVATURES CLEARANCE TYPE OF PILOT POCKET INPT 730
    2 CAGE/129H ELEMENTS DIAMETER DIAMETER ANGLE CINPT 740
    3INTER INNER INCREMENT PILOT CLEARANCE CLEARANCEINPT 750
    4 WIDTH)                         INPT 760
    WORD=W1                           INPT 770
    IF(PILOT.EQ.2).WORD=W2           INPT 780
    TEMP=2.*CLEARSI1                INPT 790
    IF(PILOT.EQ.2.0)TEMP=CLEARSI2*2.0  INPT 800
    TEMP1=POCKET-0                 INPT 810
    IF(IDENS.EC.0.)DFNS=.283        INPT 820
    WRITE(6,501XN,D,F,BAT,F(1),PD,WORD,TEMP,TEMP1,CAGFW  INPT 830
    50 FORMAT(1P7E12.4,4X,A5,3X,1P3E12.4)      INPT 840
    WRITE(6,51)                      INPT 850
    51 FORMAT(130HO I. D. OF O. D. OF I. D. OF U. D. OF INPT 860
    1 MODULUS OF ELASTICITY POISSON'S RATIO INPT 870
    2 ELEMENT/130H OUTER INNER CAGE CAGE INPT 880
    3RINGS CAGE ELEMENTS RINGS CAGE ELEMENTINPT 890
    4S DENSITY)                      INPT 900
    WRITE(6,52)-RINGD1(1),RINGD1(2),CAGED1(2),CAGED1(1),YR,YC,YF,PR,PC,INPT 910
    1PE,DENS                         INPT 920
    52 FORMAT(1P11E12.4)              INPT 930
    RETURN                            INPT 940
    END                               INPT 950
    SUBROUTINE CUTPT                 OUTP 10
    2REAL LURDEN                     OUTP 20
    COMMON HSC(40),HSI(40)            OUTP 30
    COMMON ALPHA,AA(2),AMAJ(2,40),AMIN(2,40),APOCK(40),     RET,BETANOUTP 40
    1,B(2),BP(2),PPOCK(40), CAGEW, CRV(2), CRAD, COSA,CPII,CTHET, OUTP 50
    2DPHR(5),CP(2),CF,C(2),CS(2),CIR(5), CLFARS(2),CLFAPP, DP(2,5), OUTP 60
    3G(2,2),FCF(5),DB(2,5),DEX(2),DROP,DL,DENS,DDL(4),DFL(4),DTV(5,5), OUTP 70
    4DFTRP,DFL(2),DNFLX(2,2),DXKDC(2),DFXVX(2),DFXVY(2),DFXWS(2), OUTP 80
    5DFXP(2),DFYVX(2),DFYVV(2),DFYWS(2),DFYPL(2),DOSVX(2),DOSVY(2),DOSWSOUTP 90
    6(2),DOSR(2),DFX(2,5),DFY(2,5),DOS(2,5),DFXP(5),DFP7(5),DOP(5),DYM(5),OUTP 100
    7(2),DMZ(5),DPS(5,5),DPS1(5,5),DRA(2),DUELA(2),DPA(2),DFXAL(2),DFYAOUP 110
    8(2),DOSA(2),DFXIM(2),DFYOMF(2),DOSOME(2),DFPXA(2),DFPZA(2),DOPA(2)OUTP 120
    9(2),DVARA1(5),DVARA2(5),DVOFE(5),DGA(2), E,EL OUTP 130
    COMMON EPP(5),F2,FSAVE(2),     FLAT,F(2),FK,FRADDOUTP 140
    1,STAN,FFX(2,40),FFY(2,40), GAGE,G2(2),G0(2),OUTP 150
    2,          HOP17,HOP18,HOP2,HOP3,HOP4, IQUIT, OUTP 160
    3JPASS, LPASS,LURDEN, N, OMEGAE,OMY,OMX, OUTP 170
    4D(2),GMS(2),CMFX(40),OMFY(40),OMF(40), PPOC(40),PL,OUTP 180
    5PR,PE,PC,PD,POCKET,PHT,PILOT,PL(2),PSI(5),PL(2,40), OMY,OUTP 190
    6DS(2),DJS(2,40), R,PRM(2), SINP,SPH,STIFT, OUTP 200
    7SH(2),SD(2), TOTL,TI,THET,TL(11),TCRV,TSAVE(2), OUTP 210
    8THICKP(2,40),THICKP(40), V15,VFPT,VPT1,VPT2,VPT3,VPT4,VYR(2), OUTP 220
    9VYR(2),VXR(2),VXP(40),VZP(40),VFC(5) OUTP 230
    COMMON X(1),XN,XF(4),XF(4),XH(2),XH(2),XPH(40),XHFT(2,40),XDISOUTP 240
    1(2,40),XML,XMUL, YE,YR,YC,YHM OUTP 250
    2,DMC(1),D2VYR,D2VX,D2HS,D2P2,XIN,X4ASS OUTP 260
    COMMON F(1),FY(2)               OUTP 270
    COMMON F(1),TI(40),LCTL,LTNT,LTDP,TOL(2),T1,T2,T3,Y4,Y5,Y6,Y7,Y8,Y9OUTP 280

```

1, Y10, GA(2,2), RA(2,2), DFLA(2,2), H(2), HH(2), a1(2), H2(2), SRAL(2), OUTP 290  
 2CIAL(2), DMFGA, DMF(40), DCX(2), DPSIX(2,2), DGYA(2), PA(2,2), DPSIA(2), OUTP 300  
 3XA(2), KCON, CAD(2,2), RFVB, DGYR(2), CAI, SAL, A1,A2, DN, T1, T2, T3, T4, OUTP 310  
 4FT, NUM, XA1(4C), XA2(40), IYPASS, RFVX(40), RFVZ(40) OUTP 320  
 5, CACCO(2), RINGO(2), AREA(2), VEL(2), SPRAGL(2), BDRAG, DSDRG(2,4), OUTP 330  
 6EPTPA1, EP7PA2, EP7OME  
 CMMMN/XTRA/VDPAG(2), CDPAG(2) ,CFORCE  
 WFE=3,14159  
 RP4(1)=RFM(1)/.10471976  
 RP4(2)=0PM(2)/.10471976  
 MEGAF=DMGAE/.10471976  
 WRITF(6,1111)  
 WRITF(6,1112)  
 1111 FORMAT(130H) RPM. OF RPM. OF EXTERNAL LOADS INITOUTP 420  
 1111 STARTING DEFLECTIONS FINAL DEFLECTIONS OUTP 430  
 2 RPM. OUTP 440  
 1112 FORMAT(129H) RUTEP INNER AXIAL RADIAL MISALIGGUTP 450  
 1MNT ALONG X ALONG Z ALONG X ALONG Y ALONG Z OUTP 460  
 2 (CAGE)  
 WRITE(6,1)RFM(1),PPM(2),XF(1),XF(3),DX(4),DOL(1),DOL(3),DFL(1),  
 DFL(2),DFL(3),DMF(2)  
 1 FORMAT(1P11F12.4)  
 WRITF(6,50)  
 50 FORMAT(39H) REACTION OF BEARING ON SHAFT/46HO ALONG X OUTP 520  
 1 ALONG Y ALONG Z ABOUT Y)  
 WRITF(6,1)XF(1),XF(2),XF(3),XF(4)  
 WRITF(6,11)  
 11 FORMAT(25H) BALL/RACE CONTACT DATA)  
 WRITF(6,2)  
 2 FORMAT(119H) ELEMENT ELEMENT CONTACT LOAD OUTP 580  
 1 INFLAT ANGLE PRESSURE AREA LENGTH PRESSURE AREA WIDTH) OUTP 590  
 WRITF(6,3)  
 3 FORMAT(117H) NO. AZEMUTH OUTER INNER OUTP OUTP 610  
 1FR (INNER OUTER INNER OUTER INNER) OUTP 620  
 01 4 J=1,N  
 1F(P2,J)14,4,5  
 5 WRITE(6,6)J,XPH((J),P(1,J),P(2,J),XRET(1,J),XRET(2,J),AMAJ(1,J),  
 1AMAJ(2,J),AMIN(1,J),AMIN(2,J)  
 6 CONTINUE  
 6 FORMAT(17.5X,1P10F12.4)  
 WRITF(6,7)  
 7 FORMAT(116H) ELEMENT BALL VELOCITY COMPONENTS TRROUTP 700  
 1CTION ALONG X TRACTION ALONG Y SPINNING MOMENT) OUTP 710  
 WRITE(6,8)  
 9 FORMAT(117H) NO. ABOUT X ABOUT Y ABOUT Z OUTP OUTP 730  
 1CP (INNER OUTER INNER OUTER INNER) OUTP 740  
 00 0 J=1,N  
 1F(P2,J)19,9,10  
 10 WRITE(6,6)J,CMFX(J),CMFY(J),CMEZ(J),FFX(1,J),FFX(2,J),FFY(1,J),  
 1FFY(2,J),CCSI1,J),CCSI2,J)  
 9 CONTINUE  
 WRITF(6,12)  
 12 FORMAT(94H) ELEMENT SPINNING VELOCITY MINIMUM FILM THICKOUTP 810  
 1VESS MEAN HERTZ STRESS ) OUTP 820  
 WRITF(6,13)  
 13 FORMAT(94H) NO. OUTER INNER OUTP OUTP 840  
 12 (INNER ) OUTP 850  
 01 PC J=1,N  
 1F(P2,J)RC,RC,9  
 91 HSQ(J)=4.0\*P(1,J)/(P(1)\*AMAJ(1,J)\*AMIN(1,J))  
 HS1(J)=4.0\*P(2,J)/(P(2)\*AMAJ(2,J)\*AMIN(2,J))  
 80 CONTINUE  
 01 14 J=1,N  
 1F(P2,J)14,14,15

```

15 WRITE(6,6)J,XOMS(1,J),XOMS(2,J),THICKR(1,J),THICKR(2,J),HS0(J),HSTOUTP 930
16 CONTINUE
17 WRITE(6,10)
18 FORMAT(27HO HALL/ROCKET CONTACT DATA! OUTP 940
19 FORMAT(8RH ELEMENT POCKET PRESSURE ELLIPSE OUTP 950
20 DOING VELOCITY MIN. FILM OUTP 960
21 WRITE(6,18) OUTP 970
22 FORMAT(8RH NO. FORCE LENGTH WIDTH RADOUTP1020
23 1AL AXIAL THICKNESS OUTP1030
24 01 19 J=1,N OUTP1040
25 IF(F(2,J))19,19,20 OUTP1050
26 APOCK(J)=2.*APOCK(J) OUTP1060
27 BPOCK(J)=2.*BPOCK(J) OUTP1070
28 IF(IHJCKP(J).GT.CLEARP)THICKP(J)=CLEARP OUTP1080
29 WRITE(5,6)J,PPDC(J),APOCK(J),BPOCK(J),VZP(J),VXP(J),THICKP(J) OUTP1090
30 CONTINUE
31 WRITE(6,70) BDRAG OUTP1100
32 WRITE(6,50)
33 60 FORMAT(29HO CAGE/PILOTTING SURFACE DATA/34HO VISCOSUS COULOMB OUTP1130
34 NORMAL/33H TORQUE TORQUE LOAD OUTP1140
35 70 FORMAT(25HO VISCOS DRAG ON BALL #,1PIE11,4) OUTP1150
36 TEMP=VDRAG(1)+VDRAG(2) OUTP1160
37 KPLT=PILCT+1 OUTP1170
38 YMP1=CDRAG(KPLT) OUTP1180
39 WRITE(6,1)TEMP,YMP1 ,CFORCE OUTP1190
40 RETURN OUTP1200
41 END OUTP1210

```

```

SUBROUTINE S1MULT(A,N,Q,X,KX)
DOUBLE PRECISION AMPY,EL,V,ROW,AMPYI
1 FORMAT( * ELEMENTS ALL ZERO. RDY NO.9 ,16 /)
1W=6
DIMENSION A(5,5),B(5),X(5),ROW(5),KOL(5)
20 S050 J=1,N
TEMP=0.
21 S051 K=1,N
IF(APSA(J,K)-TEMP)5051,5051,5052
5052 TEMP=APSA(J,K)
5051 CONTINUE
IF(TEMP.NE.0.) GO TO 15051
WRITE(1W,1) J
GO TO 5050
C 20 S053 K=1,N
15051 20 S053 K=1,N
5053 A(J,K)=A(J,K)/TEMP
3(J)=P(J)/TEMP
5053 CONTINUE
5000 KOL(1)=1
5001 20 S002 IROW=2,N
5002 KOL(IROW)=XCOL(IROW-1)+1
5004 20 S025 KCOUNT=1,N
1ARGST=N-KCOUNT+1
1 ASE=KOL(1)
JCOL=1
5005 1F (N-KCOUNT) 5035,5014,5006
5006 AMPY = ABS ( A(1,1) )
5007 20 S010 IROW=2,LARGST
AMPYI=ABS(A(IROW,1))
5008 1F ( AMPY - AMPYI ) 1 5009, 5010, 5010

```

SIMU	10
SIMU	20
SIMU	30
SIMU	40
SIMU	50
SIMU	60
SIMU	70
SIMU	80
SIMU	90
SIMU	100
SIMU	110
SIMU	120
SIMU	130
SIMU	140
SIMU	150
SIMU	160
SIMU	170
SIMU	180
SIMU	190
SIMU	200
SIMU	210
SIMU	220
SIMU	230
SIMU	240
SIMU	250
SIMU	260
SIMU	270
SIMU	280
SIMU	290
SIMU	300
SIMU	310

```

5009 JCCL=IROW      SIMU 320
    AMPY = A(1,1) IRROW,1,1
    IERASF=KCL(IRROW)
5010 CONTINUE      SIMU 330
5011 IF (KOL(1)=IERASF) 5012,5014,5012      SIMU 340
5012 KOL(JCOL1)=KCL(1)      SIMU 350
    KOL(1)=IERASE      SIMU 360
5014 IF(A(JCOL,1)=0.0,5015,5015      SIMU 370
5015 AMPY=A(JCOL,1)      SIMU 380
5017 DO 5019 IPOL=2,N      SIMU 390
    EL=A(JCOL,IRCW)      SIMU 400
    ROWX(IRW-1)=A(JCOL,IRCW)      SIMU 410
5018 A(JCOL,IPOL-1)=A(1,IRW-1)      SIMU 420
    ROW(N)=1./AMPY      SIMU 430
    A(JCOL,N)=A(1,N)      SIMU 440
5019 DO 5022 IRW=2,N      SIMU 450
    AMPY=A(1,IRW,1)      SIMU 460
5020 DO 5021 JCOL=2,N      SIMU 470
    EL=A(IRW,JCOL)      SIMU 480
5021 A(IRW-1,JCOL-1)=A(IRW,JCOL-1)-AMPY*ROW*JCOL-1*      SIMU 490
    A(IRW-1,JCOL-1)=EL-AMPY*ROW*(JCOL-1)      SIMU 500
5022 A(IRW-1,N)=AMPY*ROW(N)      SIMU 510
5023 DO 5024 JCOL=1,N      SIMU 520
    KOL(JCOL)=KCL(JCOL+1)      SIMU 530
5024 A(N,JCOL)=FC(JCOL)      SIMU 540
5025 KOL(N)=IERASE      SIMU 550
5026 DO 5034 KCOUNT=1,N      SIMU 560
5027 IF (KCOLUMN-KCOUNT) 5035,5034,5028      SIMU 570
5028 DO 5032 IRON=KCOUNT,N      SIMU 580
5029 IF (KOL(IRON)=KCOUNT) 5035,5030,5032      SIMU 590
5030 DO 5031 JCOL=1,N      SIMU 600
    ROW(1)=A(JCOL,IRCW)      SIMU 610
    A(JCOL,IPOL)=A(JCOL,KCOUNT)      SIMU 620
5031 A(JCOL,KCOUNT)=ROW(1)      SIMU 630
    IERASF=KCL(KCOUNT)      SIMU 640
    KOL(KCOUNT)=KCL(IRW)      SIMU 650
    KOL(IPOL)=IERASF      SIMU 660
    GO TO 5034      SIMU 670
5032 CONTINUE      SIMU 680
5033 GO TO 5035      SIMU 690
5034 CONTINUE      SIMU 700
5035 IF(KX=31599,9000,998      SIMU 710
9000 KX=0      SIMU 720
    RETURN      SIMU 730
    999 DO 5042 IRW=1,N      SIMU 740
5040 X=IRWC #Q,0      SIMU 750
5041 DO 5042 JKOL=1,N      SIMU 760
    5041 DO 5042 JKOL=1,N      SIMU 770
    EL=A(IRW,JKOL)      SIMU 780
    V=B(JKOL)      SIMU 790
5042 X=IRWC # X*IRWC*ROW,JKOL + BJKOL      SIMU 800
    5042 AMPY=AMPY+EL*V      SIMU 810
5042 X(IRW)=AMPY      SIMU 820
    KX=C      SIMU 830
    RETURN      SIMU 840
5045 KX=1      SIMU 850
    RETURN      SIMU 860
END      SIMU 870
SIMU 880
SIMU 890
SIMU 900
SIMU 910

```

```

SUBROUTINE PALETJ(RG)
REAL LUDEN
COMMON HSI(40),HSI(40)
COMMON ALPHA,AM1(2),AMAJ(2,40),AMIN(2,40),APICK(40),
      RFT,PETABALF 40
1,BR(2),BR(2),BROCK(40),CAGFW,CRV(2),CRAD,CNSR,CPH,CTHEI, BALF 50
2,CCR(5),CR(2),CF,C(2),CSP(2),COP(5),CLEARP,CLEARP,DP(2,5), BALF 60
3,DG(2,2),DCF(5),D8(2,5),DE(12),DROP,D,PENS,DNL(4),DFL(4),DT(5,5), BALF 70
4,DFTEP,DFL(2),DFELX(2,2),DXKNG(2),DFXX(2),DFXVY(2),DFXWS(2), BALF 80
5,DFXP(2),DFYVX(2),DFYVY(2),DFYWS(2),DFYP(2),DOSVX(2),DOSVY(2),DOSWSBALF 90
6,1,DO(2),DFX(2,5),DFY(2,5),DOS(2,5),DFPK(5),DFPZ(5),DOP(5),DMY(2) 100
7,1,DMZ(5),DPSI(5,5),DPSI(5,5),DPA(2),DDELA(2),DPA(2),DFXA(2),DFYABALF 110
8,R(2),DOSA(2),DFXOMF(2),DFYOME(2),DOSUMF(2),DFXA(2),DFPA(2) 120
9,1,DVARA1(5),DVARA2(5),DVQME(5),DGA(2),E,EL,BALF 130
COMMON ERR,51,F2,FSAVE(2).
1,FTAN,FFX(2,40),FY(2,40).
2,HDR1,HDR1,HDR2,HDR3,HDR4.
3J ASE,LPASS,LUDEN,N,OMEGAF,DMY,DMX,BALF 160
4,7,14S(2),CMFX(40),DMKEY(40),OMEZ(40),PPDC(40),PL,BALF 180
5,SR,SE,PC,PD,POCKET,PHI,PILOT,PX(2),PSI(5),P(2,40),OMV,BALF 190
6,DS(2),DOS(2,40),R,RPM(2),SINR,SPH,STHET,BALF 200
7,SB(2),SD(2),TDL,T1,THET,TOL(11),TCRV,TSAVE(2),BALF 210
8,THICKR(2,40),VIS,VERT,VRT1,VRT2,VRT3,VRT4,VYR(2),BALF 220
9,VYB(2),VXB(2),VXP(40),VZP(40),VEC(5)
COMMON X(5),XA,XF(4),XF(4),XK(2),XN2,XMY,XPHI(40),XRET(2,40),XMSBALF 240
1,(2,40),XMU,XMU1,YE,YR,YC,YNUM,BALF 250
COMMON D2VYR,D2VX,D2WS,D2P2,XIN,XMASS,BALF 260
COMMON FX(2),FY(2),BALF 270
COMMON IC,CTL(40),LCTL,LCNT,LOOP,TO(2),Y1,Y2,Y3,Y4,Y5,Y6,Y7,Y8,Y9BALF 280
1,Y10,GA(2,2),PA(2,2),DELA(2,2),H(2),HH(2),H1(2),H2(2),SBAL(2),BALF 290
2,SBAL(2),OMEGA,DMF(40),DCX(2),DPSIX(2,2),DGYA(2),PA(2,2),DPSIA(2),HALF 300
3,XA(2),KOMV,CAD(2,2),REV6,DFYRD(2),CAL+SL,A1,A2,ON,T1,T2,T3,T4,BALF 310
4,FT,NUM,XA(40),XA(40),ITPASS,REVX(40),REVZ(40),BALF 320
5,CAGEDJ(2),RINGD(2),APEA(2),VEL(2),SDRAG(2),DRAG,DSDRG(2,4),BALF 330
6,FPZD(1),FPZCA(2),FPZOMF,BALF 340
DIMENSION U(3),V(3),WSS(3),W1(3),W2(3),S1(3),S2(3),PHZ(3),Y(60),BALF 350
IRATIO(60),FFXX(3,3,6),FFYY(3,3,6),TM(3,3,6),BALF 360
1,IPASS,BALF 370
2,LPASS,BALF 380
3,DVYR=D2VYR*ABS(VYR(L))-VYB(L),BALF 390
4,DVX=D2VX*APS(VXR(L)),BALF 400
5,DWS=D2WS*ABS(DMS(L))/10472,BALF 410
6,OT=D2P2*PX(L),BALF 420
7,IF(DVYR.LT.0.1)DVYR=0.1,BALF 430
8,IF(DVX.LT.0.1)DVX=0.1,BALF 440
9,IF(DWS.LT.0.1)DWS=0.1,BALF 450
10,IF(OT.LT.0.1)OT=0.1,BALF 460
11,IF(OT.GE.PX(L)) OT=0.9*PX(L),BALF 470
12,THICKR(L,J)=1.E6,BALF 480
13,S1(L)=AA(L),BALF 490
14,C2(L)=BB(L),BALF 500
15,IDY=6,BALF 510
16,IVY=20,BALF 520
17,X1DY*IDY,BALF 530
18,RJ=.5*D,BALF 540
19,B3=C(L)*.5*FE2/(C8(L)+C(L)*D),BALF 550
20,WT=PX(L),BALF 560
21,WHS=(DMS(L))/104719761,BALF 570
22,WS=WHS,BALF 580
23,Y1=VYR(L),BALF 590

```

```

120 WXR(L)
VL=-VXR(L)
DU=DVYR
DW=DVK
DWS=DWS
DHS=DWS
DE=DZ
U(2)=U1+DU
U(3)=U1-DU
V(2)=V1+DV
V(3)=V1-DV
WSS(2)=WSS+DWS
WSS(3)=WSS-DWS
WTT(2)=WTT+DT
WTT(3)=WTT-DT
THETA=(T1-R2)/1.8
EXP=1./RJ+1./RP
RYP=1./RJ+1./RG
AAA=.5*RXP
DDG=.5*YP
RXP=1./RXP
RYP=1./RYP
AMC=(AAA-PPB)/(AAA+DDG)
FP=3.14159265/111.-PF**21/YE+(1.-PR**21)/YE
U(1)=UL
V(1)=VL
WSS(1)=WS
WTT(1)=WT
YY=2./X1DY
YY 200 K=2,3
TEMP=(WTT(K)/WTT(1))+4.3333333
S1(K)=S1(1)*TEMP
200 S2(K)=S2(1)*TEMP
DO 45 I=1,3
OH2(I)=1.5*WTT(1)/(3.14159265 *S1(I)*S2(I))
S1(I)=.75*WTT(I)/S1(I)
45 CONTINUE
35 VIS3=VIS*EXP(BETA*(T1-96.))
AL3=ALPHA+.930.*ALPHA*(T1-86.)/1546.* (T1+450.)
IHH=1.GR=ALPHA**.6*VIS**.7*EP**.03*RXP**.43
S1T=VIS3*(ALPHA/AL3)**.6*(VIS/VIS3)**.7
S2T=VIS3*BETA/(R.*EK*.216)
I1=1
IJ=1
KK=1
LT=1
IN=1
45 F1Y=0.
F1X=0.
T42=0.
T41=0.
CS=WSS(KK)*.10471076*11(LL)
IF((KK.EQ.11).AND.(LL.EQ.11).AND.((IJ).NE.11).OR.(IJ.NE.11))GO TO 49
IF((SS.EQ.0.0).TO 49
YS=(U(1))-U2)/SS
IF((YS.GE.1.00.(YS.LE.(-1.0)))GO TO 43
GO TO 44
43 Y(1)=1.+YY*.5
M4=1

```

```

-- G1 TO 42 --
44 NPN=J
Y(1)=YS
45 Y(NNN+1)=Y(NNN)+DY
RAT10(NNN+1)=1.-Y(NNN+1)**2
NNN=NNN+1
IF(Y(NNN).LT.(1.-5*DY)) GO TO 41
IF(Y(NNN).GE.1.1.NNN=NNN-1
Y4=NNN+1
Y(MM)=YS-DY
RAT0(MM)=1.-Y(MM)**2
IF(Y(MM).LE.(-1.1)MM=MM-1
42 Y(MM+1)=Y(MM)-DY
RAT10(MM+1)=1.-Y(MM+1)**2
MM=MM+1
IF(Y(MM).GT.(-1.+5*DY)) GO TO 42
IF(Y(MM).LE.(-1.1)MM=MM-1
43 GO TO 50 MM=2,MM
UHAR=ARS((U(I1)+U2-SS*Y(M))/5)
H=SH(LL)*RATIO(M)
HQ=HHH*UBAR**.7/H**.13
PP/Z=PH2(LL)*SCRT(RATIO(M))
US=ARS((U2-U(I1)+SS*Y(M))
G1=G1+US/(HQ*PPHZ)
G2=G2+LS**2
G3=AL3*PPHZ
CALL FRACT(TG11,G22,G33,FCOF,THETAC
C FCOE=7.5*SORT(G11)
FCOF=7.5*SORT(G11)
F1X=-FCOE*H*DY*SI(LL)
IF((U(I1)-SS*Y(M)).LT.U2)F1X=-F1X
F1Y=-FCOF*H*V(JJ)/US*DY*SI(LL)
FF1X=FF1X+F1X
FF1Y=FF1Y+F1Y
TFX=-F1X*Y(M)*SI(LL)
TM1=TM1+TFX
TFY=-FCOF*H*SS*SI(LL)**2*RATIO(M)*DY/(3.*US)
TM2=TM2+TFY
IF(HQ-TICKRL,JJ)201,201,50
201 TICKRL,JJ)=HQ
50 CONTINUE
TM=TM1+TM2
FFXX(I1,JJ,NN)=FF1X
FFYY(I1,JJ,NN)=FF1Y
TMM(I1,JJ,NN)=TM
IF((I1.GE.2).OR.(JJ.GT.1).OR.(LL.GT.1)) GO TO 55
I1=I1+1
GO TO 49
55 I1=1
IF((JJ.GE.3).OR.(KK.GT.1).OR.(LL.GT.1)) GO TO 56
JJ=JJ+1
GO TO 48
56 IJ=1
IF((KK.GE.3).OR.(LL.GT.1)) GO TO 57
KK=KK+1
NN=NN+1
GO TO 48
57 KK=1

```

BALF1190  
BALF1200  
BALF1210  
BALF1220  
BALF1230  
BALF1240  
BALF1250  
BALF1260  
BALF1270  
BALF1280  
BALF1290  
BALF1300  
BALF1310  
BALF1320  
BALF1330  
BALF1340  
BALF1350  
BALF1360  
BALF1370  
BALF1380  
BALF1390  
BALF1400  
BALF1410  
BALF1420  
BALF1430  
BALF1440  
BALF1450  
BALF1460  
BALF1470  
BALF1480  
BALF1490  
BALF1500  
BALF1510  
BALF1520  
BALF1530  
BALF1540  
BALF1550  
BALF1560  
BALF1570  
BALF1580  
BALF1590  
BALF1600  
BALF1610  
BALF1620  
BALF1630  
BALF1640  
BALF1650  
BALF1660  
BALF1670  
BALF1680  
BALF1690  
BALF1700  
BALF1710  
BALF1720  
BALF1730  
BALF1740  
BALF1750  
BALF1760  
BALF1770

```

1F(1L,GF,3100 TO 58
LL=11+1
NN=NN+1
G1 TO 49
58 CONTINUE
EXDUX=(FFXX(2,1,1)-FFXX(3,1,1))/(2.*DU)
EXDV=(FFXX(1,2,1)-FFXX(1,3,1))/(2.*DV)
EXDWS=(FFXX(1,1,2)-FFXX(1,1,3))/(2.*DWS)
EXDW=(FFXX(1,1,4)-FFXX(1,1,5))/(2.*DWT)
FYDUX=(FFYY(2,1,1)-FFYY(3,1,1))/(2.*DU)
FYDV=(FFYY(1,2,1)-FFYY(1,3,1))/(2.*DV)
FYDWS=(FFYY(1,1,2)-FFYY(1,1,3))/(2.*DWS)
FYDW=(FFYY(1,1,4)-FFYY(1,1,5))/(2.*DWT)
TMDU=(TMH(2,1,1)-TMH(3,1,1))/(2.*DU)
TMDV=(TMH(1,2,1)-TMH(1,3,1))/(2.*DV)
TMDWS=(TMH(1,1,2)-TMH(1,1,3))/(2.*DWS)
TMDW=(TMH(1,1,4)-TMH(1,1,5))/(2.*DWT)
FX(L)=FFYY(1,1,1)
FY(L)=FFXX(1,1,1)
DS(L)=TMD(1,1,1)
DXVX(L)=-FYDV
DXVY(L)=-FYDU
DXWS(L)=-FYDWS/.10471976
DXWP(L)=EXDW
DXVX(L)=-EXDV
DXVY(L)=-EXDY
DXWS(L)=-EXDWS/.10471976
DXWP(L)=EXDW
DQSvx(L)=-TMDV
DQSvy(L)=-TMDU
DQSws(L)=-TMDWS/.10471976
DQSp(L)=TMDW
25 TURN
END

SUBROUTINE BAL1
26AL LUBDEN
COMMON HSC(40),HST(40)
COMMON ALPH(1),AL(2),AM(3)(2,40),AMIN(2,40),APICK(40),
      BFT,BETABALL 40
      1,B(2),BP(2),BPCCK(40), CAGEW, COV(2), CRAD, COSB,CPH,CTHET, RALL 50
      2CCR(5),CP(2),CF(2),CSP(2),CR(5), CLFARS(2),CLFARP, DP(2,5), RALL 60
      3DG(2,2),DCF(5),DP(2,5),DEX(2),DGP,D,DENS,DDL(4),DTV(5,5), BALL 70
      4DFTEP,DFL(2),DDEFLX(2,2),DXKDG(2),DXVX(2),DXVY(2),DXWS(2), RALL 80
      5DFEXP(2),DFYVX(2),DFYHS(2),DFYPL(2),DQSvx(2),DQSvy(2),DQSWSHALL 90
      6(2),DOSD(2),DFX(2,5),DFY(2,5),DOS(2,5),DFXPX(5),DFPZ(5),DOP(5),DMY(RALL 100
      7S),DMZ(5),DPSI(5,5),DPA(2),DDEL(2),DPA(2),DFXA(2),DFYARBALL 110
      8(2),DOSA(2),DFXOME(2),DFYOME(2),DGSOME(2),DFPXA(2),DFPZA(2),DOPA(2)BALL 120
      9),DVARA(5),DVARA2(5),DVO(5),DGA(2). F,EL RALL 130
COMMON FRR(5),F2,FSAVF(2),
1,FTAN,FFX(2,40),FFY(2,40),
2 HOR17,HOR1,HOR2,HOR3,HOR4, GAGE,GZ(2),GG(2),RALL 150
3JPASS, LPASS,LUBDEN, N, OMEGAE,DMY,DMX, RALL 170
4OM7,OMS(2),OMFY(40),OMFY(40),OMEZ(40), PPMC(40),PL,RALL 190
5PR,PF,PC,PD,PUCKET,PH1,PILC7,PX12J,PS1(51),P12,40), OMV,BALL 190
6PS(2),POS(2,40), R,RP(2), SINH,SPH,S1HFT, RALL 200
7SP(2),SQ(2), TOTL,TI,THET,TOL(111),TCRV,TSAVE(2), RALL 210
8THICKP(2,40),THICKP(40), VTS,VERT,VRT1,VRT2,VRT3,VRT4,VYR(2), RALL 220
9VYR(2),VXR(2),VXP(40),VZP(40),VEC(5)
COMMON X(5),XA,XF(4),XF(4),Y(2),X4Z,X4Y,XPH(40),XBFT(2,40),XOMSRALL 240
112,40),XMU,XMU1, YF,YR,YC,YUM, RALL 250
COMMON D2VYR,D2VX,D2WS,D2P2,XIN,X4ASS RALL 260
COMMON FX(2),FY(2) RALL 270
COMMON IC,CTL(40),LCTL,ICNT,LOOP,TO(2),Y1,Y2,Y3,Y4,Y5,Y6,Y7,Y8,Y9RALL 280
1,Y10,GA(2,2),BA(2,2),ELA(2,2),H1(2),HH(2),H1(2),H2(2),SRAL(2), RALL 290
2CPAL(2),OMEGA,OMF(40),DX(2),DPSIX(2,2),DGYA(2),PA(2,2),DPSIA(2), RALL 300
3XA(2),KOMV,EAP(2,2),RFVR,DXERQ(2),CAL,SAI,A1,A2,IAS,I1,I2,I3,I4,I5,I6, RALL 310

```

```

4*E1,NUM,XA1(40),XA2(40),IPASS,REVY(40),REVZ(40)
5,CACED1(2),PINGD1(2),AREA1(2),VEL1(2),SDRAG(2),BDRAG,ESDRG(2,4),
6,BPZCA1,BPZCA2,BPZDME
7-IPASS
8=CTLE(J)
9=TAL=SE(I0)/(CF(IC)+C(IC)*D/E2)
10=ATAN(TAL)
11=SAL=SIN(ALX)
12=CAL=COS(ALX)
13=IK=1,2
14=TEMP=R(K)-ALX
15=SAL(K)=SINITMP3
16=SPAL(K)=COS(TEMP1)
17=T1=GG(1)*CBAL(2)
18=T2=GG(2)*CBAL(1)
19=DW11*T2
20=REV= E2*(RPM(1)-RPM(2))+GG(1)*GG(2)/ID*DN
21=REVX(J)=REV*B*CAL
22=REVZ(J)=REV*B*SAL
23=OMEGA=(T1+RPM(1)+T2*RPM(2))/DN
24=XMASS*.5*E2*OMEGA**2
25=XHY=XIN*OMEGA*REV*B*SAL
26=H(1)=2.*XHY/D
27=JHL21=H(1)
28=Y1=CB(IC)**2+C(IC)*G2(IC)
29=Y2=CB(IC)**2-SB(IC)**2
30=Y3=SB(IC)*CB(IC)
31=Y4=(CAL/Y1)**2
32=Y5=E2*(RPM(1)-RPM(2))/ID*DN**2
33=Y6=CMEGA*DN
34=Y7=2./D*(H1(IC)*CR(1)-H2(IC)*CR(2))
35=Y8=2./D*(H1(IC)*SP(1)-H2(IC)*SP(2))
36=Y9=.5*D*Y7
37=Y10=.5*D*Y8
38=IK=2,K=1,2
39=X=(Y1+Y2*D8(IC,K))-Y3*(-2.*Y3*D8(IC,K)+C(IC)*DG(IC,K)))+Y4
40=Z1=GG(1)*SPAL(2)*(DB(2,K)-DALX)
41=Z2=GG(2)*SPAL(1)*(DB(1,K)-DALX)
42=D04BX=Y5*(DN*1-GG(1)*DG(2,K)+GG(2)*DG(1,K))-GG(1)*GG(2)*(-Z1+CBAL(2))
43=D04EX=(DN*(RPM(1)*1-Z1)+CBAL(2)*DG(1,K))-RPM(2)*Z2+CBAL(1)*DGL2,K)IF ALL .700
44=Z1=-Y6*(-Z1+CPAL(2)*DG(1,K)-Z2-CRAL(1)*DG(2,K))/DN**2
45=DC(X(K))=XMASS*(E2*OMEGA*D04EX+.5*OMEGA**2*D(X(K)))
46=DGYRD(K)=XTN*((REV*B*D04EX+OMEGA*D04BX)+SAL+REV*B*OMEGA*CAL+DALX)
47=T1=PX(1)*CB(1)+H(IC)*SB(1)
48=T2=PX(2)*CB(2)+H(IC)*SB(2)
49=T3=PX(1)*SP(1)-H(1)*CB(1)
50=T4=PX(2)*SP(2)-H(2)*CB(2)
51=IK=1,2
52=OPSIX(1,K)=T1*DB(1,K)-T2*DB(2,K)+DP(1,K)*SB(1)-DP(2,K)*SP(2)-Y7*
53=1*DGYRD(K)
54=OPSIX(2,K)=-T3*DP(1,K)+T4*DP(2,K)+DP(1,K)*CB(1)-DP(2,K)*CB(2)+Y8
55=1*DGYRD(K)=DC(X(K))
56=PS1(1)=PX(1)*SP(1)-PX(2)*SP(2)-H(1)*Y9
57=PS1(2)=PX(1)*CB(1)-PX(2)*CB(2)+H(1)*Y10-CP
58=DF1=DP(SFX(1,1)-OPSIX(2,2)-OPSIX(2,1)+OPSIX(1,2))
59=CR(1)=(FSI(1)*OPSIX(2,2)-PSI(2)*OPSIX(1,2))/DET
60=CO4(2)=(OPSIX(1,1)*PSI(2)-OPSIX(2,1)*PSI(1))/DET
61=IK=1,2
62=X(K)=X(K)-CR(K)
63=RETURN
64=END

```

```

SUBROUTINE BALL2
REAL LURDEN
COMMON HSQ(40),HSI(40)
COMMON ALPHA,AA(2),AMAJ(2,40),AMIN(2,40),APACK(40),
     1,BL2),BB(2),BPLCK(40),CAGEM,CRV(2),CBAD,CSB,CPH,CTHET,BALL
     2,CCR(5),CP(2),CF,C(2),CSP(2),COR(5),CLEAR(2),CLFARP,DP(2,5),BALL
     3,DGL(2,2),DCFL(5),DR(2,5),DEX(2),DROP,D,DENS,DL(16),DFL(4),DTV(5,3),BALL
     4,DFTR,DFL(2),DDFLX(2,2),DXKNG(2),DFXVX(2),DFXW(2),DFXWS(2),BALL
     5,DFXP(2),DFYVY(2),DFYMS(2),DFYP(2),DOSVX(2),DOSVY(2),DOSMSBALL
     6(2),DOSP(2),DFX(2,5),DFY(2,5),DQS(2,5),DFPX(5),DFPZ(5),DQP(5),DMY(BALL
     7,5),DMZ(5),DPS(5,5),DPS(1,5,5),DBA(2),DDEL(2),DPA(2),DFXA(2),DFYABALL
     8(2),DOSA(2),DFXOMF(2),DFYOMF(2),DOSOME(2),DFPXA(2),DFPZA(2),DOPA(2)BALL
     9,1,DVARA(15),CVARA(15),DVOME(5),DGA(2),
     10,E,EL,BALL
COMMON FRR(5),F2,FSAVE(2),
     11,FIAM,FFX(2,40),FFY(2,40),
     12,HOR1,HOR1,HOR2,HOR3,HOR4,QUIT,BALL
     13,JPASS,IPASS,LURDEN,N,OMEGA,E,UMY,OMX,BALL
     14,OMZ,OMS(2),CP(40),OMEY(40),OMEZ(40),PPOC(40),PL,BALL
     15,5,R,PE,PC,PD,POCKET,PHI,PILO,PX(2),PSI(5),P(2,40),QMV,BALL
     16,605(2),QOS(2,40),R,RP(2),SINH,SPH,STHET,BALL
     17,7SB(2),SO(2),TOTL,T1,THET,TOL(11),TCPV,TSAVF(2),BALL
     18,THICKR(2,40),THICKP(40),VIS,VERT,VRT1,VRT2,VRT3,VRT4,VVR(2),BALL
     19,VYD(2),VXB(2),VXP(40),VZP(40),VEC(5),BALL
COMMON X(5),XA,XF(4),XF(4),XX(2),XMZ,XMY,XPHI(40),XRFT(2,40),XOMSBALL
     20,112,40),XMU,XMU1,YE,YR,YG,YNUM,BALL
COMMON D2VYR,F2VX,D2WS,D2P2,XIN,XMASS,BALL
COMMON FX(2),FY(2),BALL
COMMON IC,CTL(40),LCTL,ICNT,LLOOP,T0(2),Y1,Y2,Y3,Y4,Y5,Y6,Y7,Y8,Y9BALL
     1,1,Y10,GA(2,2),BA(2,2),DELA(2,2),H(2),HH(2),H1(2),H2(2),SNAL(2),BALL
     2,SNAL(2),CMFGA,CM(40),DCX(2),DPSIX(2,2),DGYA(2),PA(2,2),DPSIA(2),BALL
     3,XA(2),KCONV,(AD(2,2),REV,B,DGYB(2),CAL,SAL,A1,A2,DH,T1,T2,T3,T4,BALL
     4,DET,NUM,XA(40),XA(40),ITPASS,REVX(40),REVZ(40),BALL
     5,CAGFD(2),BINGD(2),AREA(2),VEL(2),SUPAG(2),BDrag,DSDrag(2,4),BALL
     6,FP1DA1,FP1DA2,FP1DME,BALL
     7,J=JPASS,BALL
     8,ICNT=ICNT+1,BALL
     9,DO 1 K=1,2,BALL
     10,T(1)=AA(K)*PX(K)*FSAVE(K)/CSP(K),BALL
     11,B2R1=COS(P(2)-A(1)),BALL
     12,IF(ICNT-3)2,3,3,BALL
     13,IF(LLOOP14,4,5,BALL
     14,LC1=1,BALL
     15,IC=1,BALL
     16,NUM=1,BALL
     17,RFTRDN,BALL
     18,IF(IC=1)6,6,7,BALL
     19,IF(T0(2)*B2R1-T0(1))8,8,9,BALL
     20,IC1=2,BALL
     21,DO T0 10,BALL
     22,IC1=1,BALL
     23,DO T0 10,BALL
     24,IF(T0(1)*B2R1-T0(2))11,11,12,BALL
     25,IC1=1,BALL
     26,DO T0 10,BALL
     27,IC1=2,BALL
     28,IF((IC1-IC1)3,5,13,BALL
     29,IC=IC1,BALL
     30,NUM=1,BALL
     31,RETURN,BALL

```

```

5.    CTL(J)=10
      NM=0
      DELA(2,1)=SB(2)
      DELA(2,2)=CP(2)
      RA(2,1)=CA(2)*Z2/(A2-X(2))
      RA(2,2)=-(A1-X(1))*(C2(2)/(A2-X(2)))*Z2
      GA(2,1)=-D*PA(2,1)*SB(2)/E2
      GA(2,2)=-D*RA(2,2)*SR(2)/E2
      DO 14 K=1,2
      DALA=(Y1*Y2*PA(1,C,K))-Y3*(-Z2*Y3*CA(1,C,K)+C(1)*GA(1,C,K))+Y4
      DALA=Y1*Y2*RA(1,C,K)-Y3*(-Z2*Y3*RA(1,C,K)+C(1)*GA(1,C,K))+Y4
      Z1=CG(1)*SBAL(2)*(RA(2,K)-DALA)
      Z2=GC(2)*SBAL(1)*(RA(1,K)-DALA)
      DMPA=Y5*(DN*(-GG(1)*GA(2,K)+GG(2)*GA(1,K))-GG(1)*GG(2)*(-Z1+CRAL(BALL 740
      12)*GA(1,K)-Z2-CRAL(1)*GA(2,K)))
      DMPA=(DN*(PPM(1)*(-Z1+CRAL(2)*GA(1,K))-PPM(2)*(Z2+CRAL(1)*GA(2,K)))BALL 760
      11)-Y6*(-Z1+CRAL(1)*GA(1,K)-Z2-CRAL(1)*GA(2,K))/DN*Z2
      DC LA=Y4*SS*E2*DMPA*DMPA
      DC YA(K)=XIN*((PEVP*DMPA+DMPA*REV*B*DMPA+CAL*DMPA) BALL 790
      DO 15 L=1,2
15.   PA(L,K)=1.5*SC(L)*DEFL(L,K)+DEL(L)*SORT(DEFL(L))*DXDG(L)*GA(L,K) BALL 810
      DPSIA(1)=T1*PA(1,K)-T2*PA(2,K)+PA(1,K)*SR(1)-PA(2,K)*SR(2)-Y7*DGYABALL 820
      1(K)
      DPSIA(2)=-T3*PA(1,K)+T4*PA(2,K)+PA(1,K)*CR(1)-PA(2,K)*CR(2)+Y8* BALL 840
      DGYA(K)=DCA
      XA(1)=-DPSIA(1)*DPSIX(2,2)+DPSIA(2)*DPSIX(1,2))/DET BALL 860
      XA(2)=(-DPSIA(2)*DPSIX(1,1)+DPSIA(1)*DPSIX(2,1))/DET BALL 870
      AA(2,K)=PA(2,K)+DR(2,1)*XA(1)+DR(2,2)*XA(2) BALL 880
      DELA(2,K)=DELA(2,K)+DDELX(2,1)*XA(1)+DDELX(2,2)*XA(2) BALL 890
      PA(2,K)=1.5*SC(2)*DELA(2,K)+DEI(2)*SDET(DEL(2))*DXDG(2)*(GA(2,K)+BALL 900
      1)DG(2,1)*XA(1)+DG(2,2)*XA(2)) BALL 910
14.   DGYA(K)=DGYA(K)+DGYR(1)*XA(1)+DGYR(2)*XA(2) BALL 920
      XF_1(1)=XF_1(1)+T4 BALL 930
      XF_1(3)=XF_1(3)+T2*CPH BALL 940
      DO 16 K=1,2
      Y1=PA(2,1)*PA(1,K)+PA(2,2)*DA(2,K)
      Y2=PA(2,1)*PA(1,K)+PA(2,2)*DA(2,K) BALL 960
      Y3=DGYA(1)*CAL(1,K)+DGYA(2)*DA(2,K) BALL 970
      Y4=T2*Y1+Y2*SR(2)-H2(1C)*Y3*CB(2)/D2. BALL 990
      Y5=-T4*Y1+Y2*CP(2)+H2(1C)*Y3*SR(2)/D2. BALL 1000
      DTW(1,K)=DTW(1,K)+Y6
16.   DTW(2,K)=DTW(2,K)+Y5*DPA
      RETHEN
      END

```

```

SUBROUTINE FRCTN (G1,G2,G3,FCDF,THE1A)          FRCT  10
 014E510N AG1(13),AG2(7),AG3(7),FTN(13,7,7),U7(7,7),V7(7),VTN(677)FRCT  20
 01MENSI0N A1(13),A2(13),A3(13),A4(13),A5(13),A6(13),A7(13),A8(13),FRCT  30
 1A9(13),A10(13),A11(13),A12(13),A13(13),A14(13),A15(13),A16(13),      FRCT  40
 2A17(13),A18(13),A19(13),A20(13),A21(13),A22(13),A23(13),A24(13),      FRCT  50
 3A25(13),A26(13),A27(13),A28(13),A29(13),A30(13),A31(13),A32(13),      FRCT  60
 4A23(13),A34(13),A35(13),A36(13),A37(13),A38(13),A39(13),A40(13),      FRCT  70
 5A41(13),A42(13),A43(13),A44(13),A45(13),A46(13),A47(13),A48(13),      FRCT  80
 6A49(13)                                FRCT  90
  EQUIVALENCE (VTN(1),FTN(1,1,1))           FRCT 100
  EQJIVALENCE (VTN(1),A1(1)),(VTN(14),A2(1)),(VTN(27),A3(1)),           FPCT 110
 1(VTN(40),A4(1)),(VTN(53),A5(1)),(VTN(66),A6(1)),(VTN(79),A7(1)),           FRCT 120
 2(VTN(92),A8(1)),(VTN(105),A9(1)),(VTN(118),A10(1)),(VTN(131),A11(1)FRCT 130
 3), (VTN(144),A12(1)),(VTN(157),A13(1)),(VTN(170),A14(1)),(VTN(183)FRCT 140
 4,A15(1)),(VTN(196),A16(1)),(VTN(209),A17(1)),(VTN(222),A18(1)),           FRCT 150
 5(VTN(235),A19(1)),(VTN(248),A20(1)),(VTN(261),A21(1)),(VTN(274),           FRCT 160
 6A22(1)),(VTN(287),A23(1)),(VTN(300),A24(1)),(VTN(313),A25(1)),           FRCT 170
 7(VTN(326),A26(1)),(VTN(339),A27(1)),(VTN(352),A28(1)),(VTN(365),           FRCT 180
 8A29(1)),(VTN(378),A30(1)),(VTN(391),A31(1)),(VTN(404),A32(1)),           FRCT 190
 9(VTN(417),A33(1)),(VTN(430),A34(1)),(VTN(443),A35(1)),(VTN(456),           FRCT 200
 1A35(1)),(VTN(469),A37(1)),(VTN(482),A38(1)),(VTN(495),A39(1)),           FRCT 210
 2(VTN(504),A40(1)),(VTN(521),A41(1)),(VTN(534),A42(1)),(VTN(547),           FRCT 220
 3A43(1)),(VTN(560),A44(1)),(VTN(573),A45(1)),(VTN(586),A46(1)),(VTNFRCT 230
 4(599),A47(1)),(VTN(612),A48(1)),(VTN(625),A49(1))                         FRCT 240
  DATA A1 / 0.0025, 0.0007, 0.0014, 0.0023, 0.0067,           FRCT 250
 1 0.0125, 0.021, 0.037, 0.046, 0.052, 0.0615, 0.0695, 0.0775/           FRCT 260
  DATA A2 / 0.0007, 0.002, 0.0039, 0.0065, 0.0150,           FRCT 270
 1 0.022, 0.022, 0.042, 0.0495, 0.054, 0.0625, 0.069, 0.0775/           FRCT 280
  DATA A3 / 0.0026, 0.0079, 0.014, 0.018, 0.028,           FRCT 290
 1 0.034, 0.038, 0.0485, 0.054, 0.059, 0.064, 0.0695, 0.0775/           FRCT 300
  DATA A4 / 0.0077, 0.017, 0.023, 0.027, 0.035,           FRCT 310
 1 0.04, 0.044, 0.051, 0.0545, 0.0605, 0.064, 0.071, 0.0775/           FRCT 320
  DATA A5 / 0.019, 0.0285, 0.034, 0.037, 0.044, 0.048,           FRCT 330
 1 0.05, 0.054, 0.06, 0.0635, 0.069, 0.0725, 0.0775/           FRCT 340
  DATA A6 / 0.0215, 0.032, 0.037, 0.0415, 0.0475,           FRCT 350
 1 0.051, 0.054, 0.06, 0.0635, 0.066, 0.07, 0.073, 0.0775/           FRCT 360
  - DATA A7 / 0.0245, 0.034, 0.04, 0.0435, 0.05,           FRCT 370
 1 0.054, 0.0565, 0.062, 0.0655, 0.0675, 0.071, 0.074, 0.0775/           FRCT 380
  DATA A8 / 0.0002, 0.0006, 0.0, 0.002, 0.004, 0.012,           FRCT 390
 1 0.019, 0.036, 0.047, 0.054, 0.0645, 0.0, 0.077/           FRCT 400
  DATA A9 / 0.0006, 0.002, 0.0, 0.0065, 0.015, 0.024,           FRCT 410
 1 0.028, 0.043, 0.052, 0.0575, 0.0645, 0.072, 0.077/           FRCT 420
  DATA A10 / 0.0027, 0.0061, 0.014, 0.019, 0.0285,           FRCT 430
 1 0.035, 0.0395, 0.051, 0.057, 0.061, 0.064, 0.0725, 0.077/           FRCT 440
  DATA A11 / 0.0066, 0.015, 0.021, 0.025, 0.034, 0.04,           FRCT 450
 1 0.0465, 0.054, 0.06, 0.064, 0.069, 0.073, 0.077/           FRCT 460
  DATA A12 / 0.012, 0.0225, 0.029, 0.0345, 0.043,           FRCT 470
 1 0.049, 0.052, 0.059, 0.062, 0.066, 0.070, 0.073, 0.077/           FRCT 480
  - DATA A13 / 0.019, 0.032, 0.039, 0.0415, 0.05, 0.054,           FRCT 490
 1 0.056, 0.061, 0.064, 0.067, 0.0715, 0.075, 0.077/           FRCT 500
  DATA A14 / 0.021, 0.0335, 0.041, 0.0455, 0.053,           FRCT 510
 1 0.056, 0.052, 0.064, 0.068, 0.07, 0.073, 0.076, 0.077/           FRCT 520
  DATA A15 / 0.0016, 0.0055, 0.0011, 0.0019, 0.0059, 0.011,           FRCT 530
 1 0.018, 0.033, 0.042, 0.048, 0.06, 0.068, 0.075/           FRCT 540
  DATA A16 / 0.007, 0.0021, 0.0043, 0.007, 0.015, 0.023,           FRCT 550
 1 0.027, 0.039, 0.046, 0.052, 0.062, 0.07, 0.075/           FRCT 560
  DATA A17 / 0.0018, 0.0053, 0.01, 0.015, 0.0255,           FRCT 570
 1 0.034, 0.037, 0.049, 0.054, 0.058, 0.066, 0.073, 0.075/           FRCT 580
  DATA A18 / 0.0046, 0.011, 0.018, 0.024, 0.037,           FRCT 590

```

0 0.039, 0.044, 0.0525, 0.057, 0.061, 0.068, 0.074, 0.075/	FRCT 500
DATA A19 / 0.0082, 0.017, 0.025, 0.03, 0.042,	FRCT 610
10.049, 0.052, 0.06, 0.064, 0.066, 0.075, 0.074, 0.075/	FRCT 620
DATA A20 / 0.015, 0.026, 0.034, 0.04, 0.049,	FRCT 630
1 0.054, 0.058, 0.063, 0.067, 0.069, 0.073, 0.075, 0.075/	FRCT 640
DATA A21 / 0.019, 0.028, 0.035, 0.043, 0.052,	FRCT 650
1 0.057, 0.06, 0.065, 0.065, 0.07, 0.074, 0.075, 0.075/	FRCT 660
DATA A22 / 0.0015, 0.0046, 0.001, 0.0017, 0.0025, 0.01,	FRCT 670
1 0.016, 0.034, 0.04, 0.046, 0.059, 0.067, 0.073/	FRCT 680
DATA A23 / 0.0064, 0.002, 0.0039, 0.0044, 0.015,	FRCT 690
1 0.021, 0.026, 0.032, 0.046, 0.052, 0.062, 0.068, 0.073/	FRCT 700
DATA A24 / 0.0017, 0.0048, 0.009, 0.014, 0.025,	FRCT 710
1 0.031, 0.036, 0.047, 0.053, 0.057, 0.065, 0.0695, 0.073/	FRCT 720
DATA A25 / 0.0141, 0.01, 0.017, 0.023, 0.033,	FRCT 730
1 0.049, 0.043, 0.052, 0.059, 0.061, 0.066, 0.07, 0.073/	FRCT 740
DATA A26 / 0.0079, 0.015, 0.024, 0.024, 0.04,	FRCT 750
1 0.046, 0.051, 0.057, 0.062, 0.064, 0.068, 0.071, 0.073/	FRCT 760
DATA A27 / 0.0145, 0.024, 0.033, 0.039, 0.049,	FRCT 770
1 0.053, 0.056, 0.062, 0.066, 0.067, 0.077, 0.072, 0.073/	FRCT 780
DATA A28 / 0.016, 0.027, 0.0355, 0.041, 0.052,	FRCT 790
1 0.056, 0.059, 0.064, 0.067, 0.069, 0.071, 0.073, 0.073/	FRCT 800
DATA A29 / 0.001, 0.0027, 0.0055, 0.0009, 0.0029,	FRCT 810
1 0.0059, 0.01, 0.025, 0.036, 0.043, 0.054, 0.062, 0.068/	FRCT 820
DATA A30 / 0.0044, 0.0013, 0.0026, 0.0044, 0.012,	FRCT 830
1 0.013, 0.024, 0.034, 0.044, 0.049, 0.057, 0.063, 0.068/	FRCT 840
DATA A31 / 0.001, 0.0029, 0.0056, 0.009, 0.0195,	FRCT 850
1 0.0255, 0.03, 0.042, 0.0485, 0.053, 0.06, 0.064, 0.068/	FRCT 860
DATA A32 / 0.0019, 0.0045, 0.0095, 0.013, 0.024,	FRCT 870
1 0.032, 0.036, 0.047, 0.053, 0.057, 0.063, 0.065, 0.069/	FRCT 880
DATA A33 / 0.0034, 0.0041, 0.0155, 0.021, 0.032,	FRCT 890
1 0.038, 0.042, 0.052, 0.056, 0.06, 0.064, 0.068/	FRCT 900
DATA A34 / 0.0044, 0.017, 0.0245, 0.03, 0.04,	FRCT 910
1 0.0445, 0.041, 0.058, 0.061, 0.063, 0.066, 0.067, 0.068/	FRCT 920
DATA A35 / 0.012, 0.022, 0.0295, 0.035, 0.0455,	FRCT 930
1 0.051, 0.055, 0.061, 0.063, 0.065, 0.067, 0.068, 0.069/	FRCT 940
DATA A36 / 0.0005, 0.0014, 0.0027, 0.0045, 0.014,	FRCT 950
1 0.0027, 0.0046, 0.013, 0.023, 0.028, 0.042, 0.052, 0.055/	FRCT 960
DATA A37 / 0.001, 0.0042, 0.0085, 0.014, 0.024,	FRCT 970
1 0.0084, 0.013, 0.0245, 0.032, 0.037, 0.0455, 0.053, 0.055/	FRCT 980
DATA A38 / 0.004, 0.012, 0.0074, 0.004, 0.011,	FRCT 990
1 0.017, 0.023, 0.0345, 0.037, 0.0425, 0.049, 0.0535, 0.055/	FRCT1000
DATA A39 / 0.0015, 0.0042, 0.004, 0.012, 0.023,	FRCT1010
1 0.029, 0.033, 0.0395, 0.043, 0.045, 0.052, 0.0535, 0.055/	FRCT1020
DATA A40 / 0.0034, 0.0044, 0.014, 0.019, 0.03,	FRCT1030
1 0.036, 0.04, 0.046, 0.048, 0.049, 0.051, 0.054, 0.055/	FRCT1040
DATA A41 / 0.0056, 0.013, 0.02, 0.027, 0.0375,	FRCT1050
1 0.042, 0.045, 0.049, 0.05, 0.052, 0.055, 0.056, 0.057/	FRCT1060
DATA A42 / 0.0071, 0.015, 0.023, 0.03, 0.04,	FRCT1070
1 0.045, 0.048, 0.051, 0.052, 0.053, 0.054, 0.055, 0.055/	FRCT1090
DATA A43 / 0.0003, 0.0009, 0.0014, 0.001, 0.009,	FRCT1090
1 0.0019, 0.003, 0.006, 0.016, 0.023, 0.037, 0.045, 0.051/	FRCT1100
DATA A44 / 0.001, 0.0026, 0.0054, 0.009, 0.029,	FRCT1110
1 0.0057, 0.0092, 0.021, 0.029, 0.034, 0.041, 0.047, 0.051/	FRCT1120
DATA A45 / 0.0025, 0.0074, 0.015, 0.024, 0.032,	FRCT1130
1 0.013, 0.019, 0.028, 0.035, 0.039, 0.046, 0.048, 0.051/	FRCT1140
DATA A46 / 0.0056, 0.0016, 0.0033, 0.0052, 0.014,	FRCT1150
1 0.022, 0.0265, 0.033, 0.04, 0.042, 0.0465, 0.047, 0.051/	FRCT1150
DATA A47 / 0.013, 0.0236, 0.0069, 0.011, 0.021,	FRCT1170
1 0.029, 0.0325, 0.0395, 0.044, 0.047, 0.0495, 0.059, 0.061/	FRCT1180

```

2478 A49      /0.0015, 0.041, 0.009, 0.012, 0.0235,      FRCT1190
1 0.0295, 0.033, 0.04, 0.044, 0.0465, 0.049, 0.0505, 0.051/      FRCT1200
DATA A49      /0.0018, 0.0052, 0.0096, 0.014, 0.0255,      FRCT1210
1 0.031, 0.035, 0.042, 0.045, 0.047, 0.05, 0.051, 0.051/      FRCT1220
DATA AG1      /1.E-8, 3.E-8, 6.E-8, 1.E-7, 3.E-7, 6.E-7,      FRCT1230
1 1.E-6, 3.E-6, 6.E-6, 1.E-5, 3.E-5, 1.E-4, 1.E-3/      FRCT1240
DATA AG2      /-15.E-7, 1.E-6, 5.E-6, 1.E-5, 5.E-5, 1.E-4, 1.E-3FRCT1250
1 /
DATA AG3      /13.32, 15.2, 17.8, 19., 21.19, 27.13, 100./      FRCT1260
IF(G1,F0.0,) GO TO 240      FRCT1270
IF(G2,E0.0,) GO TO 240      FRCT1280
GO TO 100 I=1,7      FRCT1290
GO TO 100 J=1,7      FRCT1300
IF(AG1=AG1(13)) GO TO 240      FRCT1310
40 IF(G1.LT.AG1(1)) GO TO 70      FRCT1320
CALL TLUG(G1,UZ(1,J),AG1,FTN(1,I,J),13)      FRCT1330
GO TO 100      FRCT1340
60 UZ(1,J)=FTN(1,I,J)      FRCT1350
GO TO 100      FRCT1360
70 UZ(1,J)=EXP(ALOG(FTN(1,I,J))+ALOG(FTN(2,I,J))-ALOG(FTN(1,I,J)))/IFRCT1380
1 ALOG(AG1(2))-ALOG(AG1(1)) * (ALOG(G1)-ALOG(AG1(1)))      FRCT1390
100 CONTINUE      FRCT1400
GO TO 200 K=1,7      FRCT1410
IF(G3-AG3(7)) 140,160,160      FRCT1420
140 IF(G3.LT.AG3(1)) GO TO 170      FRCT1430
CALL TLUG(G3,VZ(K),AG3,UZ(1,K),1,7)      FRCT1440
GO TO 200      FRCT1450
160 VZ(K)=UZ(7,K)      FRCT1460
GO TO 200      FRCT1470
170 VZ(K)=UZ(1,K)-(UZ(2,K)-UZ(1,K))/(AG3(2)-AG3(1))*(AG3(1)-G3)      FRCT1480
1F (VZ(K).LE.0.0) VZ(K)=1.E-5      FRCT1490
200 CONTINUE      FRCT1500
IF(G2-AG2(7)) 204,206,206      FRCT1510
204 IF(G2.LT.AG2(1)) GO TO 207      FRCT1520
CALL TLUG(G2,FR3,AG2,VZ,7)      FRCT1530
GO TO 210      FRCT1540
206 FR3=EXP(ALOG(VZ(6))+ALOG(VZ(7))-ALOG(VZ(6)))/ALOG(AG2(7))-ALOG(IFRCT1550
1G2(6))-ALOG(AG2(1))-ALOG(AG2(6)))      FRCT1560
GO TO 210      FRCT1570
227 FR3=EXP(ALOG(VZ(2))+ALOG(VZ(1))-ALOG(VZ(2)))/(ALOG(AG2(1))-ALOG(IFRCT1580
1G2(2))-ALOG(AG2(1))-ALOG(AG2(2)))      FRCT1590
219 FCDE=ALOG(IFP3)-0.149*(ALOG(IFH)-1)-ALOG(30.1)      FRCT1600
FCDE=EXP(IFCD)      FRCT1610
GO TO 250      FRCT1620
240 FCDE=0.      FRCT1630
250 CONTINUE      FRCT1640
RE TURN      FRCT1650
END      FRCT1660

```

```

SUBROUTINE TLU(A,B,C,D,N)
DIMENSION C(1),D(1)
IF(N-111,2,3
1 N=0.
GO TO 100
2 N=0(1)
GO TO 100
3 ML=1
MU=N
8 IF(MU-ML-1) 15,15,9
9 MU=(MU+ML)/2
1F(C(1)-C(2))11,2,10
10 IF(C(M)-A)13,12,14
11 IF(A-C(M))13,12,14
12 N=0(M)
GO TO 100
13 MU=M
GO TO 8
14 ML=M
GO TO 8
15 N=D(ML)+(C(MU)-D(ML))*((A-C(ML))/((C(MU)-C(ML)))
100 RETURN
END

```

TLUR	10
TLUR	20
TLUR	30
TLUR	40
TLUR	50
TLUR	60
TLUR	70
TLUR	80
TLUR	90
TLUR	100
TLUR	110
TLUR	120
TLUR	130
TLUR	140
TLUR	150
TLUR	160
TLUR	170
TLUR	180
TLUR	190
TLUR	200
TLUR	210
TLUR	220
TLUR	230

```

SUBROUTINE TLUG(A,B,C,D,N)
DIMENSION C(1),D(1)
IF(N-111,2,3
1 B=0.
GO TO 100
2 B=0(1)
GO TO 100
3 ML=1
MU=N
8 IF(MU-ML-1) 15,15,9
9 MU=(MU+ML)/2
1F(C(1)-C(2))11,2,10
10 IF(C(M)-A)13,12,14
11 IF(A-C(M))13,12,14
12 N=0(M)
GO TO 100
13 MU=M
GO TO 8
14 ML=M
GO TO 8
15 N=EXP(ALOG(D(ML))+ALOG(D(MU))-ALOG(D(ML)))*((ALOG(A)-ALOG(C(ML)))/
1/(ALOG(C(MU))-ALOG(C(ML)))))1
100 RETURN
END

```

TLUG	10
TLUG	20
TLUG	30
TLUG	40
TLUG	50
TLUG	60
TLUG	70
TLUG	80
TLUG	90
TLUG	100
TLUG	110
TLUG	120
TLUG	130
TLUG	140
TLUG	150
TLUG	160
TLUG	170
TLUG	180
TLUG	190
TLUG	200
TLUG	210
TLUG	220
TLUG	230
TLUG	240

APPENDIX II  
FORMAT FOR BALL BEARING COMPUTER INPUT INFORMATION

CARD	COL.	ITEM
NO.	NO.	
1	1-10	NUMBER OF BALLS
	11-20	BALL DIAMETER - IN.
	21-30	PITCH DIAMETER - IN.
	31-40	CONTACT ANGLF - DEG.
	41-50	OUTER RACE CURVATURE FACTOR.
	51-60	INNER RACE CURVATURE FACTOR.
	61-70	CHANGE IN INTERNAL CLEARANCE (+ IF INCREASED)
	71-80	DIAMETER OF CYLINDRICAL CAGE POCKET - IN.
2	1-10	YOUNG'S MODULUS FOR CAGE - PSI.
	11-20	POISSON'S RATIO FOR CAGE.
	21-30	YOUNG'S MODULUS FOR BALLS - PSI. IF BLANK PROGRAM ASSUMES 29000000.
	31-40	POISSON'S RATIO FOR BALLS. IF BLANK PROGRAM ASSUMES .25.
	41-50	YOUNG'S MODULUS FOR RINGS. - PSI. IF BLANK PROGRAM ASSUMES 29000000.
	51-60	POISSON'S RATIO FOR RINGS. IF BLANK PROGRAM ASSUMES .25.
	61-70	BALL MATERIAL DENSITY - LB/IN**3
	71-80	COEFFICIENT OF SLIDING FRICTION OF BALL IN POCKET.
3	1-10	COEFFICIENT OF SLIDING FRICTION OF CAGE ON PILOTING SURFACE.
	11-20	WIDTH OF CAGE - IN.
	21-30	I. D. OF CAGE - IN.
	31-40	I. D. OF CAGE - IN.
	41-50	I. D. OF OUTER RING - IN.
	51-60	D. D. OF INNER RING - IN.
	61-80	LEAVE BLANK
4	1-10	PRESSURE-VISCOSITY COEFFICIENT OF THE LUBRICANT - IN**2/LB.
	11-20	TEMPERATURE-VISCOSITY COEFFICIENT OF LUBRICANT - 1/F DEG.
	21-30	VISCOSITY OF LUBRICANT - LB-SFC/IN**2.
	31-40	INLET TEMPERATURE - F DEG.
	41-50	THERMAL CONDUCTIVITY OF LUBRICANT - BTU/F DEG - HR - FT.
	51-60	DENSITY OF LUBRICANT - LB*SEC**2/IN**4
	61-70	PROPORTIONATE INCREMENT FOR THE VELOCITY OF THE RACE IN THE Y DIRECTION. SET TO .05 IF LEFT BLANK
	71-80	PROPORTIONATE INCREMENT FOR THE VELOCITY OF THE BALL IN THE X DIRECTION. SET TO .05 IF LEFT BLANK
5	1-10	PROPORTIONATE INCREMENT FOR ANGULAR VELOCITY OF SPIN.
	11-20	SET TO .1 IF LEFT BLANK
	21-30	PROPORTIONATE INCREMENT FOR CONTACT LOAD. SET TO .05 IF BLANK
	31-40	TOLERANCE ON X(1) BALL CENTER COORDINATE. IF BLANK PROGRAM ASSUMES 1.E-6
	41-50	TOLERANCE ON X(2) BALL CENTER COORDINATE. IF BLANK PROGRAM ASSUMES 1.E-6.
	51-60	TOLERANCE ON BALL'S ANGULAR VELOCITY ABOUT X. IF BLANK PROGRAM ASSUMES 10 RPM.
	61-70	TOLERANCE ON BALL'S ANGULAR VELOCITY ABOUT Y. IF BLANK PROGRAM ASSUMES 1 RPM.
		TOLERANCE ON BALL'S ANGULAR VELOCITY ABOUT Z. IF BLANK

PROGRAM ASSUMES 5 RPM.

71-80 TOLERANCE ON DEFLECTION ALONG X - IN. IF BLANK PROGRAM ASSUMES  
1.E-6

6 1-10 TOLERANCE ON DEFLECTION ALONG Y - IN. IF BLANK PROGRAM ASSUMES  
1.E-6

11-20 TOLERANCE ON DEFLECTION ALONG Z - IN. IF BLANK PROGRAM ASSUMES  
1.E-6

21-30 TOLERANCE ON ANGULAR VELOCITY OF CAGE - RPM. IF BLANK  
PROGRAM ASSUMES .5 RPM

31-80 LEAVE BLANK

7 1-10 RPM OF OUTER RING.

11-20 RPM OF INNER RING.

21-30 THRUST LOAD - LB.

31-40 RADIAL LOAD - LB.

41-50 MISALIGNMENT ABOUT Y - IN/IN.

51-60 ESTIMATE OF DEFLECTION ALONG X - IN.

61-70 ESTIMATE OF DEFLECTION ALONG Z - IN.

71-80 PUNCH 2. IF REARING WHEN RUNNING WITH BOUNDARY LUBRICATION  
COULD BE EXPECTED TO HAVE 'INNER-RACE CONTROL'. IF BLANK  
PROGRAM ASSUMES THAT 'OUTER-RACE CONTROL' WOULD EXIST.

NOTES

TO RUN ADDITIONAL LOAD CASES WITH THE SAME SYSTEM REPEAT  
CARD NO. 7 FOR EACH NEW LOAD CASE

TO RUN NEW LUBRICANT PROPERTIES WITH SAME BEARING PLACE ONE  
BLANK AFTER LAST CARD NO. 7 AND READ IN NEW CARD NO. 4  
FT SEQ.

TO READ NEW REARING SYSTEM PLACE TWO BLANKS AFTER LAST CARD  
NO. 7 AND READ IN CARD NO. 1 ET SEQ.

APPENDIX III  
TYPICAL BALL BEARING PROBLEM FOR COMPUTER PROGRAM

BEARING DESIGN DATA		RACE-CURVATURES		CLEARANCE		TYPE OF POCKET		PILOT		CAGE	
NUMBER	ELEMENT	DIA.	CONTACT	ANGLE	DIA.	INNER	INCREMENT	PILOT	CLEARANCE	OUTER	WIDTH
ELEMENTS	DIAMETER	5.1500E-01	5.1500E-01	5.1500E-01	5.1500E-01	5.1500E-01	1.5000E-03	1.5000E-03	2.9000E-02	3.1000E-02	7.1600E-01
2.4222E-01	5.1100E-01	5.1724E-01	5.1724E-01	5.1724E-01	5.1724E-01	5.1724E-01					
1.2121E-01	5.0724E-01	5.1332E-01	5.1332E-01	5.1332E-01	5.1332E-01	5.1332E-01					
0.9121E-01	5.0344E-01	5.0950E-01	5.0950E-01	5.0950E-01	5.0950E-01	5.0950E-01					
0.6121E-01	5.0000E-01	5.0615E-01	5.0615E-01	5.0615E-01	5.0615E-01	5.0615E-01					
0.3121E-01	4.9656E-01	5.0271E-01	5.0271E-01	5.0271E-01	5.0271E-01	5.0271E-01					
0.0121E-01	4.9312E-01	5.0886E-01	5.0886E-01	5.0886E-01	5.0886E-01	5.0886E-01					
-0.3121E-01	4.8968E-01	5.0501E-01	5.0501E-01	5.0501E-01	5.0501E-01	5.0501E-01					
-0.6121E-01	4.8624E-01	5.0116E-01	5.0116E-01	5.0116E-01	5.0116E-01	5.0116E-01					
-0.9121E-01	4.8280E-01	5.0731E-01	5.0731E-01	5.0731E-01	5.0731E-01	5.0731E-01					
-1.2121E-01	4.7936E-01	5.1346E-01	5.1346E-01	5.1346E-01	5.1346E-01	5.1346E-01					
-1.5121E-01	4.7592E-01	5.1961E-01	5.1961E-01	5.1961E-01	5.1961E-01	5.1961E-01					
-1.8121E-01	4.7248E-01	5.2576E-01	5.2576E-01	5.2576E-01	5.2576E-01	5.2576E-01					
-2.1121E-01	4.6904E-01	5.3191E-01	5.3191E-01	5.3191E-01	5.3191E-01	5.3191E-01					
-2.4121E-01	4.6560E-01	5.3806E-01	5.3806E-01	5.3806E-01	5.3806E-01	5.3806E-01					
-2.7121E-01	4.6216E-01	5.4421E-01	5.4421E-01	5.4421E-01	5.4421E-01	5.4421E-01					
-3.0121E-01	4.5872E-01	5.5036E-01	5.5036E-01	5.5036E-01	5.5036E-01	5.5036E-01					
-3.3121E-01	4.5528E-01	5.5651E-01	5.5651E-01	5.5651E-01	5.5651E-01	5.5651E-01					
-3.6121E-01	4.5184E-01	5.6266E-01	5.6266E-01	5.6266E-01	5.6266E-01	5.6266E-01					
-3.9121E-01	4.4840E-01	5.6881E-01	5.6881E-01	5.6881E-01	5.6881E-01	5.6881E-01					
-4.2121E-01	4.4496E-01	5.7496E-01	5.7496E-01	5.7496E-01	5.7496E-01	5.7496E-01					
-4.5121E-01	4.4152E-01	5.8111E-01	5.8111E-01	5.8111E-01	5.8111E-01	5.8111E-01					
-4.8121E-01	4.3808E-01	5.8726E-01	5.8726E-01	5.8726E-01	5.8726E-01	5.8726E-01					
-5.1121E-01	4.3464E-01	5.9341E-01	5.9341E-01	5.9341E-01	5.9341E-01	5.9341E-01					
-5.4121E-01	4.3120E-01	5.9956E-01	5.9956E-01	5.9956E-01	5.9956E-01	5.9956E-01					
-5.7121E-01	4.2776E-01	6.0571E-01	6.0571E-01	6.0571E-01	6.0571E-01	6.0571E-01					
-6.0121E-01	4.2432E-01	6.1186E-01	6.1186E-01	6.1186E-01	6.1186E-01	6.1186E-01					
-6.3121E-01	4.2088E-01	6.1801E-01	6.1801E-01	6.1801E-01	6.1801E-01	6.1801E-01					
-6.6121E-01	4.1744E-01	6.2416E-01	6.2416E-01	6.2416E-01	6.2416E-01	6.2416E-01					
-6.9121E-01	4.1400E-01	6.3031E-01	6.3031E-01	6.3031E-01	6.3031E-01	6.3031E-01					
-7.2121E-01	4.1056E-01	6.3646E-01	6.3646E-01	6.3646E-01	6.3646E-01	6.3646E-01					
-7.5121E-01	4.0712E-01	6.4261E-01	6.4261E-01	6.4261E-01	6.4261E-01	6.4261E-01					
-7.8121E-01	4.0368E-01	6.4876E-01	6.4876E-01	6.4876E-01	6.4876E-01	6.4876E-01					
-8.1121E-01	4.0024E-01	6.5491E-01	6.5491E-01	6.5491E-01	6.5491E-01	6.5491E-01					
-8.4121E-01	3.9680E-01	6.6106E-01	6.6106E-01	6.6106E-01	6.6106E-01	6.6106E-01					
-8.7121E-01	3.9336E-01	6.6721E-01	6.6721E-01	6.6721E-01	6.6721E-01	6.6721E-01					
-9.0121E-01	3.8992E-01	6.7336E-01	6.7336E-01	6.7336E-01	6.7336E-01	6.7336E-01					
-9.3121E-01	3.8648E-01	6.7951E-01	6.7951E-01	6.7951E-01	6.7951E-01	6.7951E-01					
-9.6121E-01	3.8304E-01	6.8566E-01	6.8566E-01	6.8566E-01	6.8566E-01	6.8566E-01					
-9.9121E-01	3.7960E-01	6.9181E-01	6.9181E-01	6.9181E-01	6.9181E-01	6.9181E-01					
-1.0212E-01	3.7616E-01	6.9796E-01	6.9796E-01	6.9796E-01	6.9796E-01	6.9796E-01					
-1.0512E-01	3.7272E-01	7.0411E-01	7.0411E-01	7.0411E-01	7.0411E-01	7.0411E-01					
-1.0812E-01	3.6928E-01	7.1026E-01	7.1026E-01	7.1026E-01	7.1026E-01	7.1026E-01					
-1.1112E-01	3.6584E-01	7.1641E-01	7.1641E-01	7.1641E-01	7.1641E-01	7.1641E-01					
-1.1412E-01	3.6240E-01	7.2256E-01	7.2256E-01	7.2256E-01	7.2256E-01	7.2256E-01					
-1.1712E-01	3.5896E-01	7.2871E-01	7.2871E-01	7.2871E-01	7.2871E-01	7.2871E-01					
-1.2012E-01	3.5552E-01	7.3486E-01	7.3486E-01	7.3486E-01	7.3486E-01	7.3486E-01					
-1.2312E-01	3.5208E-01	7.4101E-01	7.4101E-01	7.4101E-01	7.4101E-01	7.4101E-01					
-1.2612E-01	3.4864E-01	7.4716E-01	7.4716E-01	7.4716E-01	7.4716E-01	7.4716E-01					
-1.2912E-01	3.4520E-01	7.5331E-01	7.5331E-01	7.5331E-01	7.5331E-01	7.5331E-01					
-1.3212E-01	3.4176E-01	7.5946E-01	7.5946E-01	7.5946E-01	7.5946E-01	7.5946E-01					
-1.3512E-01	3.3832E-01	7.6561E-01	7.6561E-01	7.6561E-01	7.6561E-01	7.6561E-01					
-1.3812E-01	3.3488E-01	7.7176E-01	7.7176E-01	7.7176E-01	7.7176E-01	7.7176E-01					
-1.4112E-01	3.3144E-01	7.7791E-01	7.7791E-01	7.7791E-01	7.7791E-01	7.7791E-01					
-1.4412E-01	3.2800E-01	7.8406E-01	7.8406E-01	7.8406E-01	7.8406E-01	7.8406E-01					
-1.4712E-01	3.2456E-01	7.9021E-01	7.9021E-01	7.9021E-01	7.9021E-01	7.9021E-01					
-1.5012E-01	3.2112E-01	7.9636E-01	7.9636E-01	7.9636E-01	7.9636E-01	7.9636E-01					
-1.5312E-01	3.1768E-01	8.0251E-01	8.0251E-01	8.0251E-01	8.0251E-01	8.0251E-01					
-1.5612E-01	3.1424E-01	8.0866E-01	8.0866E-01	8.0866E-01	8.0866E-01	8.0866E-01					
-1.5912E-01	3.1080E-01	8.1481E-01	8.1481E-01	8.1481E-01	8.1481E-01	8.1481E-01					
-1.6212E-01	3.0736E-01	8.2096E-01	8.2096E-01	8.2096E-01	8.2096E-01	8.2096E-01					
-1.6512E-01	3.0392E-01	8.2711E-01	8.2711E-01	8.2711E-01	8.2711E-01	8.2711E-01					
-1.6812E-01	3.0048E-01	8.3326E-01	8.3326E-01	8.3326E-01	8.3326E-01	8.3326E-01					
-1.7112E-01	2.9704E-01	8.3941E-01	8.3941E-01	8.3941E-01	8.3941E-01	8.3941E-01					
-1.7412E-01	2.9360E-01	8.4556E-01	8.4556E-01	8.4556E-01	8.4556E-01	8.4556E-01					
-1.7712E-01	2.9016E-01	8.5171E-01	8.5171E-01	8.5171E-01	8.5171E-01	8.5171E-01					
-1.8012E-01	2.8672E-01	8.5786E-01	8.5786E-01	8.5786E-01	8.5786E-01	8.5786E-01					
-1.8312E-01	2.8328E-01	8.6401E-01	8.6401E-01	8.6401E-01	8.6401E-01	8.6401E-01					
-1.8612E-01	2.7984E-01	8.7016E-01	8.7016E-01	8.7016E-01	8.7016E-01	8.7016E-01					
-1.8912E-01	2.7640E-01	8.7631E-01	8.7631E-01	8.7631E-01	8.7631E-01	8.7631E-01					
-1.9212E-01	2.7296E-01	8.8246E-01	8.8246E-01	8.8246E-01	8.8246E-01	8.8246E-01					
-1.9512E-01	2.6952E-01	8.8861E-01	8.8861E-01	8.8861E-01	8.8861E-01	8.8861E-01					
-1.9812E-01	2.6608E-01	8.9476E-01	8.9476E-01	8.9476E-01	8.9476E-01	8.9476E-01					
-2.0112E-01	2.6264E-01	9.0091E-01	9.0091E-01	9.0091E-01	9.0091E-01	9.0091E-01					
-2.0412E-01	2.5920E-01	9.0706E-01	9.0706E-01	9.0706E-01	9.0706E-01	9.0706E-01					
-2.0712E-01	2.5576E-01	9.1321E-01	9.1321E-01	9.1321E-01	9.1321E-01	9.1321E-01					
-2.1012E-01	2.5232E-01	9.1936E-01	9.1936E-01	9.1936E-01	9.1936E-01	9.1936E-01					
-2.1312E-01	2.4888E-01	9.2551E-01	9.2551E-01	9.2551E-01	9.2551E-01	9.2551E-01					
-2.1612E-01	2.4544E-01	9.3166E-01	9.3166E-01	9.3166E-01	9.3166E-01	9.3166E-01					
-2.1912E-01	2.4199E-01	9.3781E-01	9.3781E-01	9.3781E-01	9.3781E-01	9.3781E-01					
-2.2212E-01	2.3855E-01	9.4396E-01	9.4396E-01	9.4396E-01	9.4396E-01	9.4396E-01					
-2.2512E-01	2.3511E-01	9.5011E-01	9.5011E-01	9.5011E-01	9.5011E-01	9.5011E-01					
-2.2812E-01	2.3167E-01	9.5626E-01	9.5626E-01	9.5626E-01	9.5626E-01	9.5626E-01					
-2.3112E-01	2.2823E-01	9.6241E-01	9.6241E-01	9.6241E-01	9.6241E-01	9.6241E-01					
-2.3412E-01											



ELEMENT #0.	SPINNING VELOCITY JUTER WANER	SPINNING VELOCITY INNER	SPINNING FILM THICKNESS
1	-5.3744E-03 -3.7123E-04	8.9645E-05	8.5180E-05
2	-5.5199E-03 -3.7371E-04	8.9345E-05	8.5063E-05
3	-5.42250E-03 -3.4694E-04	8.9135E-05	8.4723E-05
4	-4.9501E-03 -3.4934E-04	8.8923E-05	8.4124E-05
5	-4.9398E-03 -3.2811E-04	8.8393E-05	8.3357E-05
6	-3.7359E-03 -3.0695E-04	8.7692E-05	8.2129E-05
7	-3.1068E-03 -2.7979E-04	8.6985E-05	8.1170E-05
8	-2.6574E-03 -2.5196E-04	8.6012E-05	7.9923E-05
9	-2.6292E-03 -2.3617E-04	8.5135E-05	7.8777E-05
10	-2.3746E-03 -2.2175E-04	8.4410E-05	7.7802E-05
11	-2.3229E-03 -2.1227E-04	8.3915E-05	7.7303E-05
12	-2.3195E-03 -2.0616E-04	8.3744E-05	7.7126E-05
13	-1.3328E-03 -2.1525E-04	8.3974E-05	7.7347E-05
14	-1.5249E-03 -2.1513E-05	7.4413E-05	7.7473E-05
15	-1.59330E-03 -2.3411E-04	8.5218E-05	7.8899E-05
16	-2.2355E-03 -2.5861E-04	8.6104E-05	8.0065E-05
17	-3.1765E-03 -2.8238E-04	8.6952E-05	8.1301E-05
18	-3.4779E-03 -3.0212E-04	8.7721E-05	8.2453E-05
19	-4.5855E-03 -3.3067E-04	8.8400E-05	8.3436E-05
20	-4.9982E-03 -3.5292E-04	8.8867E-05	8.4203E-05
21	-5.3204E-03 -3.6162E-04	8.9181E-05	8.4771E-05
22	-5.5171E-03 -3.7474E-04	8.9369E-05	8.5084E-05

## 8A-L/POCKET CONTACT DATA

ELEMENT #0.	POCKET DRAE	PRESSURE ELLIPTIC	SLIDING VELOCITY	MIN. FILM
	LENGTH	WIDTH	RADIAL AXIAL	THICKNESS
1	8.3896E-01	1.4521E-02	2.5331E-03	-1.9702E-03 -4.5297E-02 3.1167E-01
2	8.3320E-01	1.4694E-02	2.5529E-03	-1.9689E-03 -4.5661E-02 2.9720E-01
3	9.6533E-01	1.6930E-02	2.5990E-03	-1.7656E-03 -4.6627E-02 2.6603E-01
4	9.3844E-01	1.7215E-02	2.5394E-03	-1.9501E-03 -4.8071E-02 2.41034E-01
5	9.3520E-01	1.6935E-02	2.5998E-03	-1.9523E-03 -4.9945E-02 2.6193E-01
6	7.3291E-01	1.5767E-02	2.4222E-03	-1.9426E-03 -5.1795E-02 3.9853E-01
7	3.9144E-01	1.5137E-02	1.5703E-03	-1.7321E-03 -5.3782E-02 1.35541E-02
8	9.733E-02	7.9194E-03	1.2249E-03	-1.9220E-03 -5.5642E-02 1.55509E-02
9	-6.8858E-01	1.5175E-02	2.3779E-03	-1.9134E-03 -5.7222E-02 4.3527E-03
10	-1.2811E-03	1.9019E-02	2.9179E-03	-1.9071E-03 -5.8629E-02 1.2507E-03
11	-1.7026E-00	2.0222E-02	3.2080E-03	-1.9033E-03 -5.9180E-02 1.0526E-03
12	-1.9402E-00	2.1442E-02	3.7922E-03	-1.9023E-03 -5.9331E-02 6.3337E-04
13	-1.5569E-00	2.0755E-02	3.1974E-03	-1.9036E-03 -5.9123E-02 7.6056E-04
14	-1.2270E-00	1.8579E-02	2.8762E-03	-1.9076E-03 -5.8327E-02 1.35641E-03
15	-6.6858E-01	1.4914E-02	2.2567E-03	-1.9142E-03 -5.7074E-02 5.2707E-03
16	-3.8503E-02	5.9164E-03	9.0719E-04	-1.9230E-03 -5.5454E-02 1.45500E-02
17	4.3841E-01	1.3105E-02	2.0438E-03	-1.9333E-03 -5.3544E-02 1.3975E-02
18	7.5940E-01	1.5576E-02	2.4506E-03	-1.9437E-03 -5.1601E-02 1.3707E-03
19	9.1719E-01	1.7024E-02	2.6101E-03	-1.9533E-03 -5.5500E-02 2.5596E-03
20	9.4733E-01	1.7008E-02	2.4386E-03	-1.9408E-03 -5.7902E-02 2.4117E-03
21	9.3039E-01	1.6921E-02	2.5965E-03	-1.9666E-03 -5.6486E-02 2.6832E-03
22	8.55560E-01	1.6633E-02	2.5504E-03	-1.9692E-03 -4.5575E-02 2.6902E-03

VISCOSUS DRAG LAW B&amp;L = 3.1553E-00

VISCOSUS COUPLINGS NORMAL  
TORQUE TAUUE D<sub>0</sub>  
-2.4491E-01 -3.9156E-01 1.41963E-01

APPENDIX IV  
ROLLER BEARING COMPUTER PROGRAM FORTRAN SOURCE DECK

```

COMMON ALPHA,AL3,     BETA,      (12),CAGED1(2),CAGEW,CAGEW1,CLCAGE(200009700
X1,CCRVFR,CP,CZ,CP1,CZ1,          D,DPDP,DENS,DENLUB,DFL1,DEL(2),    00008300
-- XDFDEL(2),DFYWX(2),DFPDH12J,DFZDH12J,DFPWX12J,DFZWX12J,    00008900
XF,FL,FD,      FLAT,FLATO2,FK,FBARV,FD,FC,FY(2),FP(2),FZ(2),FY11,  00009000
XFY12,FP11,FP12,FZ11,FZ12,FLIM,FFY(3),      GAG,GAGE,G1T,G2T,  00009100
XMF,HMH,HP(2),HMN1,HMN2,HMN(2),HMRC(2),    ISYS,ILOAD,ILUB,ISIGN,  00009200
X'QUIT,   JPASS,   KPLT,KPASS,      NUM,NUMY,      OMEDCR,  00009300
XOMEgae,CMFL1,CMEGAK,CMX1,OMEX,      PD,POCKET,PILOT,POCLR,  00009400
XPX(21,PP1(9),      RADIUS,PINGD1(2),RINGYM,ROLLYM,  00009500
XPINGPR,ROLLPR,RMH,PPM(2),ROT,RFV,R(9),      STR,STS(9)  00009600
COMMON TOL,TOL(4),TOTL02,TI,THETA,TURQ,TORK,    VHMN,VIS,VEINC, 00009700
XVIS3,VY(2),VI(3),VSS,V(2),      XMUL,XMASS,XTM,XTREM,XN,  00009800
XYF,YNUM,YINC(2,50)      00009900
COMMON CPH,CAGECF,      XFZ,DELTA,DRAG,      FY1(2,50),FP1(2,500010000
X1,FZ1(2,50),FLIM(2,50),      HQR,M1(2,50),      ITER,      NOLOAD,  00010100
XCMFGX(50),      P1(2,50),PPP(9,2,50),PN,PXOUT,      RR(9,2,50),  00010200
XSTS1(2,50),SPH,      VERT,VY1(2,50),      XFZ,XTPM(2,50)  00010300
COMMON /CHEL/IV      00010400
DIMENSION WORD(2)      00010500
DATA WORD(1),WORD(2)/6H OUT,6H IN /
ISYS=0      00010600
C(1)=1,      00010700
C(2)=-1,      00010800
GO TO 5,      00010900
6 WRITE(6,650)
5 READ(5,10)XN,D,E,TOTL,FLAT,CORNER,RADIUS,DROP      00011000
IF(XN=.EQ.0.)STOP      00011100
10 FORMAT(14E12.2)
      NUM=XN      00011200
      ILOAD=0      00011300
      TURQ=0      00011400
      ISYS=ISYS+1      00011500
      GA=D/E      00011600
      PREAD(5,10)GAGF,PD,RINGD1(1),RINGD1(2),CAGED1(1),CAGED1(2),POCKET,
1 CAGEDW,RINGYM,ROLLYM,RINGPR,ROLLPR,      XMUL,CAGEW1,DENS,YNUM,(TOL(K00011900
21,K=1,4),      00011700
2 IF(DENS,FQ,0.,DENS=.283      00011800
3 IF(TOL(1),FQ,0.,ITOL(1)=.000001      00011900
4 IF(TOL(2),FQ,0.,ITOL(2)=.0000005      00012000
5 IF(TOL(3),FQ,0.,ITOL(3)=1.      00012100
6 IF(TOL(4),FQ,0.,ITOL(4)=1.      00012200
7 TOL(3)=TOL(3)*.1047198      00012300
8 TOL(4)=TOL(4)*.1047198      00012400
9 IF(XMUL,FQ,0.,XMUL=-1.      00012500
10 IF(YNUM,FE,0.,YNUM=5.      00012600
11 NMNY=YNUM      00012700
12 CALL      RCALC(TOTL,FLAT,GAGE,RADIUS,DROP)      00012800
13 XN = NO. OF ROLLS      00012900
14 D = ROLL dia. - IN      00013000
15 E = PITCH dia. - IN      00013100
16 TOTL = TOTAL LENGTH OF ROLL - IN      00013200
17 FLAT = LENGTH OF FLAT PORTION OF ROLL - IN      00013300
18 CORNER = CORNER PARTUS OF ROLL - IN      00013400
19 RADIUS = CROWN RADIUS - IN      00013500
20 DROP = DROP OF ROLL CROWN - IN      00013600
21 GAGE = DISTANCE FROM END OF ROLL TO CROWN DROP REFERENCE POINT      00013700
22 - IN      00013800
23 D0 = DIAMETRAL CLEARANCE - IN (+ IF BEARING IS LOOSE)      00013900
24 RINGD1(1) = I.D. OF OUTER RING - IN      00014000
25 RINGD1(2) = O.D. OF INNER RING - IN      00014100
26 CAGED1(1) = O.D. OF GAGE - IN      00014200
27 CAGED1(2) = I.D. OF GAGE - IN      00014300
28 POCKET = POCKET LENGTH IN ROLLING DIRECTION - IN      00014400
29      00014500
30      00014600
31      00014700

```

C CAGEW = WIDTH OF CAGE - IN 00014800  
 C RINGYM = YOUNG'S MODULUS FOR RINGS - PSI 00014900  
 C ROLLYM = YOUNG'S MODULUS FOR ROLLS - PSI 00015000  
 C PENNSP = POISSON'S RATIO FOR RINGS 00015100  
 C POLLPR = POISSON'S RATIO FOR ROLLS 00015200  
 C CAGEWY = WEIGHT OF CAGE - LB 00015300  
 C XMUL = COEFFICIENT OF COUPLING FRICTION FOR PILOT SURFACES 00015400  
 C FLATP= .5\*FLAT 00015500  
 C TOTLDP=.5\*TOTL-CORNER 00015600  
 C RPH=SQRT(RADIUS\*\*2-FLATP\*\*2) 00015700  
 C READ (1,20)  
 20 FORMAT(1H1,79H  
 1 /X,79H 00016000  
 2 ) 00016100  
 WRITE(16,20)  
 WRITE(16,3C)1SYS 00016200  
 37 FORMAT(13H0 DESIGN DATA FOR BEARING NO. ,13) 00016300  
 WRITE(16,40) 00016400  
 40 FORMAT(13H0 NO. OF ROLL PITCH TOTAL FL00016600  
 1 AT CROWN CROWN GAGE DIAMETRAL I.D. OF 00016700  
 2 O.D. OF 1/32H ROLLERS DIAMETER DIAMETER LENGTH 00016800  
 3 LENGTH PDP RADIUS POINT CLEARANCE OUTER RING 000016900  
 4 NG INNER RING) 00017000  
 WRITE(6,50)XN,D,F,TOTL,FLAT,DROP,RADIUS,GAGE,P0,RINGDI(1),RINGD(1) 200017100  
 11 00017200  
 .50 FORMAT(1P1E12.4) 00017300  
 WRITE(6,30)  
 62 FORMAT(128H0 O.D. OF I.D. OF TYPE OF CAGE/RING CLEARA 00017500  
 INCE POCKET CAGE YOUNG'S MODULUS POISSON 00017600  
 2S RAYD/129H CAGE CAGE PILOT OUTER IN00017700  
 3MFR CLEARANCE WIDTH PINGS ROLLS RINGS 00017800  
 9 ROLLSI 00017900  
 PILOT=1, 00018000  
 - IF(ABS(RINGDI(2)-CAGEDI(2)).LT. ABS(RINGDI(1))-CAGEDI(1))PILOT=2. 00018100  
 KPLT=PILOT 00018200  
 CLCAGE(1)=ABS(RINGDI(1))-CAGEDI(1) 00018300  
 CLCAGE(2)=ABS(RINGDI(2))-CAGEDI(2) 00018400  
 WRD=WRD(KPLT) 00018500  
 PCCCLR=POCKET-D 00018600  
 IF(RINGYM.EQ.C.)PINGYM=29.E6 00018700  
 IF(ROLLYM.EQ.0.)ROLLYM=29.E6 00018800  
 IF(RINGPR.EQ.0.)PINGPR=.25 00018900  
 IF(ROLLPR.EQ.0.)PCLIPR=.25 00019000  
 FL=.636198E11-RINGPR\*\*21/RINGYM\*\*11-ROLLPR\*\*21/ROLLYM) 00019100  
 WRITE(6,70)CAGEDI(1),CAGEDI(2),WRD,CLCAGE(1),CLCAGE(2),PCCCLR,CAGE 00019200  
 1W,RINGYM,ROLLYM,RINGPR,ROLLPR 00019300  
 70 FORMAT(1P2E12.4,3X,4E,3X,1P8F12.4) 00019400  
 WRITE(6,75) 00019500  
 75 FORMAT(16H0 FRICTION MATERIAL CORNER CAGE/46H C0F00019600  
 1E DENSITY RADIUS WEIGHT) 00019700  
 WRITE(6,30) XMUL,DENS,CCRNER,CAGEWY 00019800  
 XMASS=D\*\*2\*TOTL\*DENS/491.9797 00019900  
 80 READ(5,10)ALPHA,BETA,VIS,T1,FK,DEMFLUB  
 IF(ALPHA.LE.Q1)GO TO 6 00020000  
 ILUR=ILUR+1 00020200  
 C ALPHA = PRESSURE-VISCOSITY COEFFICIENT - IN\*\*2/LB 00020300  
 C BETA = TEMPERATURE-VISCOSITY COEFFICIENT - 1/(DEG F) 00020400  
 C VIS = VISCOSITY AT INLET TEMPERATURE - LB\*SEC/IN\*\*2 00020500  
 C T1 = INLET TEMPERATURE - DEG F 00020600  
 C FK = THERMAL CONDUCTIVITY - BTU/(DEG F)/HR/FT 00020700  
 C DEMFLUB = LUBRICANT DENSITY - LB SEC\*\*2/IN\*\*4 00020800  
 READ(5,30) 00020900  
 90 FORMAT(1H0,79H 00021000  
 11 20021100

```

      WRITE(6,81)
101 FORMAT(1H /1H /1H /1H /1H /1H /23H0  LUBRICANT PROPERTIES) 00021200
      WRITE(6,90)
      WRITE(6,82)ALPHA
      82 FORMAT(40H0  PRESSURE-VISCOSITY COEFFICIENT ,1PIE11.4) 00021600
      WRITE(6,83)BETA
      83 FORMAT(40H0  TEMPERATURE-VISCOSITY COEFFICIENT ,1PIE11.4) 00021800
      WRITE(6,84)VIS
      84 FORMAT(40H0  VISCOSITY AT INLET TEMPERATURE ,1PIF11.4) 00022000
      WRITE(6,85)TI
      85 FORMAT(40H0  INLET TEMPERATURE ,1PIE11.4) 00022200
      WRITE(6,86)FR
      86 FORMAT(40H0  THERMAL CONDUCTIVITY ,1PIE11.4) 00022400
      WRITE(6,87)DENLUB
      87 FORMAT(40H0  LUBRICANT DENSITY ,1PIE11.4) 00022600
115 READ(5,101)RPM11,BPML21,FBARV,ROT,OMEDCR,VELINC,HF
      IF((RPM11.EQ.0.0).AND.(RPM121.EQ.0.0))GO TO 80
      ILOAD=ILOAD+1
      WRITE(6,120)ILLOAD,TSYS

120 FORMAT(26H1  INPUT DATA FOR LOAD NO.,13,13H, BEARING NO.,13/34H0 00023100
      1RPM. OF RPM. OF RADIAL/33H CUTER INNER LO00023200
      2401
      IF(VELINC.EQ.0.0),1,VEIMC=.0025
      C
      IF(HF.EQ.0.0),1,HFE=.00001
      C
      WRITE(6,90)RPM11,RPM121,FRARY
      WRITE(6,7551)
7351 FORMAT(1X)
      WRITE(6,7550)OMEDCR
      7350 FORMAT(1X,17HPERCENT CAGE SLIP,1PIE15.4) 00024100
      RPM11=RPM11*.1047198
      RPM121=RPM121*.1047198
      OMEGAE=.5*(RPM11*(1.+GAM)+RPM121*(1.-GAM))+11.-OMEDCR) 00024300
      IF(OMEDCR.EQ.0.0),1,OMEDCR=.1*OMEGAE
      OMEGAE=OMEGAE
      OMEGAE=OMEGAE-OMEDCR
      151ON=1
      REV=0.
      IF(ROT)121,123,121
121 RRV=ROT*.1047198 00024900
      WRITE(6,122)RCT
      122 FORMAT(16H0  LOAD ROTATES AT,1PIE11.4,4H RPM) 00025100
      GO TO 125
      123 WRITE(6,124)
124 FORMAT(21H0  LOAD IS STATIONARY) 00025400
125 EP=2.7/(1.0-RINGPR**2)/RNGYM+11.0-KOLLPR**2)/ROLLYM) 00025500
      THE TA=TI-32.0/1.8 00025600
      VIS3=VIS*EXP(BETA*(TI-86.0)) 00025700
      EL3=ALPHA*930.0*ALPHA*(TI-86.0)/(546.0*(TI+460.0)) 00025800
      GIT=VIS3*(ALPHA/A13)**0.6*(VIS/VIS3)**0.7 00026000
      G2T=VIS3*BETA/(1.728*FK) 00026100
      MMH=1.58*ALPHA**0.6*VIS**0.7*EP**0.03 00026200
      IF(VD.GT.0.0),1,EL2=EL2+.5*PD 00026300
      TI=0 00026400
      TORR=0. 00026500
      TORK=-5.0
      CMF1=CMFGAE
      T26 F0=0. 00026600
      TQUIT=?
      TORG=TORK
      TORK=0.
      ON 130 K=1,2 00027100
      VY(K)=.5*(E+C(K)*D)*(RPM(K)-OMEGAE) 00027200

```

```

130 FD=FD(.25*CLCAGE(K)*TOTL*DEMUB+.25*(RINGDI(K)+CAGEDI(K))*OMEGAEE 00027300
11**2*OMEGAEE/ABS(OMEGAEE) 00027400
FC=XN455+.3*FD*OMEGAEE**2 00027500
IV=0 00027600
CALL NOCON 00027700
IF((IV>132,132,131 00027800
131 WRITF(6,8001) 00027900
8001 FORMAT(1X,30H*HP EXCEEDED 1.0E2 IN NOCON*) 00028000
GO TO 115 00028100
132 DELZ=.005*0 00028200
IF(TOIIIT1140,140,115 00028300
140 DO 240 ITER=1,15 00028400
XFZ=0. 00028500
DXFZ=0. 00028600
NOLOAD=0 00028700
DO 230 J=1,NUM 00028800
JPASS=J 00028900
XJ=J 00029000
PHI=6.283185*(XJ-1.)/N 00029100
CPH=COS(PHI) 00029200
DELTA=DELZ*CPH-.5*PD 00029300
DEL(1)=.55*DELTA 00029400
DEL(2)=DELTA-DEL(1) 00029500
DO 200 IZ=1,15 00029600
IF(DEL(2)<1.E-8)141,141,142 00029700
141 NOLOAD=NOLOAD+1 00029800
P(2,J)=0. 00029900
GO TO 230 00030000
142 DO 190 K=1,2 00030100
JPASS=K 00030200
143 CALL RCLL 00030300
IF(IOW11170,170,150 00030400
150 WRITF(6,160)J,1T,ITER,K 00030500
160 FORMAT(9HOMAIN 145,614) 00030600
GO TO 115 00030700
171 JEPAIN(J)171,171,172 00030800
171 P(2,J)=0. 00030900
NOLOAD=NOLOAD+1 00031000
GO TO 230 00031100
172 DO 180 L=1,NLMY 00031200
PR(L,K,J)=R(L) 00031300
PPP(L,K,J)=PP1(L) 00031400
180 STS1(L,K,J)=STS(L) 00031500
XTRMK(J)=XTRFM 00031600
P(K,J)=PX(K) 00031700
190 CONTINUE 00031800
PS11=-P(1,J)+P(2,J)+FC 00031900
X1=-DFDEL(1)-DFDEL(2) 00032000
X1=PS11/X1 00032100
DEL11=DEL(1)-X1 00032200
DEL(2)=DELTA-DEL(1) 00032300
JF((ABS(X1)-TCL(1))222,200,200. 00032400
201 CONTINUE 00032500
WRITF(6,210)J 00032600
210 FORMAT(9HOMAIN 200,14) 00032700
GO TO 115 00032800
220 DET=-DFDEL(1)-DFDEL(2) 00032900
DPZDEL=-DFDEL(1)/DET 00033000
XFZ=XFZ+P(2,J)*CPH 00033100
DXFZ=DXFZ+CPZDEL*DFDEL(2)*CPH**2 00033200
230 CONTINUE 00033300
X1=IXFZ-FEARV1/DXFZ 00033400
DELZ=DELZ-X1 00033500
JF((ABS(X1)-5.*TCL(1))255,240,240 00033600

```

```

240 CONTINUE          00033700
      WRITE(6,250)X1  00033800
250 FORMAT(9HOMAIN 240,1P1E12.4) 00033900
C GO TO 115          00034000
C 255 OMEGE=OMEGAF
255 TORK=0.          00034200
      TORK=0.          00034300
      HOR=0.          00034400
      VERT=0.          00034500
      DO 310 J=1,NUM   00034600
      IF(P(2,J)LT0,310,255)
2551 XJ=J           00034700
      PHI=6.283185*(XJ-1)/XM  00034800
      SPH=SIN(PHI)       00034900
      CPH=COS(PHI)       00035000
      OMEGAX=(RPM(1)-OMEGAF)*(E+0)/D  00035100
      JPASS=J           00035200
      DO 260 ITA=1,30   00035300
      CPI=CP*ABS(OMEGAX)  00035400
      C71=C2*OMEGAX       00035500
      DO 261 K=1,2       00035600
      WMPAC(K)=0.0       00035700
      RPASC=K           00035800
      DO 260 L=1,NUMY   00035900
      R(L)=RPL(K,J)      00036000
      PPL(L)=PPP(L,K,J)  00036100
260 STS(L)=STS(L,K,J)  00036200
      CALL TPAC          00036300
261 CONTINUE          00036400
      TEMP=FY(1)+FY(2)-FD  00036500
      IH=1               00036600
      IF(TEMP.LT.0.01)IH=2
      HP(1)=HF          00036700
      HP(2)=HF          00036800
      DO 262 ITB=1,30   00036900
      CALL POCFLM(IH)    00037100
      PS1=FP(IH)-APS(TEMP)
      DPS1IH=DFPDH(IH)   00037200
      TEMP1=PS1/DPS1IH   00037300
      HP(IH)=HP(IH)-TEMP1
      IF(HP(1).GT.1.0E21G0 TO 9000  00037400
      IF(HP(2).GT.1.0E21G0 TO 9000  00037500
      GO TO 2650          00037600
9000 WRITE(6,750)
7500 9HAT(1X,21H*HP EXCFEDED 1.0E24)
      YD 115             00037700
2650 A85(T,3P1),LF,YOL(2)IG0 TO 264  00037800
      C038000
2651 CONTINUE          00038100
      WRITE(6,263)J       00038200
263 FORMAT(1X,9HOMAIN 262,13)  00038300
C GO TO 115          00038400
264 PS12=(FY(1)-FY(2)-FZ(IH))*5.0D
      DHDX=DFPWX(IH)/DFPDH(IH)  00038500
      DPS12M=(DFYWX(1)-DFYWX(2))-DFZWX(IH)-DFZDH(IH)*DHDWX)*5.0D
      TEMP=PS12/OPSI2M  00038700
      OMEGAX=OMEGAX-TEMP  00038800
      IF(ABS(TEMP).LE.YOL(3))GO TO 300  00038900
265 CONTINUE          00039100
      WRITE(6,266)J       00039200
266 FORMAT(1X,9HOMAIN 265,1)
C GO TO 115          00039300
300 IF(IH,F0,1)HP(2)=POCLR-HP(1)  00039400
      IF(IH,F0,2)HP(1)=POCLR-HP(12)  00039500
      DO 305 X=1,2       00039600
      FY1(X,1)=FY1(X)  00039700
      FY1(X,2)=FY1(X)  00039800

```

```

-----FP1(K,J)=FP1(K)----- 00039900
-----FZ1(K,J)=FZ1(K)----- 00040000
-----VY1(K,J)=V(K)----- 00040100
-----FL1M(K,J)=HMRAC(K)----- 00040200
-----H1C1=H1C(K)----- 00040300
-----305 CONTINUE----- 00040400
-----OMEGX1(J)=OMEGAX----- 00040500
-----X1=-C(IH)*(FP(IH)*CPH+FZ(IH)*SPH)----- 00040600
-----X2=C(IH)*(FP(IH)*SPH-FZ(IH)*CPH)----- 00040700
-----HOR=HOR+X1----- 00040800
-----VERT=VERT+X2----- 00040900
-----TORK=TORK+C(IH)*(FP(IH)*E+FZ(IH)*POCKET)*.5----- 00041000
-----310 CONTINUE----- 00041100
-----VEL=(RPM(KPLT)-OMEGAE)*RINGDI(KPLT)*.5----- 00041200
-----XMUP=XMU1*VEL/ABS(VEL)----- 00041320
-----Y1=-XMUP*VERT+HCR----- 00041400
-----X2=XMUP*HOR+VERT----- 00041500
-----ANG=ATAN2(X1,X2)----- 00041600
-----CAGECF=CAGED1*BEV**2*SLCAGE1(KPLT)/772.8----- 00041700
-----PN=HOR/(XMUP*COS(ANG)+SIN(ANG))-CAGECF----- 00041800
-----DRAG=0.----- 00041900
-----DO 320 K=1,2----- 00042000
-----AREA=3.141593*RINGDI(K)*CAGED1(KPLT)----- 00042100
-----VEL=(RPM(K)-OMEGAE)*CAGED1(K)*.5----- 00042200
-----320 DRAG=CRAG*.COB=SQRT(SQRT(VIS*ABS(VEL)**2*DENLUB**3/1.5*CAGED1(K)))----- 00042300
-----11*VEL/ABS(VEL)*AREA----- 00042400
-----TORK=TORK+(XPUM*(PN+CAGECF)+DRAG)*CAGED1(KPLT)*.5----- 00042500
-----7900 FORMAT(1X, 9HMATN R0CT,14,1P5E13.5)
-----TOL(1)=.001
-----1F(LARS(TORK)-TEL1511390,390,330
-----330 JFL(TORK1311331,333
-----331 OMEGAE=OMEGAE-OMEDCR
-----GO TO 126
-----335 OMEDCR=OMEDCR/5.0
-----TORK=TORK
-----OMEGAE=OMEGAE-OMEDCR
-----WRITE(6,7500)111,OMEGAE,OME1,OMEDCR,TORK,TORO
-----GO TO 126
-----390 WRITE(6,2000)----- 00043400
-----2000 FORMAT(1H1)
-----WRITF(6,400)11 LOAD, ISYS----- 00043900
-----400 FORMAT(27H OUTPUT DATA FOR LOAD NO.,13,12H BEARING NO.,13)----- 00044000
-----WRITF(6,410)
-----410 FORMAT(6H0) BEARING RPM OF PERCENT TORK CAGE P00044300
-----110101----- 00044400
-----WRITF(6,420)
-----420 FORMAT(6H REACTION CAGE CAGE SLIP ON CAGE NORMAL 00044600
-----110AD)
-----OMEGAE=OMEGAE/.1047158----- 00044800
-----TEMP=(RPM(1)*(1.+GAM)*RPM(2)*(1.-GAM))/.2094396----- 00044900
-----TEMP=(TEMP-OMEGAE)/TEMP*100----- 00045000
-----WRITF(6,430)XFZ,OMEGAE,TEMP,TORK,PN----- 00045100
-----430 FORMAT(1P2E12.4,0P1F9.2,3X,1P2E12.4)----- 00045200
-----WRITF(6,440)
-----440 FORMAT(132F0) INPUT DATA FOR RACE CONTACTS----- 00045500
-----WRITF(6,450)
-----450 FORMAT(115H0 ELEMENT ELEMENT CONTACT LOAD MEAN 00045600
-----10MPRESSIVE STRESS PATTERN EXTREMITY SLIP VELOCITY) 00045700

```

```

      WRITF(6,460)
560  FORMAT(11TH   NUMBER   AZIMUTH   OUTER   INNER   OUT00045900
      1ER     INNER   OUTER   INNER   OUTER   INNER)  00046000
      00 490 J=1,NUM
      IF(P(2,J)=490,490,470
570  XJ=J
      PH1=360.*((J-1)/XN
      SSTS19,2,J)=.7853982*SSTS1(NUMY,2,J)  00046500
      SSTS19,1,J)=.7E*3SA2*SSTS1(NUMY,1,J)  00046600
      WRITF(6,480)J,PH1,P(1,J),P(2,J),SSTS19,1,J),SSTS19,2,J),KTRM1,1,J),00046700
      KTRM1(2,J),VY1(1,J),VY1(2,J)  00046800
580  FORMAT(17,5X,1PF12.4)  00046900
590  CONTINUE
      TF(1NOLOAD1515,515,500  00047100
591  CT1=.7853982*STR  00047200
      WRITF(6,510)PXMT,STR,XTM,VSC  00047300
592  FORMAT(12H _THE REST_ ,12X,1P1E12.4,12X,1P1E12.4,12X,1P1E12.4,12X,00047400
      11P1E12.4)  00047500
593  WRITF(6,520)
594  FORMAT(56HO ELEMENT   MIN. FILM THICKNESS   TRACTIVE FORCE00047700
      11
      WRITF(6,530)
595  FORMAT(57H   NUMBER   OUTER   INNER   OUTER   INNE00048000
      101
      00 550 J=1,NUM
      IF(P(2,J)=550,550,540  00048200
      00048300
596  WRITE(6,480)J,FLIM(1,J),FLIM(2,J),FY1(1,J),FY1(2,J)  00048400
597  CONTINUE
      TF(1NOLOAD1565,565,550  00048600
598  WRITE(6,640)FLIM,YF  00048700
599  WRITE(6,570)
599  FORMAT(34HO _OUTPUT DATA FOR POCKET CONTACTS_
      WRITF(6,580)
599  FORMAT(34HO ELEMENT   RPM OF   NORMAL POCKET LOAD   TANGEN00049100
      11AL POCKET LOAD   MIN. FILM THICKNESS)  00049200
      WRITF(6,590)  00049300
599  FORMAT(92H   NUMBER   ROLLER   FORE   AFT   FOR00049400
      1F     AFT   FORE   AFT)  00049500
      00 610 J=1,NUM
      IF(P(2,J)=610,610,600  00049600
      00049700
600  CMEGY(J)=CMEGX(J)/.2047198  00049800
      WRITE(6,480)J,CMEGX(J),FP1(1,J),FP1(2,J),FZ1(1,J),FZ1(2,J),H1(1,J)00049900
      1,H1(2,J)  00050000
601  CONTINUE
      TF(1NOLOAD1115,115,620  00050100
      00050200
602  DMX1=DMX1/.1047198  00050300
      WRITE(6,630)DMX1,FP11,FP12,FZ11,FZ12,HMN1,HMN2  00050400
603  FORMAT(12H _THE REST_ ,1P8E12.4)  00050500
      DC TO 115  00050600
604  FORMAT(12H _THE REST_ ,1P1E12.4,12X,1P1E12.4)  00050700
605  FORMAT(1H1)
      END  00050800

```

```

-----SUBROUTINE RCALC(TTL,FLAT,GAGE,RADIUS,DROP)----- 00056300
-----DOUBLE PRECISION DRP,RDIUS,FLT,TTL,GAG,A1,A2,DSORT----- 00056400
-----RDIUS=RADIUS----- 00056500
-----DRP=DRP----- 00056600
-----FLT=FLAT----- 00056900
-----TTL=TTL----- 00057000
-----GAG=GAGE----- 00056600
-----IF(RADIUS)>10,10,20----- 00057300
10 A1=1.500*TTL-GAG)**2----- 00057200
A2=(.500*FLT)**2----- 00057300
-----RDIUS=DSORT((A1-A2-DRP**2)/(2.00*DRP))**2+A1----- 00057400
-----RETURM----- 00057500
20 A1=DSORT(RDIUS**2-(.500*FLT)**2)----- 00057600
A2=ESRT(RDIUS**2-(.500*TTL-GAG)**2)----- 00057700
DRP=A1-A2----- 00057800
DROP=DRP----- 00057900
-----RETURK----- 00058000
-----END----- 00058100

```

SUBROUTINE PCELL 00058200  
 $\text{CMMRPN ALPHAS, AL}^2, \text{BETA}, C(?)$ , CAGEDI(2), CAGEW, CAGEWT, CLCAGE(2) 00058300  
 $X1, CCRNFR, CR, CZ, CP1, CZ1, 2, DDPD, DENS, DENLUR, DEL7, DEL(2), 00058400$   
 $XPEDEL(2), DFVWX(2), DFPNH(2), DFPDH(2), DFPWX(2), DFZWX(2), 00058500$   
 $YF, EL, FD, FLAT, FLAT(2), FK, FBARY, FD, FC, FY(2), FP(2), FZ(2), FY11, 00058600$   
 $XFY12, FP11, FP12, FZ12, FL14, FFY(3), GAM, GAGF, GIT, G?T, 00058700$   
 $XH, H4H, HD(2), HMN1, HMN2, HMN(2), HMRAC(2), ISVS, IL0AD, ILUR, ISIGN, 00058800$   
 $X1QUT, IPASS, KPLT, KPASS, NIIM, NUMY, QMENDR, 00058900$   
 $YMEGAF, CMF1, PMEGAX, CMX1, CMEX, PD, POCKET, PTOT, POCCLR, 00059100$   
 $XRX(2), PPI(9), RADIUS, RINGDI(2), RINGYM, ROLLYM, 00059100$   
 $XOTNGPR, PCELLPP, PNM, PFM(2), ROT, REV, R(9), STR, STS(9) 00059200$   
 $COMMON TOTL, TOTL(4), TOTL02, TI, THETA, TORC, TORK, V44IN, VIS, VEINC, 00059300$   
 $XVIS3, VY(2), VINC(2), VSS, V(2), X4U1, XMASS, XTH, XTREM, XN, 00059400$   
 $YVF, YNIUM, YINC(2,50) 00059500$   
 $CMMRPN CPH, CAGFCF, DXEZ, DELTA, DRAG, FY1(2,50), FP1(2,50) 00059600$   
 $X1, FZ1(2,50), FL14(2,50), HTR, H1(2,50), ITER, N0L0AD, 00059700$   
 $XH4GY(50), P(2,50), PDP(9,2,50), PN, PXQUT, RR(9,2,50), 00059800$   
 $XSTSI(2,2,50), SPH, VERT, VY1(2,50), XF7, XTRM(2,50) 00059900$   
 $J=10A55 00060000$   
 $K=KPA55 00060100$   
 $TX(K)=7, 00060200$   
 $DEDEI(K)=7, 00060300$   
 $XTREM=SORT(2,*RADTUS*DEI(K)+FLAT02**2) 00060400$   
 $TF(YDEM-TOTL02)15,15,10 00060500$   
 $11 YDEM=TOTL02 00060600$   
 $15 EFL=XDEM-ELAT02 00060700$   
 $VINC=EEI/(YNIUM-1,) 00060800$   
 $EEI=XTREM 00060900$   
 $YINC(K,J)=YINC 00061000$   
 $YH=YDEM+XTMC 00061100$   
 $CMINC=1, 00061200$   
 $NN RD L=1, NEMY 00061300$   
 $PP1(L)=7, 00061400$   
 $CTC(L)=7, 00061500$   
 $XH=XH-YINC 00061600$   
 $SM=-SMINC 00061700$   
 $TF(L-1)30,20,20 00061800$   
 $27 SM=7, 00061900$   
 $DO TD 40 00062000$   
 $37 TF(L-NUMY140,20,40) 00062100$   
 $47 DELY=EFL(K)+.5*(FLAT02**2-XH**2)/RADTUS 00062200$   
 $TF((DELY-1,E-9),LE,C,0)DO TD 90 00062300$   
 $43 D(L)=.5*D-EFL(K)*DEIX 00062400$   
 $CM=2,*P(L)/E 00062500$   
 $TCMD=F,F7*DEIX**1.111111/EFL**.111111 00062600$   
 $NN 50, IT=1,15 00062700$   
 $TF(TCMD,P0,45) 00062800$   
 $45 A1=SORT(FL*TEMP*D*(1.+C(K)*CM)) 00062900$   
 $A2=1.*RR54+A1*DG(EFL/(2.*A1)) 00063000$   
 $A3=A2*EL*TEND 00063100$   
 $A4=(A3-EFL*X1)/(EL*(A2-.5)) 00063200$   
 $TCMD=TEMP-A4 00063300$   
 $TF(A3-(A2-EFL*X1)-TD)11170,70,50 00063400$   
 $57 CONTINUE 00063500$   
 $40 FORMAT(9HCOLL 57) 00063600$   
 $57 I0J1T=1 00063700$   
 $E 2ET/IDN 00063800$

77	$PX(K) = PX(K) + TFLW * SM$	00767900
	$DEFEL(K) = DEFEL(K) + SM / (FL * (A2 - .5))$	00064000
	$DT(1,1) = TEMP$	02764100
	$STS(1) = 6366199 + TFLW / A1$	00764200
90	CONTINUE	00064300
	$A2 = XINC / 3$	00064400
	$PX(K) = PY(K) * A3 + ? + FLAT * TEMP$	00064500
	$DEFEL(K) = DEFEL(K) * A2 + ? + FLAT / (FL * (A2 - .5))$	00064600
	$OUTPUT = PX(1)$	00064700
	$DT(1,1) =$	00064800
	END	00764900
 C14ROUTINE PFCRN		
	C14MCN ALPHAS, C14Z, PETA, C(2), CACFD(?) , CAGEH, CAGEWT, CLCAGE(1200)	00055020
	Y1, CCEFH, CP, C2, CP1, CZ1, D, D0D0, DENS, DENLU9, DEL1, DEL(2),	00065200
	ZFDFL(2), ZFYWX(2), ZFPDH(2), ZFZDH(2), ZFPWX(2), ZFZX(2),	00065300
	X1, FL, FD, FLAT, FLAT02, FK, FRARY, FD, FC, FY(2), FP(2), FZ(2), FY11,	00065400
	XFY12, FZ1, FD12, FZ11, FZ12, FILM, FZY(2), GAM, GAGE, G1T, G2T,	00065500
	XHF, H4H, HD(2), HVN1, HKN2, HUN(2), HMD3C(2), ISYS, ILGAD, ILU9, ISION,	00065600
	X10117, J0ACC, KDT, KPASS, KUM, NMVY, OMEDCP,	00065700
	XCFGAE, CMF1, CYFCAX, CYMY, CMFX, PD, POCKET, Z1107, ZOCCLR,	00065800
	XZ(2), Z01(4), ZD01(2), ZING01(2), ZINGYM, ZDL1YM,	00065900
	ZDING02, ZD1102, DDM, DDM(2), DDT, DDU, O(2), STR, STS(2)	00066000
	C14MCN TET1, T(1)141, TOT102, T1, TTF11, T730, TORK, VHMN, VIS, VEINC, 00066100	
	XV12, YV121, YV122, YV123, YV124, YM02, XMASS, XTM, XTPFM, YN,	00066200
	YVF, YHN, YINC(2,50)	00066300
	C14MCN CDM, CACFD(2), DXFZ, DFL(2), DPAIG,	00066400
	Y1, FZ1(2,50), FZ14(2,50), HPH, H112, H21, ITED, NT1010,	00066500
	YC14CC(4,2), D(2,50), D2(2,50), D5(2,50), D6, DPH01,	00066600
	XZ07S(2,50), ZC1, ZEM, VERT, VY1(2,50), XF7, XTRM(2,50)	00066700
	ZMM + ZMM(2,4)	00066800
	YDASS(1)	00066900
	YDASS(2)	00067000
	ZF1111-1, ZF220	00067100
	ZF1111-1, ZF220	00067200
	ZF1111-1, ZF220	00067300
	ZF1111-1, ZF220	00067400
	ZF1111-1, ZF220	00067500
	ZF1111-1, ZF220	00067600
	ZF1111-1, ZF220	00067700
	ZF1111-1, ZF220	00067800
1	ZF1111-1, ZF220	00067900
2	ZF1111-1, ZF220	00068000
3	ZF1111-1, ZF220	00068100
	ZF1111-1, ZF220	00068200
	ZF1111-1, ZF220	00068300
4	ZF1111-1, ZF220	00068400
	ZF1111-1, ZF220	00068500
5	ZF1111-1, ZF220	00068600
	ZF1111-1, ZF220	00068700
6	ZF1111-1, ZF220	00068800
	ZF1111-1, ZF220	00068900
	ZF1111-1, ZF220	00069000
	ZF1111-1, ZF220	00069100
	ZF1111-1, ZF220	00069200
	ZF1111-1, ZF220	00069300
	ZF1111-1, ZF220	00069400
	ZF1111-1, ZF220	00069500
	ZF1111-1, ZF220	00069600
	ZF1111-1, ZF220	00069700
	ZF1111-1, ZF220	00069800
	ZF1111-1, ZF220	00069900
	ZF1111-1, ZF220	00069000
	ZF1111-1, ZF220	00069100
	ZF1111-1, ZF220	00069200
	ZF1111-1, ZF220	00069300
	ZF1111-1, ZF220	00069400
	ZF1111-1, ZF220	00069500
	ZF1111-1, ZF220	00069600
	ZF1111-1, ZF220	00069700
	ZF1111-1, ZF220	00069800
	ZF1111-1, ZF220	00069900
	ZF1111-1, ZF220	00069000
	ZF1111-1, ZF220	00069100
	ZF1111-1, ZF220	00069200
	ZF1111-1, ZF220	00069300
	ZF1111-1, ZF220	00069400
	ZF1111-1, ZF220	00069500
	ZF1111-1, ZF220	00069600
	ZF1111-1, ZF220	00069700
	ZF1111-1, ZF220	00069800
	ZF1111-1, ZF220	00069900
	ZF1111-1, ZF220	00069000
	ZF1111-1, ZF220	00069100
	ZF1111-1, ZF220	00069200
	ZF1111-1, ZF220	00069300
	ZF1111-1, ZF220	00069400
	ZF1111-1, ZF220	00069500
	ZF1111-1, ZF220	00069600
	ZF1111-1, ZF220	00069700
	ZF1111-1, ZF220	00069800
	ZF1111-1, ZF220	00069900
	ZF1111-1, ZF220	00069000
	ZF1111-1, ZF220	00069100
	ZF1111-1, ZF220	00069200
	ZF1111-1, ZF220	00069300
	ZF1111-1, ZF220	00069400
	ZF1111-1, ZF220	00069500
	ZF1111-1, ZF220	00069600
	ZF1111-1, ZF220	00069700
	ZF1111-1, ZF220	00069800
	ZF1111-1, ZF220	00069900
	ZF1111-1, ZF220	00069000
	ZF1111-1, ZF220	00069100
	ZF1111-1, ZF220	00069200
	ZF1111-1, ZF220	00069300
	ZF1111-1, ZF220	00069400
	ZF1111-1, ZF220	00069500
	ZF1111-1, ZF220	00069600
	ZF1111-1, ZF220	00069700
	ZF1111-1, ZF220	00069800
	ZF1111-1, ZF220	00069900
	ZF1111-1, ZF220	00069000
	ZF1111-1, ZF220	00069100
	ZF1111-1, ZF220	00069200
	ZF1111-1, ZF220	00069300
	ZF1111-1, ZF220	00069400
	ZF1111-1, ZF220	00069500
	ZF1111-1, ZF220	00069600
	ZF1111-1, ZF220	00069700
	ZF1111-1, ZF220	00069800
	ZF1111-1, ZF220	00069900
	ZF1111-1, ZF220	00069000
	ZF1111-1, ZF220	00069100
	ZF1111-1, ZF220	00069200
	ZF1111-1, ZF220	00069300
	ZF1111-1, ZF220	00069400
	ZF1111-1, ZF220	00069500
	ZF1111-1, ZF220	00069600
	ZF1111-1, ZF220	00069700
	ZF1111-1, ZF220	00069800
	ZF1111-1, ZF220	00069900
	ZF1111-1, ZF220	00069000
	ZF1111-1, ZF220	00069100
	ZF1111-1, ZF220	00069200
	ZF1111-1, ZF220	00069300
	ZF1111-1, ZF220	00069400
	ZF1111-1, ZF220	00069500
	ZF1111-1, ZF220	00069600
	ZF1111-1, ZF220	00069700
	ZF1111-1, ZF220	00069800
	ZF1111-1, ZF220	00069900
	ZF1111-1, ZF220	00069000
	ZF1111-1, ZF220	00069100
	ZF1111-1, ZF220	00069200
	ZF1111-1, ZF220	00069300
	ZF1111-1, ZF220	00069400
	ZF1111-1, ZF220	00069500
	ZF1111-1, ZF220	00069600
	ZF1111-1, ZF220	00069700
	ZF1111-1, ZF220	00069800
	ZF1111-1, ZF220	00069900
	ZF1111-1, ZF220	00069000
	ZF1111-1, ZF220	00069100
	ZF1111-1, ZF220	00069200
	ZF1111-1, ZF220	00069300
	ZF1111-1, ZF220	00069400
	ZF1111-1, ZF220	00069500
	ZF1111-1, ZF220	00069600
	ZF1111-1, ZF220	00069700
	ZF1111-1, ZF220	00069800
	ZF1111-1, ZF220	00069900
	ZF1111-1, ZF220	00069000
	ZF1111-1, ZF220	00069100
	ZF1111-1, ZF220	00069200
	ZF1111-1, ZF220	00069300
	ZF1111-1, ZF220	00069400
	ZF1111-1, ZF220	00069500
	ZF1111-1, ZF220	00069600
	ZF1111-1, ZF220	00069700
	ZF1111-1, ZF220	00069800
	ZF1111-1, ZF220	00069900
	ZF1111-1, ZF220	00069000
	ZF1111-1, ZF220	00069100
	ZF1111-1, ZF220	00069200
	ZF1111-1, ZF220	00069300
	ZF1111-1, ZF220	00069400
	ZF1111-1, ZF220	00069500
	ZF1111-1, ZF220	00069600
	ZF1111-1, ZF220	00069700
	ZF1111-1, ZF220	00069800
	ZF1111-1, ZF220	00069900
	ZF1111-1, ZF220	00069000
	ZF1111-1, ZF220	00069100
	ZF1111-1, ZF220	00069200
	ZF1111-1, ZF220	00069300
	ZF1111-1, ZF220	00069400
	ZF1111-1, ZF220	00069500
	ZF1111-1, ZF220	00069600
	ZF1111-1, ZF220	00069700
	ZF1111-1, ZF220	00069800
	ZF1111-1, ZF220	00069900
	ZF1111-1, ZF220	00069000
	ZF1111-1, ZF220	00069100
	ZF1111-1, ZF220	00069200
	ZF1111-1, ZF220	00069300
	ZF1111-1, ZF220	00069400
	ZF1111-1, ZF220	00069500
	ZF1111-1, ZF220	00069600
	ZF1111-1, ZF220	00069700
	ZF1111-1, ZF220	00069800
	ZF1111-1, ZF220	00069900
	ZF1111-1, ZF220	00069000
	ZF1111-1, ZF220	00069100
	ZF1111-1, ZF220	00069200
	ZF1111-1, ZF220	00069300
	ZF1111-1, ZF220	00069400
	ZF1111-1, ZF220	00069500
	ZF1111-1, ZF220	00069600
	ZF1111-1, ZF220	00069700
	ZF1111-1, ZF220	00069800
	ZF1111-1, ZF220	00069900
	ZF1111-1, ZF220	00069000
	ZF1111-1, ZF220	00069100
	ZF1111-1, ZF220	00069200
	ZF1111-1, ZF220	00069300
	ZF1111-1, ZF220	00069400
	ZF1111-1, ZF220	00069500
	ZF1111-1, ZF220	00069600
	ZF1111-1, ZF220	00069700
	ZF1111-1, ZF220	00069800
	ZF1111-1, ZF220	00069900
	ZF1111-1, ZF220	00069000
	ZF1111-1, ZF220	00069100
	ZF1111-1, ZF220	00069200
	ZF1111-1, ZF220	00069300
	ZF1111-1, ZF220	00069400
	ZF1111-1, ZF220	00069500
	ZF1111-1, ZF220	00069600
	ZF1111-1, ZF220	00069700
	ZF1111-1, ZF220	00069800
	ZF1111-1, ZF220	00069900
	ZF1111-1, ZF220	00069000
	ZF1111-1, ZF220	00069100
	ZF1111-1, ZF220	00069200
	ZF1111-1, ZF220	00069300
	ZF1111-1, ZF220	00069400
	ZF1111-1, ZF220	00069500
	ZF1111-1, ZF220	00069600
	ZF1111-1, ZF220	00069700
	ZF1111-1, ZF220	00069800
	ZF1111-1, ZF220	00069900
	ZF1111-1, ZF220	00069000
	ZF1111-1, ZF220	00069100
	ZF1111-1, ZF220	00069200
	ZF1111-1, ZF220	00069300
	ZF1111-1, ZF220	00069400
	ZF1111-1, ZF220	00069500
	ZF1111-1, ZF220	00069600
	ZF1111-1, ZF220	00069700
	ZF1111-1, ZF220	00069800
	ZF1111-1, ZF220	00069900
	ZF1111-1, ZF220	00069000
	ZF1111-1, ZF220	00069100
	ZF1111-1, ZF220	00069200
	ZF1111-1, ZF220	00069300
	ZF1111-1, ZF220	00069400
	ZF1111-1, ZF220	00069500
	ZF1111-1, ZF220	00069600
	ZF1111-1, ZF220	00069700
	ZF1111-1, ZF220	00069800
	ZF1111-1, ZF220	00069900
	ZF1111-1, ZF220	00069000
	ZF1111-1, ZF220	00069100
	ZF1111-1, ZF220	00069200
	ZF1111-1, ZF220	00069300
	ZF1111-1, ZF220	00069400
	ZF1111-1, ZF220	00069500
	ZF1111-1, ZF220	00069600
	ZF1111-1, ZF220	00069700
	ZF1111-1, ZF220	00069800
	ZF1111-1, ZF220	00069900
	ZF1111-1, ZF220	00069000
	ZF1111-1, ZF220	00069100
	ZF1111-1, ZF220	0

```

*END=FY(11)-5
14=7
UN(2)=HC
23 40 ITAE=1,60
CALL 225FL(11H)
DS(1)=FS(1E)-APS(TEVN)
DS(1)H=FFFFH(1H)
TF(2)=FS(1)/FS(1H)
UN(1H)=FP(1H)-TEN(1)
IF(ABS(TFMP)) .IF. .T. )100 TO 45

67 CONTINUE
45 DS12=FY(1)-F7(1H))*.500
PDWDX=-DPDWX(1H)/DPDWH(1H)
DPST2W=(DPWDX(1)-DFZWX(1H)-DFZDH(1H)*DHWKX)*.500
TEM0=PS12/DO512W
TEM0=.5*FS12/FS12W
DMEGAX=CMEGAX-TEMP
TE(ABS(TFMP)).LF.TOL(3))50 TO 55

50 CONTINUE
55 HP(1)=PPCCIR-HP(2)
FY12=0.
FD11=FP(1)
FP12=FP(2)
F711=F7(1)
F712=F7(2)
XTM=XTPFM
STRSTS(NIMY)
VSS=V(1)
FILM=YHMJN
YF=FY(1)
HMN1=HMN(1)
HMN2=HMN(2)
HMN1=FOCCIR-FMA2
DMX1=CMEGAX
GRETURN
END
00074500

SUBROUTINE PUFFLM(1H)
COMMON ALPHA,AL2, BETA, C(1),CAGE01(2),CAGFW,CAGFWT,CLCACF(200074700
Y1,CCP1,FO,FO1,C2,CPI1,C71, 0,DPD0,PFNS,PFNLUR,PFLZ,PF1(2), 00074900
X*FO1(2),DPYH(2),DPYDH(2),DFZDH(2),DFP4X(2),DFZDX(2), 00074900
YC,FL,FO, FLAT,FLAT2,FK,FR3PV,FO,FC,FY(2),FP121,FZ(2),FY11, 00075000
XFY12,FO11,FO12,F711,F712,FLM,FFY(3), GAM,GAGE,GIT,G2T, 00075100
YF,MMH,MH(2),HMN1,HMN2,HMN(2),HMPC(2), ISYS,IPAD,IPB,IS12H, 00075200
XIMIIT, IPASS, KPLT,KPASS, NJM,NJMY, OMEDCR, 00075300
YMEGAE,CYF1,C*FGAX,CYX1,DMEX, PD,PCKET,PILOT,PPCCIR, 00075400
XOXY12,OP11G, RADIUS,PTNG01(2),PTNG1,PTLY4, 00075500
YVINCD,PTL1PD,PMH,PPM(2),PTT,PTV,P(01, STA,STS191, 00075600
COMMON TOT1,TOL(4),TOTL02,T1,THET1,TDRG,TJOK, VHMN,VIN,VEINC, 00075700
XV1S,VV1(2),YINC(2),VCS,V(2), XH11,XMASS,XTM,XTPFM,VY1, 00075800
XYF,YNUM,YINC(2,50)
COMMON COH,CAGECE, DXEZ,DELTA,DRAG, FY1(2,50),FP1(2,500077600
X1,F711(2,50),FL1M(2,50), HPH,HI(2,50), ITER, NOLNAN, 00076100
Y*REGX(150), F12,FO1,FPH19,2,501,PN,DX011, PR19,2,501, 00076200
XESTS(0,2,50),SPH, VEP1,VY1(2,50), YF1,XTRM(2,501, 00076300
FF1=TCT1C2-F1AT02 00076400

```

7 INC=FF1 /1YRUM-1.)	00076500
TEM01=7INC/2.	00076670
DO 5 K=1,2	00076770
DO (K)=7,	00076800
EZ(K)=0,	00076900
DE00H(K)=0,	00077000
DE04X(K)=0.0	
DE7W(X(K)=0.0	
5 DE70H(K)=0,	00077100
K=1H	00077200
CNTINC=2,	00077300
XH=TDTI 72+7INC	00077400
DO 6C I=1,51 MY	00077500
SM=2,-511AC	00077600
EZ(I)-1120,7C,21	00077700
17 SM=1.	00077800
DO TO 71	00077900
27 E711-N1MY122,10,21	00078000
29 CNTINC=SMINC	00078100
XH=YH-2 INC	00078200
A1=0WH-SCRT(POANTHS*02-XH00*2)	00078300
A1=EX5=(XH00*2-F1ATD2*02)/POANTHS	
HWX=HPK(K)+A1	00078400
EZ(HWY=1-E-H140,40,31	
31 A2=-,6C,-91	00078500
C2=2001+12*02	00078600
EZ(Y-121+12*02*SCPT(A2))	00078700
EZ(L1+SE(Z(K))+SM*CCP1/HPK	00078800
TEM01=CPT(HPK)	00078900
EZ(K)=EZ(K)+SM*CCP1/T1/HD	00079000
DE00H(K)=DE00H(K)-SM*CCP1/HDX*02	00079100
DE04H(K)=DE04H(K)-,5*SM*CCP1/(HDY*TCMD)	00079200
63 CONTINUE	
HMN(X)=HDX	00079300
EP(K)=E,EP(K)+TEM01+CCP1+F1AT/HPK	00079400
EZ(K)=E,EP(X)+TEM01+CCP1+F1AT/T1/HD	00079500
DE00H(K)=E,DE00H(K)+TEM01-CCP1+F1AT/HDX*02	00079600
DE04H(K)=E,DE04H(K)+TEM01-(CZ1+F1AT/(HDY*TCMD))*5	00079700
DE06H(K)=EP(K)/AP(S(CM*GAX))	00079800
57 DEZHY(X)=EZ(K)/CMFGAX	00079900
RETURN	00080000
END	00080100
SIHED/HTHE TDC	20080200
COMM1 ALFA,712, PFTA, (7), CAGF01(7), CAGFW, CAGEW, CLCAGE(2) 20090300	
X1, COOPED, CP, C7, C01, EZ, 0, 0200, DCNS, DEMILUP, DFI, Z, DEL121,	00090400
XZFC01(7), CXYLY(7), DE00H(7), DE10U(7), DEPWY(7), DE74X(7),	00090500
YF, C1, F2, FLAT, FLAT2, FK, FPARV, FD, FF, FY(2), EP(2), EZ(2), FYL,	00090600
XY(2), EP(2), FZ(2), FZ1, FZ1H, FZY(2), G4M, GAGF, GLT, H2T,	00090700
XH, HFK, HD(2), HMA(2), HMN(2), HMPAC(2), ISYS, J1, JAD, J1, JUB, LSIGN,	00090800
XTO-11T, JPASS, KMT, KPASS, NM, NMV, QMFDR,	00090900
YMEGAE, YMEF, CAGFAK, EMV1, QMFX, PD, POCKET, PILOT, POCCLR,	00091000
XRY(2), PDI(9), RADIUS, RINGO(2), RINGYM, RGLEYM,	00091100
XZ1NCPE, OJ110D, PMH, PEM(2), OCT, PEV, P(9), STR, STS(9)	00091200
COMM1 TOT1, 101141, TOTL02, T1, THFTA, TORO, TORK, V4MIN, VIS, VFINC, 00091300	
XVTS2, VY(2), VINC(2), VCS, V(2), XH1, XMASS, XTM, XTRIM, XN,	00091400
XV, YV1M, YINC(2), F01	00091500
COMM1 CPK, CAGECF, FYEZ, PELTA, DRAG, FY112, 501, F0312, 5000081620	
X1, EZ1(2,501), ELT(2,501), FPK, H1(2,501), IFR, NOLNAU,	00091700
Y04EGX(5,1), P(2,501), PDP(9,2,501), PN, PYCUT, PR(2,2,501),	00091800
X5ST51N, 7, S11, CPK, VFRY, VY1(2,501), XE7, XTRM(2,501)	00091900
I-JPASS	00092000
VEKPASS	00092100
??=-1(K)*, F=(F+C(K)*0)	00092200

```

      DFN=2.*VFINC*APS(CMEGAX)          000842300
      DD 80 L=1,3                      00082400
      CMEFX=CMEGAX+VINC(L)*APS(CMEGAX)
      CM(NC)=1                           00082500
      CFV(L)=?.
      DD 70 L=1,NIMY                  00082620
      CM=2.-SMINC                      00082700
      DXP=1./L./D2+1./D(L)
      TFL=1120.10.20                   00083000
      17 CM=1                           00083100
      DD TO 31                         00083200
      21 TF(L-NIMY) 10.10.30          00083300
      21 CMINC=-CMINC                 00083400
      TF(DP(L)-L170,70,70,4)          00083500
      47 VDP1=CMEFX*D(L)*C(K)        00083600
      VS=VV(K)-VDP1                   00083700
      TF(VC151,50,51)
      57 W0(TF(5,53)VV(K),VPC1,VS,CMEFX,2(L),C(K))
      57 FORMAT(1X,4HTRAC,1PF15.4)
      51 VPARP=(VV(K)+VPC1)*.5         00083800
      51 VMAP=APC1/VPARP              00083920
      US=APS(VS)                      00084000
      VHMIN=HHH0(IPB9**.7/PP(L)**.13*RXP**.43 00084100
      G1=G1*T*US/(VHMIN*STC(L))
      G2=G2*US**2                     00084200
      G3=AL*STC(L)                   00084400
      C CALL COFFT(G1,G2,G3,COF,THETA)
      C CALL COFFT(G1,G2,G3,COF,THETA)
      C COF=5.7*SCPT(C1)
      COF=7.5*SCPT(L)
      FFY(1)=FFY(1)+SCPT(L)*COF       00084600
      70 CONTINUE                      00084800
      FFY(1)=2.*FFY(1)+VINC(K,1)/3.+PP1(NIMY)+FLAT02-COET*US/VS 00084900
      91 CONTIME
      FFY(K)=FFY(1)                  00085100
      FFYH(Y(K))=(FFY(2)-FFY(3))/DFN  00085200
      VMRAF(K)=VHMIN                00085300
      V(K)=VS                         00085400
      RETURN                          00085500
      END                            00085600

      SUBROUTINE THIA,B,C,D,N)
      DIMENSIN C(11,21)
      IC(N-1) 1,2,?
      1 D=?
      DD TO 100
      2 B=D(1)
      DD TO 100
      3 M1=1
      K1=A
      9 IF(M1=M1-1) 1E,15,0
      9 K=(M1+M1)/2
      1E(C(1)-C(2)) 1,2,10
      17 IC(M)=B1 12,12,14
      11 IC(A-C(M)) 12,12,14
      12 D=D(M)
      DD TO 100
      13 D=D(M)
      DD TO 4
      14 M=?
      DD TO 9
      15 D=D(M)+IC(M)-C(M)*((A-C(M))/((C(M))-C(M)))
      ??7 DF TO 0
      171

```

```

SUBROUTINE COEFCT(G1,G2,G3,FCOE,THETAI)
DIMENSION AG1(13),AG2(7),AG3(7),FTN(13,7,7),U7(7,7),V2(7),VTN,677)FRCT 2
DIMENSION A1(13),A2(13),A3(13),A4(13),A5(13),A6(13),A7(13),A8(13),FRCT 3
1A9(13),A10(13),A11(13),A12(13),A13(13),A14(13),A15(13),A16(13), FRCT 4
2A17(13),A18(13),A19(13),A20(13),A21(13),A22(13),A23(13),A24(13), FRCT 5
3A25(13),A26(13),A27(13),A28(13),A29(13),A30(13),A31(13),A32(13), FRCT 6
4A33(13),A34(13),A35(13),A36(13),A37(13),A38(13),A39(13),A40(13), FRCT 7
5A41(13),A42(13),A43(13),A44(13),A45(13),A46(13),A47(13),A48(13), FRCT 8
6A49(13) FRCT 9
EQUIVALENCE(VTN(1),FTN(1,1,1))
EQUIVALENCE(VTN(1),A1(1)),(VTN(14),A2(1)),(VTN(27),A3(1)),(VTN(40),A4(1)),(VTN(53),A5(1)),(VTN(66),A6(1)),(VTN(79),A7(1)),(VTN(92),A8(1)),(VTN(105),A9(1)),(VTN(118),A10(1)),(VTN(131),A11(1))FRCT 11
2(VTN(192),A9(1)),(VTN(195),A9(1)),(VTN(164),A12(1)),(VTN(157),A13(1)),(VTN(170),A14(1)),(VTN(193))FRCT 12
3A15(1)),(VTN(156),A16(1)),(VTN(209),A17(1)),(VTN(222),A18(1)),(VTN(235),A19(1)),(VTN(248),A20(1)),(VTN(261),A21(1)),(VTN(274),A22(1)),(VTN(287),A23(1)),(VTN(300),A24(1)),(VTN(313),A25(1)),(VTN(326),A26(1)),(VTN(339),A27(1)),(VTN(352),A28(1)),(VTN(365),A29(1)),(VTN(378),A30(1)),(VTN(391),A31(1)),(VTN(404),A32(1)),(VTN(417),A33(1)),(VTN(430),A34(1)),(VTN(443),A35(1)),(VTN(456),A36(1)),(VTN(469),A37(1)),(VTN(482),A38(1)),(VTN(495),A39(1)),(VTN(508),A40(1)),(VTN(521),A41(1)),(VTN(534),A42(1)),(VTN(547),A43(1)),(VTN(560),A44(1)),(VTN(573),A45(1)),(VTN(586),A46(1)),(VTN(599),A47(1)),(VTN(612),A48(1)),(VTN(625),A49(1))FRCT 13
DATA A1 / 0.0025, 0.0007, 0.0015, 0.0023, 0.0067, FRCT 25
1 0.0135, C.C21, 0.027, 0.046, 0.152, 0.0615, 0.1685, 0.0775/ FRCT 26
DATA A2 / 0.0007, 0.002, 0.0039, 0.0765, 0.0150, FRCT 27
1 0.022, 0.022, 0.042, 0.0495, 0.054, 0.0625, 0.059, C.0775/ FRCT 28
DATA A3 / 0.0026, 0.0078, 0.014, 0.018, 0.028, FRCT 29
1 0.034, 0.0395, 0.0485, 0.054, 0.058, 0.064, 0.0695, 0.0775/ FRCT 30
DATA A4 / 0.0077, 0.017, 0.023, 0.027, 0.035, FRCT 31
1 0.04, 0.044, 0.051, 0.0565, 0.0605, 0.0646, 0.071, 0.0775/ FRCT 32
DATA A5 / 0.019, 0.0285, 0.034, 0.037, 0.044, 0.048, FRCT 33
1 0.05, C.046, 0.05, 0.0675, 0.069, 0.0725, 0.0775/ FRCT 34
DATA A6 / 0.0215, 0.0232, 0.037, 0.0415, 0.0475, FRCT 35
1 0.051, 0.054, 0.06, 0.0635, 0.065, 0.07, 0.073, 0.0775/ FRCT 36
DATA A7 / 0.0245, 0.024, 0.04, 0.0425, 0.05, FRCT 37
1 0.054, C.0565, 0.062, 0.0655, 0.0675, 0.071, 0.074, 0.0775/ FRCT 38
DATA A8 / 0.0002, 0.0015, 0.0012, 0.002, 0.006, 0.012, FRCT 39
1 0.019, C.036, 0.047, 0.054, 0.0645, 0.072, 0.077/ FRCT 40
DATA A9 / 0.0006, 0.0021, 0.004, 0.0065, 0.015, 0.024, FRCT 41
1 0.028, 0.043, 0.052, 0.0575, 0.0585, 0.072, 0.077/ FRCT 42
DATA A10 / 0.0027, 0.0181, 0.014, 0.019, 0.0245, FRCT 43
1 0.035, 0.0395, 0.051, 0.057, 0.061, 0.069, 0.0725, 0.077/ FRCT 44
DATA A11 / 0.0C64, 0.015, 0.021, 0.025, 0.034, 0.04, FRCT 45
1 0.045, 0.054, C.06, 0.064, 0.069, 0.073, 0.077/ FRCT 46
DATA A12 / 0.012, 0.0225, 0.029, 0.0345, 0.043, FRCT 47
1 0.049, C.052, 0.059, 0.063, 0.065, 0.073, 0.077/ FRCT 48
DATA A13 / 0.019, 0.032, 0.039, 0.0415, 0.05, 0.054, FRCT 49
1 0.056, C.061, 0.064, 0.067, 0.0715, 0.075, 0.077/ FRCT 50
DATA A14 / 0.021, 0.0335, 0.041, 0.0455, 0.053, FRCT 51
1 0.056, 0.059, 0.064, 0.068, 0.07, 0.073, 0.076, 0.077/ FRCT 52
DATA A15 / 0.00016, 0.00055, 0.0011, 0.0019, 0.0059, 0.011, FRCT 53
1 0.019, 0.022, 0.042, 0.048, 0.054, 0.068, 0.075/ FRCT 54
DATA A16 / 0.0007, 0.0021, 0.0043, 0.007, 0.015, 0.023, FRCT 55
1 0.027, 0.039, 0.044, 0.052, 0.067, 0.07, 0.075/ FRCT 56
DATA A17 / 0.0018, 0.0053, 0.01, 0.015, 0.0255, FRCT 57
1 0.034, 0.037, 0.049, 0.054, 0.058, 0.066, 0.073, 0.075/ FRCT 58
DATA A18 / 0.0246, 0.011, 0.018, 0.024, 0.037, FRCT 59

```

U	0.020	0.044	0.0525	0.057	0.061	0.068	0.074	0.075/	FRCT	60	
DATA A20	/	0.0082	0.017	0.025	0.031	0.042			FRCT	61	
1	0.048	0.052	0.061	0.066	0.071	0.074	0.075/		FRCT	62	
DATA A20	/	0.015	0.024	0.034	0.04	0.051			FRCT	63	
1	0.044	0.058	0.063	0.067	0.071	0.073	0.075/		FRCT	64	
DATA A21	/	0.015	0.028	0.036	0.043	0.052			FRCT	65	
1	0.057	0.06	0.069	0.071	0.074	0.075	0.075/		FRCT	66	
DATA A22	/	0.0015	0.0016	0.001	0.0017	0.005	0.01		FRCT	67	
1	0.016	0.014	0.014	0.016	0.017	0.017	0.017/		FRCT	68	
DATA A22	/	0.0004	0.0002	0.0019	0.0064	0.015			FRCT	69	
1	0.021	0.026	0.029	0.046	0.05	0.062	0.078	0.073/		FRCT	70
DATA A24	/	0.0017	0.0048	0.009	0.0116	0.025			FRCT	71	
1	0.023	0.026	0.047	0.053	0.057	0.065	0.0695	0.073/		FRCT	72
DATA A25	/	0.043	0.051	0.061	0.071	0.073	0.073		FRCT	73	
1	0.030	0.042	0.052	0.059	0.061	0.066	0.07	0.073/		FRCT	74
DATA A26	/	0.0078	0.016	0.024	0.029	0.04			FRCT	75	
1	0.044	0.045	0.057	0.062	0.066	0.071	0.073/		FRCT	76	
DATA A27	/	0.0145	0.024	0.033	0.039	0.069			FRCT	77	
1	0.052	0.055	0.062	0.066	0.067	0.072	0.073/		FRCT	78	
DATA A28	/	0.016	0.027	0.035	0.041	0.052			FRCT	79	
1	0.056	0.059	0.064	0.067	0.071	0.073	0.073/		FRCT	80	
DATA A29	/	0.001	0.0027	0.0055	0.009	0.029			FRCT	81	
1	0.0250	0.021	0.025	0.036	0.042	0.048			FRCT	82	
DATA A29	/	0.0044	0.014	0.026	0.044	0.072			FRCT	83	
1	0.039	0.024	0.036	0.044	0.049	0.057	0.063	0.068/		FRCT	84
DATA A31	/	0.001	0.0029	0.0255	0.049	0.085			FRCT	85	
1	0.0255	0.02	0.042	0.0495	0.052	0.06	0.064			FRCT	86
DATA A32	/	0.0015	0.0045	0.0095	0.013	0.024			FRCT	87	
1	0.032	0.034	0.047	0.057	0.063	0.069	0.069/		FRCT	88	
DATA A33	/	0.0026	0.0093	0.0155	0.021	0.032			FRCT	89	
1	0.038	0.042	0.052	0.056	0.06	0.064	0.066			FRCT	90
DATA A34	/	0.0008	0.017	0.0245	0.033	0.04			FRCT	91	
1	0.0445	0.045	0.058	0.061	0.067	0.066	0.068/		FRCT	92	
DATA A35	/	0.0012	0.022	0.0295	0.035	0.0455			FRCT	93	
1	0.051	0.058	0.061	0.063	0.067	0.068	0.068/		FRCT	94	
DATA A36	/	0.0005	0.0014	0.0027	0.0045	0.014			FRCT	95	
1	0.0127	0.0146	0.013	0.023	0.029	0.037	0.055/		FRCT	96	
DATA A37	/	0.0012	0.0042	0.0085	0.014	0.044			FRCT	97	
1	0.0084	0.013	0.0245	0.033	0.037	0.045	0.053	0.055/		FRCT	98
DATA A38	/	0.0014	0.012	0.027	0.04	0.071			FRCT	99	
1	0.017	0.023	0.0245	0.034	0.0425	0.049	0.0535	0.055/		FRCT	100
DATA A39	/	0.0015	0.0047	0.008	0.012	0.023			FRCT	101	
1	0.029	0.032	0.0395	0.043	0.045	0.059	0.0535	0.055/		FRCT	102
DATA A41	/	0.0014	0.0084	0.014	0.0195	0.03			FRCT	103	
1	0.024	0.04	0.046	0.048	0.051	0.054	0.055/		FRCT	104	
DATA A43	/	0.0056	0.013	0.027	0.026	0.0375			FRCT	105	
1	0.042	0.045	0.049	0.05	0.052	0.0525	0.054	0.055/		FRCT	106
DATA A43	/	0.0071	0.015	0.023	0.03	0.04			FRCT	107	
1	0.043	0.048	0.051	0.054	0.053	0.055	0.055/		FRCT	108	
DATA A43	/	0.0003	0.0009	0.0021	0.003	0.009			FRCT	109	
1	0.0219	0.027	0.039	0.0416	0.043	0.047	0.051/		FRCT	110	
DATA A44	/	0.0001	0.0026	0.0058	0.009	0.029			FRCT	111	
1	0.0057	0.0092	0.021	0.029	0.034	0.041	0.047	0.051/		FRCT	112
DATA A45	/	0.0025	0.0274	0.0015	0.0224	0.0272			FRCT	113	
1	0.012	0.019	0.028	0.035	0.037	0.045	0.048	0.051/		FRCT	114
DATA A46	/	0.0054	0.016	0.023	0.033	0.052	0.074		FRCT	115	
1	0.012	0.026	0.035	0.04	0.042	0.0465	0.049	0.051/		FRCT	116
DATA A47	/	0.0013	0.0038	0.0069	0.011	0.023			FRCT	117	
1	0.029	0.0325	0.035	0.044	0.046	0.0495	0.050	0.051/		FRCT	118

```

DATA AG8 /0.0015, 0.041, 0.303, 0.012, 0.0235/ FRCT 119
2 0.0795, 0.033, 0.04, 0.044, 0.0475, 0.049, 0.0505, 0.051/ FRCT 120
DATA AG9 /0.1018, 0.0612, 0.0004, 0.014, 0.0155/ FRCT 121
1 0.031, 0.025, 0.042, 0.045, 0.047, 0.05, 0.051, 0.051/ FRCT 122
DATA AG1 /1.E-8, 3.E-8, 6.E-8, 1.E-7, 2.E-7, 6.E-7/ FRCT 123
1 1.F-6, 3.F-6, 6.F-6, 1.F-5, 3.F-5, 1.F-4, 1.0-3/ FRCT 124
DATA AG2 /5.E-7, 1.E-6, 5.E-6, 1.E-5, 5.E-5, 5.E-4, 1.E-3/ FRCT 125
1 /
DATA AG3 /13.32, 15.2, 17.8, 14., 21.19, 27.13, 100./ FRCT 126
1E(G1.EQ.0.) GO TO 240
1E(G2.EQ.0.) GO TO 240
DO 100 I=1,7
DO 100 J=1,7
1E(G1-AG1(1,3)) 40,60,60
4) 1E(G1.LT.AG1(1,1)) GO TO 72
CALL TLUG(G1,U7(I,J),AG1,FTN(1,I,J),13)
GO TO 100
6) U7(I,J)=FTN(13,I,J)
GO TO 100
7) U7(I,J)=EXP(ALOG(FTN(1,I,J))+ALOG(FTN(2,I,J))-ALOG(FTN(1,I,J))/(
1+LOG(AG1(2))-ALOG(AG1(1)))+ALOG(G1)-ALOG(AG1(1)))
177 CONTINUE
DO 200 K=1,7
1E(G3-AG3(7)) 140,160,160
14) 1E(G3.LT.AG3(1)) GO TO 170
CALL TLUG(G3,V7(K),AG3,U7(1,K).7)
GO TO 200
160 V2(K)=U7(7,K)
GO TO 200
170 V7(K)=U7(1,K)-(U7(2,K)-U7(1,K))/(AG3(2)-AG3(1))*(AG3(1)-G3)
1E(V7(K).LE.0.0) V7(K)=1.E-5
202 CONTINUE
1E(G2-AG2(7)) 204,206,206
204 1E(G2.LT.AG2(1)) GO TO 207
CALL TLUG(G2,EP3,AG2,V7,7)
GO TO 210
226 FR3=EXP(ALOG(VZ(6))+ALOG(VZ(7))-ALOG(VZ(6)))/(ALOG(AG2(7))-ALOG(A
1G2(6)))*(ALOG(G2)-ALOG(AG2(6)))
GO TO 210
227 EP3=EXP(ALOG(VZ(2))+ALOG(VZ(1))-ALOG(VZ(2)))/(ALOG(AG2(1))-ALOG(A
1G2(2)))*(ALOG(G2)-ALOG(AG2(2)))
217 FCDF=ALOG(FR3)-0.149*(ALOG(THETA)-ALOG(30.))
FCDF=EXP(FCCF)
GO TO 250
240 FCDF=0.
250 CONTINUE
RETURN
END

```

```

SUBROUTINE TLUG(A,B,C,D,N)
DIMENSION C(1),D(1)
1E(1B-11),2.E-2
1 P=0.
GO TO 100
2 R=C(1)
GO TO 100
3 M=1
MU=N
A 1E(MU-ML-1) 1E,15,9
9 MU=(ML+ML)/2
17 1E(C(1)-C(2));1,2,10
17 1E(C(M)-A);13,12,14

```

	TLUG00010
DIMENSION C(1),D(1)	TLUG00020
1E(1B-11),2.E-2	TLUG00030
1 P=0.	TLUG00040
GO TO 100	TLUG00050
2 R=C(1)	TLUG00060
GO TO 100	TLUG00070
3 M=1	TLUG00080
MU=N	TLUG00090
A 1E(MU-ML-1) 1E,15,9	TLUG0120
9 MU=(ML+ML)/2	TLUG0110
17 1E(C(1)-C(2));1,2,10	TLUG00120
17 1E(C(M)-A);13,12,14	TLUG00130

11	TF(A-C(M))11^2,12,14	TLU00140
12	R=D(M)	TLU00150
	GO TO 100	TLU00160
13	MJ=M	TLU00170
	GO TO R	TLU00180
14	M1=M	TLU00190
	GO TO S	TLU00200
15	R=C(M1)+(C(M1)-D(M1))/((A-C(M1))/(C(M1)-C(M1)))	TLU00210
177	RETURN	TLU00220
	END	TLU00230

SUBROUTINE TLUG(A,B,C,D,N)		TLUG0010
DIMENSION C(),D()		TLUG0020
IF(N=1)11,2,3		TLUG0030
1	M=0.	TLUG0040
	GO TO 100	TLUG0050
2	R=D(1)	TLUG0060
	GO TO 100	TLUG0070
3	M1=1	TLUG0080
	M1=N	TLUG0090
4	TF(M1-M1-1)=15+15,9	TLUG0100
5	M=(M1+M1)/2	TLUG0110
	TF(C(1)-C(2))11,2,10	TLUG0120
17	TF(C(M)-A)12,12,14	TLUG0130
11	TF(A-C(M))11^2,12,14	TLUG0140
12	R=D(M)	TLUG0150
	GO TO 100	TLUG0160
13	MJ=M	TLUG0170
	GO TO R	TLUG0180
14	M1=M	TLUG0190
	GO TO S	TLUG0200
15	R=EXP(ALOG(D(M1))+((ALOG(D(M1))-ALOG(D(M1)))*((ALOG(A)-ALOG(C(M1))))/((ALOG(C(M1))-ALOG(C(M1)))))))	TLUG0210
	/((ALOG(C(M1))-ALOG(C(M1))))	TLUG0220
177	RETURN	TLUG0230
	END	TLUG0240

Reproduced from  
test available copy.

APPENDIX V  
FORMAT FOR ROLLER BEARING  
COMPUTER PROGRAM INPUT INFORMATION

MAIN PROGRAM			00000100
CARD	COL.	ITEM	00000200
1	1-10	NO. OF ROLLS (50 MAXIMUM)	00000300
	11-20	ROLL DIA. - IN.	00000400
	21-30	PITCH DIA. - IN.	00000500
	31-40	TOTAL LENGTH OF ROLL - IN.	00000600
	41-50	LENGTH OF FLAT PORTION OF ROLL - IN.	00000700
	51-60	ROLL CORNER RADIUS - IN.	00000800
	61-70	ROLL CROWN RADIUS - IN. DO NOT READ IF CROWN DROP IS000000900 GIVEN	00001000
	71-80	ROLL CROWN DROP - IN. DO NOT READ IF CROWN RADIUS IS000001100	00001200
2	1-10	DISTANCE FROM ROLL END TO POINT WHERE CROWN DROP IS	00001300
		MEASURED - IN.	00001400
	11-20	DIAMETRAL CLEARANCE - IN. + IF LOOSE.	00001500
	21-30	I.D. OF OUTER RING - IN.	00001600
	31-40	O.D. OF INNER RING - IN.	00001700
	41-50	O.D. OF CAGE - IN.	00001800
	51-60	I.D. OF CAGE - IN.	00001900
	61-70	LENGTH OF CAGE POCKET IN THE ROLLING DIRECTION - IN.	00002000
	71-80	WIDTH OF CAGE - IN.	00002100
3	1-10	MODULUS OF ELASTICITY FOR RINGS - PSI. IF BLANK	00002200
		PROGRAM ASSUMES 29,000,000.	00002300
	11-20	SAME FOR ROLLS.	00002400
	21-30	POISSON'S RATIO FOR RINGS. IF BLANK PROGRAM ASSUMES	00002500
		.25	00002600
	31-40	SAME FOR ROLLS.	00002700
	41-50	COEFFICIENT OF SLIDING FRICTION FOR CAGE/PILOT CONTACT.	00002800
	51-60	WEIGHT OF CAGE - LB.	00002900
	61-70	ROLL DENSITY - LB/IN**3. IF BLANK PROGRAM ASSUMES	00003000
		.283	00003100
	71-80	TOLERANCE ON ELASTIC APPROACH OF ROLL TO RACE - IN.	00003200
		IF BLANK PROGRAM ASSUMES .000,000.1	00003300
4	1-10	TOLERANCE ON FILM THICKNESS AT ROLL/POCKET CONTACT	00003400
		- IN. IF BLANK PROGRAM ASSUMES .000,000.5 IN.	00003500
	11-20	TOLERANCE ON ANGULAR VELOCITY OF ROLL ABOUT OWN CENTER - RPM. IF BLANK PROGRAM ASSUMES 1.	00003600
	21-30	TOLERANCE ON ANGULAR VELOCITY OF CAGE - RPM. IF BLANK PROGRAM ASSUMES .1	00003700
	31-40	LEAVE BLANK.	00003800
	1	PUNCH 1 (NO DECIMAL POINT)	00003900
	2-80	TITLE CARD. WRITE ANYTHING.	00004000
6	1	LEAVE BLANK.	00004100
	2-80	WRITE ANYTHING.	00004200
7	1-10	PRESSURE-VISCOSITY COEFFICIENT OF LUBRICANT. IN**2/LB.	00004300
	11-20	TEMPERATURE-VISCOSITY COEFFICIENT OF LUBRICANT -	00004400
		1/DEG F	00004500
	21-30	VISCOSITY OF LUBRICANT AT INLET TEMPERATURE -	00004600
		LB*SEC/IN**2.	00004700
	31-40	INLET TEMPERATURE OF LUBRICANT - DEG F.	00004800
	41-50	Thermal Conductivity of Lubricant -	00004900
		BTU/(DEG F)/HR/FT.	00005000
	51-60	LUBRICANT DENSITY - LB*SEC**2/IN**4.	00005100
	61-80	LEAVE BLANK.	00005200
8	1	PUNCH ZERO	00005300
	2-80	IDENTIFICATION DATA FOR LUBRICANT. PUNCH ANYTHING.	00005400
			00005500
			00005600
			00005700
			00005800

9	1-17	RPM OF OUTER RING.	00005900
	11-20	RPM OF INNER RING.	00006000
	21-30	RADIAL LOAD - LB. (POSITIVE SIGN)	00006100
	31-40	RPM OF ROTATING LOAD. IF LOAD IS STATIONARY LEAVE BLANK.	00006200
	41-50	FACTOR WHICH MULTIPLIES CAGE SPEED TO GET CAGE SPEED DECREMENT. IF BLANK PROGRAM ASSUMES .1	00006300
	51-60	PROPORTIONALITY FACTOR FOR FINITE DIFFERENCE IN THE ANGULAR VELOCITY OF A ROLL ABOUT ITS OWN CENTER. IF BLANK PROGRAM ASSUMES .05	00006400
	61-70	STARTING VALUE FOR MINIMUM FILM THICKNESS AT ROLL/POCKET CONTACT - IN. IF BLANK PROGRAM ASSUMES .0005 IN.	00006500
	71-90	LEAVE BLANK.	00006600
		TO RUN ADDITIONAL LOAD CASES WITH SAME LUBRICANT REPEAT CARD 9 AS REQUIRED	00006700
		TO RUN ADDITIONAL LUBRICANTS PLACE ONE BLANK AFTER LAST CARD 7 AND READ CARD 5 ET. SEQ.	00006800
		TO RUN NEW BEARING CONFIGURATION PLACE TWO BLANKS AFTER LAST CARD 7 AND READ CARD 1 ET. SEQ.	00006900
		TO STOP PLACE THREE BLANK CARDS AFTER LAST CARD 7.	00007000
			00007100
			00007200
			00007300
			00007400
			00007500

APPENDIX VI  
TYPICAL ROLLER BEARING  
PROBLEM FOR COMPUTER PROGRAM

## INPUT DATA FOR LOAD NO. 1 BEARING NO. 2

BEARING REACTION	PERCENT CAGE SLIP	FORCE ON CAGE	CAGE PILOT NORMAL LOAD
7.001E-02	4.003E-03	10.02	6.6691E-01 1.9830E-01

## INPUT DATA FOR RACE CONTACTS

ELEMENT NUMBER	ALPHUTH	CONTACT LOAD INNER	MEAN COMPRESSIVE STRESS	PATTERN EXTREMITY	SLIP VELOCITY
1	7.0	1.6226E-02	1.4205E-02	8.5242E-04	0.7831E-04 1.6415E-01 1.6092E-01 9.7870E-01 1.2710E-02
2	6.0000E-01	7.8287E-01	5.0124E-01	6.0051E-04	5.8051E-04 1.4723E-01 1.4271E-01 8.3379E-01 1.4168E-02
3	3.0001E-02	7.8206E-01	2.2206E-01	6.0050E-04	5.8051E-04 1.4723E-01 1.4271E-01 6.3180E-01 1.4168E-02
THE REST	7.0026E-01			3.1867E-04	1.3217E-01 2.7620E-01

ELEMENT NUMBER	MIN. FILM THICKNESS	TRACTIVE FORCE
1	6.2125E-05	0.22645E-05
2	6.7474E-05	0.2945E-05
6	6.7474E-05	4.6495E-05
THE REST	7.7176E-05	1.1060E-02

## INPUT DATA FOR POCKET CONTACTS

ELEMENT NUMBER	ROW OF ROLLERS	MORAL POCKET LOAD	TANGENTIAL POCKET LOAD	MIN. FILM THICKNESS
1	-7.7022E-04	1.4628E-01 0.0	-5.4400E-02 0.0	5.0747E-015 0.8492E-01
2	-7.6696E-04	5.5004E-04 0.0	-3.3110E-02 0.0	1.5070E-06 0.7492E-03
6	-2.6696E-04	3.3064E-04 0.0	-3.3110E-02 0.0	1.5074E-05 0.7492E-03
THE REST	-5.8634E-04	0.0	4.0133E-02 0.0	4.7111E-03 1.9804E-04

**APPENDIX VII**  
**MIL-L-23699-TYPE OIL PROPERTIES**  
**AVAILABLE FOR USE IN PROGRAM INPUTS**

The following pressure-viscosity data\* for Aeroshell Turbine Oil 555 is typical of the Mil-L-23699 class of lubricants. Pertinent properties for the formulated fluid are as follows:

<u>Thermal Conductivity</u> <u>(Btu/ft - hr- °F-ft)</u>	<u>Kinematic Viscosity</u> <u>(cs)</u>	<u>Density</u> <u>(g/ml)</u>	<u>Reciprocal Asymptotic Isoviscous Pressure,</u> <u>((psi)<sup>-1</sup>)</u>
100° F .098	28.2	.980	.942
210° F -	5.3	.935	.691
300° F .078	2.4	.897	.602
500° F .075	-	-	-

\*Data provided by William R. Jones, Jr., Research Engineer, NASA Lewis Research Center, Cleveland, Ohio.

APPENDIX VIII  
SOLUTION FOR ROLLER BEARING CASE  
OPERATING AT 20,000 RPM AND RADIAL LOAD OF 200 POUNDS

Reproduced from  
best available copy.

